2009

Morphodynamics of ebb tidal delta sandbanks in a meso to macro tidal environment; Teignmouth, UK.

Aird, Nigel P.

Morphodynamics of ebb tidal delta sandbanks in a meso to macro tidal environment; Teignmouth, UK.

By

Nigel P. Aird

A thesis submitted to the University of Plymouth

in partial fulfilment for the degree of

Doctor of Philosophy

School of Earth, Ocean and Environmental Sciences

Faculty of Science

June 2009

Copyright Statement

Abstract

Morphodynamics of ebb tidal delta sandbanks in a meso to macro tidal environment; Teignmouth, UK.

Nigel P. Aird

This contribution utilises a multifaceted approach to investigate the physical processes responsible for the onshore migration of ebb tidal sandbanks at an estuarine inlet dominated by low energy waves.

A coastal video system was used to obtain two-weekly quantitative measurements of the position, plan form and crest depth of the landward migrating sandbanks over a five year period which encompassed four consecutive events. These data were supplemented with a 35 year photographic record of the inlet's development. Onshore sandbank migration was characterised by mean and maximum rates of 1 to 2 $m.day^{-1}$ and 5 $m.day^{-1}$ respectively. The migration rate was found to be highly correlated ($R^2 = 0.7$) with, and linearly related to the ratio of the incident wave height to the crest depth particularly prior to shore-attachment. The plan form, area and crest depth of the sandbanks are a function of the sediment availability. In the inlet's current morphologic mode two plan form geometries are typically observed. These are crescentic and elongate forms (high aspect ratios) where the latter have their major axis transversely-orientated with respect to the coast. Which of these forms develops is dependent on the chronology of wave energy and the crest depth in relation to the tidal water level variation. Elongate transverse morphologies are associated with low relief sandbanks which are synonymous with periods of relatively low sediment availability. Conversely the crescentic morphologies typically occur when sediment availability is higher and the depth to the sandbank crests is shallower.

A unique set of in-situ measurements of waves, currents and sediment transport were obtained from four positions on a sandbank in the mid term of its onshore migration. Analysis of the data revealed that the sandbank was dominated by onshore directed sediment transport in the shallow surf zone where current maxima occurred. The gradients in transport were highest on the flood tide. An energetics analysis of the data revealed that short wave stirring and wave driven mean flows were the physical processes responsible for morphological change. The mean flows are in effect longshore currents since they are generated by strong refraction and focussing of the incident waves by the morphologies. These generate a zone of wave convergence over the sandbanks when in the submerged state and very oblique wave breaking along the flanks when the features are exposed by the tide. A numerical model (MIKE 21) was subsequently applied in order to simulate the wave driven patterns of erosion and deposition over the sandbanks using both idealised and measured boundary conditions. The numerical experiments determined that there exists a dichotomy in the patterns of erosion and deposition which are laterally constrained in the submerged state and divergent in the exposed state. Morphological evolution was therefore governed by the variable residence times of the causative wave driven processes at different tidal elevations. It was found that low energy waves when combined with neap tides promoted shoreward elongation through the dominance of the patterns of deposition in the shallow submerged state. Higher energy conditions were predicted to promote a degree of broadening in the longshore dimension and increased crest elevation. This was caused by the patterns of deposition being dominated by both the laterally constrained (high tide) and divergent (low tide) patterns due to their longer residence times.

Contents

Abstract.....iii.
Contents.....iv.
List of Figures.....ix.
List of Tables.....xvii.
Acknowledgements.....xix.
Author Declaration.....xx.

Chapter 1: Introduction.....1.

1.1 The importance of coastlines and sediment transport.....1.

1.2 Specific objectives.....5.

1.3 Thesis overview... .....6.

Chapter 2: Literature review.....9.

2.1 Basic inlet concepts and nomenclature.....9.

2.1.1 Physical characteristics of ebb tidal delta sandbanks.....12.

2.2 Morphologic models of ebb tidal deltas.....14.

2.2.1 Natural sediment bypassing at inlet entrances.....20.

2.3 Empirical relationships.....25.

Chapter 3: Introduction to the Teign inlet.....30.

3.1 Physical setting.....30.

3.2 Environmental conditions.....32.

3.3 Sediment characteristics and littoral circulation.....35.

3.4 Nearshore morphodynamics: an historical perspective.....39.

Chapter 4: Video remote-sensing.....48.

4.1 Argus video system.....50.

4.1.1 Brief history of the Teignmouth Argus station.....51.

4.1.2 Camera model and coordinate transformation.....53.

4.2 Contour extraction methodology and sampling strategy.....56.

4.3 Sandbank descriptive parameters.....62.

4.3.1 Image spatial resolution and coordinate transformation accuracy.....62.

4.3.2 Estimation of sandbank crest depth from Argus images.....67.

4.4 Results.....69.

4.4.1 Introduction.....69.

4.4.2 Contour times series and their qualitative description.....70.

4.4.3 Temporal variability in sandbank descriptive parameters.....84.

4.4.3.1 Cross-shore and longshore centre of mass position.....84.

4.4.3.2 Cross-shore migration rate.....89.

4.4.3.3 Crest depth .....96.

4.4.3.4 Correlation between raw cross-shore migration rate and the ratio of mean offshore significant wave height to minimum crest depth.....101.

4.4.3.5 Plan view geometry.....104.

4.5 Summary.....109.

Chapter 5: In-situ measurements.....113.

5.1 Data analysis techniques.....113.

5.1.1 Sampling theory.....113.

5.1.2 Time series analysis.....114.

5.1.2.1 Sediment transport calculations.....116.

5.1.3. Frequency domain analysis and the Fast Fourier Transform.....117.

5.1.4 Spectral analysis.....119.

5.1.5 Co-spectral analysis.....121.

5.1.6 Energetics analysis.....123.

5.2 Instrumentation.....125.

5.2.1 Synchronised logger for investigation into the transport of sediment (SLOT)) .....126.

5.2.2 Pressure transducer.....127.

5.2.3 Electromagnetic current meter.....129.

5.2.4 Optical back scatter sensor.....130.

5.3 Data collection strategy.....132.

5.4 Data processing.....133.

5.5 Fieldwork environmental conditions.....134.

5.6 Results.....138.

5.6.1 Introduction to the raw data.....138.

5.6.2 Overview of the observed of the observed current regime.....140.

5.6.3 Comparison of cross-shore hydrodynamics and sedimentation under calm and low energy conditions.....147.

5.6.4 Comparison of third order cross-shore velocity moments under calm and low energy conditions.....155.

5.6.5 Co-spectral analysis of the cross-shore current and sediment transport fluxes under low energy conditions.....158.

5.7 Summary.....161.

Chapter 6: Numerical modelling.....166.

6.1 MIKE21: NSW, HD and ST modules .....168.

6.2 Model calibration and validation .....170.

6.3 Idealised simulations.....174.

6.3.1 Methodology and model setup.....174.

6.3.2 Results.....177.

6.3.2.1 Comparison of modelled hydrodynamics and sedimentation for circular and elliptic sandbanks under emerged and submerged states.....177.

6.3.2.2 The propensity of different combinations of hydrodynamic conditions to alter the aspect ratio of an offshore sandbank.....187.

6.3.2.3 Wave driven morphological change over spring and neap tidal ranges.....191.

6.3.3 Summary .....199.

6.4 Teignmouth simulation.....201.

6.4.1 Methodology and model setup.....201.

6.4.2 Results.....203.

6.4.2.1 Qualitative validation of the modelled and measured hydrodynamics using the data for the offshore extremity position.....203.

6.4.2.2 Spatial and temporal variation in the modelled hydrodynamics and sedimentation.....208.

6.4.2.3 Temporal variation in the relative importance of the wave driven and tidal components of the mean flow regime.....218.

6.5.3 General summary.....221.

Chapter 7: Discussion and Synthesis.....230.

7.1 Primary physical controls on short to medium term shoal morphodynamics.....225.

7.2 Refraction, diffraction and sheltering effects.....230.

7.3 Long term trends in the morphological evolution of the ebb tidal delta and landward migrating sandbanks.....232.

7.3.1 Seasonal trends (lower macro time scale).....232.

7.3.2 Supra-annual trends (upper macro time scale).....235.

7.4 Conceptual model of the plan form morphological evolution of Teign inlet ebb tidal delta sandbanks.....238.

Chapter 8: Conclusions.....244.

Appendices.....249.

Appendix A1 Teign inlet: c.1976-2009.....249.

Appendix A2 In-situ measurement data quality tables for the different SLOT rig deployment positions during the May 2003 Coastview fieldwork program.....253.

Appendix A3 Proceedings paper: 29th International Conference on Coastal Engineering, Lisbon, Portugal.....258.

References.....271.

List of Figures

Chapter 1

Figure 1.1: Spatial and temporal scales in relation to coastal morphological change, (modified from Cowell *et al.*, 2003). 4.

Chapter 2

Figure 2.1: Typical ebb shoal morphology with tidal flow residuals and dominant transport directions indicated by arrows (after Hayes, 1975, 1980). 11.

Figure 2.2: Morphologic inlet models of barrier island inlets (left panel) after Galvin, (1971) and estuarine inlets (right panel) after Hicks and Hume, (1996). 15.

Figure 2.3: Morphologic models of barrier island inlet ebb tidal delta geometry, Georgia, southeast USA, left panel after Oertel, (1975), and right panel after Hubbard *et al.* (1979). 18.

Figure 2.4: Examples of conceptual models of inlet ebb shoal evolution from the United States Army Corps of Engineers: a) stable inlet processes (model 1), b) ebb tidal delta breaching (model 3), and c) outer channel shifting (model 4). T1 to T3 denote time chronology (after FitzGerald *et al.*, 2000). 22.

Figure 2.5: Conceptual profile model of onshore sandbank migration on the ebb tidal delta (after FitzGerald, 1988). 23.

Figure 2.6: Inlet shoal bypassing interval in the context of inlet tidal prism (left panel) and ebb tidal delta volume (right panel) after Gaudiano and Kana (2001) (modified from Burningham and French, 2006). 27.

Chapter 3

Figure 3.1: Location of the Teign inlet: U.K. (left panel) and Lyme Bay (right panel) coastlines. (Vertical datum: shoreline at mean high water, data source: NOAA Geophysical Data Centre (http://rimmer.ngdc.noaa.gov/mgg/coast/getcoast.html). 30.

Figure 3.2: Low tide images of the Teign inlet. Upper left panel: inlet entrance flanked by the Ness headland to the south with Denn Spit and Spratt Sand to the north (2001). Upper right panel: south end of Teignmouth beach with shore-attached transverse sandbank (2001). Lower panel: a typical configuration of sandbanks on the ebb tidal delta (2007). (Upper panel aerial images are courtesy of Prof. K. Dyer, Futurecoast Project, Department of the Environment, Food and Rural Affairs., U.K., 2000-2002). 33.

Figure 3.3: Teign inlet channel and nearshore bathymetry superposed with the areal distribution of surficial sediments (Grain types: > 2 mm: gravel; 1-2 mm: very coarse sand; 500-1000 μm: coarse sand; 250-500 μm: medium sand; 125-250 μm: fine sand) (after van Lancker et al., 2004). 36.

Figure 3.4: Conceptual model of the littoral circulation for the Lyme Bay coastal region from The Parson and Clerk headland, Holcombe to the Hope's Nose, headland,

Torquay, and in the vicinity of the Teign inlet entrance (inset) (after Bray *et al.*, 2004). 37.

Figure 3.5: Teign inlet morphological evolution from February 1967 to September 1970 after Robinson (1975). (Dark grey shading denotes land; light grey shading denotes sedimentary features, and arrows indicate the prevailing tidal current direction. 40.

Figure 3.6: Spatial representation of the dominant hydrodynamic forces (left panel),and littoral sediment budget at the Teign inlet after Siegle (2003). 43.

Chapter 4

Figure 4.1: Argus image types from camera 3 showing Teignmouth town, the main beach and pier: a) snapshot, b) timex, c) variance, and d) daytimex. 50.

Figure 4.2: a) Argus station location, b) station viewpoint, c) camera rig, d) Argus II collection strategy (after Holman and Stanley, 2007). 52.

Figure 4.3: a) Rectified Teignmouth Argus image, b) camera model parameters (after Holland *et al.*, 1997). 54.

Figure 4.4: The manual contour extraction process using a focussed region of a rectified Argus image containing the sandbank. A set of descriptive parameters that define the feature are subsequently extracted using the Matlab 'regionprops' function. The derived contour is displayed on the right side of the diagram overlaid with major and minor axes which cross at the centre of mass of the sandbank. 58.

Figure 4.5: Contour depth histograms for individual events. 59.

Figure 4.6: Cross-shore 2D section through the offshore sandbank from May 2003. The horizontal lines depict the target contour tidal level (-1.80 m ODN) and the depth of the shallowest contour (-1.25 m ODN). 61.

Figure 4.7: Cross- and longshore pixel footprint maps for the Teignmouth camera setup. 63.

Figure 4.8: Contour coordinates dataset and pixel footprint variability in the a) cross-shore direction, and the b) longshore direction. 64.

Figure 4.9: Event 1 contour times series. 72.

Figure 4.10: Event 1 root-mean-square wave height (upper panel) and period (lower panel) time series. Bold lines indicate a 7-day running mean. 73.

Figure 4.11: Event 2 contour time series. 75.

Figure 4.12: Event 2 root-mean-square wave height (upper panel) and period (lower panel) time series. Bold lines indicate a 7-day running mean. 76.

Figure 4.13: Event 3 contour time series. 78.

Figure 4.14: Event 3 root-mean-square wave height (upper panel) and period (lower panel) time series. Bold lines indicate a 7-day running mean. 79.

Figure 4.15: Event 4 contour time series. 81.

Figure 4.16: Event 4 root-mean-square wave height (upper panel) and period (lower panel) time series. Bold lines indicate a 7-day running mean. 82.

Figure 4.17: Time series of the cross-shore (points) and longshore (stars) coordinates of the sandbank's centre of mass position for all events. The vertical hatched lines indicate the approximate time of sandbank shore-attachment. Event colour key: event 1: black, event 2: red, event 3: green, event 4: blue. 85.

Figure 4.18: Argus image time series depicting the offshore genesis of a new sandbank and its subsequent merging with the elongate event 1 sandbank. 87.

Figure 4.19: Time series of cross-shore COM position (red line), raw migration rate (thin black line) and, smoothed and interpolated migration rate (thick black line) for events 1 to 4. The lines denoted by A1 to A4 (vertical) and S1 to S3 (horizontal) indicate the approximate time of shore-attachment and common trends (medium to long term) in average migration rate respectively. Key: raw cross-shore COM position: red line, raw migration rate: thin black line, smoothed & interpolated migration rate: thick black line. 90.

Figure 4.20: Scatter plots of cross-shore COM position versus migration rate with polynomial trend-line (dashed line) for events 1 to 4. The trend-lines highlight periods of acceleration and deceleration in the sandbank morphodynamics. 91.

Figure 4.21: Time series of the estimated sandbank crest depth with error bars. The vertical lines denoted by A1 to A4 indicate the approximate time of sandbank shore-attachment (Colour key: event 1: black, event 2: red, event 3: green, event 4: blue). 97.

Figure 4.22: Sandbank crest depth time series for individual events. The vertical lines denoted by A1 to A4 indicate the approximate time of sandbank shore-attachment. 99.

Figure 4.23: Time series of cross-shore migration rate (black) and the ratio of offshore significant wave height to crest depth (red) for the onshore migration events 2 to 4: a) event 1, b) event 2, and c) event 3. Vertical hatched lines indicate the approximate time of shore-attachment. 103.

Figure 4.24: Time series of geometric sandbank parameters for all events: a) area, b) length of cross-shore (black) and longshore (red) axes, and c) aspect ratio (cross-shore length/longshore length). The approximate times of sandbank shore-attachment for events 1 to 4 are denoted by the vertical hatched lines A1 to A4 respectively. Event key: event 1 diamonds, event 2: asterisks, event 3: triangles, event 4: stars. 106.

Figure 4.25: Scatter plots of geometric sandbank parameters for all events: a) area, b) length of cross-shore (dots) and longshore (diamonds) axes and c) aspect ratio. Colour denotes event number. 107.

Chapter 5
Figure 5.1: Classification of time series data (after Bendatt and Piersol, 1986). 115.

Figure 5.2: Argand diagram depicting the complex number representation of a vector. 118.

Figure 5.3: Spectral peak coefficient (y-axis) versus degrees of freedom (x-axis) with curves denoting the 80, 90 and 99% confidence levels for the upper and lower error bars. 121.

Figure 5.4: The Valeport SLOT system secured *in-situ* using steel tubing. 126.

Figure 5.5: Contour plot of the bathymetry and topography of the study site during the May 2003 fieldwork program with SLOT and ADCP positions (▲) superimposed. The contours are in metres referenced to ODN. 134.

Figure 5.6: Images depicting the sea state at Teignmouth on a) the 14th May (calm conditions) and b) the 16th May (low energy conditions). (SLOT 1A deployment position is pictured in the foreground). 136.

Figure 5.7: Wind and offshore ADCP (h = -5.8 m ODN) wave measurements during the fieldwork program. The vertical lines denote times when there was a noticeable change in the significant wave height conditions. Note: wind direction is measured relative to True North and indicates the direction the wind is coming from. Wave direction is measured relative to the shore normal where a 180° wave direction indicates that the waves are propagating onshore in a perpendicular manner to the beach face). 137.

Figure 5.8: Raw data time series from run 3 (inner surf zone) on the 16th May for water depth (h), cross-shore current (u), longshore current (v), and suspended sediment concentration (c). Note for u and v, a positive value denotes an onshore directed current, and a negative value denotes an offshore directed current. 139.

Figure 5.9: a) current vector time series from each SLOT rig deployment position using data averaged over 17 minute intervals for the duration of one tidal cycle. For scaling purposes a vertical vector denoting an onshore directed current of 0.5 $m.s^{-1}$ is positioned to the right of each vector time series plots, b) sandbank bathymetry with SLOT rig deployment positions overlaid. The abbreviations AM and PM relate to the 1st and 2nd tides of the day. 141.

Figure 5.10: Comparison of hydrodynamics and sediment suspension under calm (dots) and low energy conditions (circles) for the offshore extremity SLOT position (1A): a) water depth ($< h >$), b) wave height ($< H_s >$), c) mean cross-shore current ($< \bar{u} >$), d) the standard deviation of the cross-shore current (oscillatory component) ($< u' >$), e) the mean suspended sediment concentration ($< c >$). Note: each plotted point is a 17 minute time average of the data. 148.

Figure 5.11: Comparison of the cross-shore sediment transport under calm (black dots) and low energy conditions (white circles) at the offshore extremity SLOT position (1A): a) net cross-shore sediment transport ($< uc >$), the mean component of the cross-shore sediment transport ($< \overline{uc} >$), and the oscillatory component of sediment transport ($< uc' >$). Each plotted point is a 17 minute time average of the data. 153.

Figure 5.12: Third order cross-shore velocity moments computed for the offshore extremity position (1A) at the inner, mid- and outer surf zone positions for: a) calm conditions (14th May), and b) low energy conditions (16th May). The runs relate to the flood tide and positive values denote offshore transport, negative values denote onshore transport. 156.

Figure 5.13: Cross-spectral analysis of suspended sediment concentration and cross-shore velocity for run 3, 16th May: a) SSC auto-spectrum, b) *u* velocity auto-spectrum, c) *c-u* co-spectrum, d) *c-u* phase spectrum where white circles = non coherent phase relation, black circles = coherent phase relation, e) *c-u* cross-spectrum, and f) *c-u* coherence spectrum. 159.

Figure 5.14: Sensors at the shoreward extremity SLOT rig position after excavation on the 16th May. 165.

Chapter 6

Figure 6.1: MIKE 21 modular framework. 168.

Figure 6.2: Teignmouth bathymetry with the stations used in the Siegle (2003) model calibration and validation. 171.

Figure 6.3: Contour plots showing the bathymetries for a subset of the model domain focussed on the sandbank morphologies: a) circular and b) elliptic. The contour units are depths (m) relative to an arbitrary datum and the cross-shore and longshore axes are relative to the model domain origin. 175.

Figure 6.4: Modelled hydrodynamics and sedimentation for the emerged and submerged states of the circular morphology. Emerged state (h = -2.0 m): a) wave height and direction (vectors) with water depth (colour), b) current strength and direction (vectors) with H_s/h (colour), c) sediment flux strength and direction (vectors) with initial rate of bed level change (colour), Submerged state (h = -1.0 m): d) wave height and direction (vectors) with water depth (colour), e) current strength and direction (vectors) with H_s/h (colour), f) sediment flux strength and direction (vectors) with initial rate of bed level change (colour). 178.

Figure 6.5: Modelled hydrodynamics and sedimentation for the emerged and submerged state of the elliptic morphology. Emerged state (h = -2.0 m): a) wave height and direction (vectors) with water depth (colour), b) current strength and direction (vectors) with H_s/h (colour), c) sediment flux strength and direction (vectors) with initial rate of bed level change (colour), Submerged state (h = -1.0 m): d) wave height and direction (vectors) with water depth (colour), e) current strength and direction (vectors) with H_s/h (colour), f) sediment flux strength and direction (vectors) with initial rate of bed level change (colour). 179.

Figure 6.6: Hydrodynamic and sedimentation parameters for circular (black) and elliptic (red) morphologies from Table 7.4: a) ratio of maximum shoaling wave height to water depth, b) maximum current strength ($m.s^{-1}$), c) maximum sediment flux ($m^3.day^{-1}.m^{-1}$), and d) mean initial rate of bed level change per unit area ($cm.day^{-1}.m^{-1}$). Offshore significant wave heights of 0.5, 1.5, and 2.5 m are denoted by circles, triangles and squares respectively. 183.

Figure 6.7: Conceptual diagram of the mechanisms of broadening and elongation due to the patterns of erosion (light grey shading) and accretion (dark grey) around the sandbank. The large circle denotes the plan form of the underlying sandbank. 188.

Figure 6.8: Comparison of the ratio of the longshore lengths scales of the erosion and accretion contours relating to initial bed level change rates of ±0.1 cm.day^{-1} per unit area under a range of water levels (h = -2.0, -1.0, +1.0, +2.0 m), and offshore significant wave heights (H_s = 0.5, 1.5, 2.5 m) for the: a) circular morphology, b) elliptic morphology. The H_s/h ratios are computed from the offshore significant wave height and the minimum depth over the crest of the sandbank which is located at a level of -1.42 m relative to the arbitrary datum (h = 0 m). Negative H_s/h ratios indicate that the morphology is emerged. 189.

Figure 6.9: 3D contour plots showing the original circular sandbank morphology (black contours) and the estimated morphology after (red contours) 30 cycles of neap (tidal range = 2 m) and spring (tidal range = 4 m) tides under a range of offshore wave heights: a) H_s = 0.5 m, neap tide, b) H_s = 1.5 m, neap tide, c) H_s = 2.5 m, neap tide, d) H_s = 0.5 m, spring tide, e) H_s = 1.5 m, spring tide, and f) H_s = 2.5 m, spring tide. The contours are at 0.5 m intervals and all axes dimensions are specified in meters relative to an arbitrary datum (h = 0 m). 193.

Figure 6.10: 2D plan view contour plots from the -2.0 m level from the original (black contours) and updated (red) sandbank morphologies in Figure 7.7: a) H_s = 0.5 m, neap tide, b) H_s = 1.5 m, neap tide, c) H_s = 2.5 m, neap tide, d) H_s = 0.5 m, spring tide, e) H_s = 1.5 m, spring tide, f) H_s = 2.5 m, spring tide. Contours are in specified meters at 0.5 m intervals and referenced to an arbitrary datum. 195.

Figure 6.11: Modelled and measured current vector time series for the offshore extremity SLOT rig position (1A) under similar hydrodynamic conditions. a) in-situ measurement data from May 16th, 2003, and b) modelled data. A vector denoting a 0.5 m.s^{-1} onshore directed current is plotted to the right of the time series for scaling purposes. 204.

Figure 6.12: Modelled (black circles) and measured (white circles) hydrodynamics and sedimentation under comparative offshore wave and tide conditions for the offshore extremity SLOT rig position (1A): a) water depth, b) cross-shore current velocity, and c) cross-shore sediment flux (model) with the estimated suspended cross-shore sediment transport rate after Jaffe *et al.* (1984) (*in-situ* measurements). 207.

Figure 6.13: Simulated hydrodynamics and sedimentation in the vicinity of the offshore sandbank at Teignmouth for the 16th May, 2003. Time ≈ high tide: a) current strength and direction, b) sediment flux strength and direction. Black hatched lines indicate the shoreline position and black triangles indicate the nearest grid point to the SLOT rig positions used in the fieldwork program. Reference vectors are plotted at the furthest right hand grid point position for scaling purposes. 209.

Figure 6.14: Simulated hydrodynamics and sedimentation in the vicinity of the offshore sandbank at Teignmouth for the 16th May, 2003 Time ≈ high tide +2 hours: a) current strength and direction, b) sediment flux strength and direction. Black hatched lines indicate the shoreline position and black triangles indicate the nearest grid point to the SLOT rig positions used in the fieldwork program. Reference vectors are plotted at the furthest right hand grid point position for scaling purposes. 210.

Figure 6.15: Simulated hydrodynamics and sedimentation in the vicinity of the offshore sandbank at Teignmouth for the 16th May, 2003. Time ≈ high tide +4 hours: a) current strength and direction, b) sediment flux strength and direction. Black hatched lines indicate the shoreline position and black triangles indicate the SLOT positions during the fieldwork program. Reference vectors are plotted at the furthest right hand grid point position for scaling purposes. 211.

Figure 6.16: Simulated hydrodynamics and sedimentation in the vicinity of the offshore sandbank at Teignmouth for the 16th May, 2003. Time ≈ low tide: a) current strength and direction, b) sediment flux strength and direction. Black hatched lines indicate the shoreline position and black triangles indicate nearest grid point to the SLOT rig positions used in the fieldwork program. Reference vectors are plotted at the furthest right hand grid point position for scaling purposes. 212.

Figure 6.17: Simulated hydrodynamics and sedimentation in the vicinity of the offshore sandbank at Teignmouth for the 16th May, 2003. Time ≈ low tide +2 hours: a) current strength and direction, b) sediment flux strength and direction. Black hatched lines indicate the shoreline position and black triangles indicate nearest grid point to the SLOT rig positions used in the fieldwork program. Reference vectors are plotted at the furthest right hand grid point position for scaling purposes. 213.

Figure 6.18: Simulated hydrodynamics and sedimentation in the vicinity of the offshore sandbank at Teignmouth for the 16th May, 2003. Time ≈ low tide +4 hours: a) current strength and direction, b) sediment flux strength and direction. Black hatched lines indicate the shoreline position and black triangles indicate the nearest grid point to the SLOT rig positions used in the fieldwork program. Reference vectors are plotted at the furthest right hand grid point position for scaling purposes. 214.

Figure 6.19: Comparison of modelled cross-shore current strength due to the combined effects of wave and tidally driven currents (black circles), the tide only (red circles), and waves only (blue circles) for the four SLOT rig deployment positions on the 16th May 2003: a) shoreward extremity (2A), b) central crest (1B), c) southern flank (2B), and d) offshore extremity (1A). Positive values denote onshore directed currents and vice versa. Abbreviation key: WD denotes wave dominance and TD denotes tidal dominance. 220.

Chapter 7

Figure 7.1: Histogram of monthly average significant wave height compiled from hourly pier-mounted pressure transducer data for a) event 1, b) event 2, c) event 3, d) event 4, and e) ensemble average. 233.

Figure 7.2: Camera 4 image showing the relict sandbank on the terminal lobe on the 14th May, 1999. 235.

Figure 7.3: Index of the boreal winter (December-March) mean NAO constructed as the difference in sea level pressure between Lisbon, Portugal and Stykkisholmur/Reykjavik, Iceland from 1960 to 2007. The black line represents the index smoothed to remove fluctuations with periods less than 4 years. 236.

Figure 7.4: Sensitivity of winter monthly mean significant wave height to NAO around northern Europe. (Image supplied to the Department for the Environment, Food and Rural Affairs courtesy of David Woolf, National Oceanographic Centre, Southampton). 237.

Figure 7.5: Conceptual model of shoal geometry evolution during onshore migration at the Teign inlet. Light and dark grey shaded areas represent regions of erosion and deposition respectively. Q_{IN} and Q_{OUT} represent supply to the ebb tidal delta. DL and EL are the longshore length scales of the regions of deposition and erosion. Box codes denote the post genesis mechanisms of morphological change due to the tendency towards the predominance of submerged (PG1) or emerged (PG2) patterns of erosion and deposition. 241.

Appendices

Figure A1: Chronology of the Teign inlet ebb shoal system photographed from the Ness headland, 1976-1979. (Courtesy of S.Hook). Upper panel: main ebb channel is orientated north due to the well developed Ness bar, an irregular-shaped, shore-attached sandbank is in the process of being dissipated. Middle panel: the main channel is orientated east, genesis and mid-term migration sandbanks are present. Lower panel: the main channel is orientated east, the migrating sandbank has a large area with crescentic horns developing at the landward margin of both flanks. 249.

Figure A2: Chronology of the Teign inlet ebb shoal system photographed from the Ness headland, 1982-1984. (Courtesy of S.Hook). Upper panel: the main channel is orientated to the east, offshore sandbanks are developing on the terminal lobe and a relict shore-attached bar on Teignmouth main beach is in evidence. Middle panel: sandbank in mid-term onshore migration with crescentic horns on the landward side, the terminal lobe is completely submerged. Lower panel: the main ebb channel is orientated to the east and the Ness bar is well-developed, mid-term migration and shore-attached sadbanks are observed indicating high sediment availability. 250.

Figure A1: Chronology of the Teign inlet ebb shoal system photographed from the Ness headland, 1986-1990. (Courtesy of S.Hook). Upper panel: the main ebb channel is orientated to the north due to the well-developed Ness bar, the irregular-shaped, shore-attached bar is in the process of being dissipated. Middle panel: a large shore-parallel sandbank in mid-term migration has developed horns on the landward side. Lower panel: a single sandbank is in mid-term migration, there are no shore-attached bars in evidence on the main beach and the terminal lobe is completely submerged. 251.

Figure A2: Chronology of the Teign inlet ebb shoal system photographed from the Ness headland, 1992-2009. Upper panel: A large oblique sandbank gas developed on the terminal lobe, the main channel has been deflected to the east, a shore-attached bar is in evidence (Courtesy of S.Hook). Middle panel; inner (shore-attached) and outer sandbanks occupy the nearshore region, both features are elongate and transversely oriented, (Argus image panorama). Lower panel: the sandbanks in the previous image have merged to form a single transverse bar approximately 600 m in length (Argus image panorama). 252.

List of Tables

Chapter 4
Table 4.1: Contour dataset summary statistics. 59.

Table 4.2: Sandbank descriptive parameters. 62.

Table 4.3: Summary of the pixel footprint variability between morphological stages. 65.

Chapter 5
Table 5.1: Third order velocity moments generated by the expansion of the cubed cross-shore velocity component. A tilde denotes the oscillatory component and angle brackets denote a time average. 124.

Table 5.2: Velocity moment terms that constitute the sediment transport at the offshore extremity. 156.

Chapter 6
Table 6.1: Significant wave height validation parameters (Siegle, 2003). 171.

Table 6.2: Water level validation parameters (Siegle, 2003). 171.

Table 6.3: Horizontal current velocity validation parameters (Siegle, 2003). 172.

Table 6.4: Summary of key hydrodynamic and sedimentation experimental parameters for circular and elliptic morphologies under a variety of stationary water level and wave height conditions. Values of Hs/h, current strength, and sediment fluxes are maximum values extracted from around the morphologies. The initial rate of bed level change is the mean value per unit area based on a 1 km^2 region of the model domain that encompasses the features. 182.

Appendices
Table A3.1: Data quality tables for the in-situ measurements at SLOT rig deployment position 1A (SLOT1 P1) from the 14th May to the 16th May, 2003. P1 and P2 denote the first and second deployment positions respectively. AM and PM denote the first and second respective tides for a particular date; *u* and *v* denote the orthogonal current direction. Instrument abbreviations: EM: electromagnetic current meter, PT: pressure transducer, and OBS: optical back scatter sensor. 254.

Table A3.2: Data quality tables for the in-situ measurements at SLOT rig deployment positions 1A (SLOT1 P1) and 1B (SLOT1 P2) from the 16th May to the 18th May, 2003. P1 and P2 denote the first and second deployment positions respectively. AM and PM denote the first and second respective tides for a particular date; *u* and *v* denote the orthogonal current direction. Instrument abbreviations: EM: electromagnetic current meter, PT: pressure transducer, and OBS: optical back scatter sensor. 255.

Table A3.3: Data quality tables for the in-situ measurements at SLOT rig deployment positions 2A (SLOT2 P1) and 2B (SLOT2 P2) from the 15th May to the 17th May,

2003. P1 and P2 denote the first and second deployment positions respectively. AM and PM denote the first and second respective tides for a particular date; *u* and *v* denote the orthogonal current direction. Instrument abbreviations: EM: electromagnetic current meter, PT: pressure transducer, and OBS: optical back scatter sensor. 256.

Table A3.4: Data quality tables for the in-situ measurements at SLOT rig deployment positions 2B (SLOT2 P2) from the 17th May to the 18th May, 2003. P1 and P2 denote the first and second deployment positions respectively. AM and PM denote the first and second respective tides for a particular date; *u* and *v* denote the orthogonal current direction. Instrument abbreviations: EM: electromagnetic current meter, PT: pressure transducer, and OBS: optical back scatter sensor. 257.

Acknowledgements

First and foremost, I would like to extend my deepest gratitude to Dr. Mark Davidson for his guidance, patience and ceaseless support, without which, it would not have been possible to complete this research. Many interesting moments were shared by student and supervisor alike when studying the energetic surf zone conditions of the SW French coast at first hand. These times, which I also had the pleasure of sharing with Dr. Paul Russell and Dr. Jon Miles, were among the most memorable and enjoyable of my PhD experience.

I would also like to thank my second supervisor Prof. David Huntley who provided invaluable guidance through the course of this research project. In addition to this, I would like to thank Pete Ganderton for his expertise during the fieldwork measurement program in May 2003. Under Pete's guidance it was possible to successfully deploy instrumentation in the highly challenging marine environment of an offshore sandbank in the mid term of it's onshore migration cycle.

I would also like to thank The European Commission and the Coastview Project for funding this research.

Finally, I would like to thank my parents for their patience and support, and my friends for just being there during the many challenging times, in particular: Helen, Ismael and Cecillia, Marcos, Tom, Simone and Chris, Julian and Faye, Ian.

AUTHOR'S DECLARATION

At no time during the registration for the degree of Doctor of Philosophy has the author been registered for any other University award.

This study was financed with the aid of a studentship funded by the European Union V Framework program (1998-2002) and the Coastview Project (1998-2002) (contract no. EVK3-CT-2001-0054).

The author attended regular internal seminars attended by PhD research colleagues and members of the academic staff. The author also attended a series of bi-annual meetings between Coastview Project partners from Holland, Italy and Spain (European academic institutes) and coastal management professionals. Three presentations of the in-situ measurements analyses of the present study were given at internal research group and Coastview Project meetings between August 2002 and March 2004, and a further presentation was made at the Plymouth Marine Laboratory (January, 2005). In addition to the above, the author also attended the 29th International Conference on Coastal Engineering, Portugal, 2004 and presented research integrating field measurements with video remotely-sensed data.

Signed: 

Date: 06/08/10

1 Introduction

1.1 The importance of coastlines and sedimentation transport

Coastlines are of significant socio-economic importance due to their being heavily populated. For example it has been estimated that there are 1.2 billion people living within a 100 km^2 stretch of coastline with densities three times larger than the global average (Small and Nicholls, 2003). The attraction of the coastline stems from its usefulness as a resource and consequently extensive areas of land in close proximity to the shoreline are developed. Climate change is generally considered to be driving changes to the prevailing nearshore hydrodynamic conditions of the world's coastlines. The most important changes with respect to coastal habitats are considered to be sea level rise and an increased incidence of storms which put coastal developments at an increased risk of inundation, and damage due to elevated wave energy levels. For the U.K. it has been estimated that coastal vulnerability to inundation due to sea level rise and increased storminess could cause the '1 in 100 year flood factor' to become a '1 in 10 year factor' by 2100 (House of Commons Science and Technology Committee, 2007). The changes in wave energy levels associated with climate change have an additional importance with regard to sedimentary coasts because they initiate changes to the littoral transport. Beaches are the buffer zone between the turbulent ocean and developed coastal environments and their physical state is determined by the net sediment budget of the system. In respect of the estimated total length of the coastline of England and Wales, this is particularly significant because 30% (1532 km) is comprised of sandy beaches, of which 96% (1475 km) is unprotected (www.geog.plymouth.ac.uk/research/gmasselink/classification.html).

Nearshore sandbanks occur in a wide range of marine environments but in the coastal zone they are particularly important because they interact and modify the characteristics of the local wave and tidally driven current regimes, and thereby exert a physical control on the morphological adjustment and stabilisation of the adjacent coastline (Dyer and Huntley, 1999). Nearshore sandbanks are increasingly being used as a resource, for example for beach nourishment intervention schemes and as aggregates for the construction industry. Around the U.K. in the decade preceding 2004, it was estimated that between 13 and 16 million cubic metres of sand and gravel were mined per year (Hitchcock and Bell, 2004). Studies have revealed that the removal of large volumes of sediment from nearshore features have lead to local increases in the wave energy incident at the shoreline (Byrnes *et al.*, 2004; Maa *et al.*, 2004; Stone *et al.*, 2004). Therefore anthropogenic modification of nearshore accumulations of sediment can also lead to changes in the net sediment budget along a section of coastline hence initiate changes to the evolution of shoreline.

On sedimentary coastlines shoreline change is typically manifest by the erosion and accretion of beaches, therefore their morphodynamic state is considered to be particularly important in relation to the ability of a section of coastline to mitigate the effects of change (Stive, 2004). The shoreline response typically associated with climate change and the mining of nearshore sandbanks as defined earlier is often characterised by erosion. For the U.K. coastline a recent estimate stated that 17% of it is eroding, but in respect of the combined English and Welsh coastlines this figure is significantly higher at 53% due to their large proportion of sandy beaches (Marine Climate Change Impacts Partnership, 2008). This highlights the necessity for better scientific understanding of the physical processes concerned so that these populated and eroding sections of coastline can be properly managed.

Sections of sedimentary coastline in which there are inlets often contain large volumes of sediment in the nearshore beaches and sandbanks and consequently the morphodynamics are particularly complex (Komar, 1996; Mehta, 1996). Our ability to understand these important marine environments is hindered by the lack of thorough understanding of nearshore physical processes. Mehta (1996) stated that this lack of understanding, and specifically in the case of littoral bypassing in the vicinity of inlet entrances, has been a deterrent to the development of global models for the prediction of these phenomena which are of significant importance to the evolution of the adjacent shorelines. Mehta (1996) also concluded that ebb tidal delta and swash platform hydro- and sediment dynamics are poorly understood and should therefore be a high research priority derived from detailed fieldwork and numerical modelling studies. Similarly, the motivation for the Gaudiano and Kana (2001) ebb shoal research was cited as being the fact that relatively little is known about the frequency and magnitude of discrete shoal bypassing events despite their great importance. Evidently, more research is required to improve our knowledge of the physical processes that govern their morphodynamic evolution in order to aid the development of improved approaches to numerical modelling and the predictability of these highly complex marine environments.

In respect of the above the aim of the present study is to contribute to the knowledge of ebb shoal morphodynamics by investigating the Teign inlet on the south Devon coast of the U.K. This is achieved using a multifaceted approach that integrates video remote sensing with in-situ measurements and numerical modelling. The forces that act to on the system and the morphodynamic response are investigated in detail over a range of spatial and temporal scales which are defined in Figure 1.1.

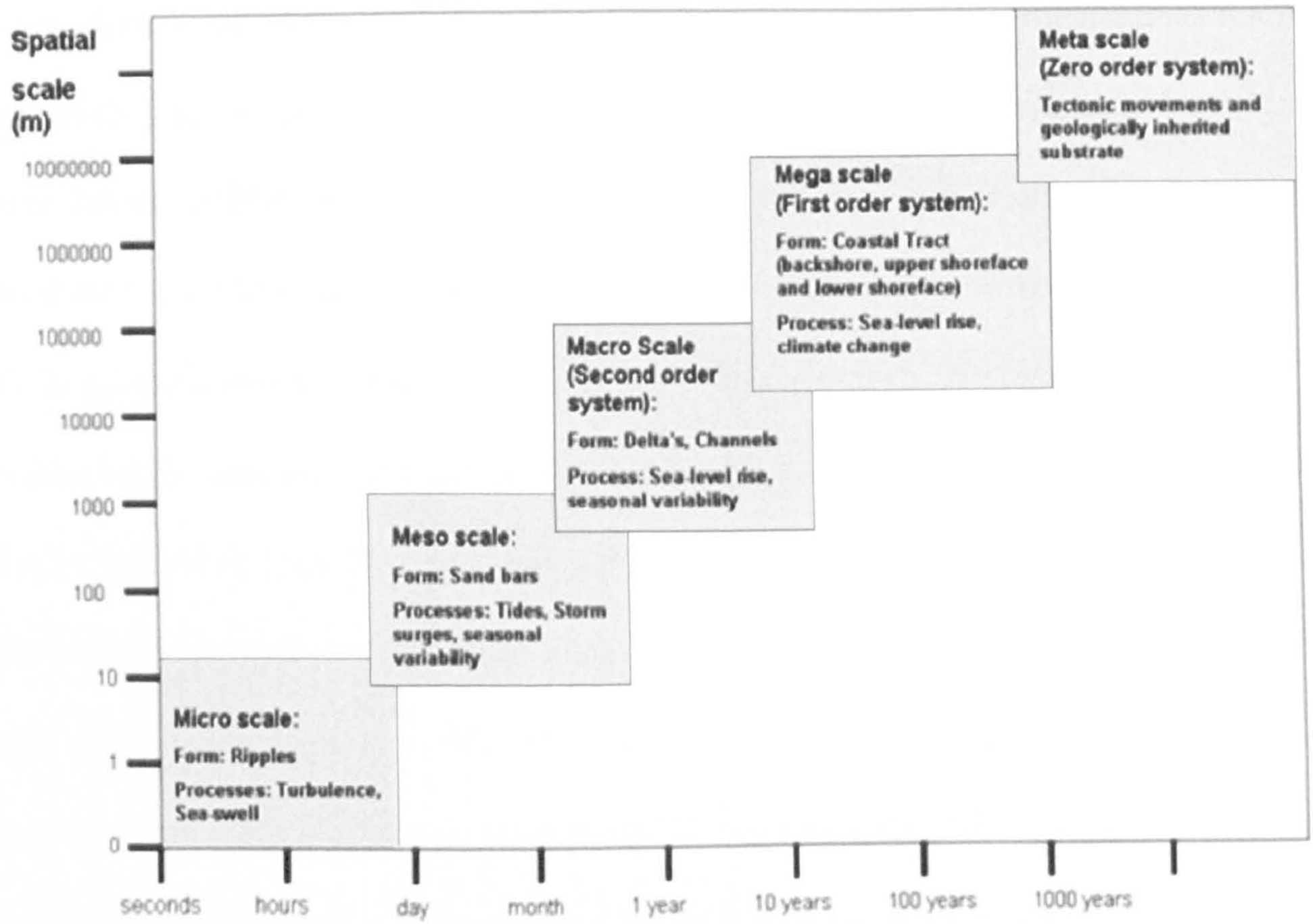

Figure 1.1: Spatial and temporal scales in relation to coastal morphological change, (modified from Cowell *et al.*, 2003).

The smallest scales of interest are the micro scale physical processes associated with the shoaling and breaking of individual waves which occur over time and spatial scales of seconds, and centimetres to meters respectively. Also of interest to the present study are the aggregated effects of the wave and tidally driven processes over a single tidal cycle (micro temporal scale) and over the multiple tidal cycles that comprise the spring-neap variation (micro to meso time scale). These aggregated physical processes alter the morphology of the ebb tidal delta's individual shoals and channels on spatial scales in the range of meters to hundreds of meters (micro to lower macro spatial scales) where the latter are the largest spatial scales of interest to the present study. The largest temporal scales of interest concern the morphodynamic periodicity of individual sandbanks on the ebb tidal delta which occur over years (macro time scale), and of the volume changes to the delta which occur over decades (lower mega time scales).

The present study was funded by the European Union V Framework program (1998-2002), and the Coastview Project (contract no. EVK3-CT-2001-0054). The latter also provided the resources to conduct the fieldwork program. For further detailed information on the project the reader is referred to the project website (http://thecoastviewproject.org).

1.2 Specific objectives

The general aim of gaining a better understanding of the Teign inlet ebb shoal morphodynamics is comprised of the following set of specific objectives:

1. To characterise and quantify the nature of the ebb shoal morphodynamics over short to long term time scales (weeks to years), in which the principle component is the episodic landward migration of large discrete shoals.

2. To determine which physical processes are responsible for the observed behaviour.

3. To determine the relative contributions of the primary hydrodynamic forces due to wave and tidal energy through a tidal cycle (short term).

4. To determine the role of the spring-neap variation in tidal water level on the landward migration of the ebb shoals.

5. To explain the persistent elongate and transversely oriented geometry of the shoals through the course of their landward migration.

In order to achieve the primary objectives, the study focuses on the morphodynamics of individual shoals on the ebb tidal delta from genesis to shore-attachment and their subsequent dissipation.

1.3 Thesis overview

The present study begins in Chapter 2 with a general review of the knowledge concerning inlet sandbank (ebb shoal) morphodynamics. The nomenclature is defined and the hydrodynamics and sedimentation are described over a range of temporal and spatial scales. In this chapter the Teign inlet is also framed in context with the observed trends in geomorphology and energy.

In Chapter 3 there is a general description of the Teign inlet geomorphology and environmental settings in order to provide the reader with the relevant background knowledge concerning the primary factors that determine the nature of the ebb shoal morphology at the location. This is followed by a review of ebb tidal delta morphodynamics utilising a combined photographic archive and scientific research database spanning 35 years of the inlet's development. This provides an invaluable insight in to the inter-decadal morphological evolution.

In Chapter 4 the nature of the landward migration of the sandbanks on the ebb tidal delta is characterised and quantified. This was achieved using a set of descriptive parameters that were derived from a time series of plan view contours of discrete sandbanks. The chapter details the methodology and defines the dataset which were extracted from Argus video images (Holman and Stanley, 2007). During this time the Argus station recorded four individual sequences of the onshore migration of a sandbank on the ebb tidal delta. Their derived parameters are compared and contrasted, in order to identify trends that help to elucidate the physical processes responsible for the observed behaviour.

Chapter 5 concerns the analysis of a unique dataset of co-located, near bed Eulerian measurements that were taken from the surface of a shoal in mid term migration. The fieldwork measurement program was undertaken in order to aid in the determination of the physical hydrodynamic and sediment transport processes responsible for the observed morphodynamic behaviour. The parameters measured were water surface elevation, orthogonal current strength and direction, and suspended sediment concentration. The chapter presents the analyses of the measured parameters in the time and frequency domains.

Chapter 6 is the description and presentation of the numerical modelling experiments undertaken which were twofold. Initially, simplified boundary conditions are used to investigate the combined effect of wave-driven processes and variable water levels (stationary) on the patterns of erosion and accretion on a discrete nearshore sandbank. The variability in the patterns of erosion and deposition is demonstrated to exert an important control on the sandbank's sedimentation through a series of highly idealised or synthetic experiments. In order to determine the effects of the meso to macro tidal current component of the hydrodynamic regime, subsequent numerical simulations were conducted using the in-situ data and measured bathymetry as model boundary conditions. Bed level updating was not incorporated into these experiments so the morphological feedback mechanisms are not included in the analysis.

In Chapter 7, the results of the primary data analyses are synthesised with the secondary data to provide an explanation for the observed persistent onshore migration of the nearshore sandbanks on the Teign inlet ebb tidal delta over a range of spatial and temporal scales. A conceptual model that accounts for the plan form morphological evolution of the migrating sandbanks is proposed.

The final chapter in the thesis (Chapter 8) summarises the principle findings of the study in a formal set of conclusions framed in the context of the specific objectives that were set out in Chapter 1.

2 Literature review

2.1 Basic inlet concepts and nomenclature

The term inlet is often applied to a wide variety of environments and this is illustrated by the following sample definition which relates to the coastal engineering discipline and states that an inlet is:

"A region connecting two or more large bodies of water by a relatively short and narrow channel. The water bodies may be an ocean and lagoon, a large lake and a bay, or a river entering a sea or lake" (Seabergh, 1999).

For the purpose of this review the definition is used to refer to the juncture between the ocean and landward bodies of water at river mouths (estuarine inlets) and barrier island inlets. As with the term inlet, estuary can also be applied to a range of river mouth inlets but in this review the definition is limited to those with enclosed (narrow) entrances, for example due to the growth of a spit as observed at the Teign and adjacent Exe inlets. Estuarine and lagoonal inlets have markedly different physiography of the inland area. River valleys are typically narrow and sinuous inland, and widen toward the mouth, whilst barrier island lagoons are bodies of water separated from the ocean by a relatively narrow, essentially shore-parallel band of land. Hayes (1975) studied the morphology of sand accumulations in inlets in the United States of America (U.S.A.), and despite their diversity, common attributes were found which permitted the definition of a number of key components that constitute the basic tidal inlet system. The model which was based on studies of meso-tidal inlets comprises a main channel with two sedimentary features deposited at each end. These are termed the flood and ebb tidal deltas in the respective landward and seaward distal portions of the channel. Though the basic inlet model was originally derived for lagoonal inlets, it is equally applicable to estuarine inlets that share the same key attributes. The components of the system are described in the following paragraph to familiarise the reader with inlet

nomenclature. However, since this study is an investigation in to the morphodynamics of components of the ebb tidal delta sedimentary system, the flood tidal delta is omitted from further consideration, other than to acknowledge that their presence (e.g. The Salty inside the Teign inlet entrance), represent a potential source or sink for marine sediments to or from the ebb tidal delta respectively. The important influence of the ebb tide currents that propagate through the entrance of inlets on the formation and morphodynamic evolution of ebb tidal deltas is .encapsulated in the name of these sedimentary features. The plan form geometry of the ebb and flood tidal deltas varies considerably in response to the resulting complex three-dimensional flow regime. In some cases, one of these two shoal systems may become well developed whilst the other is entirely absent depending on the nature of sediment exchange between inner and outer regions of the inlet (FitzGerald *et al.*, 2002).

The generic components of an ebb tidal delta are defined schematically in Figure 2.1 where the main channel is incised into a sand (swash) platform that defines the general extent of the sedimentary feature. The seaward extremity of the distal portion of the channel is marked by an accretionary region called the terminal lobe. Secondary channels, often termed flood or spill-over channels link with the main channel and lie between the tidally exposed sandbanks on the sand platform. The sandbanks lying on the sand platform comprise the transversely oriented marginal linear bars which flank the main channel, and the more morphologically irregular sandbanks that form in the region of the terminal lobe (Hayes, 1975, 1980; Hine, 1975; Oertel, 1972). The latter have been termed swash bars (see Figure 2.1) by some authors due to their formation being associated with wave action but since they are morphologically different to the swash bars associated with natural beaches, hereafter they are simply referred to as sandbanks or shoals. The primary sediment transport pathways in Figure 2.1 which are

denoted by the black arrows indicate that the longshore transport is directed toward the inlet entrance and offshore in the main channel where sediment is subsequently transported offshore to the terminal lobe. One of the key components that define inlet sedimentation is whether the reversing currents in the main channel are dominated by those during the ebb or flood tide. The current dominance in the main channel is principally a function of the balance between tidal and fluvial discharges but is also affected by the level of wave energy incident at the entrance (Section 2.2). In the meso-tidal model in Figure 2.1 it is the former that dominate the regime and lead to the well-developed ebb tidal delta depicted in the figure.

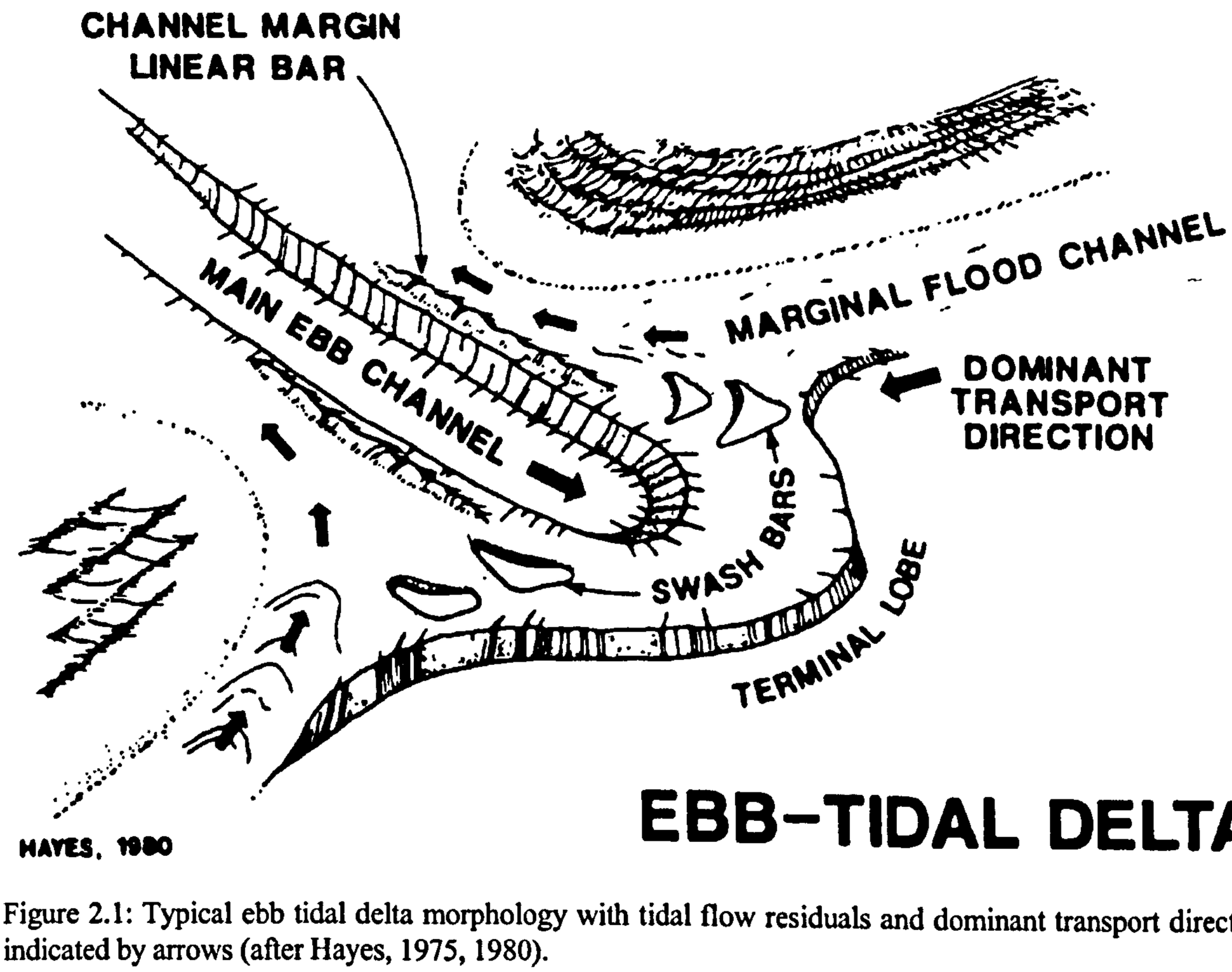

Figure 2.1: Typical ebb tidal delta morphology with tidal flow residuals and dominant transport directions indicated by arrows (after Hayes, 1975, 1980).

Ebb tidal flows dominate the main channel at the Teign inlet and consequently the model defined in Figure 2.1 is broadly representative of the observed morphology in the nearshore region. The primary difference is geomorphological whereby the Ness headland on the southern flank creates an offset configuration of the points of land

forming the inlet entrance. This configuration has resulted in the ebb tidal delta developing an asymmetric plan form in the nearshore region to the north of the channel (Section 3.2). The Teign inlet's ebb tidal delta shares other common attributes with the meso-tidal model shown in Figure 2.1 such as well defined main channel with a marginal linear bar on the northern flank (Spratt Sand), and additional sandbanks (swash bars) that form further offshore. Similarly, the nearshore region adjacent to the inlet is considered to be a sediment convergence zone as in the case of the meso-tidal model and this in evidence by the well developed system of sandbanks around the entrance.

The geometry and distribution of the ebb tidal delta's channel margin linear bars and sandbanks, and their morphodynamic evolution are controlled by a wide range of factors (Section 2.2). Channel margin bars are often relatively static and in a moribund state, whereas the sandbanks that form on the terminal lobe are dynamic. Because the latter transport large volumes of sediment $O(10^3$ to 10^6 $m^3)$ landward they are considered particularly important to the development of the adjacent shorelines (FitzGerald, 1988; Gaudiano and Kana, 2001). It is this type of sandbank that is the subject of the present morphodynamic study, and hence the review focuses on inlet sedimentation in relation to these features. The less important channel margin linear bars are not considered further, but it is acknowledged that these features are also intrinsic to inlet sedimentation as in the case of the flood tidal delta.

2.1.1 Physical characteristics of ebb tidal delta sandbanks

The discrete sandbanks that are observed on the terminal lobe are considered to be formed under the swash action the incident waves (Hayes, 1975; Hine, 1975). The scale, geometry and distribution of the ebb tidal delta and the overlying sedimentary features

is dependent on the supply of sediment, the relationship between incident wave and tidally-driven flow fields, freshet effects and geomorphologic factors such as headland sheltering, inlet throat geometry (FitzGerald, 1988, 1996; FitzGerald *et al.*, 2002; Hayes, 1975, 1980; Hubbard *et al.*, 1979; Hume and Herdendorf, 1990, among others). The most important of these factors are considered to be the geometry of the points of land forming the entrance, and the balance between the wave and tidally driven hydrodynamic forces where the latter can be significantly affected by large fluvial discharges during periods of high rainfall (Fitzgerald *et al.*, 2002). The sandbanks that form on the terminal lobe exhibit diverse plan form geometry and orientation during their evolution in response to the chronology of the forcing. They are considered to have typical elevations in the range 1 to 3 m, major axis length scales of the order of hundreds to thousands of metres, minor axis length scales *O*(50-100 m) (Fitzgerald *et al.*, 2000), and gradients of up to 4–6° with seaward slopes typically 1–2° steeper than landward slopes (Buonaiuto and Kraus 2003).

The diverse morphology and dynamic of these features is encapsulated in the selection of conceptual morphologic models of their evolution after FitzGerald (1988) as shown in Figure 2.4 (Section 2.2.1). The models depict the morphodynamic evolution of the discrete sandbanks associated with three inlet types through their representation in three vertically aligned chronological time steps. Elongate features with a range of orientations from shore-parallel to transverse are in evidence, along with relatively rotund (similar major and minor axis length scales) and arcuate or crescentic features. These can either be inter- or sub-tidal, and may be shore-attached or detached, and they are characterised by relatively steeper landward facing gradients (slip faces) than seaward facing gradients (see Figure 2.5, Section 2.2.1). These inlet models encapsulate the irregular morphology and changes in area of the sandbanks that form on the terminal

lobe through their evolution in response to the forcing chronology, and the geomorphological constraints of the different types of inlet system. Before these are further discussed (Section 2.2.1) the following section provides an overview of the relevant more generally applicable morphologic models of inlet ebb tidal deltas.

2.2 Morphologic models of ebb tidal deltas

Since the 1970's intensive inlet research particularly in the U.S.A. has resulted in the development of many conceptual morphologic models of inlets for example those after Galvin Jr. (1971), Hayes (1975, 1980), Hubbard *et al.* (1979), Oertel (1975, 1977), Sha and Vandenberg (1993), and Hicks and Hume (1996) among others. Two important generic concepts emerge from these models which are that the ebb tidal delta morphodynamics are governed firstly by the geometry or configuration of the land points forming the inlet entrance, and secondly by the hydrodynamic balance between the wave and tidal regimes which in turn control the inlet sedimentation processes. In this section an overview is presented of a selection of the morphologic models that demonstrate the observed variability in respect of these key components of the inlet system.

Galvin Jr. (1971) proposed a classification system for barrier island inlets based on the configuration or geometry of the entrance points which is equally applicable to estuarine inlets in terms of their basic form. The classification comprises four inlet types which are the over-lapping, updrift, downdrift, and negligible offset inlets (left panel, Figure 2.2). The concept is based on a qualitative relationship between morphological development shoreline and the magnitude of net longshore transport (littoral drift). In the figure the magnitude is depicted by the balance between the opposing transport components Q_{Rt} and Q_{Lt} which are directed toward the right and left respectively.

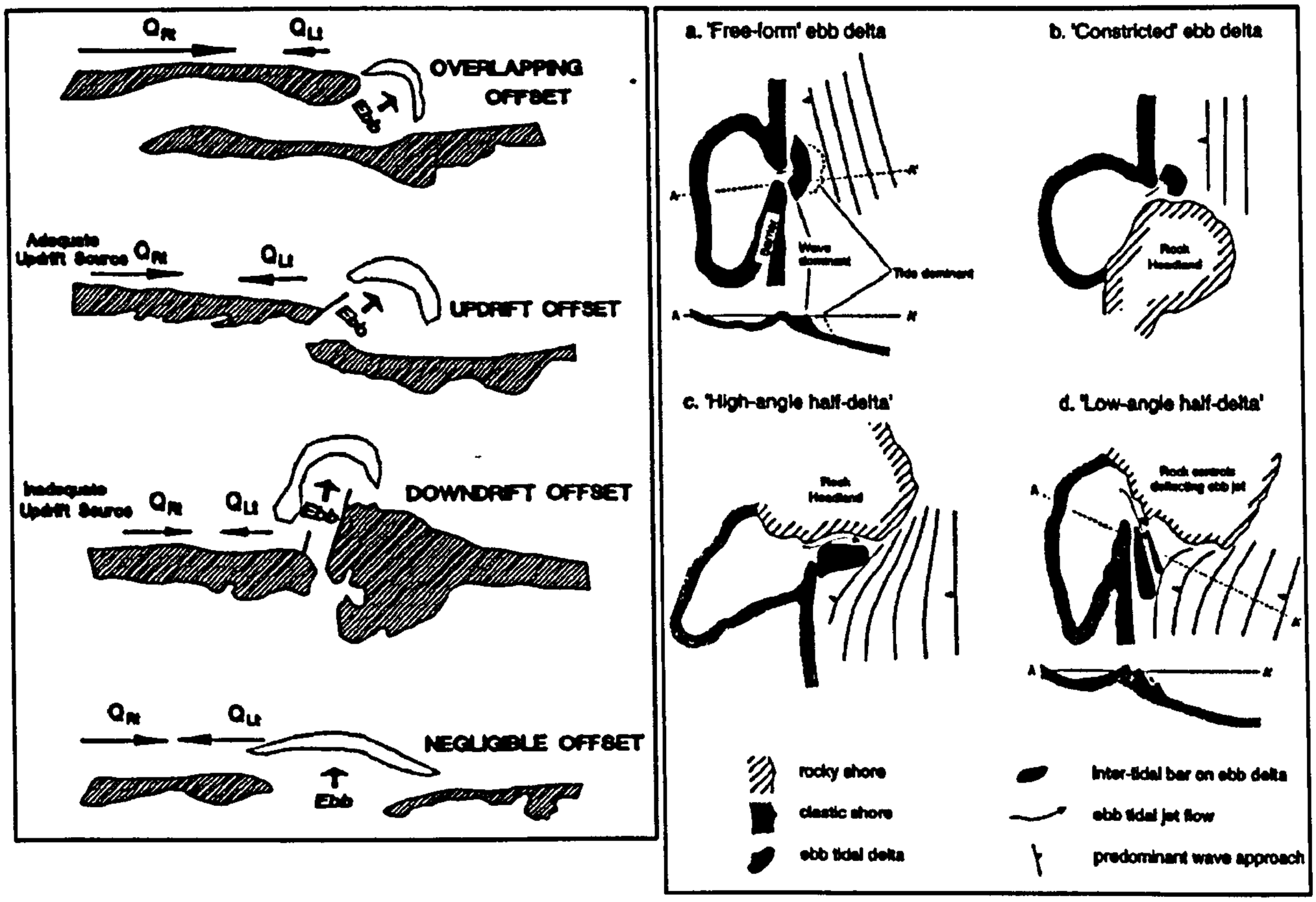

Figure 2.2: Morphologic inlet models of barrier island inlets (left panel) after Galvin (1971), and estuarine inlets (right panel) (after Hicks and Hume, 1996).

The inlet types form a continuum in terms of the net longshore transport (toward the right of the figure) where the largest is associated with the overlapping offset and this decreases to approximately zero net transport in the negligible offset inlet type. Coasts with high net longshore transport rates, such as in the overlapping and updrift offset inlets cases, are typically wave-dominated and high sediment supply to the updrift shoreline enables it to accrete (seaward growth). In the downdrift offset case, sediment supply due to the net longshore transport is comparatively small and the wave refraction and sheltering effects of the well-developed asymmetric ebb tidal delta on the downdrift shoreline are considered to be the key processes in the formation of this type of offset (Douglass, 1991; Hayes *et al.*, 1970). In the negligible offset inlet, the net longshore transport is close to zero and there is no preferential accretion or erosion on either shoreline but in contrast to the other inlet types, the ebb tidal delta is relatively symmetrically-distributed about the entrance.

Inlets occur in a wide range of settings and consequently it has long been recognised that some have positional stability whilst others have been observed to be more transient (Escoffier, 1940). Galvin Jr. (1971) proposed a classification for inlet positional stability in which there are three classes: the primary, secondary and temporary types. The first two represent stationary and migratory (transient) inlets entrances and the third type represent ephemeral inlets caused for example, by the storm-induced breach of a barrier island. Examples of the primary type which are positionally stable include estuarine inlets on rocky coasts such as the Teign inlet where the stability is derived from the stratigraphy. The secondary and temporary types are typically found on sandy barrier island coasts for example on the southeast Atlantic coast of the U.S.A., which are prone to morphological change due to the channel bank composition not being resistant to the erosive hydrodynamic processes (FitzGerald, 1988). Secondary inlet entrances that migrate tend to do so in the direction of dominant littoral drift, these changes and those associated with the temporary type occur on time scales from the frequency of individual storm events (seasonal) to hundreds of years (Van Rijn, 1998).

Hicks and Hume (1996) classified the natural (estuarine) inlets of the rocky pocket-bay east coast of North Island, New Zealand based on ebb tidal delta shape which are often laterally constrained by the presence of rock outcrops. Four inlet types were proposed which are the free form, constricted, high angle half delta, and low angle half delta types (right panel, Figure 2.2). The free form type denotes the case where the ebb tidal delta is symmetrically distributed about the main channel, and where the major axis is alongshore oriented due to high littoral drift conditions for example on exposed coasts. The remaining three types have markedly different ebb tidal delta geometry but are geomorphologically similar due to the offset imposed by the presence of rock outcrops. The constricted type is where the relationship between the incident wave conditions and

the effects of the offset permit only negligible growth of the ebb tidal delta in both the alongshore and cross-shore dimensions. In the case of the low angle half delta inlet type the underlying geology forces the channel to be aligned with a small angle relative to the shoreline and consequently sediment is deposited on the sheltered shoreward flank in elongate shore-parallel deposits. Alternatively, in the high angle half delta case the channel is positioned against the rock outcrop causing its transverse orientation and the growth of the ebb tidal delta offshore on the opposing side; wave sheltering and refraction effects of the rock outcrop and ebb tidal delta are considered important. These characteristics most closely resemble the Teign inlet configuration in that it is a rock bound estuarine inlet due to the presence of the Ness headland that has an elongate and relatively static channel margin bar (Spratt Sand) (Figure 3.2).

Oertel (1975, 1977) classified inlets on the coast of Georgia, South East, U.S.A. based on the geometry of the ebb tidal delta as determined by the balance of longshore currents due to waves and the transverse tidal currents in the main channel. The concept concerns inlets of the negligible offset configuration after Galvin Jr. (1971) and four types are proposed which are shown in the left panel of Figure 2.3 in which the black arrows indicate the relative forces due to the orthogonal current components. In Type A inlets the longshore currents predominate and the offshore directed current in the main channel is relatively weak whilst the opposite occurs in Type D inlets. The resulting ebb tidal deltas reflect the relative strengths of the main channel currents where in the Type A inlet the channel is shorter and terminated by a well-developed terminal lobe on account of the offshore directed channel currents being comparatively weak. However, in the Type D inlet the stronger reversing currents cause the channel to extend further offshore and the terminal lobe to be less well developed. The Type D inlet main channel

currents are also responsible for the formation of channel margin bars and for deposits of sediment in the inlet entrance.

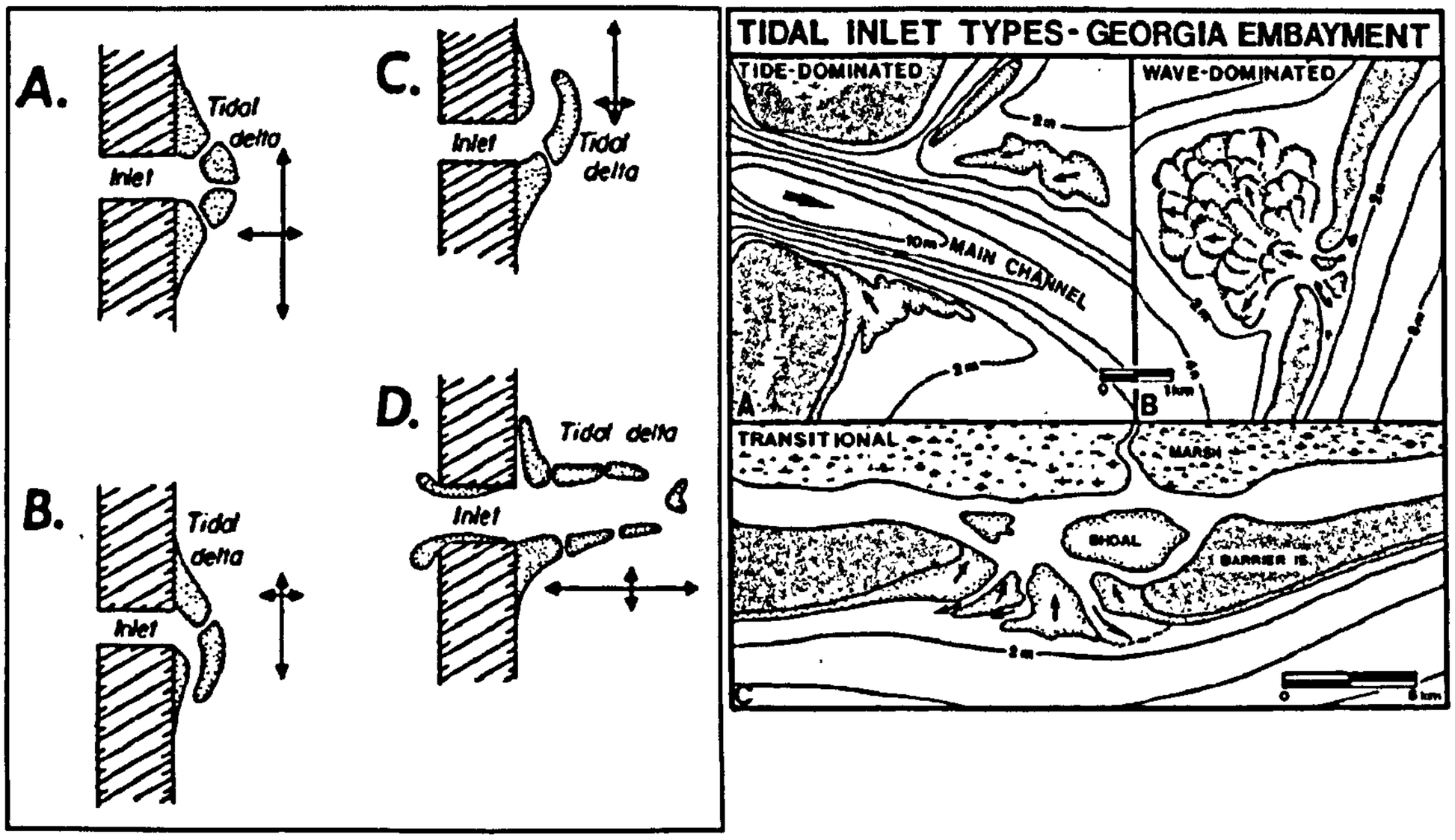

Figure 2.3: Morphologic models of barrier island inlet ebb tidal delta geometry, Georgia, southeast USA, left panel after Oertel (1975), and right panel after Hubbard *et al.* (1979).

The Teign inlet is considered to approximate to an offset variation of the Type D inlet since it is defined by the principle Type D inlet attributes such as strong ebb tide channel currents and marginal bars. Oertel (1975) also describes the bars as having gently sloping offshore facing slopes and steep shoreward facing slip faces which is also a characteristic of the dynamic Teign inlet sandbanks that are the focus of the present study (Figure 4.6). The principle difference of the Teign inlet from the Type D inlet being that the former has an asymmetric ebb tidal delta on account of it being rock bound to the south by the Ness headland. The remaining two inlet types concern variations of the Type A inlet where one or other of the longshore currents dominates the nearshore leading to asymmetric ebb tidal delta growth in the downdrift direction.

Hubbard *et al.* (1979) also classified Georgia inlet ebb tidal deltas on the basis of the morphology and distribution of the shoals which in this model is considered to be

primarily a function of the hydrodynamic balance between wave and tidal energy. The model is based on the concept that deposition in the vicinity of inlet entrances occurs in regions where the two current regimes are in approximate equilibrium and defines three inlet types which are the wave-dominated, tide-dominated and transitional types (right panel, Figure 2.3). In the case of the wave-dominated inlets, sediment is pushed through entrance as the onshore wave driven current component exceeds the ebb tide dominance in the main channel which typically occurs in micro-tidal settings. Consequently the ebb tidal delta is poorly developed or absent, but in transitional inlets which tend to have the widest entrances, sediment is deposited in close proximity to the entrance under the influence of approximately equal wave driven and tidal forces. The tide-dominated inlet resembles the basic inlet model defined by Hayes (1975, 1980), and described in Section 2.1 in which the primary components comprise the main channel, channel marginal bars and the terminal lobe at the distal end of the channel. These inlets typically occur where conditions are meso tidal or larger allowing the reversing currents in the narrow and deep main channel to develop jet-like flow conditions during peak ebb tide (flow acceleration). Conversely on the flood tide the inlet entrance hydraulics more closely resemble funnel conditions (flow deceleration) hence there is a tendency for there to be complex flow asymmetry over the tidal cycle and particularly in the main channel. Flow asymmetry can be manifest in terms of the relationship between the times of peak flow rates and high or low tide, in the magnitude of the ebb and flood tide current maxima, and in the duration of the flood and ebb tides (Hayes, 1980; Walton, 2002). The tide-dominated inlets defined in this model are also distinguished by the presence of landward oriented sandbanks on the ebb tidal delta and this factor along with those previously cited, strongly reflects the nature of the Teign inlet ebb tidal delta system though the offset entrance configuration means that the shoal system has developed only on one side of the main channel.

The presence of a well-developed ebb tidal delta in tide-dominated inlets is due to the ebb dominance of the flow regime in the main channel under typical hydrodynamic conditions. However, with the exception of sheltered coasts, superposed on the tidal current effects are those due to waves which further complicate the hydrodynamic regime by assisting and opposing the flood and ebb tide currents respectively. The importance of the wave-driven component is also evident in the morphodynamic response of the individual landward migrating sandbanks which initiate significant shoreline changes upon attachment. Sediment involved in this process has often been transported to the updrift side of the inlet entrance by the prevailing longshore transport and then bypassed around the inlet entrance. This important process in natural inlet morphodynamics is term sediment bypassing and this is defined and discussed in the flowing section.

2.2.1 Natural sediment bypassing at inlet entrances

The basic inlet sediment bypassing concept is that sediment supplied to the updrift side of an inlet is transported to the downdrift side by involvement of the channel and ebb tidal delta (FitzGerald *et al.*, 2000). The models shown in Figure 2.4 are part of a set of nine morphologic bypassing models defined in the United States Army Corps of Engineers (U.S.A.C.E.) technical report on natural inlet bypassing mechanisms by FitzGerald *et al.* (2000). The models are based on the work of Bruun and Gerritsen (1959) and FitzGerald (1982, 1988) among others and depict inlet evolution in terms of the growth and migration of the sandbanks that form on the terminal lobe and the development of the main channel which may change position or orientation in response changing hydraulics. The temporal evolution of the sandbanks is depicted in relation to typical tide dominated inlet conditions as opposed to those due to extreme events such as storm surges that can overwhelm the ebb dominated main channel flow regime and

significantly alter the natural sedimentation processes (FitzGerald *et al.,* 2000). In order to be concise the following review of bypassing models is limited to three types which are the most morphologically similar to the Teign inlet. These are the stable inlet (model 1), the ebb tidal delta breaching inlet (model 3), and the outer channel shifting inlet (model 4) as shown in Figure 2.4. The principle attributes that the Teign inlet ebb tidal delta shares with these three models are the landward migrating sandbanks that form at the distal margins of the main channel and the migration of the channel under changing hydraulics. The inlet types omitted are those in which the morphological evolution is related to the breaching or migration of entrance spits, wave dominance or human intervention (e.g. construction of entrance jetties). Whilst the Teign inlet entrance is enclosed by the Denn spit, the feature is not subject to significant morphological change or prone to breaching as in the case of the spit related models. Therefore, other than to enclose the Teign inlet entrance the Denn spit is not considered have a primary role in the morphodynamics of the sandbanks on the ebb tidal delta over the time scales of interest (Section 1.1).

One of the most important aspects of the morphodynamic evolution of these inlets is the formation and landward migration of large coalescing sandbank complexes. A primary cause of the release of the sandbanks from the outer margin of the ebb tidal delta (terminal lobe) is considered to be the realignment of the main channel (Gaudiano and Kana, 2001), though exceptions to this do occur (model 1, Figure 2.4). The subsequent landward migration of the sandbanks is considered to be caused by landward directed currents over the features due to the action of wave swash hence the term swash bars as used by some authors (Borrelli and Watts, 2003; Hayes, 1975; Hine, 1975; Robin *et al.*, 2007).

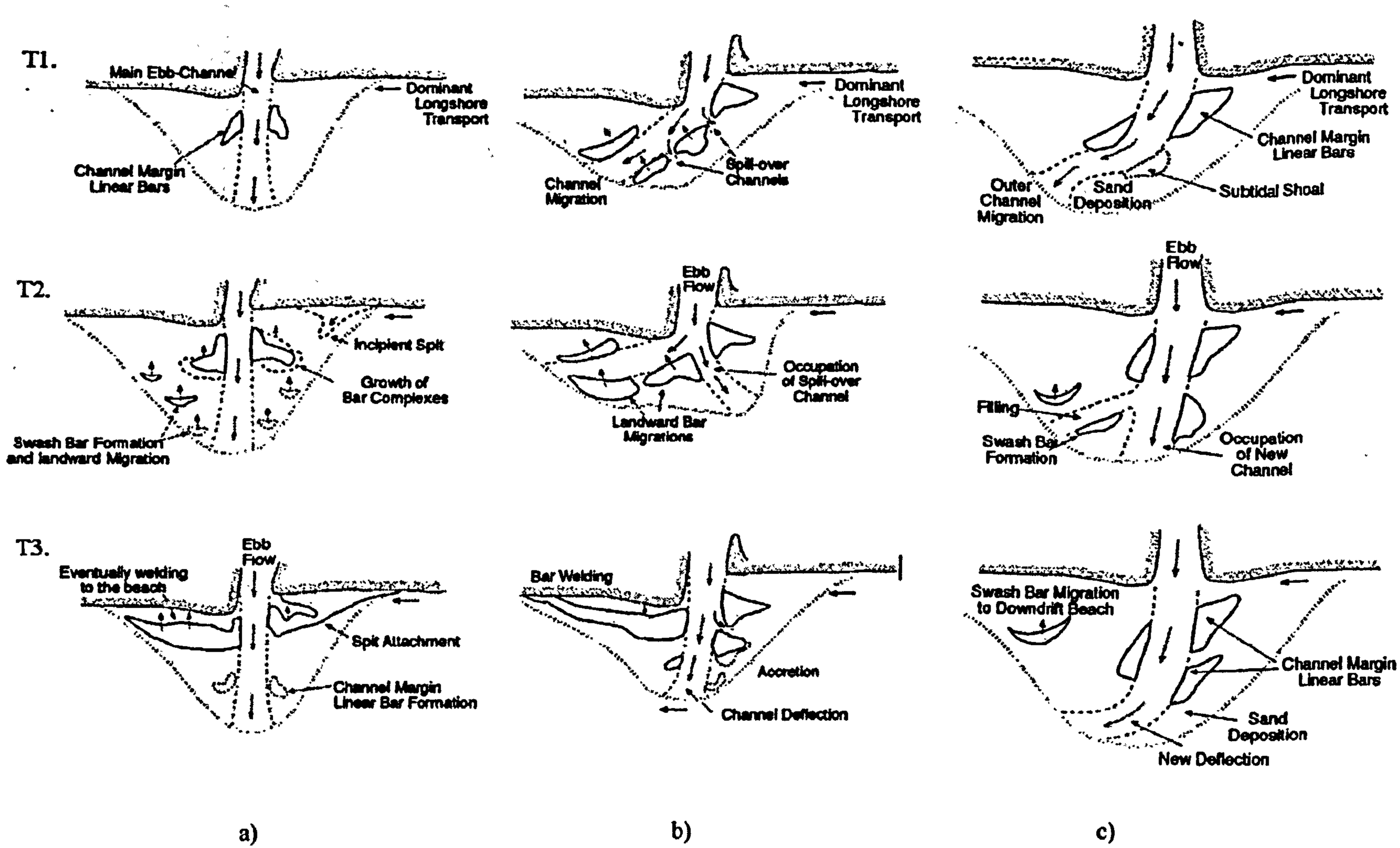

Figure 2.4: Examples of conceptual models of inlet ebb shoal evolution from the United States Army Corps of Engineers: a) stable inlet processes (model 1), b) ebb tidal delta breaching (model 3), and c) outer channel shifting (model 4). T1 to T3 denote time chronology (after FitzGerald *et al.*, 2000).

The coalescence of sandbanks is also hypothesised to be caused by the features decelerating with their progression up the shore face under decreasing exposure to the hydrodynamic sediment transport processes (FitzGerald, 1988). This is depicted in Figure 2.5 which illustrates the difference in exposure for a landward migrating sandbank of a constant elevation. As a consequence of the increasing subaerial exposure the outer bars are considered to have higher migration rates than inner bars for a given wave energy level.

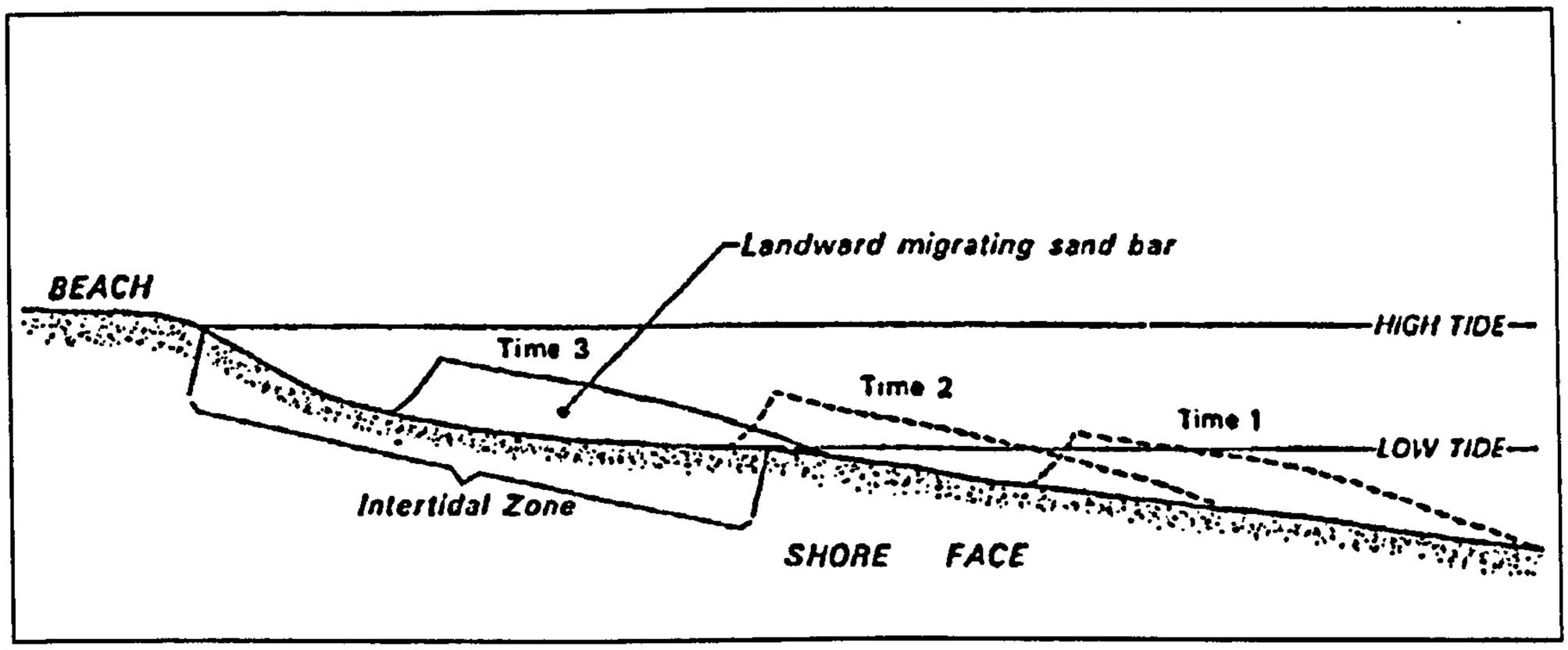

Figure 2.5: Conceptual profile model of onshore sandbank migration on the ebb tidal delta (after FitzGerald, 1988).

Prior to shore-attachment, the sheltering effects of a migrating sandbank may initiate a temporary reversal of the prevailing longshore current direction on the adjacent shoreline and at such times sediment is typically transported toward the inlet entrance leading to the temporary recirculation of sediment around the entrance as opposed to it being transported farther down the coast and out of the inlet sedimentation system. Upon shore-attachment, the migratory sandbanks release large volumes of sediment to the downdrift shoreline providing a natural form of beach nourishment which typically recurs over a 4 to 10 year period. The process is usually shorter for smaller inlets which have smaller ebb tidal deltas (Walton Jr and Adams, 1976), therefore smaller volume bypassing sandbanks. These are formed closer to the shoreline due to the smaller ebb

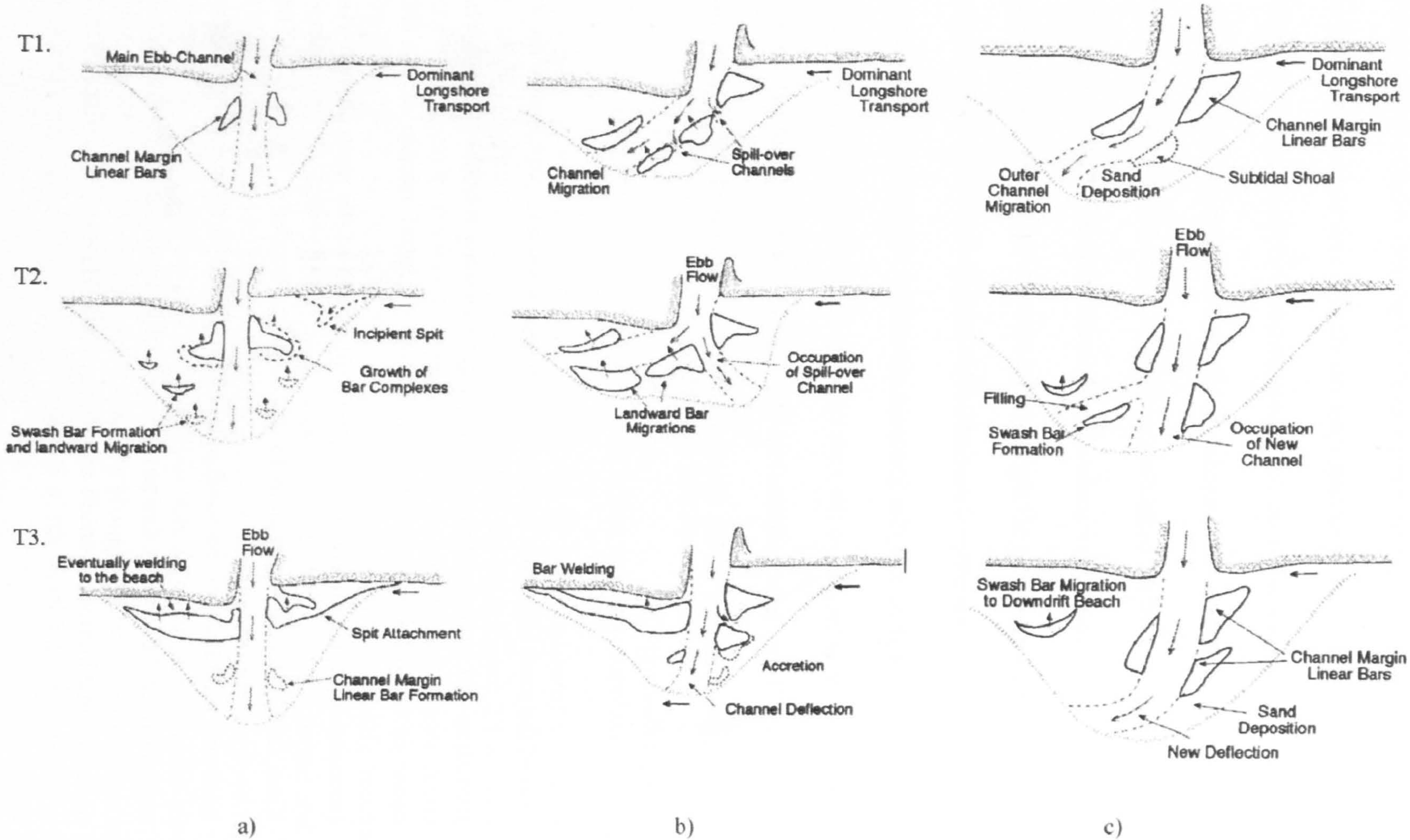

Figure 2.4: Examples of conceptual models of inlet ebb shoal evolution from the United States Army Corps of Engineers: a) stable inlet processes (model 1), b) ebb tidal delta breaching (model 3), and c) outer channel shifting (model 4). T1 to T3 denote time chronology (after FitzGerald *et al.,* 2000).

The coalescence of sandbanks is also hypothesised to be caused by the features decelerating with their progression up the shore face under decreasing exposure to the hydrodynamic sediment transport processes (FitzGerald, 1988). This is depicted in Figure 2.5 which illustrates the difference in exposure for a landward migrating sandbank of a constant elevation. As a consequence of the increasing subaerial exposure the outer bars are considered to have higher migration rates than inner bars for a given wave energy level.

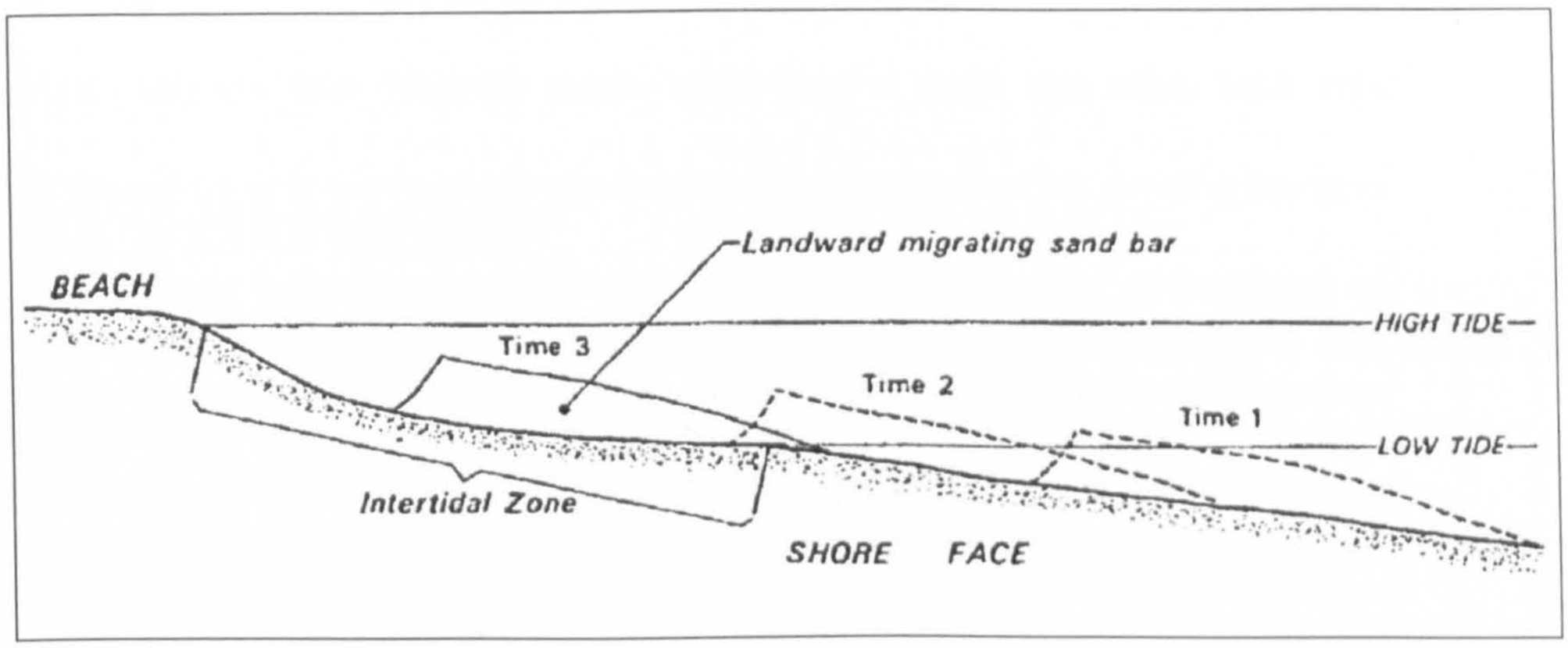

Figure 2.5: Conceptual profile model of onshore sandbank migration on the ebb tidal delta (after FitzGerald, 1988).

Prior to shore-attachment, the sheltering effects of a migrating sandbank may initiate a temporary reversal of the prevailing longshore current direction on the adjacent shoreline and at such times sediment is typically transported toward the inlet entrance leading to the temporary recirculation of sediment around the entrance as opposed to it being transported farther down the coast and out of the inlet sedimentation system. Upon shore-attachment, the migratory sandbanks release large volumes of sediment to the downdrift shoreline providing a natural form of beach nourishment which typically recurs over a 4 to 10 year period. The process is usually shorter for smaller inlets which have smaller ebb tidal deltas (Walton Jr and Adams, 1976), therefore smaller volume bypassing sandbanks. These are formed closer to the shoreline due to the smaller ebb

tidal delta thereby providing less time for coalescence and migration to occur before shore-attachment and dissipation (FitzGerald, 1988; FitzGerald *et al.*, 2000).

Ebb tidal delta breaching inlets (Figure 2.4b) also have stable entrances but the main channel cyclically undergoes a gradual rotation toward the downdrift shoreline under the preferential deposition of sediment on the updrift side of the ebb tidal delta. The increasing deflection of the main channel which can become acute, causes increasingly inefficient hydraulics until conditions eventually allow the flow regime to breach the ebb tidal delta and form a new more direct channel with similar alignment to the original prior to deflection. Breaching typically occurs over 6 to 12 month time scales or in response to individual storms and once this has occurred, the abandoned channel undergoes a natural process of infilling. These inlets also experience the same sandbank morphodynamics as in the case of stable inlets but may involve larger volumes of sediment and this bypassing process is estimated to repeat over similar intervals as those in the stable inlet type (5 to 10 years). Outer channel shifting (Figure 2.4c) involves the same process as ebb tidal delta breaching but on a smaller scale since it only concerns the outer or distal portion of the channel. The smaller scale of this type of bypassing is therefore associated with smaller volumes of sediment in the bypassing sandbanks than in the previous types.

Outer channel shifting was observed to occur at the Teign inlet during the decade following 1964 (Robinson, 1975) and from the photographic archive used in the present study that spans a period of 35 years, this is commonly observed until *c.*1995. From the post mid 1990's to the present time, the main channel appears to have greater positional stability hence the Teign inlet may be better represented by the stable bypassing model over this period. The morphodynamics of the individual sandbanks on the Teign inlet's

ebb tidal delta over the 35 year period encapsulated by the photographic archive are fully described in the next chapter. Due to the occurrence of bypassing being observed repeatedly at some inlets, such events are frequently referred to as cyclic which implies that they are periodic (Bruun and Gerritsen, 1959; Cheung *et al.*, 2007; Israel and Dunsbergen, 1999; Robinson, 1975; Sha, 1989, among others). However, in practice the timing and duration of consecutive events have often been found to vary hence bypassing phenomena are also termed episodic in the literature in recognition of this variability (Gaudiano and Kana, 2001; Kana *et al.*, 1999).

2.3 Empirical relationships

The intensive research into the morphodynamic evolution of inlets has led to the formulation of many empirical equations that relate the tidal prism to the cross-sectional area of the inlet entrance (e.g. O'Brien, 1931, 1969; Jarrett, 1976), or to the volume of sediment stored in the ebb tidal deltas and shoals (e.g. Gaudiano and Kana, 2001; Hicks and Hume, 1996; Marino and Mehta, 1987; Walton Jr and Adams, 1976). These relationships are based on the principle that the inlet entrance dimensions or ebb tidal delta volume oscillate about an equilibrium value in response to long term changes (years to decades) to the prevailing conditions of sedimentation. The tidal prism-entrance area relationships suggest that there is a dynamic equilibrium between the supply of sediment via longshore (littoral) transport which tends to close the inlet entrance and the flow rate which opposes the closure due to higher current velocities as the entrance becomes more constrained (O'Brien, 1969; Van Rijn, 1998). Townend (2005) collated data for 153 estuaries from around the U.K. mainland in order to examine them in context with these empirical relationships for inlets in other countries. Despite uncertainties in the dataset Townend (2005) was able to demonstrate that the U.K.'s estuaries including the Teign inlet exhibit similar trends in the tidal prism versus

cross-sectional area data as observed in the Holland, New Zealand and the U.S.A. The study found that the data formed two sub-groups which were determined by their geomorphology. These sub-groups were broadly defined as either unfilled geological basins or those that have been filled with sediment during the Holocene period.

The empirical tidal prism-volume relationships are based on a similar principle in which changes to the tidal prism effect changes to the flow rate in the channel that define the general morphology of the ebb tidal delta hence volume. Large inlets are associated with larger ebb tidal delta volumes and *vice versa.* Walton and Adams Jr. (1976) utilised a 'wave energy factor' to determine the effect of varying wave energy levels and found that larger volumes of sediment are stored in ebb tidal deltas of low wave energy coasts when compared with high energy coasts. This was considered to be caused by larger volumes of sediment being driven landward and returned to the adjacent shorelines, or being transported through the inlet entrance under higher wave energy conditions. Hicks and Hume (1996) also found that ebb tidal delta volume was a primary function of the tidal prism and further suggested that the angle between the main channel and the shoreline was an additional contributing factor. The channel angle affected the efficacy of the offshore directed ebb tidal currents to oppose the onshore directed currents due to waves hence smaller ebb tidal deltas were observed at inlets with acute channel angles.

The majority of the studies of inlet morphodynamics are focussed on macro scale temporal and spatial changes to ebb tidal deltas whereas there are comparatively few studies concerning the meso-scale features such as the discrete sandbanks that overly the ebb tidal delta. In order to begin to address this gap in the research Kana (1995) and Gaudiano and Kana (2001) studied sand bypassing at inlets on the southeast coast of the

U.S.A. In the latter study data were collated data from nine inlets in which they found that trends in the volume of individual bypassing sandbanks and the average bypassing interval were empirically related to the tidal prism (Figure 2.6). This is intuitive given the apparent control that the tidal prism has on the size of the ebb tidal delta as summarised in the preceding paragraph. Smaller inlets typically have smaller volume ebb tidal deltas therefore smaller bypassing sandbanks. As a consequence of their smaller scale it was concluded that the average bypassing interval of smaller inlets also tends to be shorter than at larger ones because the cross-shore distance to traverse is shorter plus there is a smaller mass of sediment to be transferred. However Gaudiano and Kana's theory may not be universally applicable as when Burningham and French (2006) compared the bypassing interval of the meso-tidal gravel rich Deben estuary on the southeast coast of the U.K. with the Gaudiano and Kana (2001) data, they found that the estuary was an outlier due to the mega time scale of its cyclic morphodynamic behaviour (Figure 2.6). The long duration of the bypassing interval was attributed to reduced sediment transport efficiency due to the coarse-grained nature of the sediment which is predominantly in the sand-gravel fraction.

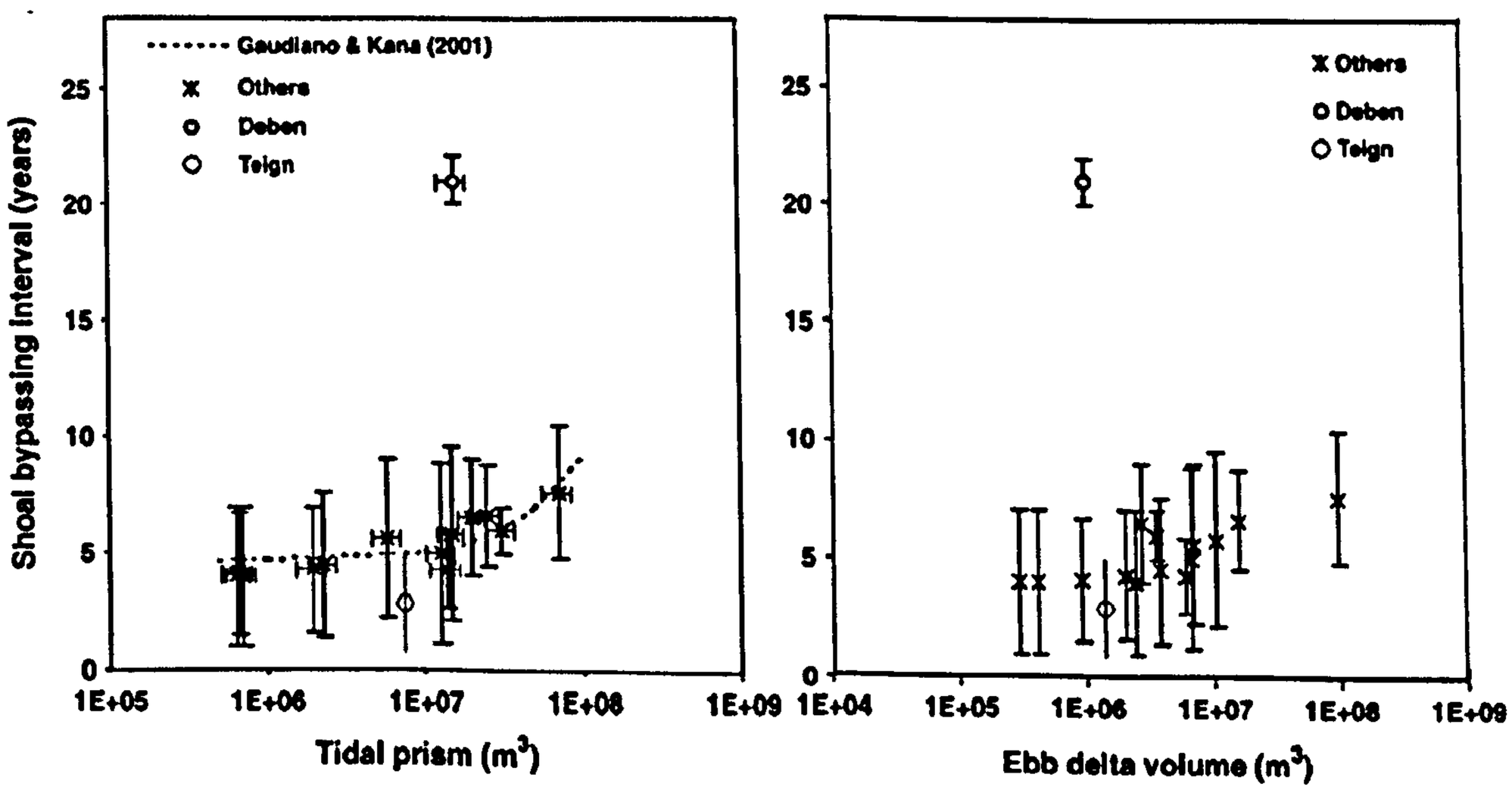

Figure 2.6: Inlet shoal bypassing interval in the context of inlet tidal prism (left panel) and ebb tidal delta volume (right panel) after Gaudiano and Kana (2001) (modified from Burningham and French, 2006).

The periodicity of the morphological change at the Teign inlet has been estimated at between 1 and 5 years (Kingston 2005; Robinson, 1975; Siegle 2003) and the mean tidal prism at 7.8 x 10^6 m^3 after Bernardes (2005). The average inter-tidal volume of the nearshore region from Kingston *et al.* (2005) has been used as a rough approximation of the ebb tidal delta volume and is estimated at 1.4 x 10^6 m^3. These data have been used to plot the Teign inlet with the Gaudiano and Kana (2001) data in Figure 2.6 from which it can be seen that the Teign inlet broadly fits within the error bars of both datasets. However, it is only during times when the morphological periodicity is in the 4 to 5 year range that the inlet best fits the trends.

The empirical tidal prism-area equations proposed by numerous authors have been collated and analysed by Van Rijn (1998) in which there appears to be considerable variation in the coefficients ($O(10^4)$ for area-prism relationships); the variability of the exponents ($O(10^1)$) is also not insignificant whilst the results of Walton Jr. and Adams (1976). The results of Townend (2005) and Gaudiano and Kana (2001) were also subject to scatter, and the Burningham and French (2005) study highlighted the inability of the bypassing interval relationship to account for the Deben estuary. Some authors cite variable levels of human intervention (e.g. stabilisation structures) and data continuity issues as potential causes of the scatter (O'Brien, 1969; Gaudiano and Kana, 2001; Townend, 2005). FitzGerald (1996) suggested that the uncertainty in these empirical relations may be partly attributable to the temporal variability induced by natural inlet cycles which is unaccounted for in the relationships. The fact that there is uncertainty in these relationships reflects the complexity of the physical processes and highlight the need for more detailed research particularly with regard to the dynamic bypassing sandbanks. The present study compliments the work of Gaudiano and Kana (2001) and makes an important contribution to the research concerning inlet bypassing.

The study characterises and quantifies inlet bypassing over meso time scales (weeks) and identifies trends over macro (years) time scales which is rarely undertaken in the research. Some authors have also highlighted the fact there are few studies concerning inlets with large tidal ranges (i.e. macro- and mega-tidal) (Robin *et al.,* 2007), or that there are few concerning inlets with coarse-grained sediment (Burningham and French, 2006), and that there a few that utilise in-situ measurements (Vinther *et al.,* 2005). The spring tidal cycle of the Teign inlet is in the macro-tidal category during spring tides (Section 3.2), the ebb shoals are comprised of sediment in the coarse to very coarse fraction (Section 3.3), and the study utilises a unique set of in-situ measurements obtained from the surface a dynamic shoal in mid term migration (Chapter 5) hence the present study helps to address these other gaps in the research concerning the morphodynamic behaviour of inlets.

In the following chapter the characteristics of the study site are defined in terms of its geomorphology, hydrodynamics and sedimentation. The research concerning the Teign inlet ebb tidal delta morphodynamics is discussed in the final section (Section 3.4) and the manner in which this work moves the research forward is summarised at the end of the section.

3 Introduction to the Teign inlet

3.1 Physical setting

The Teign inlet is situated at Teignmouth on the South Devon coast which lies in an approximately central location of the broad semi-circular shaped Lyme Bay that faces southeast into the English Channel (left panel, Figure 3.1). The coastline of Lyme Bay stretches 80 km from Portland Bill in the northeast to Start Point in the south. To the south of the Teign inlet the coast becomes less exposed than it is to the north owing to a succession of small headland confined bays. The Lyme Bay coastline in the vicinity of the Teign inlet is dominated by cliffs of widely differing composition with few beaches present. Where beaches do occur they are small and comprised largely of coarse clastic grains eroded from the New Red Sandstone breccias, which causes their distinct red hue.

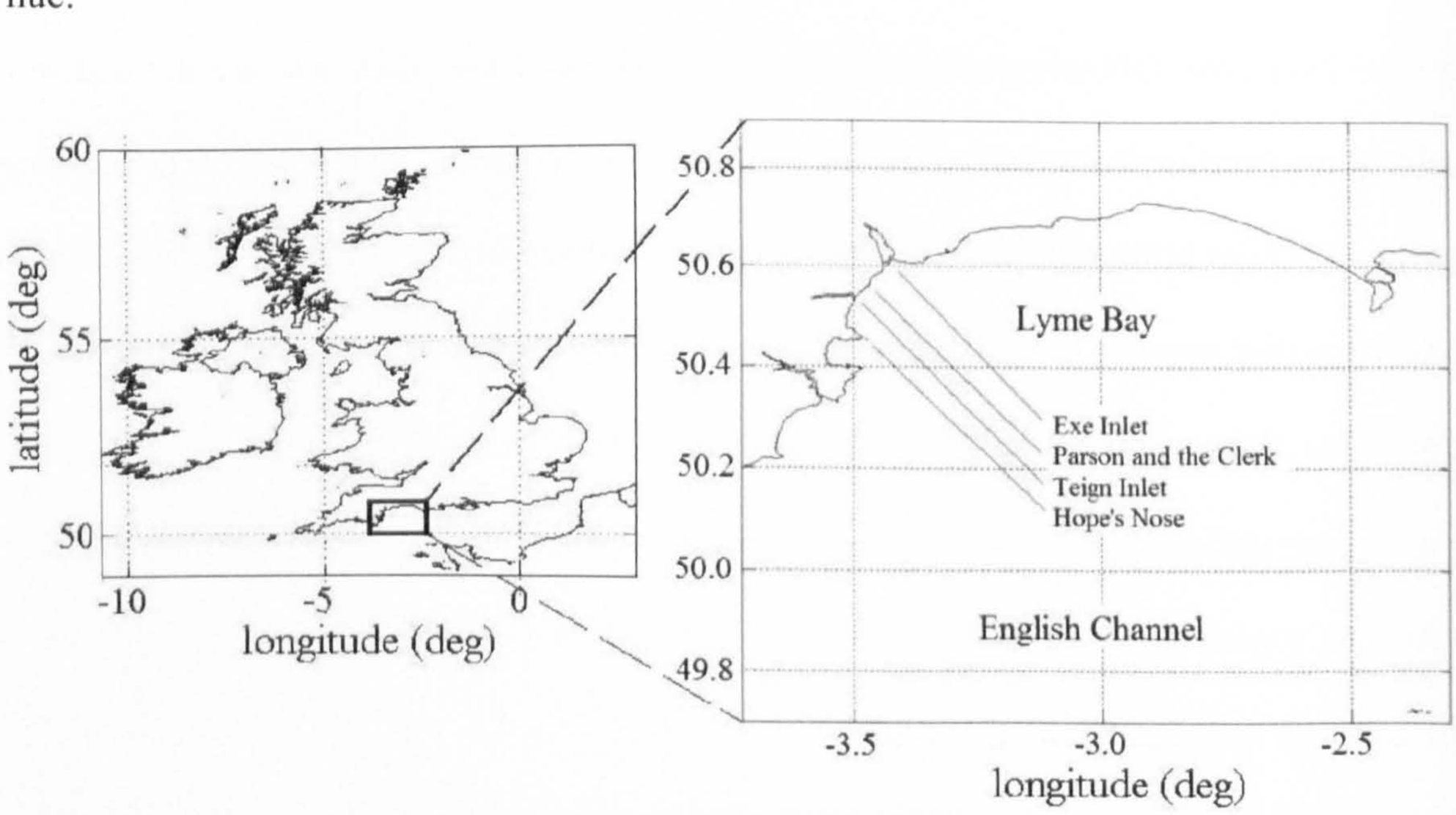

Figure 3.1: Location of the Teign inlet, U.K. (left panel) and Lyme Bay (right panel) coastlines. (Vertical datum: shoreline at mean high water, data source: NOAA Geophysical Data Centre (http://rimmer.ngdc.noaa.gov/mgg/coast/getcoast.html).

At a distance of approximately 10 km to the north of Teignmouth the cliffs are interrupted by the bar-built or spit-enclosed Exe estuary at Exmouth. The intervening section of coastline is partially segmented by the projecting headland known as The Parson and Clerk whilst the stretch of coastline to south of the Teign estuary is demarcated by the rocky headland known as the Hope's Nose at a distance of approximately 10 km. The orientation of this section of the Lyme Bay coast and the 2 km long beach at Teignmouth face ESE into the English Channel (right panel, Figure 3.1). The bathymetric contours of the bay are predominantly shore-parallel with seabed gradients in the range 0.001 to 0.005 between the depths of -50 to -25 m w.r.t. Chart Datum. However, toward to the west of Portland (longitude $\approx$ -2.4° W, Figure 3.1) and the Teign inlet, the contours are interrupted by localised shoals which reduce depths by as much as 10 m (Nunny, 1995).

The Teign and Exe estuaries were formed through the post-glacial submergence of former river valleys during the early Holocene period which commenced approximately 10,000 years before the present time. The former estuary is small in comparison to the latter and this is reflected in the estimated total area of the Teign estuary which is approximately one fifth that of the Exe estuary at 3.7 km^2 compared with 18.7 km^2 respectively. The inter-tidal area of the Teign inlet represents a large proportion of the total inlet area due to the meso-to macro-tidal regime of the region (Teign inlet inter-tidal area = 2.2 km^2, mean spring tidal range $\approx$ 4.2 m) (Buck, 1997). At lower states of tide, the 7 km long river channel is forced to circumnavigate a series of sharp meanders due to the Salty flood shoal in the outer reaches of the inlet, and the Denn Spit that encloses the entrance. The tidal regime is semi-diurnal (M_2 primary harmonic

constituent) owing to the Channel's link with the Atlantic Ocean, where the tidal wave propagates west to east during the flood and *vice versa* on the ebb tide.

3.2 Environmental conditions

The Teign inlet entrance (Figure 3.2) is situated at the southern end of the main beach at Teignmouth, and the main ebb channel is flanked on its southern side by the Red Sandstone rock outcrop (headland) known locally as the Ness, and on its northern side by a channel margin linear bar known as Spratt Sand. In the outer estuary there is a small commercial port which necessitates the daily drag-dredging (flattening) of the terminal lobe so that vessels may navigate safely to the deeper section of the channel on the landward side. This activity has only been partly successful in achieving its objective as evidenced by the occasional grounding incidents which persist to the present time, for example five incidents were recorded between 1999 and 2002 (ABP Marine Environmental Research 2002, hereafter ABP MER). The inlet's terminal lobe which is responsible for the navigation difficulties is clearly depicted in the lower panel of Figure 3.2 by the white line of foam caused by wave breaking along its margin. Along with revealing the form of the terminal lobe, the images in Figure 3.2 also show two examples of the migratory sandbank in its shore-attached mode (upper right and lower panels), and this is a common plan form of the feature at this stage of its evolution as observed during the last decade, but which is observed less frequently in the period between 1964 and the mid 1990's. In addition to the commercial use of the port in the outer estuary, Teignmouth is a popular summer tourist venue which imposes a seasonal recreational demand on the inlet environment.

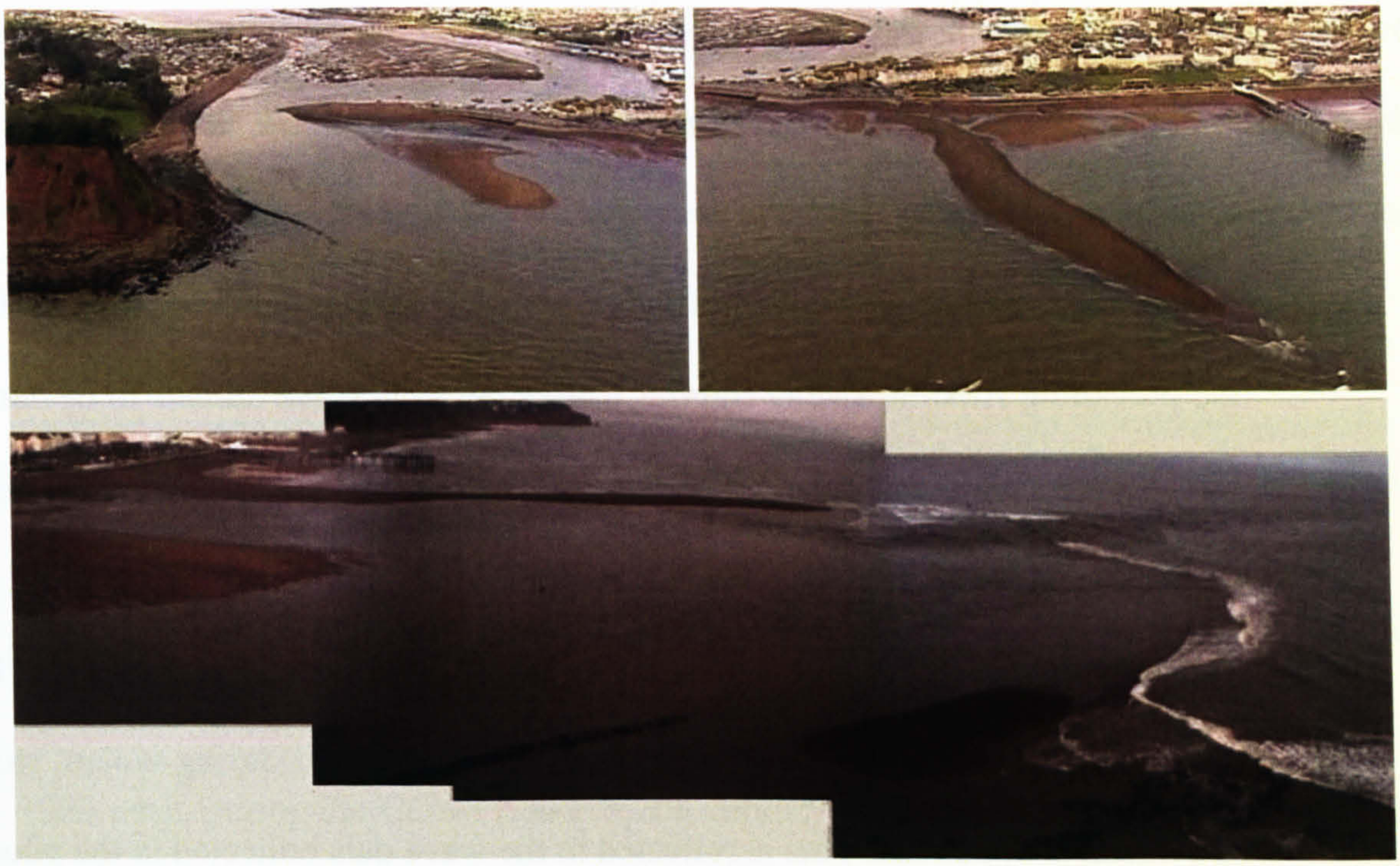

Figure 3.2: Low tide images of the Teign inlet. Upper left panel: inlet entrance flanked by the Ness headland to the south with Denn Spit and Spratt Sand to the north (2001). Upper right panel: south end of Teignmouth beach with shore-attached transverse sandbank (2001). Lower panel: a typical configuration of sandbanks on the ebb tidal delta (2007). (Upper panel aerial images are courtesy of Prof. K. Dyer, FutureCoast Project, Department of the Environment, Food and Rural Affairs., U.K., 2000-2002).

The mixed meso- to macro-tidal spring-neap cycle (mean range: 1.7 to 4.2 m) at the inlet combined with the spit-enclosed entrance (depth to width ratio $\approx$ 0.03) results in high current velocities through the mouth at times of peak flood and ebb flow (O(2 to 3 $m.s^{-1}$)), which can be significantly increased at times of high river discharge due to the 380 km^2 catchment area (Craig-Smith, 1970). Discharge rates are typically at a minimum during summer (< 20 $m^3.s^{-1}$), and maximum during the autumn to winter period ($\approx$ 50-100 $m^3.s^{-1}$) (Miles *et al.*, 1997). ABP MER (2002) analysed a 43 year discharge dataset for the Teign inlet (1956-1999) and concluded that discharge rates O(10 $m^3.s^{-1}$) represent 4 and 9% of the spring and neap tidal prisms respectively, and that under more extreme events, these rates increase by an order of magnitude (O(100 $m^3.s^{-1}$)). Under such conditions the strong ebb dominance of the main channel will be significantly enhanced and if sediment supply via littoral transport is high as at times of

elevated wave energy levels, it is hypothesised that large quantities of sediment will be transported offshore to the terminal lobe.

Due to the orientation of the coastline (Figure 3.1), Teignmouth beach is sheltered from the prevailing Atlantic swells and this causes the local wave climate to be dominated by fetch-limited wind sea during the relatively infrequent occurrences of winds from the east. Draper (1991) assessed the wave climate of the coastline of the U.K. in which Teignmouth was characterised by significant wave heights of less than 0.5 m for 75% of the time, but wave heights as large as 3 m can be attained during violent storm events (Davidson *et al.,* 1992). This is reflected in the wave data collected in the pilot study for the COAST3D project (EC MAST Project No. MAS3-CT97-0086) in which the computed $H_{90\%}$ exceedence statistic indicated that waves of 0.83 m were only exceeded by 10% of the observations. Therefore, henceforth the Teignmouth wave climate is defined as a low wave energy regime after Jackson *et al.,* (2002). At times of easterly winds, the combination of waves and large tides produces reflective conditions around the high tide mark due to the steep upper beach gradient (≈ 0.1 to 0.14), and dissipative conditions on the shallow low tide terrace gradients (≈ 0.02 to 0.07) at lower states of tide (Davidson *et al.*, 1992; Miles and Russell, 2004). Teignmouth beach can therefore be classed as an intermediate beach after Wright-Short (1984). Under the combined wave and tidal regime, the nearshore region can be classed as a mixed energy environment after Davis and Hayes (1984).

The presence of the ebb shoal system focuses the wave energy which is strongly refracted and diffracted by the irregular morphology. When the local water level is shallow enough to permit wave breaking, dissipation over the sandbanks causes lower

than expected wave energy levels on the lee shoreline when compared with the exposed shoreline of the adjacent beach. Furthermore, the refraction and diffraction effects result in little directional spread of the shoaling and breaking waves at the shoreline and on the shoals (Bird *et al.*, 2001).

3.3 Sediment characteristics and littoral circulation

The beach sediment at Teignmouth is comprised of fine to medium sand ($d_{50} \approx 250$ μm) on the low tide terrace, which becomes coarse to very coarse on the upper beach ($d_{50} \approx$ 1000 μm). During the COAST3D Project, similarly coarse sediment was found in three lobes distributed around the main channel that defined the outer margin of the ebb-tidal delta and reflected the previous history of earlier channel and shoal configurations (Figure 3.3) (Van Lancker *et al.*, 2004). The northern-most lobe that protrudes toward the pier would also appear to indicate the region where migratory sandbanks are released from the terminal lobe to begin their landward migration. Ebb-tidal delta grain size data were not sampled as part of the Coastview Project measurement program, but samples taken from the beach for an undergraduate study in 2003 were characterised by medium grain sizes as found by Van Lancker *et al.* (2004). Additional samples taken indicated that the surficial sediments of the migrating sandbank were predominantly coarse-grained and more closely resembled the sediment that formed the three lobes around the main channel. It is assumed that the presence of coarse grained sediment around the marginal areas of the ebb shoal is a persistent feature of the environment due to the winnowing action of the wave driven processes and the strong spatial gradients in flow regime which remove finer grains from the population.

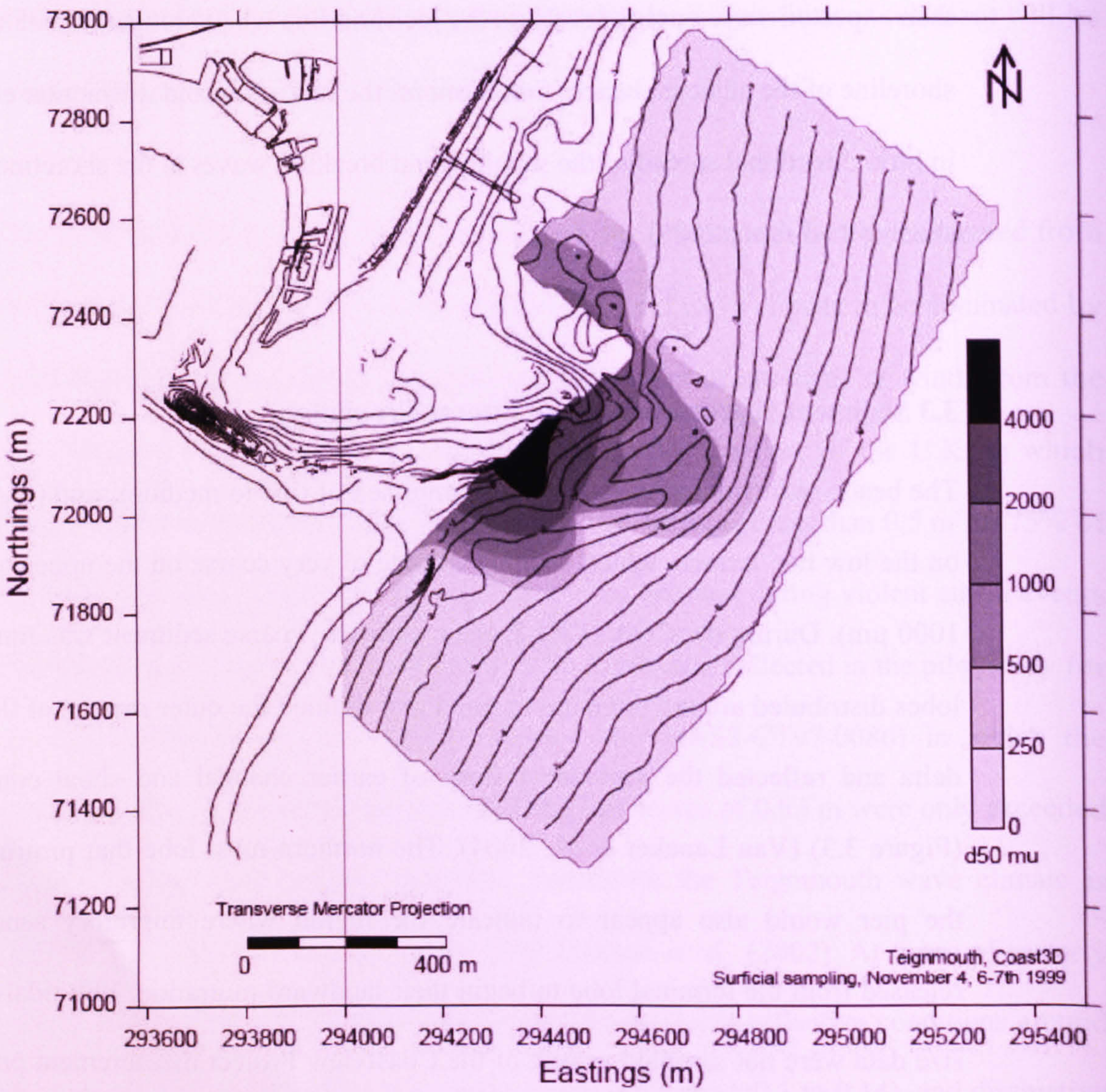

Figure 3.3: Teign inlet channel and nearshore bathymetry superposed with the areal distribution of surficial sediments (Grain types: > 2 mm: gravel; 1-2 mm: very coarse sand; 500-1000 μm: coarse sand; 250-500 μm: medium sand; 125-250 μm: fine sand) (after van Lancker *et al.,* 2004).

Littoral transport adjacent to inlets exerts a primary control on the morphological evolution of these environments. The southern U.K. coast littoral cell that includes the Teign inlet has been defined as the stretch of coast from Hope's Nose in the south to the Parson and Clerk in the north after Bray *et al.* (2004) (Figure 3.4). Their work on the inlet sediment budget (net exchange of sediment sources and sinks) qualitatively suggests that at the present time the Teign inlet nearshore region is a sediment convergence zone as indicated by the opposing direction of the littoral transport on

either side of the inlet (LT1 and LT2). Their work supports the findings of a morphodynamic modelling study by Siegle (2003) (Section 3.4) in which littoral drift was determined to be to a primary source to the inlet sediment budget under high wave energy conditions.

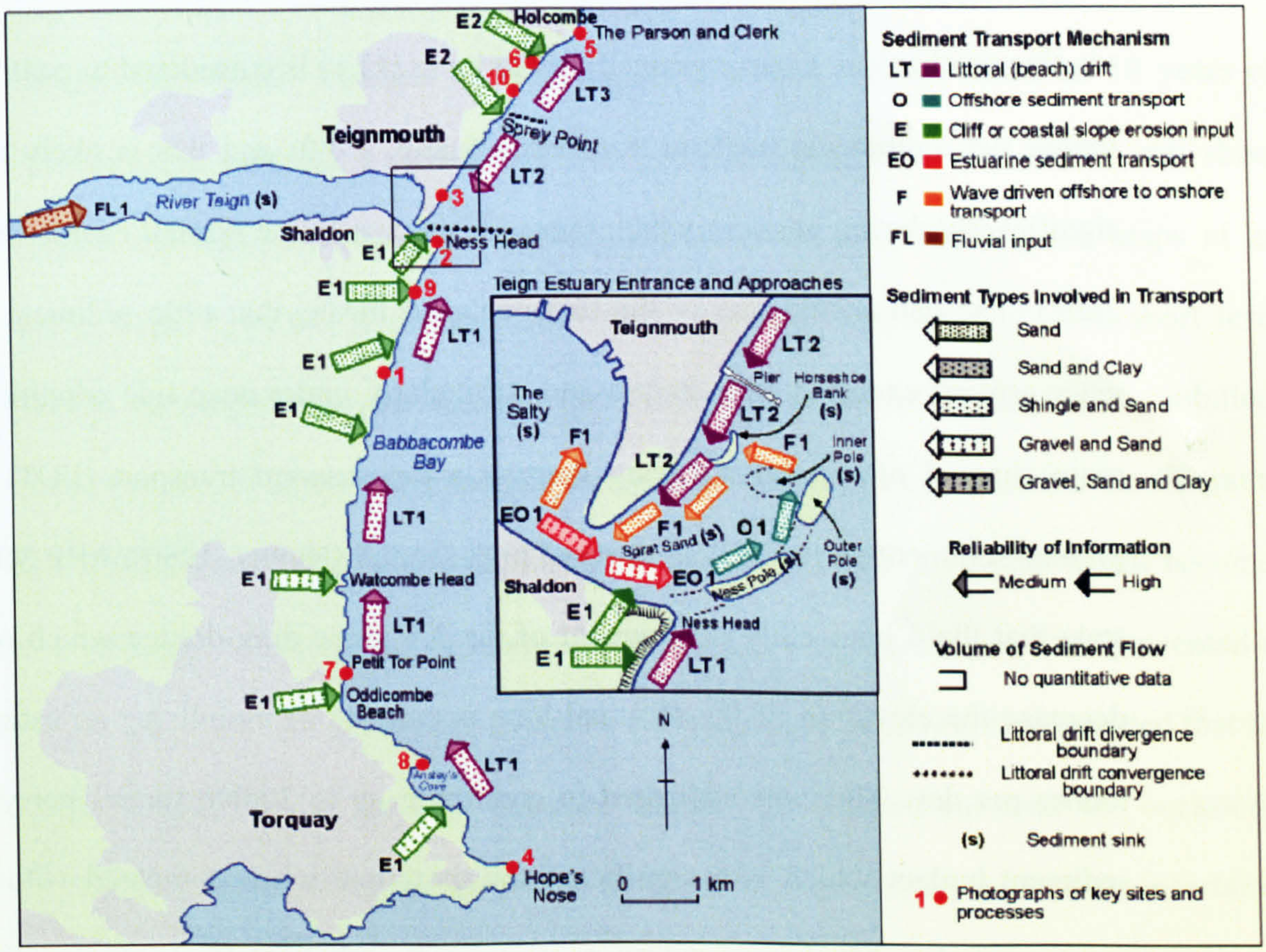

Figure 3.4: Conceptual model of the littoral circulation for the Lyme Bay coastal region from The Parson and Clerk headland, Holcombe to the Hope's Nose, headland, Torquay, and in the vicinity of the Teign inlet entrance (inset) (after Bray *et al.*, 2004).

However, it has also been suggested that the input from the north (LT2) is likely to be interrupted under incident wave angles > 140° when the longshore current is prone to short-term reversal (Siegle, 2003; Whitehouse *et al.*, 2001). In addition, Siegle (2003) found that the main longshore transport input (from the north) became negligible under significant wave heights of less than 0.5 m. The exchange of sediment with the Lyme Bay offshore region is not thought to be significant (Robinson, 1975) which is intuitive given the coarse nature of the sediment that form the sandbanks on the ebb tidal delta.

The erosion of the sandstone cliffs on the adjacent coastlines (E1) is a primary input of sediment to the nearshore and these are estimated to be eroding at a rate of 0.1-0.2 $m.yr^{-1}$. Based upon this ABP MER (2002) estimated that as much as 2000 tonnes per annum could be contributed to the nearshore region for an eroding section of cliff 15 m in height and 500 m in length. Conversely, Robinson (1975) proposed that little is added via this mechanism. Coarse grained fluvial input (FL1) is considered to contribute 6000 tonnes per annum via bedload transport (Nunny, 1980) and this is likely to increase significantly during years in which there are more extreme rainfall events (ABP MER, 2002). The ebb dominance of the main channel means that little sediment is able to enter estuary except during storms and particularly under neap tide conditions. In the main channel of the outer estuary there is a net seaward transport (EO1) of coarse grained sediment particularly at times of high rainfall (Nunny, 1980). ABP MER (2002) state that the 6 hour daily deployment of the 3.5 tonne drag-dredge which operates to decrease the elevation of the terminal lobe is capable of mobilising an estimated 100 tonnes per day. This was estimated to contribute up to 30,000 tonnes per year to the sediment budget which is a significant transport rate when compared with the other input estimates. Much uncertainty is associated with the effects of the drag-dredge operations at the inlet which hinders the estimation of a reliable budget for the location. The hydrodynamic forces governing the ebb tidal delta sediment transport regime have been observed to re-circulate sediment in the inlet entrance on variable time scales of 1 to 5 years (Kingston, 2005; Robinson, 1975; Siegle, 2003). This circulation of sediment in the inlet entrance is defined in the inset diagram in Figure 3.4 and the research concerning associated morphodynamics is described and discussed in more detail in the following section.

3.4 Nearshore morphodynamics: an historical perspective

The need to better understand the morphological evolution of the Teign inlet by the scientific, commercial and recreational communities that use the resource has led to a number of studies dating back 200 years. One of the principle contemporary studies was undertaken by Robinson (1975) who used a largely qualitative approach to analyse and explain the complex changes to the irregular ebb shoal system based on 10 years of observational evidence (1964-1974). The morphological evolution of the ebb shoal system was analysed using a chronological series of plan view sketch maps at an approximate 6 month resolution. The study was also supplemented with short term current measurements and tracer experiments. In order to describe the evolution, Robinson (1975) adopts the historical terminology for shoals such that the bar closest to the Ness is termed the Ness pole, farther to the north is the outer pole which becomes the inner pole upon migrating landward. A subset of the sketch maps are presented in Figure 3.5. From the qualitative evidence compiled Robinson (1975) concluded that the cycle of sediment in the inlet entrance lasted 3 to 5 years but with the occasional occurrence of shorter duration events of 12 to 13 months. However the uncertainty associated with the latter estimate is high given the low temporal resolution of the dataset therefore the reliability of this result is questionable.

The morphological diagrams in Figure 3.5 reflect those depicting the United States Army Corps of Engineers' (USACE) natural bypassing models (Figure 2.4) and illustrate the sandbank dynamics and their irregular plan form evolution. They also depict the manner in which the shoals evolve from elongate shore-parallel forms to crescentic forms after genesis which is a common feature seen in the S. Hook photographic archive over the subsequent 15 to 20 year period.

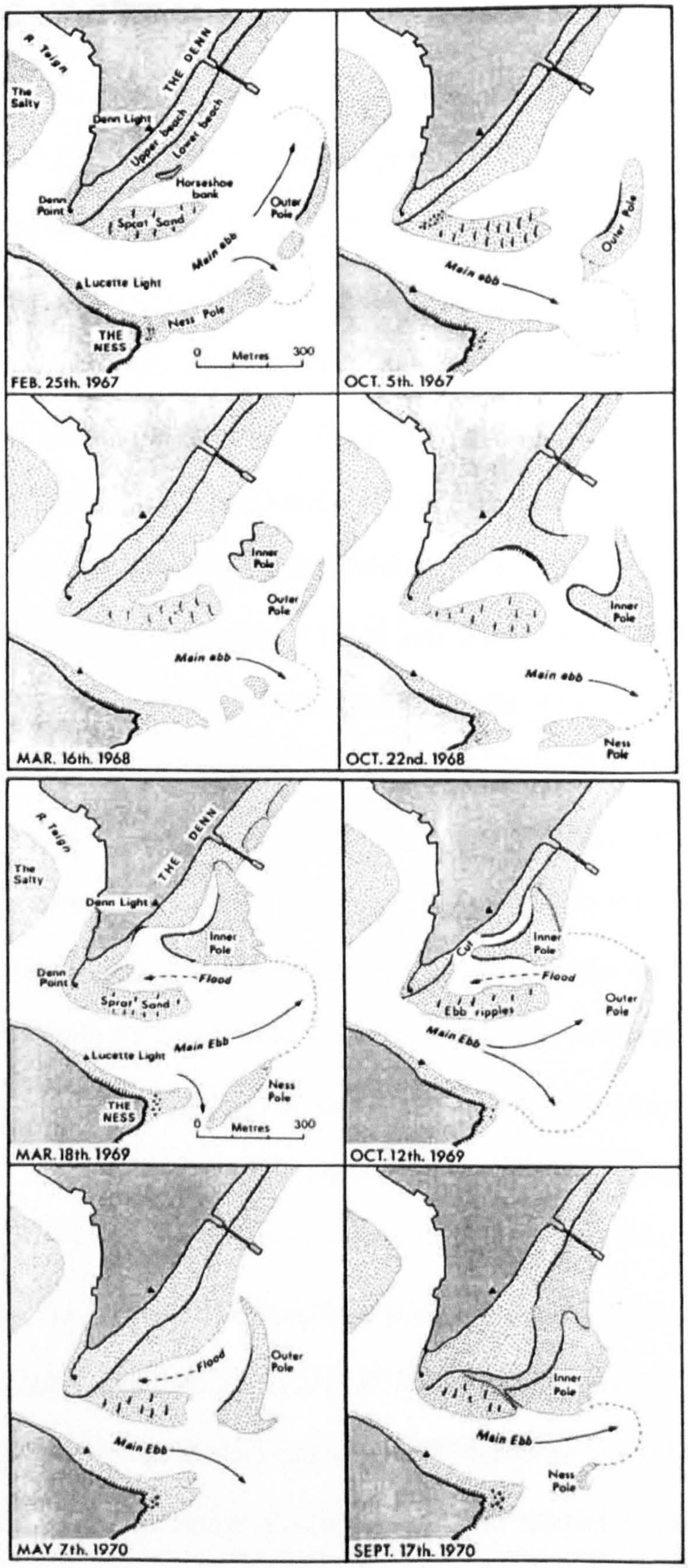

Figure 3.5: Teign inlet morphological evolution from February 1967 to September 1970 after Robinson (1975). (Dark grey shading denotes land; light grey shading denotes sedimentary features, and arrows indicate the prevailing tidal current direction.

A representative subset of this archive is presented in Appendix A1. Robinson (1975) also reported that the outer to inner pole transition is accompanied by increases in the elevation of the migrating sandbanks from initial values of 0.5 m to 2.5-3.0 m (w.r.t chart datum). Additionally Robinson (1975) states that the migrating sandbanks can experience bed level changes of up to 0.7 m and changes in position of 5 m between successive tides.

In the first of the sequence of morphological maps (top left panel, Figure 3.5) the Ness bar is well-developed and there appears to be a newly released outer pole which migrates landward during the winter and is subsequently replaced by a new outer pole. From March to October 1968 the sequence is unclear due to an apparent significant change through the winter of 1967, but by October 1968 a large crescentic inner pole had developed. This sandbank is large enough to dominate the Teignmouth inter-tidal morphology over the subsequent 12 months where it eventually becomes shore-attached forming a small lagoon on the upper low tide terrace. The inner pole attachment initiates a large shoreline change during this onshore migration event. By comparison, the Ness pole appears small in area, but this increases between October 1969 and May 1970 and during this time a new large shore-parallel and elongate outer pole has formed. This sandbank subsequently migrates landward, where it once more develops a crescentic plan form (September, 1970).

The sequence illustrates the characteristics of the Teign ebb tidal delta morphodynamics and clearly depicts the growth and landward migration (bypassing) of the sandbanks on the swash platform. Robinson (1975) proposes that features are released from the terminal lobe due to changing channel configuration under high sediment availability

conditions. The study also concluded that the morphodynamics are controlled by the balance of wave and tide driven currents with the largest changes occurring during storms. Finally, the analysis undertaken by Robinson (1975) seems to suggest that the Teign inlet fits in to the USACE inlet framework with the morphodynamic attributes of the natural bypassing inlets described in Section 2.2.1.

Siegle (2003) investigated the Teign inlet ebb shoal morphodynamics for the period 1999 to 2001 using video remote sensing coupled with a depth integrated 2D numerical model. The study utilised the deterministic MIKE21 model to explain the cyclic sedimentation of the ebb shoal system in terms of the spatial and temporal variation in the balance of forces that drive the hydrodynamics and sedimentation of the nearshore region. This balance of forces was summarised by the author in the diagram presented in Figure 3.6 (left panel). Siegle (2003) found that the main channel was dominated by offshore directed tidal currents whilst over the submerged terminal lobe, the interaction of tide and wave driven current regimes was complex. At this location the direction and strength of sediment transport depended on the balance between the onshore directed wave driven currents and the reversing tidal currents, which are in turn affected by the extent of river discharge. Over the migrating shoals the sediment transport was dominated by onshore directed currents under wave driven processes which begin to mobilise appreciable quantities of sediment under significant wave heights in excess of 0.5 m. Siegle (2003) went on to determine the sediment budget of inlet using a 13 day time series of measured boundary conditions (right panel, Figure 3.6). The transport regime defined strongly reflects that of Bray *et al.* (2004) (inset Figure 3.4) with the main littoral input from the north and a secondary input from the south. Note that the

terminal lobe is represented as a sink to sediment which is intuitive given the ebb tidal dominance and the drag-dredge operations which occur throughout the tidal cycle.

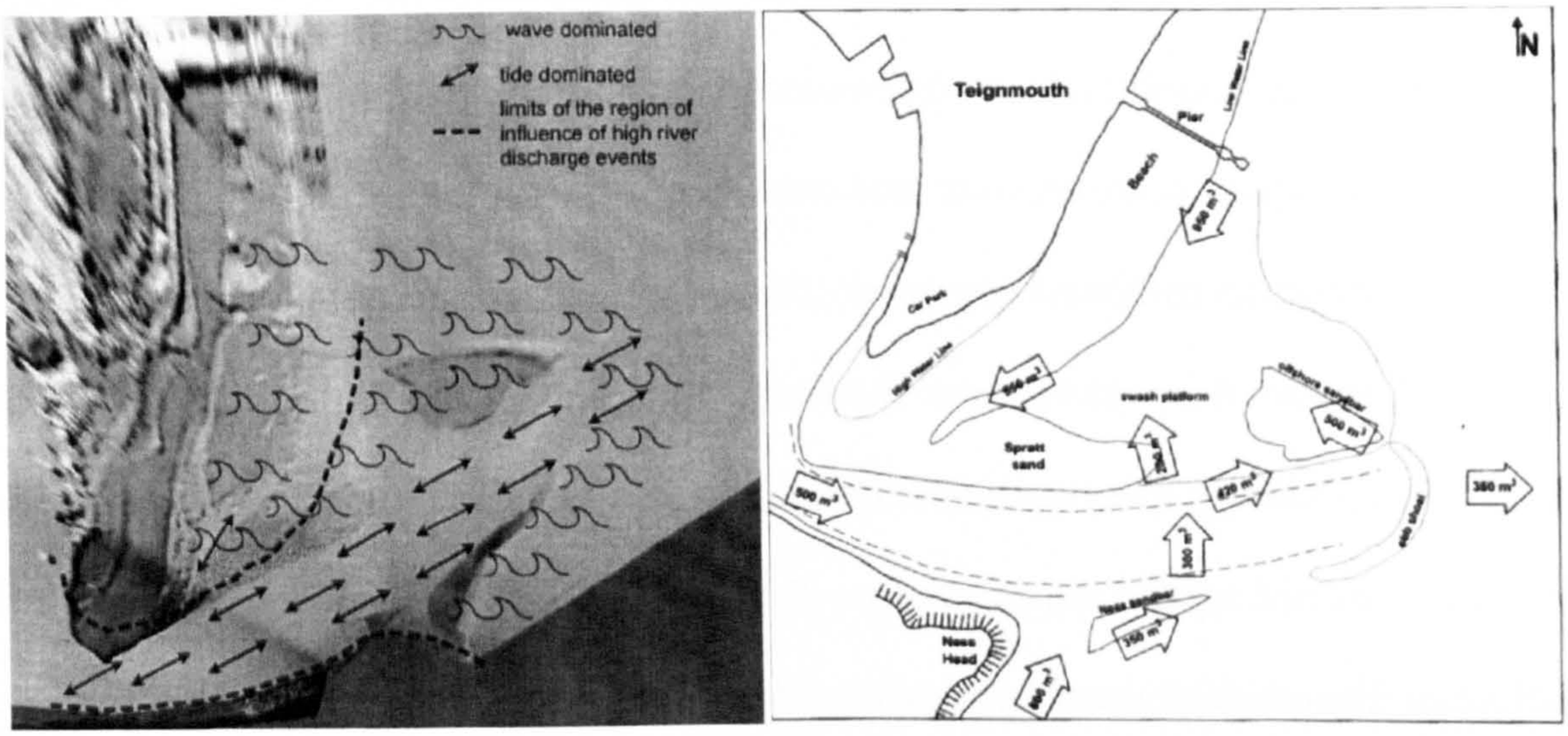

Figure 3.6: Spatial representation of the dominant hydrodynamic forces (left panel) and littoral sediment budget at the Teign inlet after Siegle (2003).

The balance of wave and tidally driven forces results in an anticlockwise sediment transport gyre as originally described by Oertel (1972). Siegle (2003) concluded that the magnitude and intensity of the resulting morphological change was primarily a function of high energy wave events that predominate during the winter months. The winter was therefore considered to be the season in which the most significant morphological change occurred whilst during the summer the morphology was considered to be comparatively stable. In addition it was found that most nearshore bed level change occurred during neap tides and this was attributed to the increased residence time of the hydrodynamic forces under the smaller tidal ranges. During the 3 year study period Siegle (2003) observed a single cycle of sediment which involved the sandbank genesis offshore, its onshore migration, shore-attachment and subsequent dissipation, and the start of genesis of the next offshore sandbank. This led to the conclusion that the morphological periodicity was approximately 3 years.

Marino-Tapia *et al.* (2006) investigated the physical processes acting over short time scales (seconds to hours) that control the sediment transport regime over the migratory sandbank at the Teign inlet in its shore-attached mode. It was found that under high energy conditions strong wave set-up in the surf zone leads to offshore directed undertow currents over and around the feature causing it to elongate in the same direction (offshore migration). The outer shoals differ in this respect as onshore wave driven flows have been shown to dominate these features under high wave energy conditions (Siegle, 2003). Conversely, under lower wave energy conditions (offshore wave height = 0.5 m) Marino-Tapia *et al.* (2006) showed that the strong refraction of the incident waves by the shore-attached bar caused them to be obliquely incident which resulted in onshore currents and sediment transport around the flanks (emerged low tide state). During higher states of the tide when the bar is submerged, the small waves lacked sufficient energy to mobilise the sediment therefore the transport rate was small. The low energy sediment transport regime over the shore-attached sandbank strongly reflects that on the offshore sandbank under the similar conditions, as described by Siegle (2003). Marino-Tapia *et al.* (2006) concluded that wave driven mean flows dominate the shore-attached shoal hydrodynamics which move the feature onshore and offshore under lower energy and storm conditions respectively. The results of Marino-Tapia *et al.* (2006) are comparable with those of Siegle (2003) in that they show larger morphological change during energetic conditions. The study by Marino-Tapia *et al.* (2006) observed a 30 m onshore bar migration during a 7 day period of low wave energy, whilst under the storm the feature elongated 90 m in the offshore direction over a 3 day period on account the strong mean undertow currents.

Kingston *et al.* (2005) studied the Teign inlet ebb tidal delta over medium to long time scales (months to years) in relation to the stability of the main channel and volume changes to the ebb tidal delta using a shoreline detection algorithm on a 5 year Argus image archive (1999-2004). They used a dataset of 64 shorelines at a 6 month temporal resolution to determine shoreline change down to a depth of -10 m w.r.t. Ordnance Datum Newlyn (ODN). From the results it was concluded that the morphological periodicity had reduced with 4 events occurring in the 5 year time span and this was hypothesised to be related to changes in the long term drag-dredging strategy. The main channel was found to oscillate between more easterly and northerly orientations where in the former the channel follows the line of the Ness headland. Both channel states had approximately equal residence times but the degree of lateral deflection was larger in the outer channel section (70 m) when compared with the inner section (12 m). Kingston *et al.* (2005) also suggested that the nearshore inter-tidal region had undergone a marginal decrease in volume whilst the nearshore region which encompassed the Denn spit and inlet throat had experienced a small decrease in volume. The latter result concurs with the findings of Bernardes (2005) who found that the inlet was undergoing a period of infilling with a net overall gain, but net loss from the nearshore region between December 2002 and November 2004. The numerical modelling study by Bernardes (2005) investigated the medium to long term (months to years) morphodynamics of the Teign inlet for the above period using the 2D Telemac system. The author concluded that there was a distinct seasonal pattern of deposition and erosion at the inlet. During the more energetic periods in the winter and autumn sediment is imported to both the nearshore and outer estuary regions under higher sediment availability conditions. The majority of the sediment is considered to be imported via increased littoral drift due to the more frequent higher energy wave

conditions for the time of year. Conversely, during the spring and summer months the paucity of higher energy waves allows the comparatively strong ebb tide currents in the outer estuary and inlet entrance to export sediment into the main channel where it is transported offshore.

The image time series of the Teign inlet ebb shoal system taken from the Ness headland by S. Hook is too large to present in the thesis but a selection of images are presented in Appendix A1 for reference purposes. The images were sampled at random low tide intervals so the variable temporal resolution of the time series means that the archive serves only as a useful qualitative visual record of the morphology for the 15 year period following 1975. The morphology of the shoals and their dynamic continued to exhibit the characteristics described by Robinson (1975) with the genesis and landward migration of large sandbanks of irregular form in which there were repeated occurrences of the crescentic plan form depicted in Figure 3.4. Similarly, the channel behaviour for the period strongly reflected the two state model proposed by Kingston *et al.* (2005) with several gradual transitions between the northerly and easterly orientations occurring. A qualitative assessment of the S. Hook archive has been undertaken by the present author observed the genesis of 15 distinct offshore sandbanks from October 1976 to March 1990, though there were only 11 complete cycles due to the occurrence of several bar coalescence events. From the available archive it was estimated that the sedimentation cycle had a mean periodicity of approximately 22 months with maximum and minimum periodicities of 11 and 28 months respectively.

The present work makes an important contribution to the work of previous authors and advances the knowledge of Teign inlet morphodynamics in a number of ways. On short

time scales this contribution analyses the hydrodynamic and sedimentation processes acting on the sandbank in mid term onshore migration using physical measurements obtained from its surface. The in-situ measurement analysis (Chapter 5) complements the work of Marino-Tapia *et al.* (2006) who conducted a similar analysis using measurements from the sandbank in its shore-attached mode. The study enlarges upon that by Siegle (2003) whose modelling work was limited to one sedimentation cycle, whereas the dataset used herein captures multiple (4) events. The resolution of the dataset permits the short term (weeks) morphodynamic behaviour to be quantified and the macro time scale (years) of the Argus image archive has enabled the identification of medium to long term (months to years) morphological trends (Chapter 4). The study by Robinson (1975) of the 10 year period in the inlet's evolution was based on a comparatively low frequency dataset (~bi-annual) of a qualitative nature that negated the quantification of relevant parameters. This research has benefited from advances in remote sensing technology so that the history of morphological change has been documented using a high resolution dataset of contours derived from a geo-referenced video system. This permits the quantification of relevant morphological parameters from which a more robust set of conclusions can be drawn than from qualitative data. By virtue of the fact that the migrating sandbanks that are the focus of this research are the most morphodynamic component of the ebb tidal delta, the variability captured in the contour dataset accounts for much of the observed morphodynamic variability of the system. In the next chapter the study begins with the characterisation and quantification of the sandbank morphodynamics from the remotely sensed video image archive.

4 Video remote sensing

In order to investigate morphodynamic processes in the nearshore it is necessary to sample key variables over a wide range of spatial and temporal scales (e.g. surface water elevation (η), cross-shore (u) and longshore (v) current velocities, suspended sediment concentration (c) and the rate of bed level change ($\delta z/\delta t$)). Traditionally, nearshore field studies involve the cumbersome deployment of multiple arrays of expensive instrumentation within the inter-tidal region which is both technically and logistically challenging, and poses a significant financial risk when fieldwork programs coincide with high energy conditions. Furthermore, the difficulty in obtaining these data at an adequate spatial resolution using conventional methods often results in a relative paucity of data when considering the complexity and scale of the phenomena being studied. This hinders the challenging task of understanding the morphodynamics.

The application of relatively cheap optical remote sensing equipment to nearshore studies was investigated at Oregon State University's in the 1980's when the usefulness of imaging for this purpose was first being realised. This usefulness stems from the fact that many of the key geophysical variables have optical signatures which are manifest in the pixel data. The principle advantages of imaging over traditional methods is that it enables the collection of important variables (e.g. wave period, wave direction) at the required temporal and spatial resolution without the aforementioned problems, and can continue autonomously for an indefinite period with minimal running costs. Additionally, remote sensing of the nearshore in this manner offers a safer way of obtaining observations during the important periods of high energy conditions, and represents a significantly lower financial risk in the event of equipment being damaged or lost altogether. Since the 1980's the Coastal Imaging Laboratory at Oregon State

University have developed and incorporated the technology into the Argus system for coastal research. The specific capability of being able to resolve inter-tidal bathymetry using the collected images makes the Argus station an invaluable tool for the study of medium to long term morphodynamics.

4.1 Argus video system

An Argus station (Holman and Stanley, 2007) comprises an elevated remote camera system focused on a coastal region of interest and an internet-connected PC for system control and data transmission to the archive facility. Typically, each station has five digital video cameras with a combined field of view of 180° covering a stretch of coastline up to a 5 km in length. The process of data collection and storage is fully automated with the default setting usually configured to collect three image products routinely which are defined as follows:

1. Snapshot: this is a single standard image which serves as a qualitative visual reference source for conditions at the data collection event.
2. Ten minute time-exposure image (timex images): this represents the mathematical time-mean of all images sampled at a frequency of 2 Hz over a ten minute period. The averaged pixel intensity data are particularly useful for identification of regions of wave breaking which have then been used to determine the location of submerged morphological features (Lippmann and Holman, 1989).
3. Ten minute variance image: this represents the mathematical time-mean of the variance of the image intensities sampled in the timex images. The averaged pixel variance data distinguish between regions where pixel intensities vary strongly (bright

signal) from those where there is little or no variation (dark signal) during the sampling interval.

Each image product is collected at hourly intervals with a further timex image known as a 'daytimex' image being generated from the average of the hourly timex images collected each day (Figure 4.1a to d). A single 24-bit 640 x 480 pixel RGB image contains approximately 900 KB of data in its raw format hence the use of jpeg compression for archiving purposes. This reduces the file size to between 10 and 30 KB depending on image type. The Argus system can also be set up to record intensity data from user-defined individual pixels or pixel arrays thus permitting the collection of pixel intensities at high temporal resolution (e.g. 2 Hz) without generating unmanageable quantities of data.

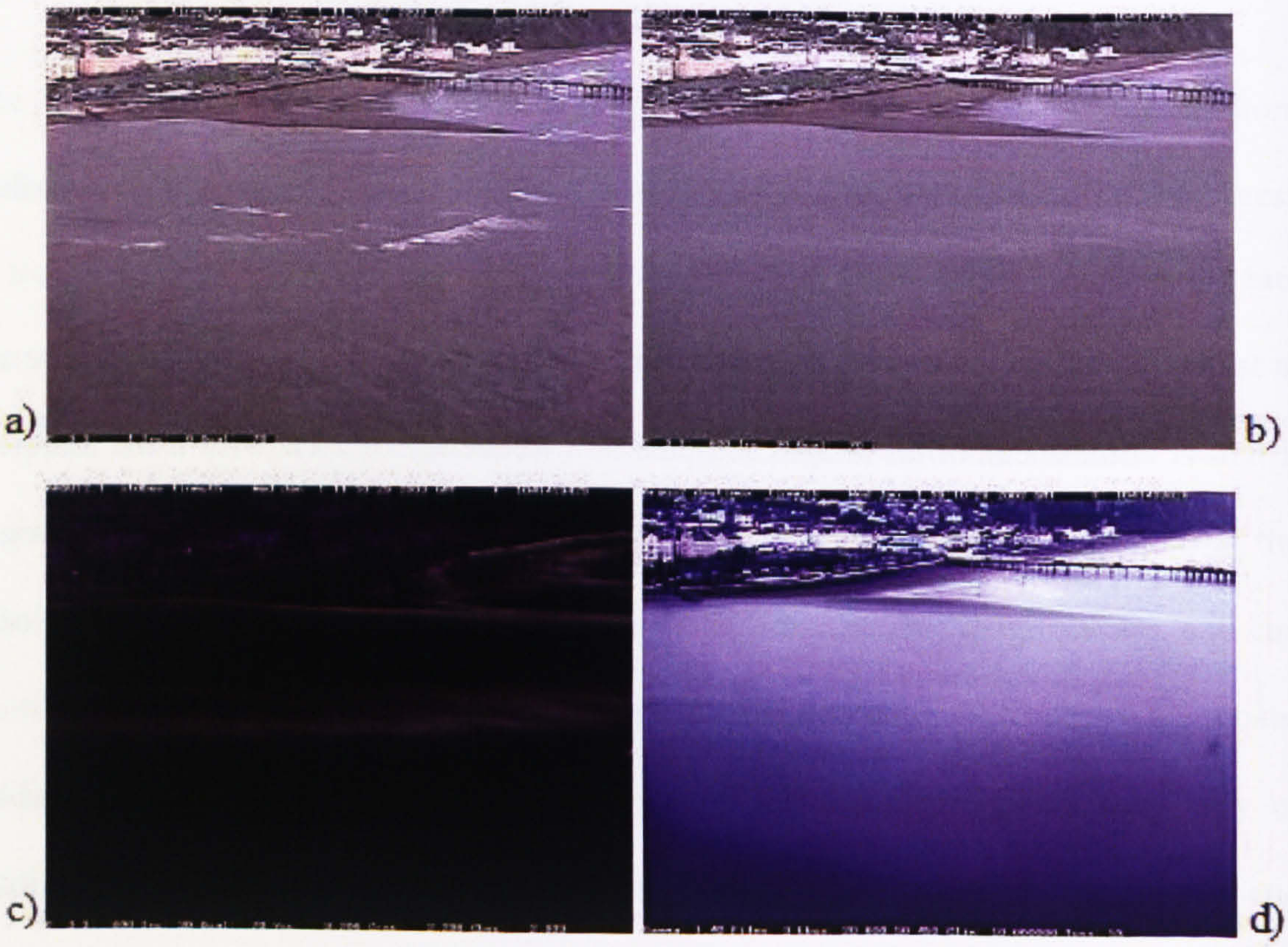

Figure 4.1: Argus image types from camera 3 showing Teignmouth town, the main beach and pier: a) snapshot, b) timex, c) variance, and d) daytimex.

The relative low cost and effectiveness of the Argus station has led to their increasing use in the investigation of a wide range of nearshore phenomena which have been broadly categorised into three groups (Aarninkhof, 2003). The first group utilise timex images to identify nearshore regions of preferential wave breaking in order to derive the spatial and temporal variability of sub-tidal morphological features (Van Enckevort and Ruessink, 2003a, b; Lippmann and Holman, 1989; Konicki and Holman, 2000; Lippmann and Holman, 1990). The second group utilise high resolution pixel data to resolve hydrodynamic processes including the phase speed, angle and period of breaking waves (Lippmann and Holman, 1991), wave run-up (Holland *et al.*, 1995), and the magnitude of surface currents (Chickadel *et al.*, 2003). The third group utilise daily snapshot and timex images to resolve 2D and 3D sub-aerial topography (Holman *et al.*, 1991), inter-tidal bathymetry (Davidson *et al.*, 1997; Madsen and Plant, 2001; Aarninkhof *et al.*, 2003; Siegle, 2003), and sub-tidal bathymetry (Stockdon and Holman, 2000; Aarninkhof *et al.*, 1997). These techniques require the generation of time series of shoreline position at different tidal elevations which can then be integrated and mapped.

4.1.1 Brief history of the Teignmouth Argus station

The Argus II video station (Holman and Stanley, 2007) was first installed on The Ness headland at Teignmouth in February 1999 (Figure 4.2a to d). The system uses an SGIO2 Unix work station with frame grabber which routinely samples and archives the three different image types using five analogue cameras. The analogue images which measure 640 x 480 pixels were digitised using an external Kramer digitisation unit. However, owing to the Argus II system having only one video input, each data

collection event was comprised of three sub-collection events in order to collect images from all of five cameras (Figure 4.2d).

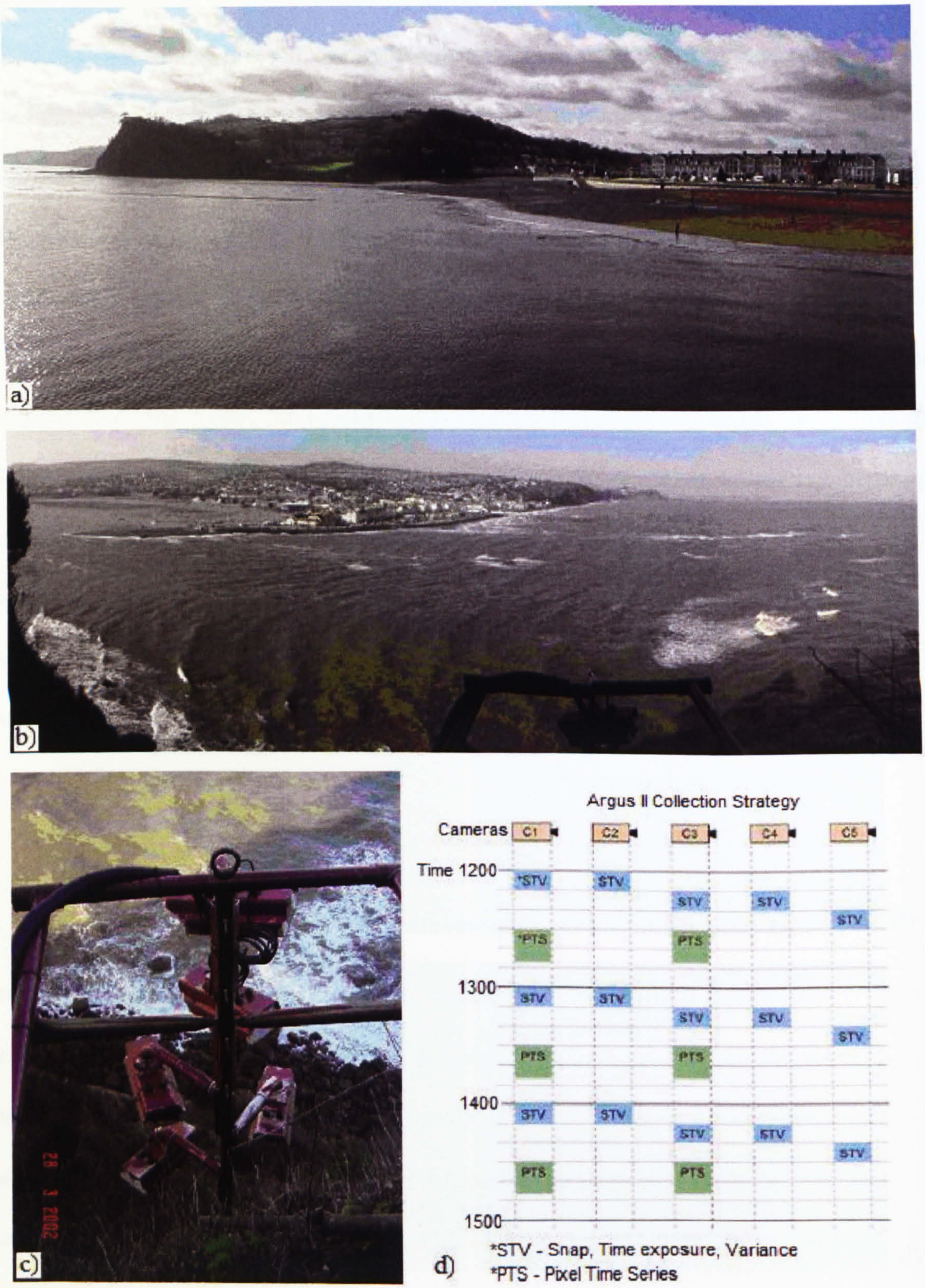

Figure 4.2: a) Argus station location, b) station viewpoint, c) camera rig, d) Argus II collection strategy (after Holman and Stanley, 2007).

Consequently the sub-collection events and consecutive image pairs are asynchronous with an approximate 0.25 s offset between them. This does not hinder shoreline extraction utilising 10 minute timex images, but does create a significant processing problem when resolving video-derived data that require high temporal resolution. The Argus station at Teignmouth has proved to be particularly reliable apart from a brief period during January 2001 which resulted in a depleted image archive for that period. The longevity of the station's operational time has meant that it has been possible to compile a unique six year image time series of the ebb tidal delta system at Teignmouth. These data are combined with the contemporaneous wave climate and environmental data in order to characterise the geometry and dynamics of the migratory sandbanks on the ebb tidal delta.

4.1.2 Camera model and coordinate transformation

Obtaining quantitative data from oblique images for the analysis of nearshore processes involves merging the images from each camera into a single image and transforming them into a geo-referenced and geometrically correct plan view image (image rectification) as shown in Figure 4.3a. The image rectification process utilises a calibrated camera model to transform between 3D world coordinates and 2D image coordinates which requires the determination of two sets of camera parameters:

1. Intrinsic parameters: these parameters describe the physical characteristics of the camera, lens and image acquisition hardware. The parameters concerned are the lens radial distortion coefficients: k_1, k_2, the position of image optical centre: U_o, V_o, the vertical and horizontal pixel scale factors: λ_u, λ_v, and the effective focal length, f.

2. Extrinsic parameters: these parameters describe the cameras geometrical position (x_c, y_c, z_c) and orientation in terms of tilt, azimuth and roll (i.e. τ, ϕ and σ respectively) in relation to the reference frame chosen (see Figure 4.3b).

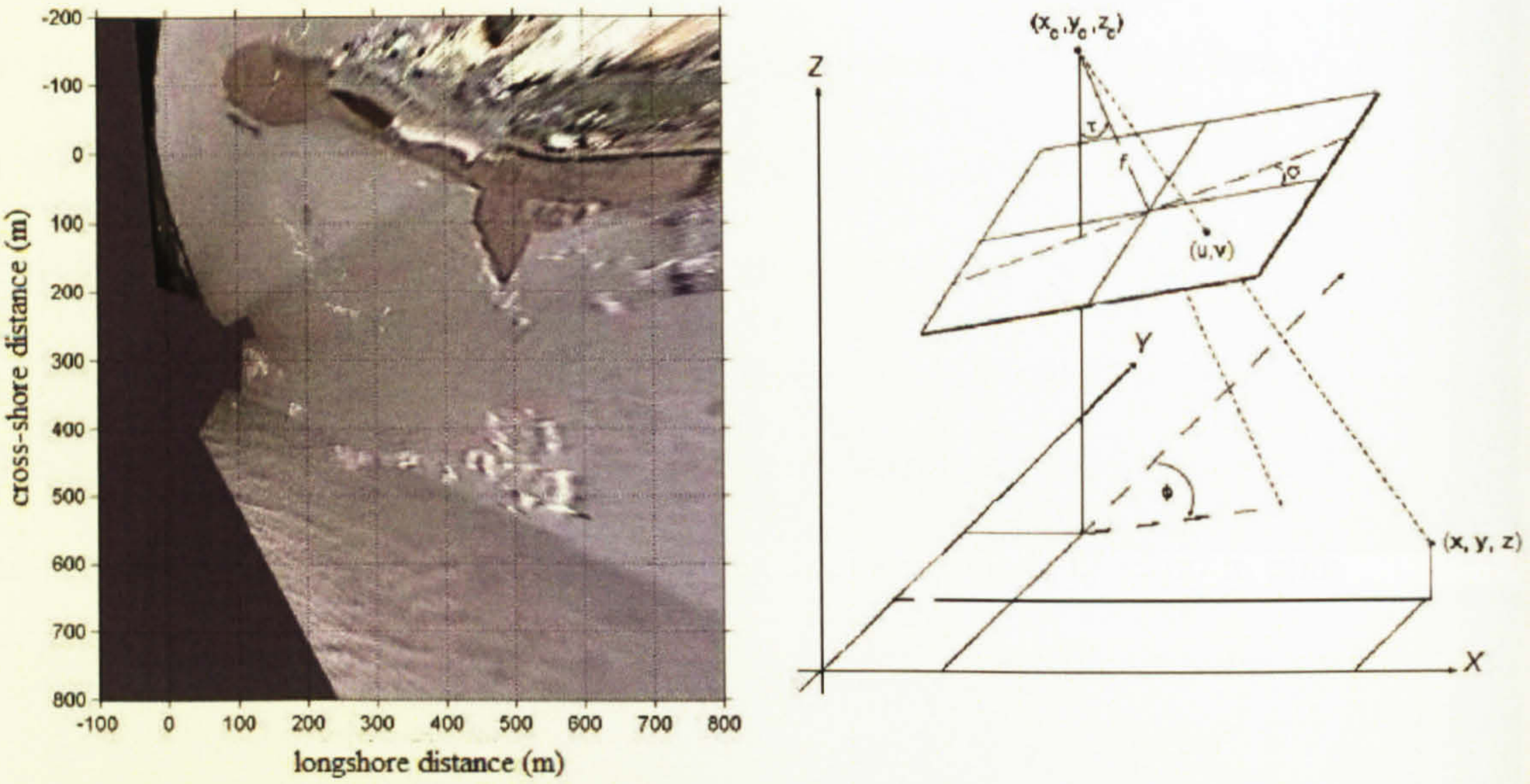

Figure 4.3: a) Rectified Teignmouth Argus image, b) camera model parameters (after Holland *et al.*, 1997).

The camera model used in the Argus algorithm has been derived using the standard direct linear transformation (DLT) method from photogrammetry which accounts for camera roll and lens distortion effects, and digital sampling imperfections caused by the offset between the location of the optical and image centres and the pixel scale factor (Holland *et al.*, 1997). The transformation between 3D world and 2D image coordinates uses linear versions of the co-linearity equations as follows:

$$U = \frac{L_1 x + L_2 y + L_3 z + L_4}{L_9 x + L_{10} y + L_{11} z + 1} \tag{4.1}$$

$$V = \frac{L_5 x + L_6 y + L_7 z + L_8}{L_9 x + L_{10} y + L_{11} z + 1} \tag{4.2}$$

Where U and V are the image coordinates, x, y, and z are the world coordinates and the coefficients L_j for j = 1 to 11 are the DLT coefficients which incorporate the camera's intrinsic and extrinsic parameters. The solution to the camera model involves a two step explicit-implicit method to solve for the intrinsic and extrinsic camera parameters and perform the transformation between real world and image coordinates (Holland *et al.*, 1997). Initially, the lens distortion coefficients, the position of the image optical centre, and the vertical and horizontal pixel scale factors are determined in the laboratory leaving the effective focal length and the 6 extrinsic parameters to be determined in the field. If the camera position (x_c, y_c, and z_c) is surveyed, then the remaining 4 intrinsic camera parameters (τ, φ, σ and f) can be solved explicitly using the coordinates of 2 surveyed ground control points that lie within the camera field of view. Two permutations of the transformation between 3D world and 2D image coordinates exist which require different approaches in order to obtain the final solution which are summarised as follows:

1. Transformation from 3D world to 2D image coordinates: determination of the extrinsic and intrinsic camera parameters permits direct computation of the 2D image coordinates by direct substitution.
2. Transformation from 2D image to 3D world coordinates (image rectification): rearrangement of the equations for u and v (equations 7.1 and 7.2) to form two simultaneous equations permits an iterative least squares solution using matrix algebra provided that $z = z_{tide}$ where z_{tide} = tidal level.

For more detailed camera model calibration information the reader is referred to (Holland *et al.*, 1997; Lippmann and Holman, 1989).

4.2 Contour extraction methodology and sampling strategy

The principle objective of the video image work in the present study is to extract a plan view contour time series at a particular tidal reference level in order to be able to quantify the dynamics and characterise the geometrical evolution of the sandbank from the offshore accretion stage to the beach dissipation stage. The six year Teignmouth archive has captured four consecutive cycles of this morphological behaviour and hence the contour time series are an invaluable resource that enables the identification of similar trends between individual cycles in the offshore sandbank's morphodynamics through the period of onshore migration.

Since the inception of the Argus video system a range of shoreline detection algorithms have been used to resolve nearshore morphology in two and three dimensions (Section 4.1). Typically the techniques involve the processing of lengthy image time series necessitating automation for the efficient retrieval of the data. The algorithms delineate the wet and dry regions of the nearshore using their different pixel intensity or colour characterisation to determine the position of the shoreline. The application of a shoreline detection algorithm to the present study was found to be particularly problematic when part or the entire contour to be determined was contained within the inter-tidal region whilst it was exposed by the tide. The pixel signatures of minor adjacent inter-tidal morphological features were difficult to distinguish from those of the study feature due to their having nearly identical characteristics.

The sampling strategy for this study was constrained by the resolution of the image archive and the vertical extent of the sandbank in relation to that of the tidal cycle. After undertaking a qualitative assessment of the image dataset with due consideration of the constraints, it was decided to use a manual contour extraction method as this was

considered to be the most robust approach. Based on the start and end dates of the Argus archive, a contour time series sampled at a frequency of one per spring tide for the duration of the archive would generate a data set containing approximately 130 images, and a manageable quantity for manual contour extraction. The choice of the optimum tidal reference level was governed by the requirement that a representative contour could be extracted from the sandbank throughout its entire onshore migration from offshore genesis to the beach dissipation. A target tidal reference level of -1.80 m ODN was chosen which corresponds to the approximate local mean spring low water (MSLW) level. This reference level was considered to be the optimum level under the constraints of the methodology as it is deemed to be sufficiently placed within the vertical space occupied by the sandbank through the entirety of its onshore migration to be representative of the features morphology.

The manual extraction process involved the visual delineation of the sandbank in each rectified Argus image and the recording of the coordinate set. This was undertaken using a Matlab algorithm based on the 'ginput' function that acquires the *xy* coordinates of the cursor relative to the plotted reference frame upon operation of the mouse button; the values obtained from the rectified Argus image were therefore the Argus *xy* coordinates (m). The timex image type was the primary image product chosen for the purpose of the contour extraction but at times when spatial uncertainty existed in a contour, it proved beneficial to consult images from the adjacent chronology, and to make use of the variance and daytimex images which at times enhanced the sandbank's delineation. An example of the contour extraction process described is represented in Figure 4.4 in which an arbitrary tidal reference level of -1.18 m ODN has been used to extract a contour from a clearly delineated sandbank.

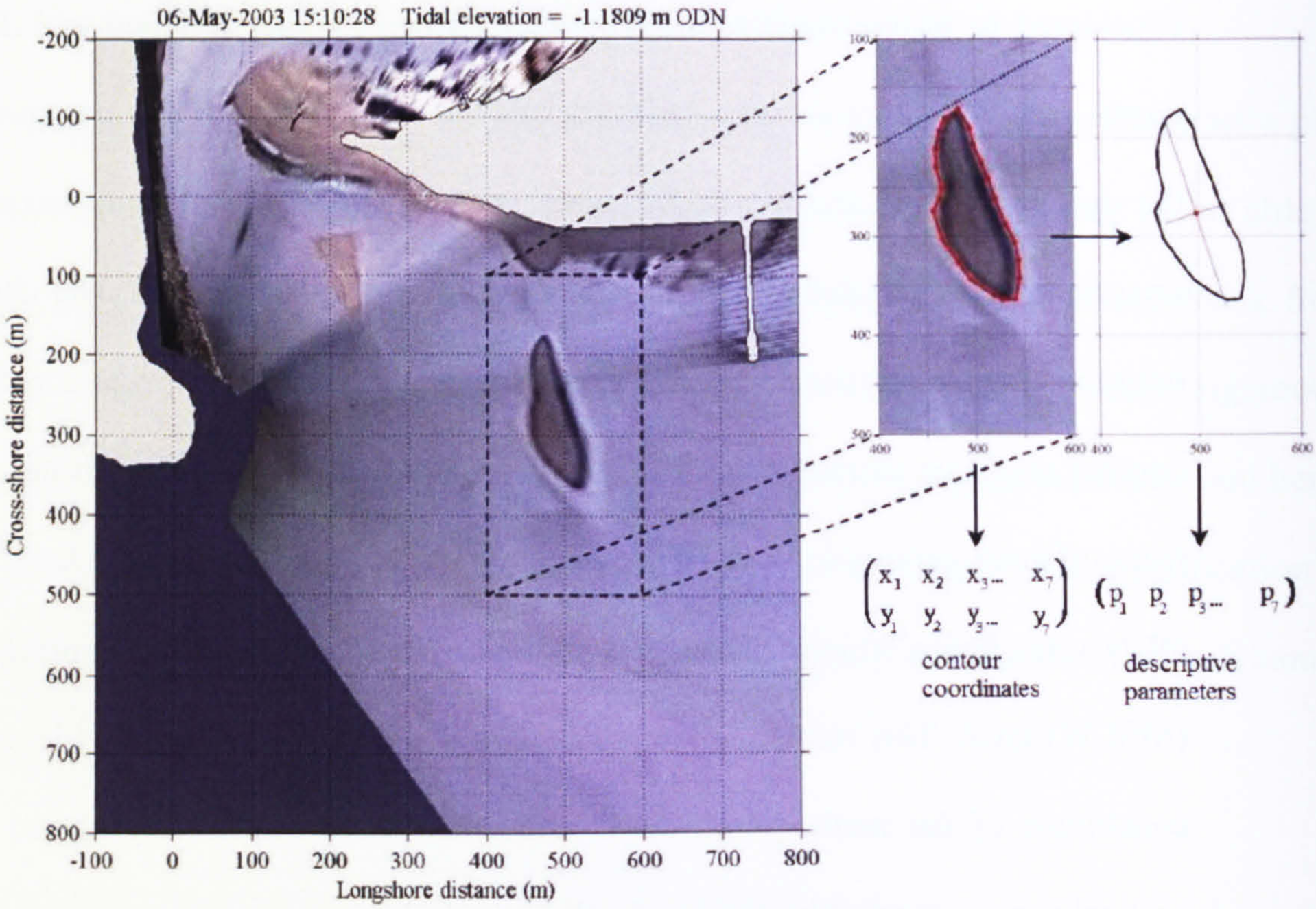

Figure 4.4: The manual contour extraction process using a focussed region of a rectified Argus image containing the sandbank. A set of descriptive parameters that define the feature are subsequently extracted using the Matlab 'regionprops' function. The derived contour is displayed on the right side of the diagram overlaid with major and minor axes which cross at the centre of mass of the sandbank (red dot).

The delineation of the shoreward boundary of the sandbank during the shore-attached stage was sometimes particularly difficult to determine. In such cases this section of the extracted contour is prone to the most subjectivity though the task was often facilitated by the different hues of the sandbank and beach sediments. The reader is referred to Section 4.3.1 for an analysis of the inherent uncertainty in contour position due to the methodology. The maximum possible shoreward cross-shore limit of the sandbank was defined as that of the coastal boundary as demarcated in the EDINA digital map of Teignmouth.

The target tidal reference for the purpose of contour extraction was -1.80 m ODN but the constraints of both the temporal resolution of the Teignmouth Argus archive and the methodology resulted in a contour dataset obtained from a range of tidal values about the target level which have been plotted in Figure 4.5 and summarised in Table 4.1.

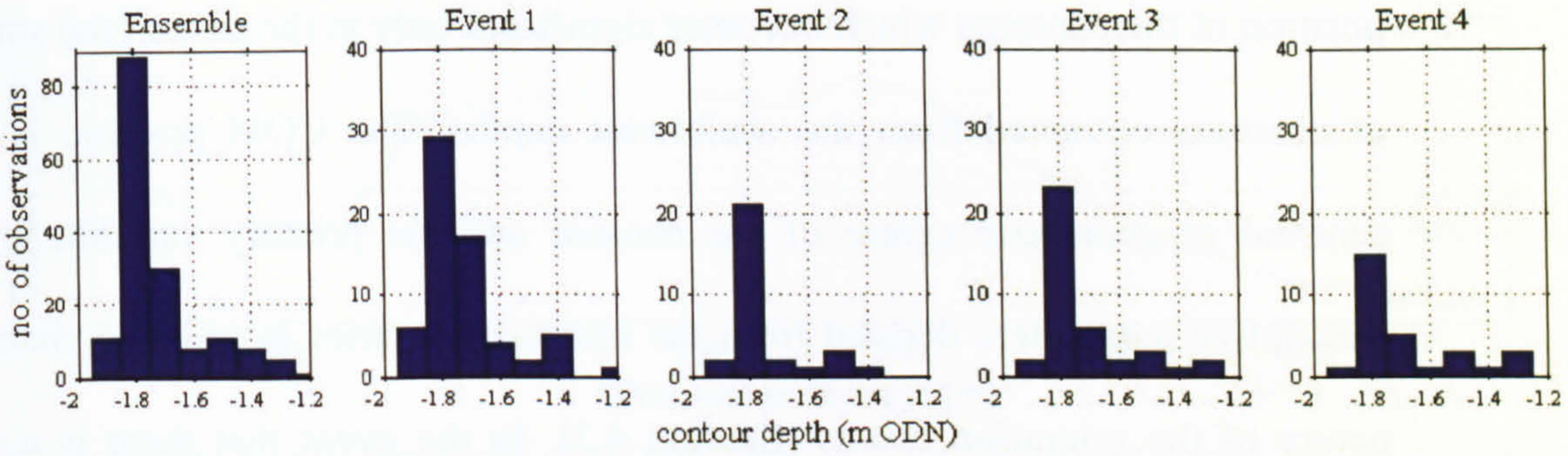

Figure 4.5: Contour depth histograms for individual events.

The maximum and minimum mean tidal levels for individual contour datasets are -1.75 m ODN for event 2 and -1.68 m ODN for event 4 respectively whilst the mean of the ensemble dataset is -1.72 m ODN. The comparatively low mean value for event 4 indicates that this dataset contains a higher proportion of shallower contours.

	Maximum contour depth (m ODN)	Mean contour depth (m ODN)	Minimum contour depth (m ODN)	Range (m)	No. of observations
All events	-1.89	-1.72	-1.25	0.65	164
event 1	-1.89	-1.72	-1.25	0.65	66
event 2	-1.86	-1.75	-1.42	0.43	30
event 3	-1.87	-1.72	-1.27	0.60	39
event 4	-1.87	-1.68	-1.26	0.61	29

Table 4.1: Contour dataset summary statistics.

The maximum and minimum contour depths are -1.89 m ODN and -1.25 m ODN respectively which are both found in the event 1 dataset and consequently this dataset has the maximum range in contour tidal levels of 0.65 m. The event 2 dataset has the smallest range at 0.43 m, and the mean value closest to that of the target contour tidal level of -1.80 m ODN. All the datasets are strongly positively skewed towards the target tidal reference level (Figure 4.5).

In relation to the spread in the depth values in the contour dataset in which the outlying points are as much as 0.6 m distant from the target tidal level, there is a potential effect to be considered. This effect concerns the displacement of the centre of mass (COM)

position of the contours which becomes significant only in the case of the small quantity of contours extracted from the shallowest depths. The COM position is simply the centroid or geometric centre of the contour and the primary variable in the set of descriptive parameters derived from the image time series in order to characterise the nature of the migration events (Section 4.3). In the event that there is a cross-shore displacement of the COM position of a contour, this would subsequently affect the cross-shore migration rate of the individual points affected in relation to adjacent points.

The cross-shore migration rate time series constitutes the primary dataset to be generated from the video work in the current study and the remainder of this section is a qualitative assessment of the potential impact of this effect on this dataset. The magnitude of a displacement in the cross-shore COM position is dependent on both the size of the difference between the extraction depth and the target tidal level, and on the gradients in the morphology of the shoreward and offshore extremities of the sandbank. From examination of the available Teignmouth nearshore bathymetric data, it is evident that the offshore extremity of the sandbank has consistently shallower gradients when compared with those of the shoreward extremity, and therefore it this section of contour on the offshore extremity of the sandbank that would be most affected by the phenomenon. Before shore-attachment, and in the depth range between -1.25 and -1.89 m ODN, the shoreward extremity typically has a much steeper gradient (3 to 5°) than offshore extremity (1 to 2°) and this is illustrated in the cross-shore 2D section through the sandbank in Figure 4.6. Two horizontal lines have also been plotted on the figure depicting the target tidal level of -1.80 m ODN and the shallowest contour depth of -1.25 m ODN which help to visualise the potential impact on the COM position.

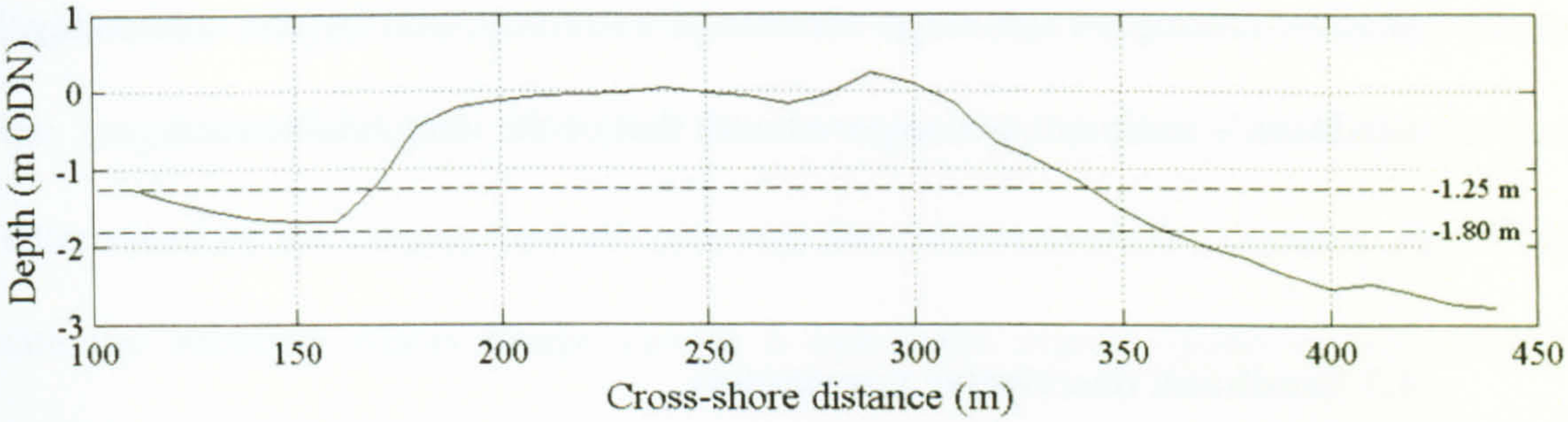

Figure 4.6: Cross-shore 2D section through the offshore sandbank from May 2003. The horizontal lines depict the target contour tidal level (-1.80 m ODN) and the depth of the shallowest contour (-1.25 m ODN).

The gradients in this scenario result in the shallowest contours being associated with a shoreward displacement *O*(18 m) in the line of the contour on the offshore extremity, but the potential impact of this on the COM position is mitigated by the offshore displacement in the line of the contour *O*(13 m) on the shoreward extremity. The resultant cross-shore COM displacement would therefore be *O*(5 m) for contours extracted from the minimum depth in this scenario. This could have the effect of artificially increasing the onshore migration rate of the COM by as much as 0.33 $m.day^{-1}$ based on an average contour sample interval of 15 days. This error source is infrequent and random in nature but since the largest deviations from the target tidal level only concerns a particularly small subset of the dataset the error source is not considered to have a significant impact on the results. Once shore-attachment has occurred, the mitigating effect of the shoreward gradient in reducing the potential impact of a shallow contour on the COM is lost and thereby these contours may be particularly susceptible to error in the COM position. Shoreward of the inner extremity of the sandbank, a channel in the bathymetry exists which also has the potential to result in a shoreward displacement of the line of the contour and by as much as 40 m in this example. However, it should be emphasised that the sandbank is typically clearly delineated due it being completely surrounded by the sea. The delineation does become more difficult once the sandbank encroaches on the inter-tidal terrace but is much improved by the

shadow-casting of the steep shoreward extremity, and by the contrasting hues of the sandbank's sediment as compared with that of the inter-tidal terrace.

4.3 Sandbank descriptive parameters

The dynamics and plan view geometric evolution of each onshore migration event captured in the Teignmouth archive are described and quantified using a set of six sandbank descriptive parameters. The parameters which have been defined in Table 4.2 were derived from the application of the Matlab 'regionprops' function to binary matrices generated from individual sandbank contours. The sandbank parameters of primary importance in this study are the centre of mass (COM) or centroid of the contour which is used to quantify the sandbank's migration rate variability, and its minimum crest elevation. The remaining parameters are used to define the plan form geometry of the sandbanks through their morphological evolution in terms of their physical proportions, area and orientation.

Parameter	Description
Centre of mass position	Coordinate of the contour centroid or geometric centre of mass, (Argus *y*, Argus *x*)
Cross-shore axis length	Length between contour extremities (m)
Longshore axis length	Length between contour extremities (m)
Crest depth	Minimum depth of the sandbank crest (m ODN)
Area	Area enclosed by contour (m^2)
Aspect ratio	Cross-shore axis length divided by longshore axis length (non dimensional)

Table 4.2: Sandbank descriptive parameters.

4.3.1 Image spatial resolution and coordinate transformation accuracy

The sandbank descriptive parameters are derived from sets of contour coordinates so their accuracy is governed by the projection and calibration errors in relation to the spatial resolution of the domain covered by the rectified Argus image. A Teignmouth

Argus video image comprises 640 pixels in the cross-shore dimension and 480 pixels in the longshore dimension. The pixel matrix represents a finite physical area that is determined by the camera field of view and the camera-to-object distance. At the study site the rectified Argus image covers a nearshore region spanning 900 m in the longshore direction and 1000 m in the cross-shore direction (see Figure 4.7). The spatial resolution of the image can therefore be defined in terms of the pixel 'footprint' variability which concerns the physical dimensions that each pixel represents at ground plane level (i.e. where $z = 0$ within the site specific reference frame). The size of each pixel footprint is a function of the slant range between the camera and ground plane, and the relative position of the pixel within the image frame. Calculation of the footprint matrices for each camera permits the mapping of the spatial resolution of a merged and rectified video image (Figure 4.7).

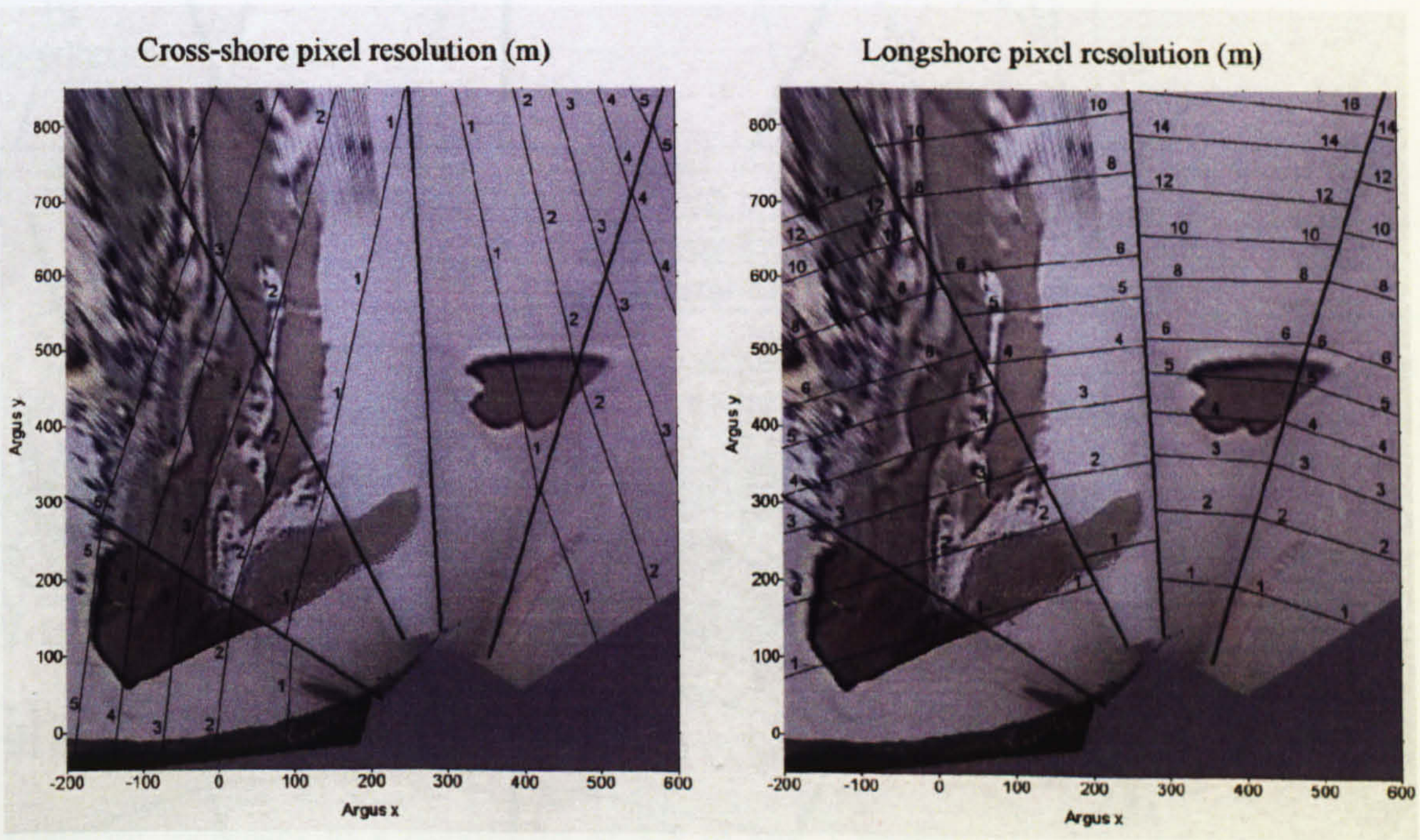

Figure 4.7: Cross- and longshore pixel footprint maps for the Teignmouth camera set up.

For both of the cross-shore and longshore pixel resolution maps the image spatial resolution degrades in a near linear manner in the cross range direction (Argus x) but as R^2 in the range direction (Argus y) hence as the target-to-camera distance increases in

the latter direction, so the footprint size stretches out significantly (Holman and Stanley, 2007).

In order to better visualise the effect of pixel resolution variability on the contour coordinate datasets, these datasets have been plotted on the pixel resolution map for the cross-shore and longshore dimensions (Figure 4.8).

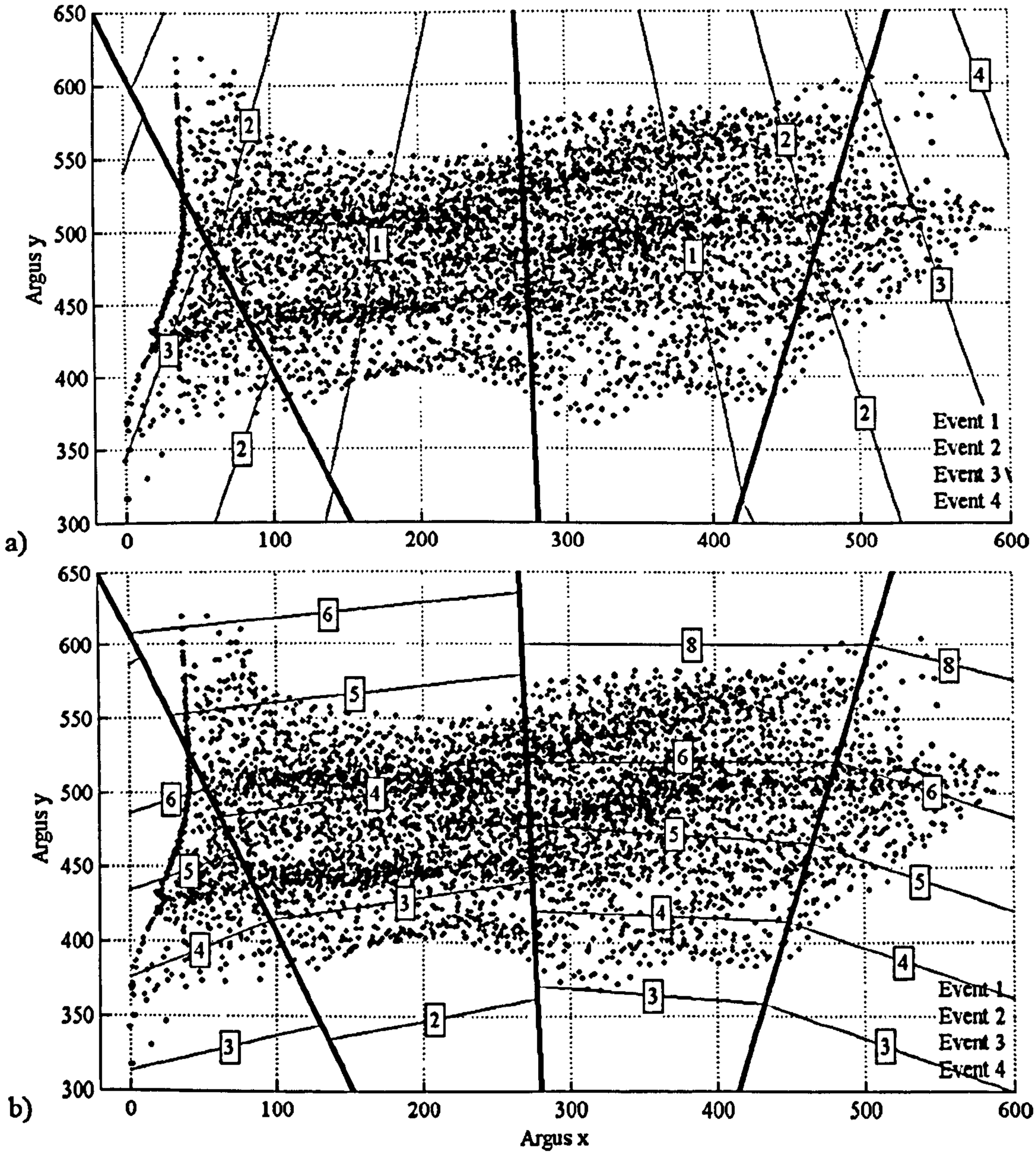

Figure 4.8: Contour coordinates dataset and pixel footprint variability in the a) Cross-shore direction, and the b) longshore direction.

The combination of the higher pixel resolution in the cross-shore dimension (Argus y) and the near linear manner in which the pixel footprint degrades in this dimension, as compared with that in the longshore direction (Argus x), means that the cross-shore coordinates are predominantly more accurate than their corresponding longshore coordinates. The onshore migration of the sandbank can be represented by three morphologic stages in the cross-shore dimension which are the offshore genesis stage, the elongation and onshore migration stage, and the shore-attachment and dissipation stage, for which qualitative definitions are provided in Section 4.4.1. The Argus coordinate ranges relating to each stage are detailed in Table 4.3 which summarises the pixel footprint variability across the stages. The greater accuracy of the cross-shore coordinates as compared with the longshore coordinates is clearly evident. In the cross-shore dimension, the pixel footprint is in unity in the range from 150 m and 400 m, and consequently the corresponding Argus x coordinates of the contours potentially have the smallest error bounds.

	Sandbank morphological stage					
	Offshore genesis		Elongation & migration		Beach attachment & dissipation	
	Coordinate range (m)	Footprint range (m)	Coordinate range (m)	Footprint range (m)	Coordinate range (m)	Footprint range (m)
Cross-shore	350 to 600	1 to 3.5	350 to 100	1 to 1.5	100 to 0	1.5 to 3
Longshore	400 to 600	4.5 to 8	350 to 550	2.5 to 7.5	350 to 600	3 to 6

Table 4.3: Summary of the pixel footprint variability between morphological stages.

In the regions further offshore and inshore of the centralised pixel unity region, the pixel footprint increases to a maximum of 3.5 m and 3 m respectively, and with the lower resolution there is the greatest potential for inaccuracy ($O(\pm 2$ m$)$) in the corresponding cross-shore coordinates. These peripheral regions concern contour coordinates associated with the sandbank's early genesis and the latter period of the beach

dissipation stage. The longshore coordinates are subject to the greatest potential inaccuracy with the pixel footprint variability in the range from 3 m to 8 m, and particularly coordinates from the furthest flank of the sandbank during the genesis and early migration-elongation stages where the pixel footprint reaches a maximum of approximately 8 m (±4 m). The pixel footprint variability for the longshore coordinates from the nearside flank of the sandbank is in the range from 2.5 to 4 m and are therefore subject to improved potential accuracy.

The accuracy of object coordinates between transformations is governed by the accuracy of the geometry solution as determined by the extrinsic camera parameters. The position of the camera is surveyed using a Leica TC1600 total station which has typical accuracies of ±3 mm in distance and $\pm 5^{cc}$ in angle ($1^{cc} \approx \pi/2 \times 10^{6}$ radians). In order to retain coordinate accuracy, the extrinsic camera angles need to be determined to an accuracy commensurate with the cross range pixel resolution (Holman and Stanley, 2007) which is estimated at 0.047° per pixel for the Teignmouth cameras (Siegle, 2003). Measuring the camera angles to this level of accuracy is physically not possible but instead their accurate derivation is achieved through the use of multiple ground control points (GCP) during the calibration procedure. Provided a sufficient number of GCP's are used (> 2), post transformation errors between measured and predicted coordinates pairs are of the order of 1 to 2 pixels (Holland *et al.*, 1997). Based on the pixel footprint variability in Table 4.3, this equates to a maximum Argus x coordinate error of 7 m which is less than 3% of the mean cross-shore axis length scale hence this error source is considered to be negligible. Furthermore, it only applies to a small subset of the Argus x coordinate dataset which are those on the lateral margins of Figure 4.8a.

4.3.2 Estimation of sandbank crest depth from Argus images

In relation to the morphodynamic evolution of the sandbank, the crest depth is an important parameter since the depth of the sandbank crest beneath the sea surface controls the extent of wave breaking during periods when the sandbank is submerged. For the purpose of this study the crest depth is defined as the depth over the shallowest part of the sandbank referenced to 0 m ODN. In the absence of high frequency bathymetric and topographic data, the Argus image archive was used to estimate the approximate crest depth position of the sandbank for the duration of the observation period. The crest depths were sampled using the same intervals as the contour time series. This was achieved by averaging the tidal levels of the Argus images in which the sandbank was first observed to emerge on the ebbing tide and *vice versa* for the flooding tide, and this was aided by making use of the images from the adjacent chronology which helped to verify the values. The diurnal tidal water level variation means that two depths were obtained for each stage of the tidal cycle and these were first averaged giving a single estimate to provide an estimate for the ebb and the flood tide stages, the mean of these was then taken to obtain the final sandbank crest depth estimate.

The accuracy of the crest depth estimates is primarily dependent on the accuracy of the Argus system time which governs the time stamp attributed to the pier mounted pressure transducer measurements in the field data archive. The Argus system time is maintained through regular automated updates via the internet so the internal clock is accurate hence this error source is negligible. A secondary potential source of error concerns water surface topography in the region encompassing the sandbank and the pier-mounted pressure transducer. In order for the tidal levels of the Argus images to be valid for the purpose of crest depth extraction, it is necessary for the local water level

topography between the pier the position of the sandbank to be level. The local water level is controlled by both the tidal cycle and by the wave generated setup. In a previous study it was discovered that tidally induced water level variations as large as 0.9 m occurred between the estuary channel and the adjacent coastal region during the occurrence of spring tides, whilst being negligible (5 cm) during neap tides (Siegle, 2003). The magnitude of the variation in local water level between the pier and the sandbank has never been quantified but the physical phenomenon decreases with distance from the channel and is considered negligible in the vicinity of the sandbanks and pier (Siegle, 2003). The effects of wave generated setup are more complex to evaluate as the extent of the setup varies both with wave height and with cross-shore position. However, Siegle (2003) established that the principle wave generated variation in water level topography in the vicinity of the migrating sandbanks occurred between the offshore and inshore extremities. This was calculated to be as high as 0.15 m with a significant wave height of 1.8 m. However, since Teignmouth is categorised as a low wave energy environment, the incidence of wave heights over 0.5 m is occur less than 10% of the time (Chapter 3) and thereby the effect of wave generated setup on the crest depth dataset is also considered to be negligible. The uncertainty in the crest depth approximation in relation to the methodology was evaluated by generating error bars derived from the depth of the corresponding flood- or ebb-averaged value. A comparison of the estimated crest depths with the surveyed bathymetries indicates the method to be robust. For example, the surveyed sandbank crest depth from the May 2003 Coastview field work determined that the minimum crest depth was at approximately 0 m ODN (Figure 4.6), and this is in good agreement with the image derived crest depth estimate for the same period (Figure 4.22c).

4.4 Results

4.4.1 Introduction

The primary objective of the video work is to characterise the morphological evolution of the onshore migration events in the ebb tidal delta sedimentation cycle in terms of the geometry of the feature, and to quantify the dynamics based on the centre of mass. Three generic morphological stages were introduced in Section 4.3.1 (see Table 4.3) and these are defined as follows:

1. Offshore genesis: the initial period after the first observation when the sandbank is usually observed to grow in area but with an approximately stationary centre of mass (COM) position.
2. Elongation and migration: the sandbank's COM propagates towards the beach which is observed to coincide with elongation in the cross-shore dimension and growth in area
3. Attachment and beach dissipation: the shoreward extremity of the sandbank merges with the beach face forming a shore-attached transverse bar feature which gradually diminishes in area and cross-shore extent.

The genesis stage in the contour time series begins after the sandbank has first been observed in the Argus image frame during the spring tide observation window. The first contour is only extracted when the sandbank has accreted sufficiently in vertical extent to be observable over consecutive tides which does not necessarily coincide with the first observation. The end of each event time series was determined when it became no longer possible to properly delineate the sandbank from the surrounding beach morphology. The morphological behaviour outlined above is manifest in all four of the events though despite the similarities there are also significant differences in the

observed behaviour between individual events which are elaborated upon in the following sections.

4.4.2 Contour times series and their qualitative description

Notes on the presentation of the contour time series

The contour time series are presented in chronological order from event 1 to event 4. The series are presented in their entirety where practicable with the contours being displayed in a panel of plots comprised of up to six contours per row. The contour plots are focused on the Argus image area between 0 m to 650 m in the cross-shore dimension (Argus x) and 300 m to 700 m in the longshore dimension (Argus y). Representative major and minor axes have been added to the contour plots with the intersection of the two being the position of the COM. The image date, the tidal level at the time the contour was extracted and the cross-shore migration rate computed from the difference in the cross-shore coordinate of the COM between consecutive contours are displayed in the individual plot windows. Episodes of onshore migration of the COM are denoted by negative values and *vice versa* for offshore migration episodes. The EDINA coastal boundary, which has been defined as the onshore limit of the migration of the sandbank for the purpose of this study is depicted by a grey shaded region and this represents the boundary denoted by the Teignmouth seawall defence on the main beach in accordance with the Ordnance Survey map data. The inter-tidal terrace typically occupies the cross-shore region between 50 m and 175 m offshore. The figures of the individual event contour time series are followed by plots of the root-mean-square (H_{RMS}) wave height and period (T_{RMS}) for the time corresponding to each set of contours. The measurements were obtained from the pier-mounted transducer and gaps in the wave time series correspond to periods of system downtime. The data are

presented in order to provide the reader with a general overview of the wave energy conditions hence the trends in the data have been highlighted using a 7 day running mean. The time series are characterised by calm and stormy periods when typical maximum H_{RMS} values are in the range 1 to 1.2 m conditions. The T_{RMS} time series oscillate between fetch-limited and long period swell conditions with typical values in the range 5 to 14 s. From the time series for event 2 the seasonal signal in wave energy levels is readily discernible (Figure 4.12).

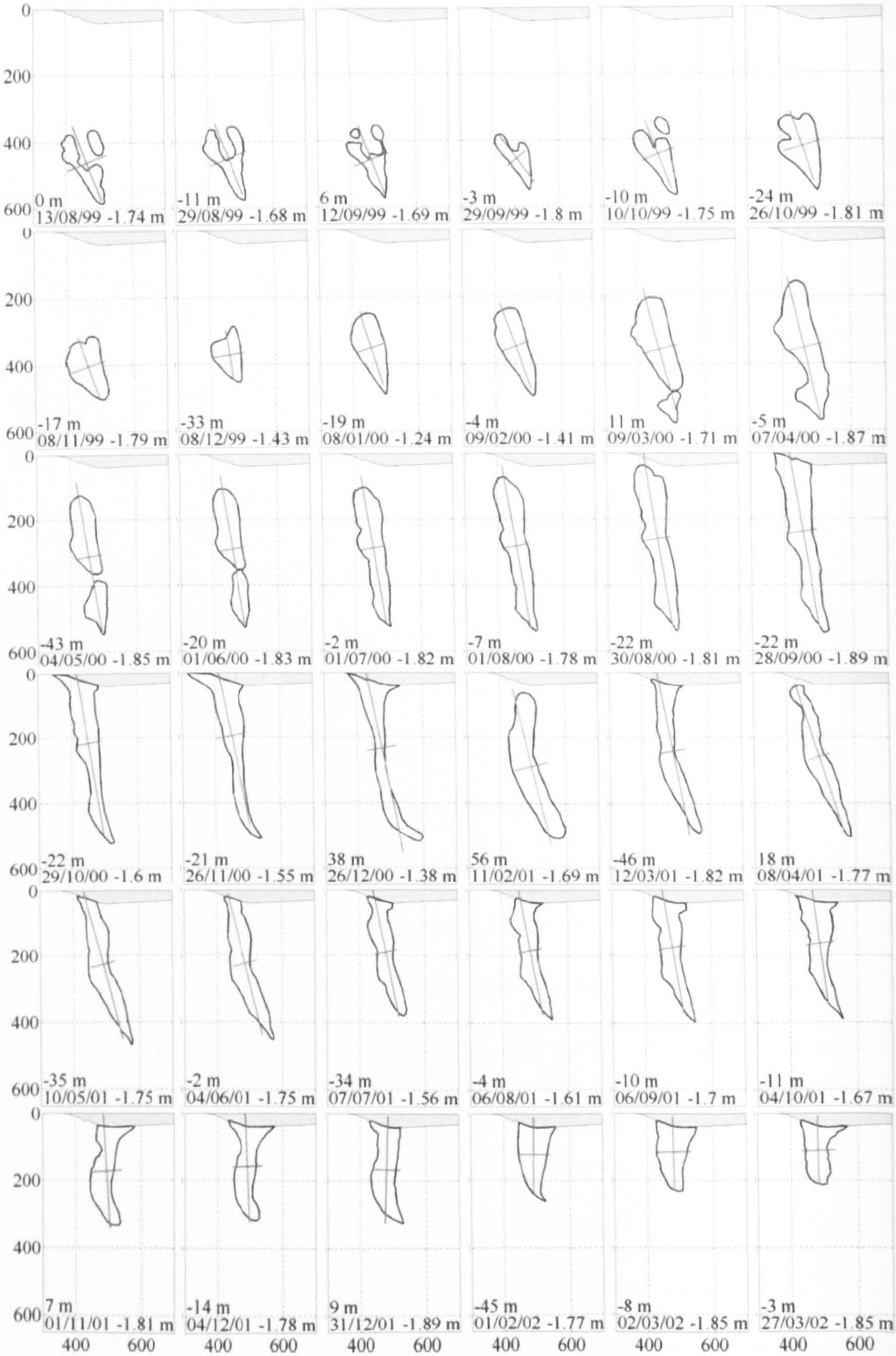

Figure 4.9: Event 1 contour times series.

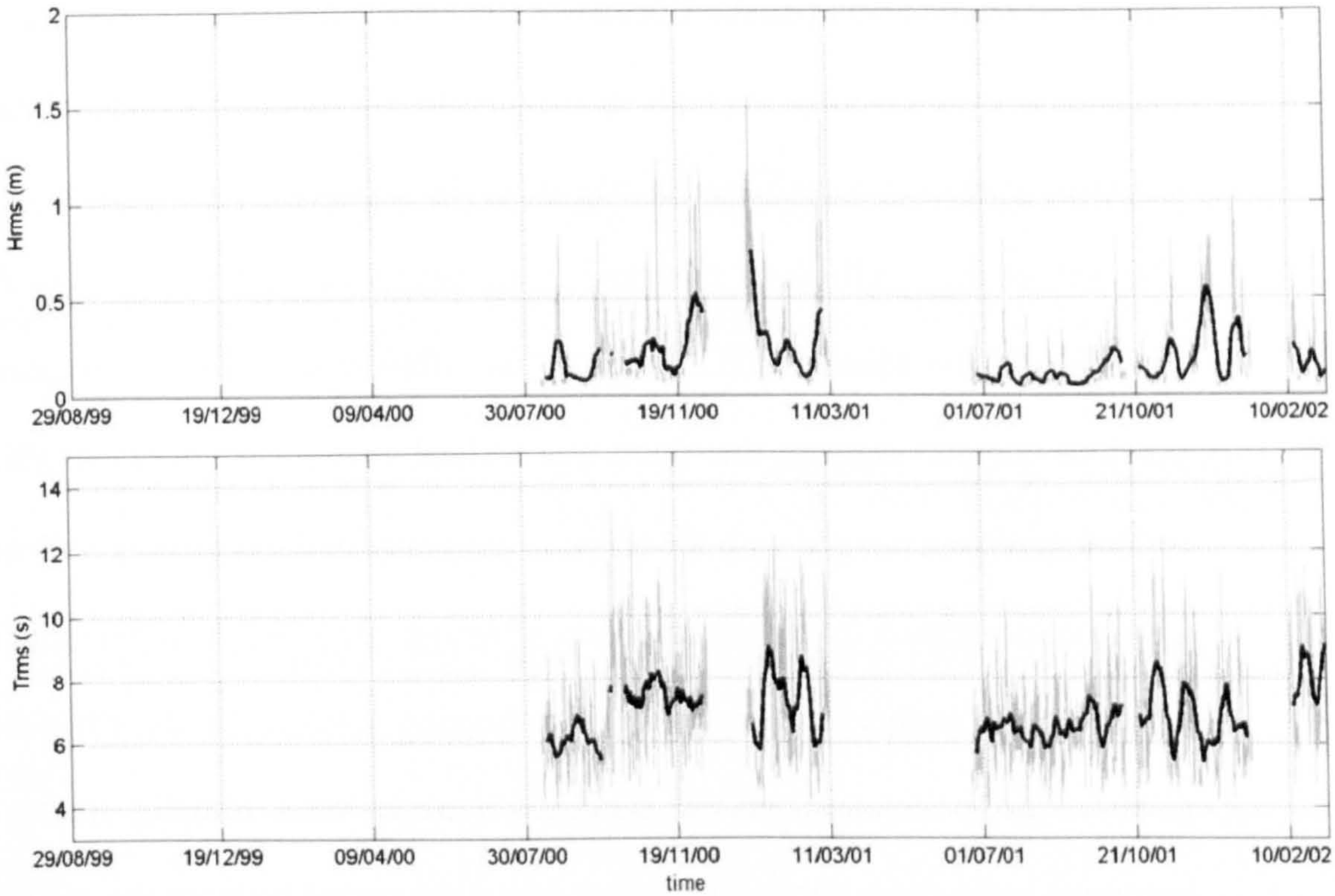

Figure 4.10: Event 1 root-mean-square wave height (upper panel) and period (lower panel) time series. Bold lines denote a 7-day running mean.

Event 1

Event 1 is the most enduring of the four observed onshore migration events with 957 days between the start and end dates of the contour time series and 66 individual contours. A subset of the contours is presented comprising every other contour excepting the first seven which are without omission. The January 2000 contour is also absent from the time series due to there having been a short period of station downtime. The COM of the first contour in event 1 is located at 463 m and 464 m in the offshore and longshore dimensions respectively, and the orientation of the major axis is towards the estuary mouth. The sandbank genesis is evident in the image archive as early as April 1999 but it was not until October 1999 when the first contour is extracted as this is when it first becomes clearly defined in the Argus images at the target tidal reference level. The event 1 genesis is marked by a horse-shoe shaped morphology which is not observed in any of the subsequent events. The genesis lasts until early October 1999, after which the COM is observed to begin migrating shoreward, with elongation first

becoming evident between the December 1999 and January 2001 contours. The event 1 elongation is noteworthy for both its magnitude and duration which culminates in the sandbank spanning approximately 550 m in the cross-shore dimension by May 2001. The area of the sandbank at this time is the largest of the entire contour dataset. The extension of the March 2000 contour in the offshore direction as compared with the previous contour suggests that there was a shoal coalescence event in which a newly formed sandbank merged with the offshore extremity in the preceding four week period. This was confirmed from the inspection of images from the preceding and subsequent weeks and is analysed in more detail in Section 4.4.3.1. As the elongation process persists, the orientation of the sandbank's major axis initially rotates clockwise becoming more shore normal. However during the period between the end of December 2000 and mid-February 2001, the outer half of the sandbank rotates anti-clockwise re-orientating itself towards the estuary mouth and giving it the appearance of having been bent. The shoreward end of the sandbank first encroaches on the inter-tidal terrace during April 2000, initially becoming shore-attached towards the end of September. During the subsequent 6 month period, the transverse sandbank is seen to twice become detached again suggesting successive periods of erosion and accretion. The offshore end of the sandbank begins to recede during the summer of 2001 which causes it to return to a more shore-normal orientation. The sandbank becomes fully dissipated early in the summer of the following year. It should be noted that due to technical problems with the Argus station and pier mounted pressure transducer in January and February 2001, there is a period of just over one month during which no contours were obtained causing a two point data gap in the time series.

Figure 4.11: Event 2 contour time series.

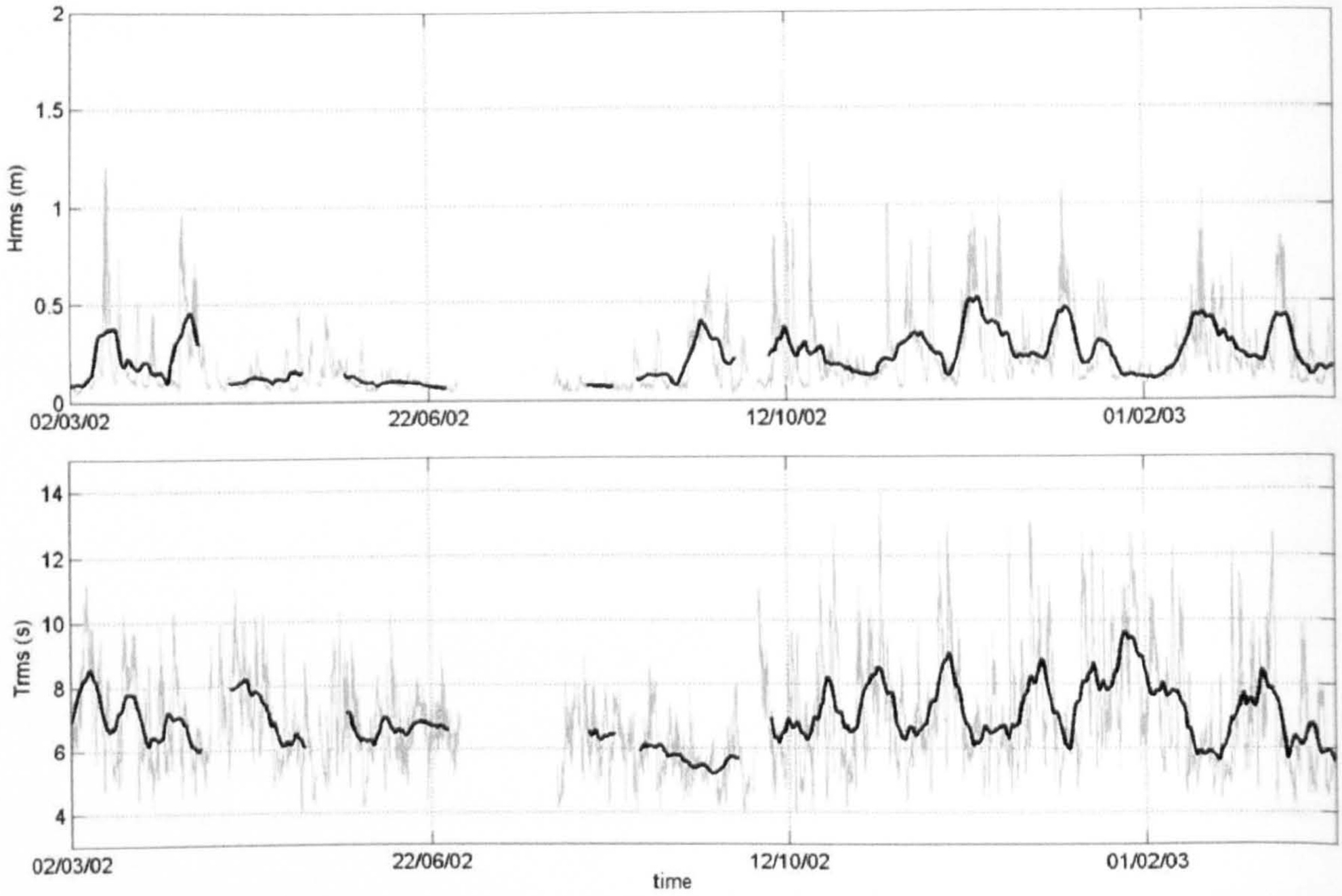

Figure 4.12: Event 2 root-mean-square wave height (upper panel) and period (lower panel) time series. Bold lines denote a 7-day running mean.

Event 2

The event 2 onshore migration is the third longest in the series spanning 429 days between the first and last observations and comprising 30 contours which are presented in their entirety. The genesis of the event 2 sandbank first became apparent in December 2001 though it was not until February 2002 when it became clearly defined that first contour of the time series is extracted. The initial contour has a COM located 410 m offshore and 514 m longshore, an elliptic morphology and with the major axis orientated towards the estuary mouth. The genesis period is considered to have ended by the beginning of March 2002 as the sandbank is observed to begin its shoreward migration. The onset of the associated elongation in morphology in this event is delayed as the process first becomes apparent in September which is several months following the start of the onshore migration phase. Once the elongation process begins, it occurs over a relatively short period lasting approximately 6 weeks and culminates in attachment and a major axis length of approximately 350 m. The COM of the event 2 at

the start of the sandbank's elongation was between 80 m and 90 m further inshore when compared with event 1. The shoreward growth of the morphology results in a clockwise rotation of the major axis which becomes orientated in a near shore-normal direction. Attachment occurs in the latter part of October 2002 after which the offshore extremity of the sandbank is observed to gradually diminish in cross-shore extent and become fully dissipated by April 2003.

Figure 4.13: Event 3 contour time series.

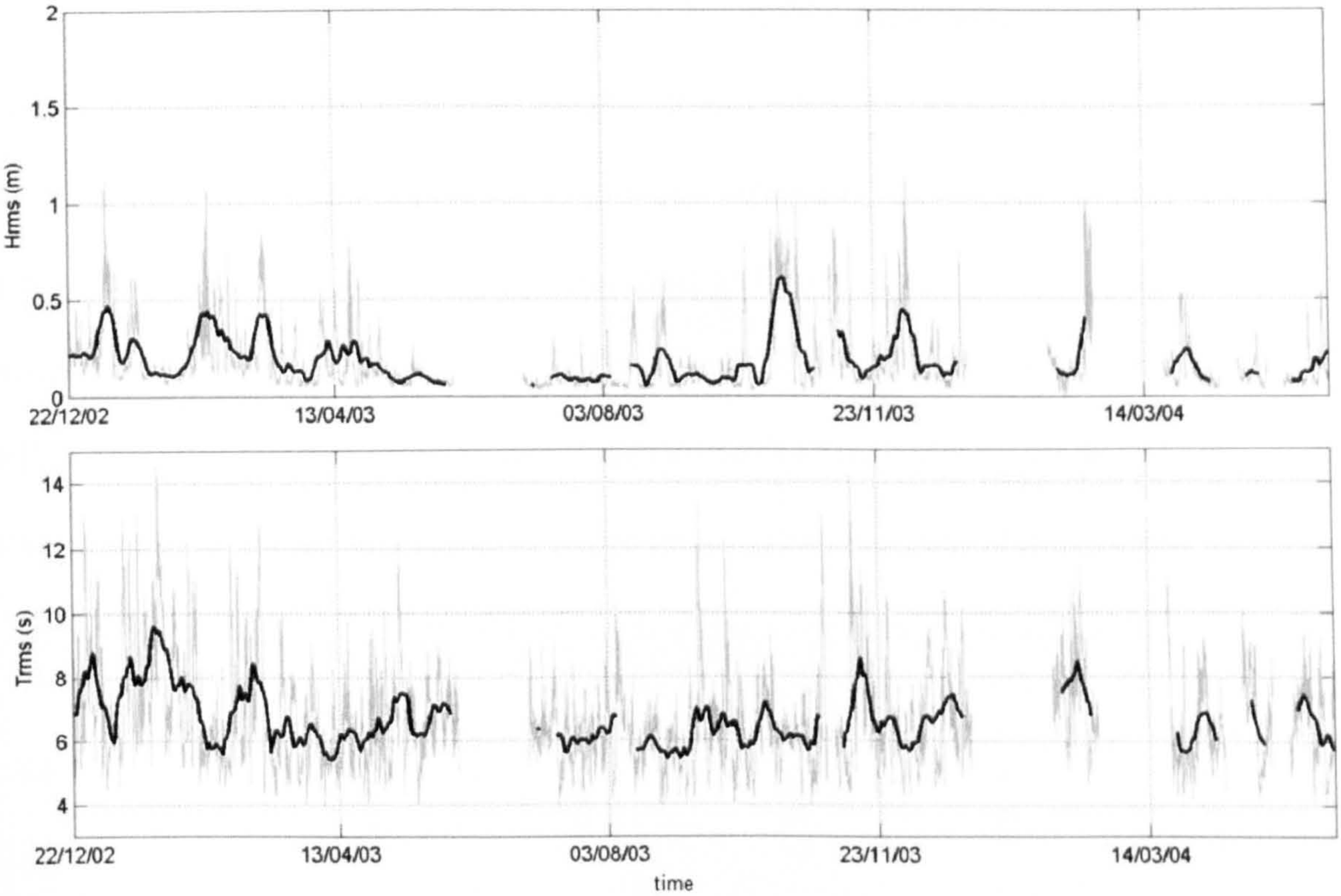

Figure 4.14: Event 3 root-mean-square wave height (upper panel) and period (lower panel) time series. Bold lines indicate a 7-day running mean.

Event 3

Event 3 constitutes the second longest time series with 559 days between first and last observations and comprising 39 contours of which those on the 30th June 2003, 22nd February 2004, and the 18th June 2007 have been omitted from the presented times series. The genesis of the event 3 sandbank was first detected as early as April 2002 when it was observed to be part of the submerged terminal lobe at the distal end of the estuary channel. The feature was subject to intermittent erosion and accretion over the following 8 months and hence it was frequently absent from the low tide Argus images. The first contour was extracted in December 2002 after the sandbank had accreted sufficiently in elevation to remain in view at the target tidal level. The sandbank morphology is initially elliptic with the COM located 482 m offshore and 532 m longshore, and with the major axis orientated towards the estuary mouth. The genesis stage is brief but marked by the morphology of the feature becoming more circular and gaining in area. At then end of January 2003, the sandbank is observed to begin

migrating shoreward with the elongation first becoming noticeable in March. During the six month period to September the shoreward elongation continues in a gradual manner and the subsequent clockwise rotation of the major axis which evolves to form a shore normal or transverse bar. The transverse bar becomes shore-attached by early October 2003 at which time the feature reaches its maximum length of approximately 350 m. The shore-attached end of the morphological feature initially broadens in the longshore dimension before narrowing again as the offshore end begins to decrease in cross-shore extent. The feature becomes fully dissipated by the end of summer 2004.

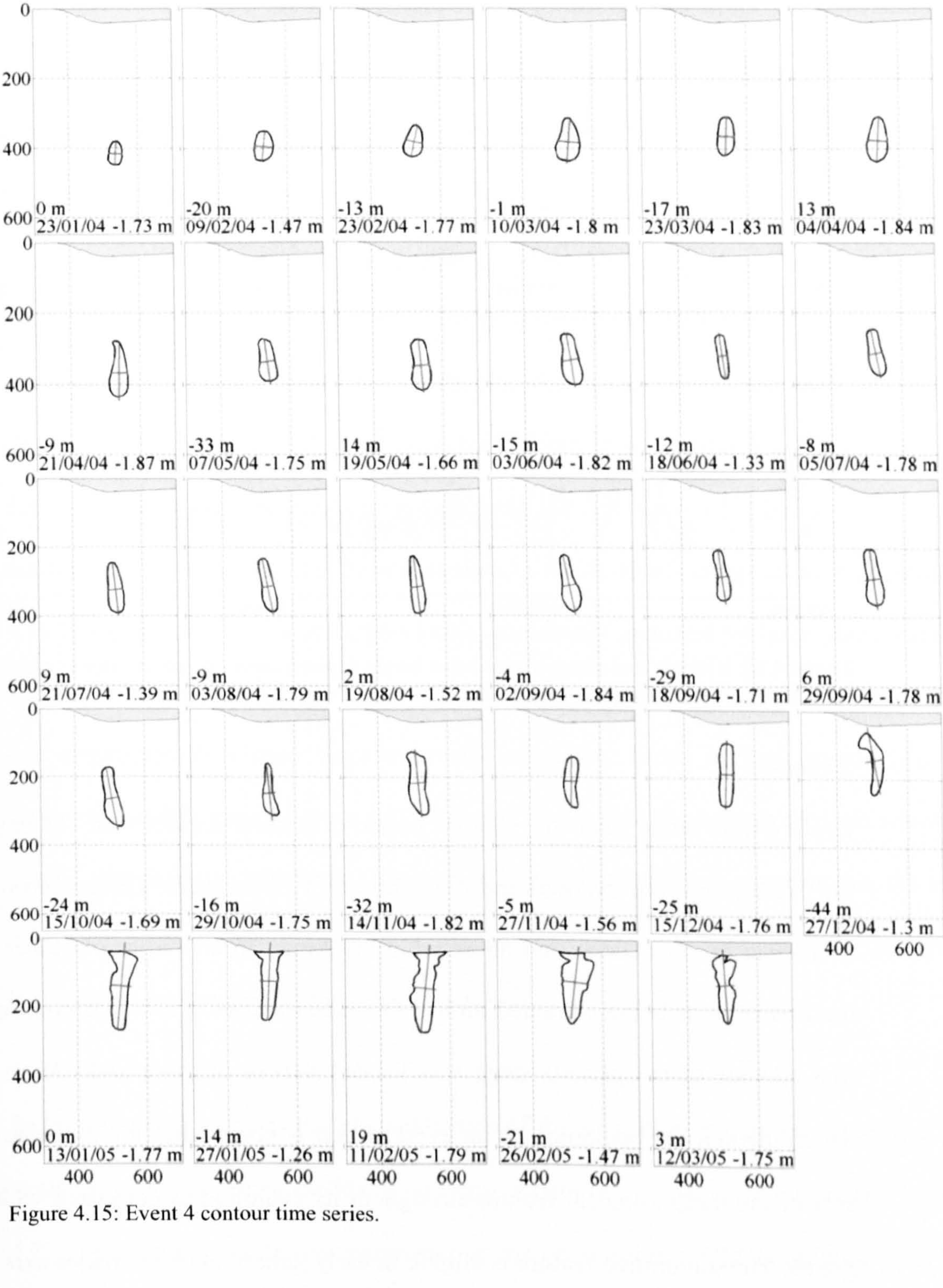

Figure 4.15: Event 4 contour time series.

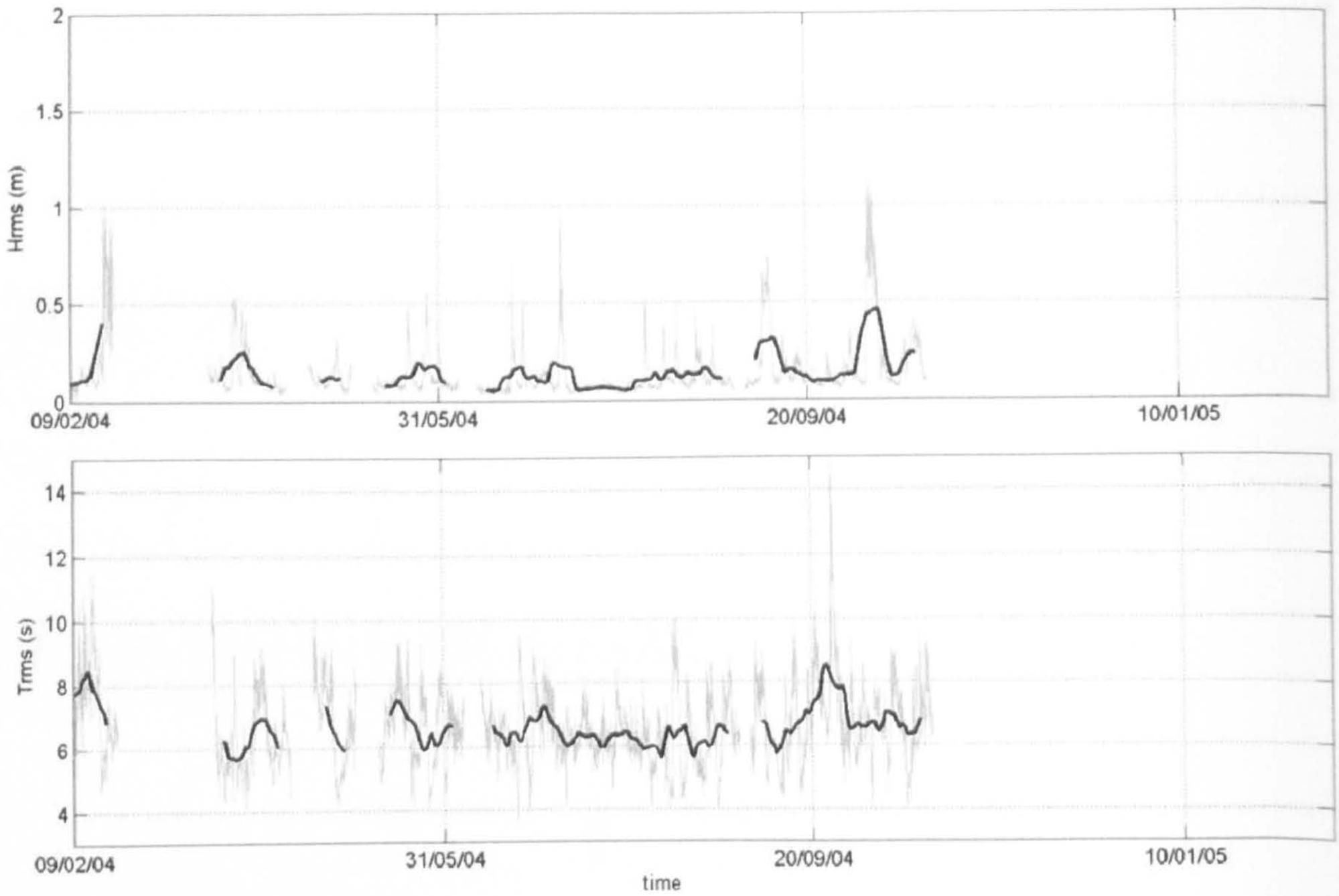

Figure 4.16: Event 4 root-mean-square wave height (upper panel) and period (lower panel) time series. Bold lines indicate a 7-day running mean.

Event 4

Event 4 time series spans the shortest period of contour dataset with 414 days between the first and last observations and is comprised of 29 contours. The genesis of the event 4 offshore sandbank was first observed in the Argus archive in late October 2003 with the first contour being extracted on the 23rd January 2004. The COM coordinate of the first contour of the genesis stage was located 416 m offshore and 535 m longshore which marked the beginning of an event which is noteworthy for the relatively small area of the morphological feature throughout its evolution as compared with the other events. The diminutive feature is elliptic in early genesis with the major axis orientated in a near shore-normal direction. The genesis stage is brief as the COM is observed to begin migrating shoreward from the outset with the process of elongation becoming evident in the third contour dated the 23rd February 2004. The morphological feature continues to be subject to gradual elongation for the remainder of the time series reaching a length of 187 m before becoming shore-attached. Thereafter the sandbank

reaches its maximum cross-shore length at 263 m in February 2005. Shore-attachment occurs at the end of December. The final contour in event 4 of the 12th March 2005 depicts a sandbank that is in a partially dissipated state but owing to station downtime, no further images of the feature were available.

To summarise the contour time series clearly define the onshore migration phase of the morphological behaviour of the sandbanks the Teign ebb tidal delta in which similarities can be observed. The individual events show similar plan form geometry during their evolution which is in contrast to the period between 1964 and *c.*1990 as per the findings of Robinson (1975) and as seen in the S. Hook image archive (Appendix A1) The migration events were previously commonly manifest by large shore-parallel swathes of sediment (e.g. top panel of Figures A1 and A3; top left panel, Figure 3.5) that sometimes developed large transverse crescentic forms as they approached the shore (e.g. middle panel, Figure A3). However, the events depicted in the time series all evolve into elongate transverse forms prior to attachment which suggests that the inlet ebb shoal system has undergone a significant change in sedimentation processes between the two periods in the inlet's evolution.

In the following sections the characteristics of the migration events are quantified and analysed using the set of sandbank descriptive parameters that were introduced Section 4.3. The primary descriptive parameter is the cross-shore COM coordinate which is used to quantify the cross-shore migration rate and hence the dynamic of the migrating sandbanks. The remaining parameters which are area, aspect ratio (cross-shore/longshore axis length) and eccentricity are used to define the plan form geometry of the features through their morphological evolution.

4.4.3 Temporal variability in sandbank descriptive parameters

4.4.3.1 Cross-shore and longshore COM position

The COM cross-shore and longshore time series for each onshore migration event are presented in Figure 4.17 along with the approximate time of sandbank shore-attachment as denoted by hatched lines. The cross-shore COM time series for each onshore migration event are also presented in Figure 4.17 in which the most significant feature is the persistent onshore migration of the sandbank and the relative paucity of offshore directed migration. This persistent onshore migration of a sedimentary feature exposed to wave action is atypical morphodynamic behaviour when compared with features on open coast beaches which typically migrate both on and offshore, e.g. shore parallel bar dynamics (Van Enckevort and Ruessink, 2003a). However, at tide dominated and mixed energy inlets the episodic or quasi-periodic onshore directed migration of ebb tidal delta sandbanks is the typical morphodynamic behaviour of such features (Section 2.2.1). In contrast to the dynamic cross-shore position variability, the longshore position of the onshore migration events is relatively static and constrained to the region between 450 and 550 m alongshore. The time series suggest that the longshore position of the COM of the sandbanks has slowly migrated northwards by a maximum of approximately 100 m between events 1 and 4. The northward trend in the alongshore migration COM position is likely to be a function of the longshore position at genesis where sandbank sediment transport is governed by waves, tides and river discharge (Figure 3.6) (Siegle, 2003). Therefore over macro-times scales (years) the northward trend in the longshore position at genesis may be indicative of a long term gradual increase in the combined tidal and river discharge component of flow.

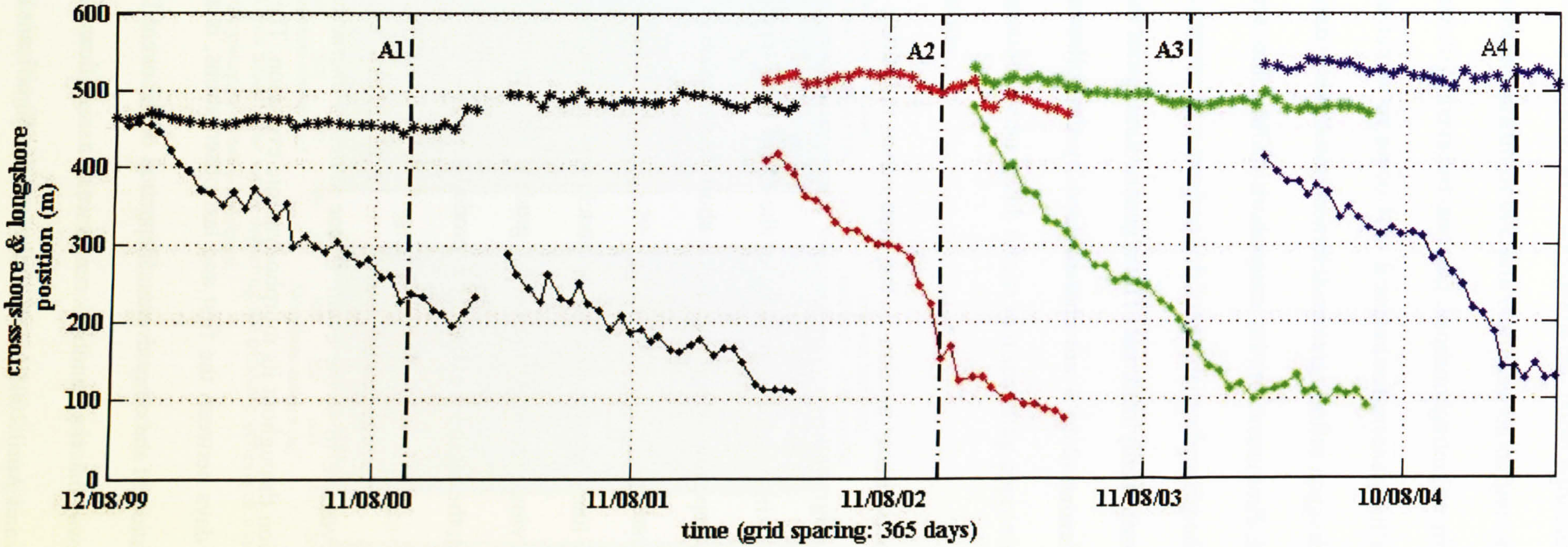

Figure 4.17: Time series of the cross-shore (points) and longshore (stars) coordinates of the sandbank's centre of mass position for all events. The vertical hatched lines indicate the approximate time of sandbank shore-attachment. Event colour key: event 1: black, event 2: red, event 3: green, event 4: blue.

In the cross-shore dimension, the initial period of offshore genesis for all of the events is centred on the region between 400 and 500 m offshore after which the COM of the sandbanks begin migrating onshore. Genesis for event 1 occurs in autumn (August, 1999), whereas the genesis for events 2 to 4 occur in winter between December and February which may reflect greater sediment availability during the higher energy winter months. Prominent in the cross-shore COM time series are clear generic similarities in the general variability of this parameter for events 2 to 4, whilst the event 1 time series is markedly different. These generic similarities in the cross-shore COM variability for events 2 to 4 are characterised by the following three chronological stages:

1. An initial quasi linear section in the time series indicating a period of relatively steady onshore migration.
2. A brief period in which the gradient of the COM time series is observed to flatten briefly before steepening which signifies a short deceleration in the onshore migration rate then acceleration.
3. A final quasi linear section after shore-attachment in which the gradient is less steep than in the previous sections, indicating gradual deceleration during the dissipation process in which the offshore extremity is eroded.

In contrast to events 2 to 4, the event 1 time series is characterised by a quasi-linear onshore migration throughout its morphodynamic evolution. The protracted duration of event 1 at 958 days between the first and last observations, is approximately twice as long as the duration of the other events. Inspection of the event 1 contour time series in Figure 4.9 shows that the sandbank underwent a significant morphological change between March and April 2000 in which there was a significant addition of sediment to

the offshore extremity of the sandbank which first becomes noticeable in December 1999. This morphological change is documented in Figure 4.18 which comprises a time series of three Argus images spanning the period from December 23rd 1999 to April 7th 2000 in which the supply of the new sediment to the offshore extremity is clearly evident. The cross-shore location of the new sediment suggests that it is the genesis of a new offshore sandbank which merges with the event 1 sandbank's offshore extremity. The merging of the two sandbanks occurs due to the offshore extremity of the event 1 sandbank still being in close proximity to the distal end of the inlet's ebb channel where genesis ordinarily occurs. Consequently, event 1 is comprised of the aggregation of two onshore migration events which results in it spanning approximately 550 m in the cross-shore dimension.

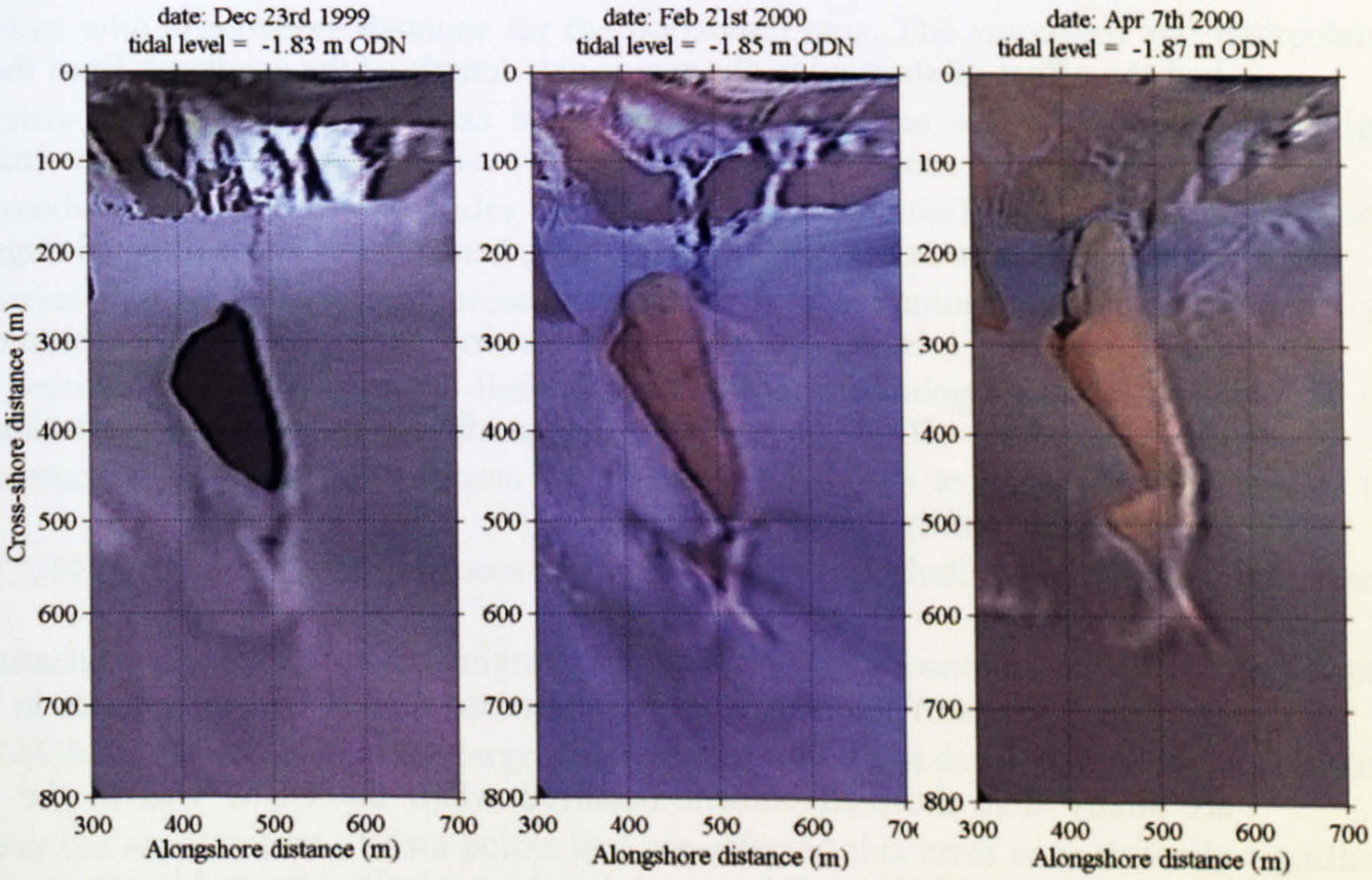

Figure 4.18: Argus image time series depicting the offshore genesis of a new sandbank and its subsequent merging with the elongate event 1 sandbank.

This resulting sandbank is significantly larger than the subsequent features (Figure 4.24), which provides an explanation for its atypical cross-shore COM position time series in relation to the other events. A further distinguishing feature of the event 1

cross-shore COM position time series relates to the period between the end of November 2000 and mid February 2001, when there is a significant offshore trend in the position of the COM of the shore-attached sandbank. This is the only significant offshore movement in the sandbank COM observed in the study. During this period the COM moved offshore by approximately 100 m, which partly coincided with the period of station downtime. This resulted in the loss of two contours creating a discontinuity in the cross-shore COM position time series. Inspection of the available contours (Figure 4.9) and Argus images for the period indicate that the offshore migration is caused by the erosion of the shore-attached extremity of the sandbank which subsequently becomes detached from the beach face. This is a hypothesis based on the observational evidence as the shoreward extremity appears to recede and become disconnected but the mechanism for this is unclear. The erosion of the shoreward extremity appears to have had the effect of shortening the major axis length of the sandbank from the shoreward extremity by as much as 70 m, whilst the position of the offshore extremity remained stationary at approximately 500 m offshore, hence the offshore directed migration of the COM. After the missing observations in the time series, the initial onshore migration of the cross-shore COM position of the sandbank reflects the reattachment of the shoreward extremity during March 2000.

Two final points of interest regarding the cross-shore COM time series in Figure 4.17 are firstly that shore-attachment occurred when the COM was in the cross-range between 130 and 240 m offshore and that this typically occurred in autumn (September-October) though in event 4 it was a couple of months later (January 2005). Secondly, there is typically an overlap between events such that genesis occurs during the dissipation of the previous shore-attached sandbank. Therefore the shore-attached feature is subject to a degree of sheltering of the incident wave energy by the offshore

sandbank which is a function of both the area of the latter feature, and of the duration of the temporal overlap. The time series indicate that the duration of temporal overlap is shortest between events 1 and 2 when compared with subsequent events. Therefore the sheltering effect of the event 2 offshore sandbank in genesis on the wave energy reaching the event 1 shore-attached sandbank is lower than in subsequent events hence this may have assisted the dissipation process.

4.4.3.2 Cross-shore migration rate

In Figure 4.19 the cross-shore COM position time series of the individual events have been plotted with the raw, and smoothed and interpolated cross-shore migration rate. In Figure 4.20 on the following page the same migration rate data are presented in scatter plots with cross-shore distance for the horizontal axis. The smoothed and interpolated cross-shore migration rate has been plotted on the time series in order to highlight trends over the meso time scales (months) which are partially obscured in the raw time series due to the inherent noise introduced by the contour extraction methodology (Section 4.2). The primary limitation of the methodology causes variation in the extraction depth of the contours which has been shown to cause displacement of the COM position of the contours extracted from the shallowest depths after shore-attachment. The estimated migration rate error for a contour extracted from depths O(0.6 m) shallower than the target tidal level is O(0.33 m.day^{-1}) using typical gradients. For the small subset of data points that are affected this error is statistically significant in relation to the migration rate variability which predominantly fluctuates in the range 0 to 2 m.day^{-1}. The smoothed migration rate time series were calculated by first applying a three point average to the raw cross-shore COM time series and then interpolating the data on to a monotonic 7 day sample frequency.

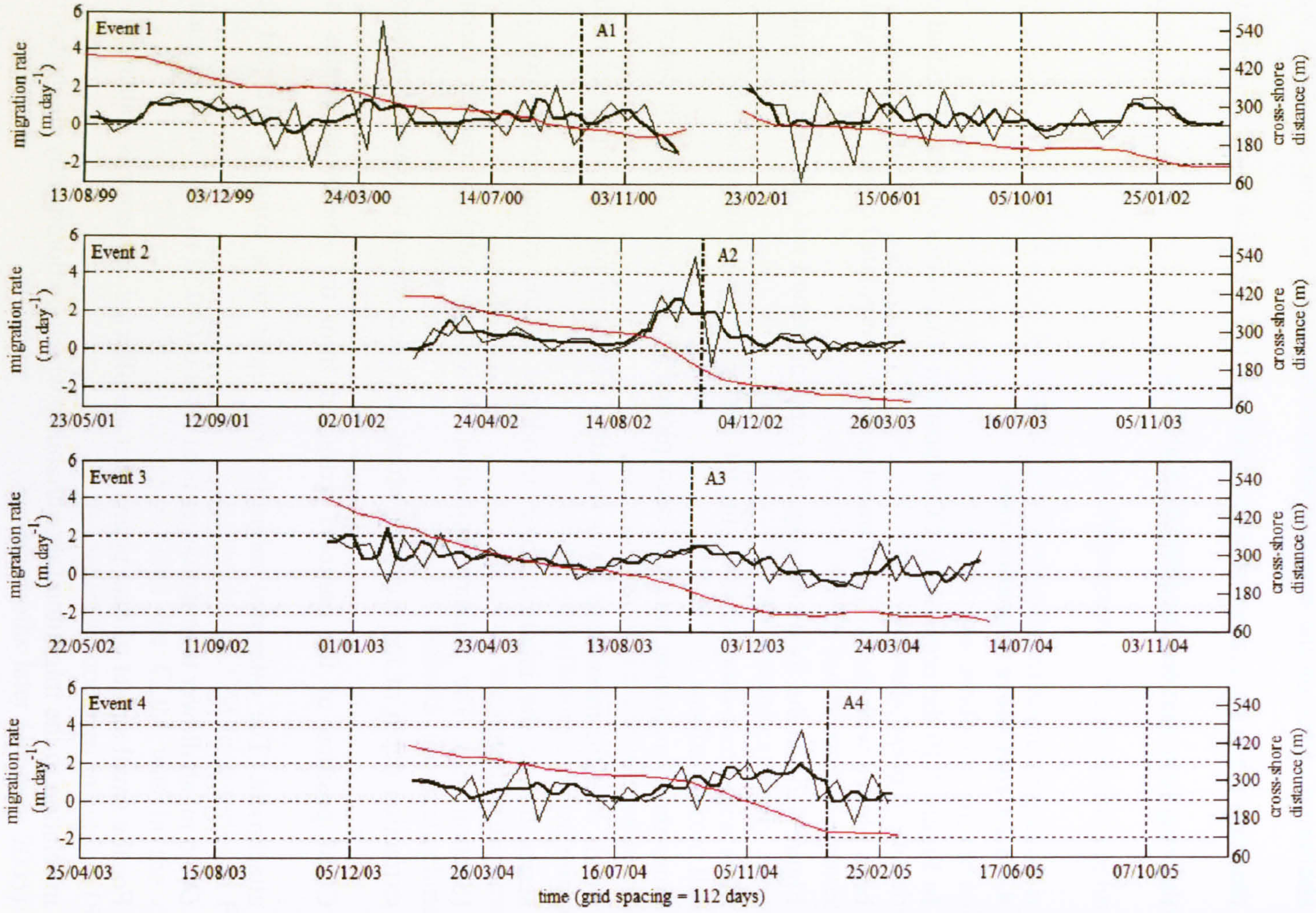

Figure 4.19: Time series of cross-shore COM position (red line), raw migration rate (thin black line) and, smoothed and interpolated migration rate (thick black line) for events 1 to 4. The lines denoted by A1 to A4 (vertical) and S1 to S3 (horizontal) indicate the approximate time of shore-attachment and common trends (medium to long term) in average migration rate respectively. Key: raw cross-shore COM position: red line, raw migration rate: thin black line, smoothed & interpolated migration rate: thick black line.

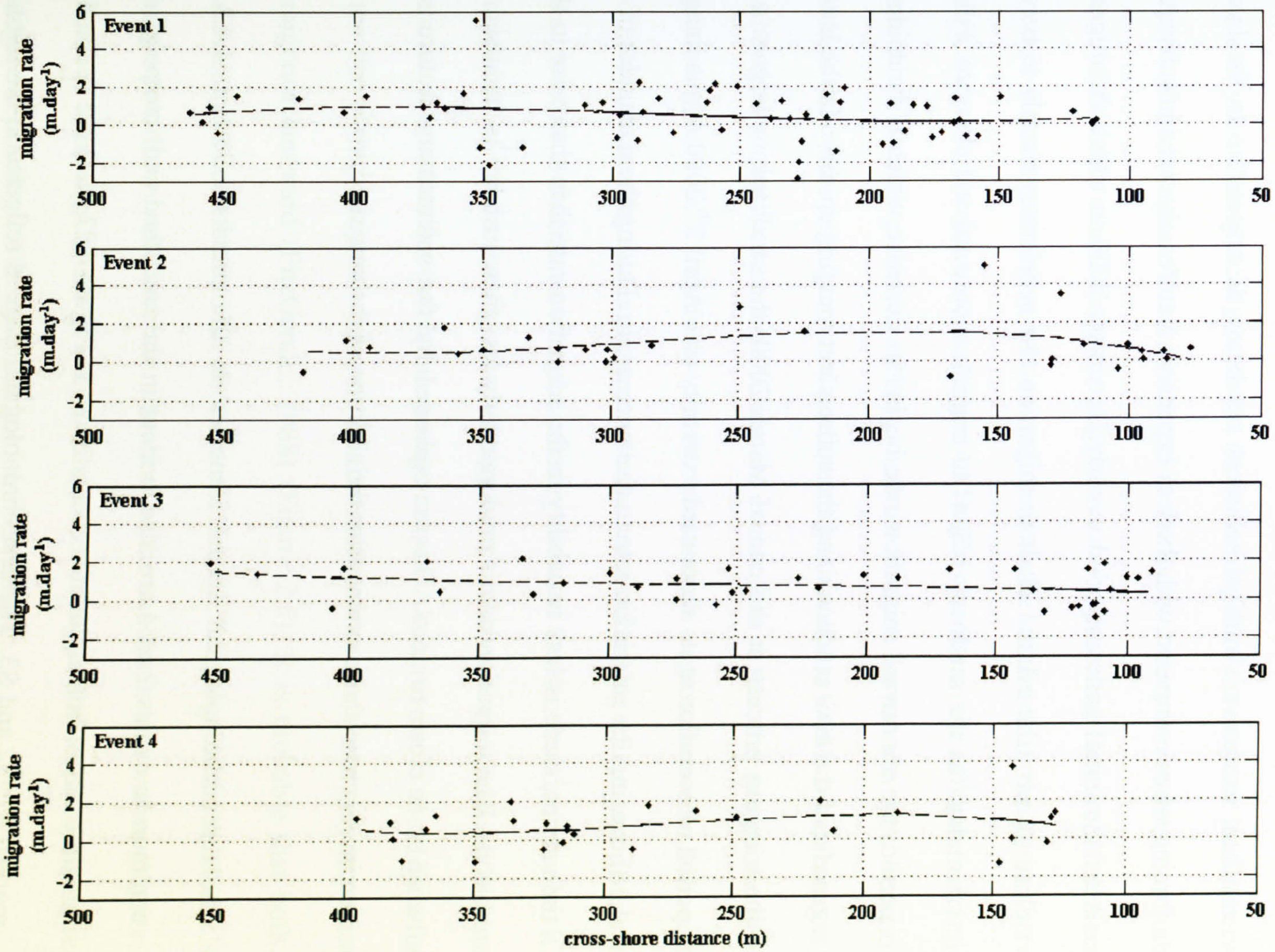

Figure 4.20: Scatter plots of cross-shore COM position versus migration rate for events 1 to 4 with best-fit trend-line (dashed line) added.

In Section 4.4.3.1 it was determined that the event 1 sandbank had an atypical cross-shore COM position time series when compared with the other events on account of it having been formed from the coalescence of two offshore sandbanks. The behaviour is also manifest in the migration rate time series due to the COM parameter of the resultant extensive swath of sediment not being as responsive to the hydrodynamic forcing when compared with the less expansive features observed in subsequent events. After the initial genesis period in early December 2000 in which the migration rate is close to zero, the event 1 onshore migration rate accelerates sharply to between 1 and 1.5 $m.day^{-1}$ as the sandbank begins to migrate shoreward and elongate. Following this period, the shoreward migration rate begins to decrease which is coincident with the genesis of the new sandbank and the subsequent merging episode. In the latter stages of the merging process at the end of March 2000, the sandbank undergoes a significant period of accretion at its shoreward extremity (see April 7th 2000 Argus image in Figure 4.18) causing the migration rate to rise once again. During the remainder of the event 1 time series, there is less variability in the migration rate than that prior to the merging episode. The migration rate is predominantly less than 1 $m.day^{-1}$ with sustained periods when it is close to zero. This is explained by the sedimentary feature reaching its maximum cross-shore extent after the addition of the new sand.

The three chronological stages identified in the previous Section 4.4.3.1 that are common to events 2 to 4 are also evident in the smoothed and interpolated migration rate time series. In the plots for events 2 to 4 in Figure 4.23 these are denoted by regions marked S1, S2 and S3. The first chronological stage is reflected in the initial section of the COM migration rate time series by a sustained period of gentle deceleration in which the smoothed onshore migration rate reduces from between 1 and 2 $m.day^{-1}$ to approximately zero (S1). A regression analysis of this chronological stage in the

migration rate time series produces similar deceleration values for the three events where event 2 is -0.006 m.day^{-2} (R^2 = 0.9), event 3 is -0.007 m.day^{-2} (R^2 = 0.8) and event 4 is -0.004 m.day^{-2} (R^2 = 0.4) respectively (data not presented). In addition to this, all three deceleration periods terminate within three weeks of each other relative to the time of year. This typically occurs at the latter stages of the summer period between late July and mid August. The initial trend in the event 2 time series does not quite follow that of the other events since the migration rate begins close to zero before acceleration occurs following an influx of new sediment to the sandbank in the period between the first and second contours (see Figure 4.11). This results in the offshore extremity of the sandbank accreting further offshore and an increase in its area (see Section 4.4.3.5) which delays the initial onset of onshore migration of the COM. It can be seen from the smoothed migration rate time series for events 2 to 4 that the end of the deceleration period occurs in a relatively narrow cross-shore region between 260 and 320 m offshore. When this is considered with the seasonal timing of the end of this stage it is not possible to determine what the primary cause of the deceleration may be. It could be a product of the decreasing wave energy which reaches a minimum in the latter part of the summer when the deceleration stage ceases. Alternatively, it could be a function of the decreasing temporal exposure of the sandbank to the wave driven processes as it migrates landward (FitzGerald, 1988) (Figure 2.5). It is probable that both of these mechanisms contribute to the deceleration through this stage of the sandbank's onshore migration. However, since the elevation of the sandbank also varies (Figure 4.21 and 4.22) in time then this will either enhance or mitigate the level of exposure to some degree depending on the magnitude of the variability.

The second chronological stage (S2) involves a period in which the onshore migration rate accelerates as the sandbank approaches and attaches to the shore and this is

particularly pronounced in the event 2 time series. The marked onshore directed acceleration in the event 2 time series is caused by significant onshore directed changes in the cross-shore COM position between observations during this period. These increases were primarily the result of a period of significant elongation in the sandbank's morphology of *O*(150 m) during September and October 2002 which culminates in shore-attachment (see Figure 4.11) The onshore acceleration of the event 2 sandbank's COM increased the migration rate from an initial value close to zero to a peak of 2.7 m.day^{-1}. This is the highest migration rate of the four time series and a regression analysis shows the associated acceleration to be 0.06 m.day^{-2} (R^2 = 0.95) and is an order of magnitude larger than the initial deceleration (S1). The less pronounced onshore accelerations in the event 3 and 4 time series result in peaks in the cross-shore COM position migration rates of 1.5 and 1.9 m.day^{-1} respectively, whilst the regression analyses produces corresponding accelerations of 0.01 m.day^{-2} (R^2 = 0.8) for both events. The shore-attachment of the sandbanks in events 2 to 4 is observed to occur close to the peak in the migration rate during the onshore directed acceleration though it should be noted that the shore-attachment line is only an approximate indication. Following the peak in the migration rate, there is a subsequent period of deceleration in which the offshore extremity of the shore-attached sandbank begins to be eroded. Regression analysis of this stage shows that event 4 experiences the most rapid deceleration of -0.07 m.day^{-2} (R^2 = 0.9), whilst events 2 and 3 experience similar deceleration magnitudes of -0.03 (R^2 = 0.9) and -0.02 m.day^{-2} (R^2 = 0.9) respectively. Typically, the end of the deceleration process occurs when the COM of the sandbank has a cross-shore range of approximately 120 m and coincides with the offshore extremity arriving on the low tide terrace (cross-shore range: 200-300 m). Note that the S2 acceleration-deceleration stage occurs through the winter season before ending prior

to the start of spring. The termination of the deceleration period marks the time when the offshore extremity begins to traverse the inter-tidal terrace.

The final S3 stage in the smoothed and interpolated migration rate time series appears to be a period in which there is no sustained acceleration or deceleration during in which the migration rate predominantly fluctuates between zero and 1 $m.day^{-1}$. The S3 phase of the evolution marks the time when the intermittent submergence and exposure of the feature by the tidal water level variation is at its maximum. The rate of dissipation of the offshore extremity is therefore a primary function of the balance between wave energy levels and water level variation, with a secondary dependence on the degree of sheltering due to the genesis of the offshore sandbank.

The mean migration rates of the four events have been estimated by taking the mean of the absolute values from the time series and these are 0.91, 1.0, 0.94 and 1.0 $m.day^{-1}$ respectively. These magnitudes infer similar migration rate variability between events which is estimated at 27 to 30 m over a 30 day period. However, if the mean migration rate is calculated from using the cross-shore distance traversed by the COM between the first and last contours and the total duration of each onshore migration event then the estimated values are somewhat different at 11, 23, 21 and 21 m per 30 day period respectively. This statistic better reflects the observed morphological change insomuch as the calculation differentiates between event 1 and the other events where the duration of the former was approximately twice that of the other events as a result of the sandbank merging with another feature (4.4.3.1).

The differences between the scatter plots of migration rate versus cross-shore position in Figure 4.20 infers that the influence of the cross-shore position on the sandbank's

migration rate is complex as there are no distinctly similar trends across all of the events. Events 2 and 4 do exhibit a similar form in the trend-lines but it in general it is difficult to draw any reliable conclusions from the plots.

4.4.3.3 Crest depth

The time series of crest depth estimates for the observation period are plotted in Figure 4.21 which includes error bars indicating the uncertainty associated with each estimate and the approximate time of sandbank shore-attachment. The discontinuities in the crest depth time series occur when it has not been possible to obtain data at both of the tidal levels necessary to make an estimate on either the flood or ebb tide. The most striking trend in Figure 4.21 is the increasing depth of the sandbank's crest from event 1 to event 4 which is reflected in the average crest depth statistic where events 1 to 4 have mean values of 0.6, -0.2, 0.1 and -1.1 m ODN respectively. The maximum crest depth in the dataset is +2.4 m ODN which relates to the event 1 sandbank at around the time of shore-attachment but this is not reflected in the other events where the peak in crest depth occurs both before and after shore-attachment.

To assist with the purpose of a more detailed comparison of the four events the individual crest depth time series are presented separately in Figure 4.22. The only trend that these time series appear to share is one of increasing elevation during the onshore migration and elongation stage after genesis. Apart from this there appear to be no other common trends in the minimum sandbank crest depth parameter which seem to increase and decrease randomly.

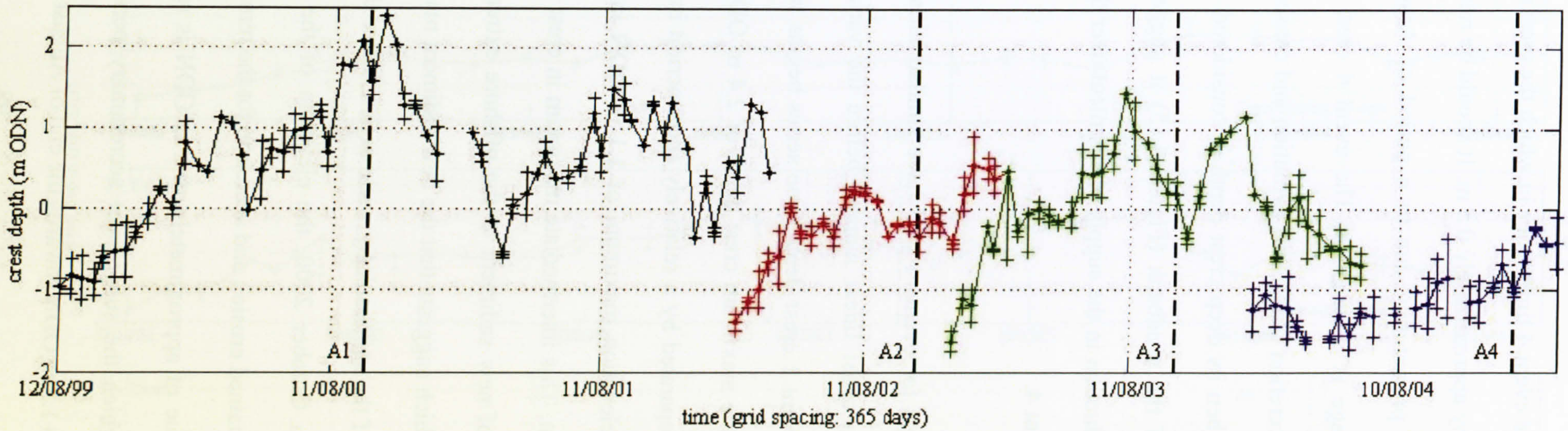

Figure 4.21: Time series of the estimated sandbank crest depth with error bars. The vertical lines denoted by A1 to A4 indicate the approximate time of sandbank shore-attachment (Colour key: event 1: black, event 2: red, event 3: green, event 4: blue).

The initial sustained increases in the crest depth elevation in events 1 to 3 is not reflected in the event 4 time series in which the crest depth appears to be eroded shortly after genesis by approximately 0.5 m. It should be reiterated that the event 4 time series is terminated prematurely due to a period of Argus system downtime and so the dissipation stage is incomplete. The event 4 crest elevation does not undergo any appreciable accretion through its evolution and consequently it is atypical in relation to the others. When its deep crest depth is considered in conjunction with the markedly small area of the sandbank (Figure 4.15) it suggests that there may have been a significant reduction in the supply of sediment over the meso to macro time scale from event 1 to event 4.

The time series for events 1 to 3 have similar initial trends in which the crest depth increases in a quasi linear manner before the variability becomes more random in nature. The event 1 crest depth time series begins with two quasi linear sections that culminate in the maximum crest depth of 2.4 m ODN in mid October 2000. The two sections are separated by a relatively short period in which the crest depth reaches an intermediate elevation maximum of 1.1 m ODN in early March 2000, before being eroded by 1 m. This intermediate maximum in crest depth elevation is coincident with the addition of new sediment to the offshore extremity as discussed in the previous subsection, which suggests that the new sediment may have been redistributed over the central area of the sandbank by wave action. After the peak in the event 1 crest depth time series in October 2000, the elevation of the sandbank undergoes consecutive periods of sustained erosion and accretion for the remainder of its life cycle. The event 1 minimum value of approximately -0.6 m ODN is reached towards the end of March 2001, after which the subsequent accretionary period culminates in an intermediate maximum of +1.5 m ODN towards the end of August 2001.

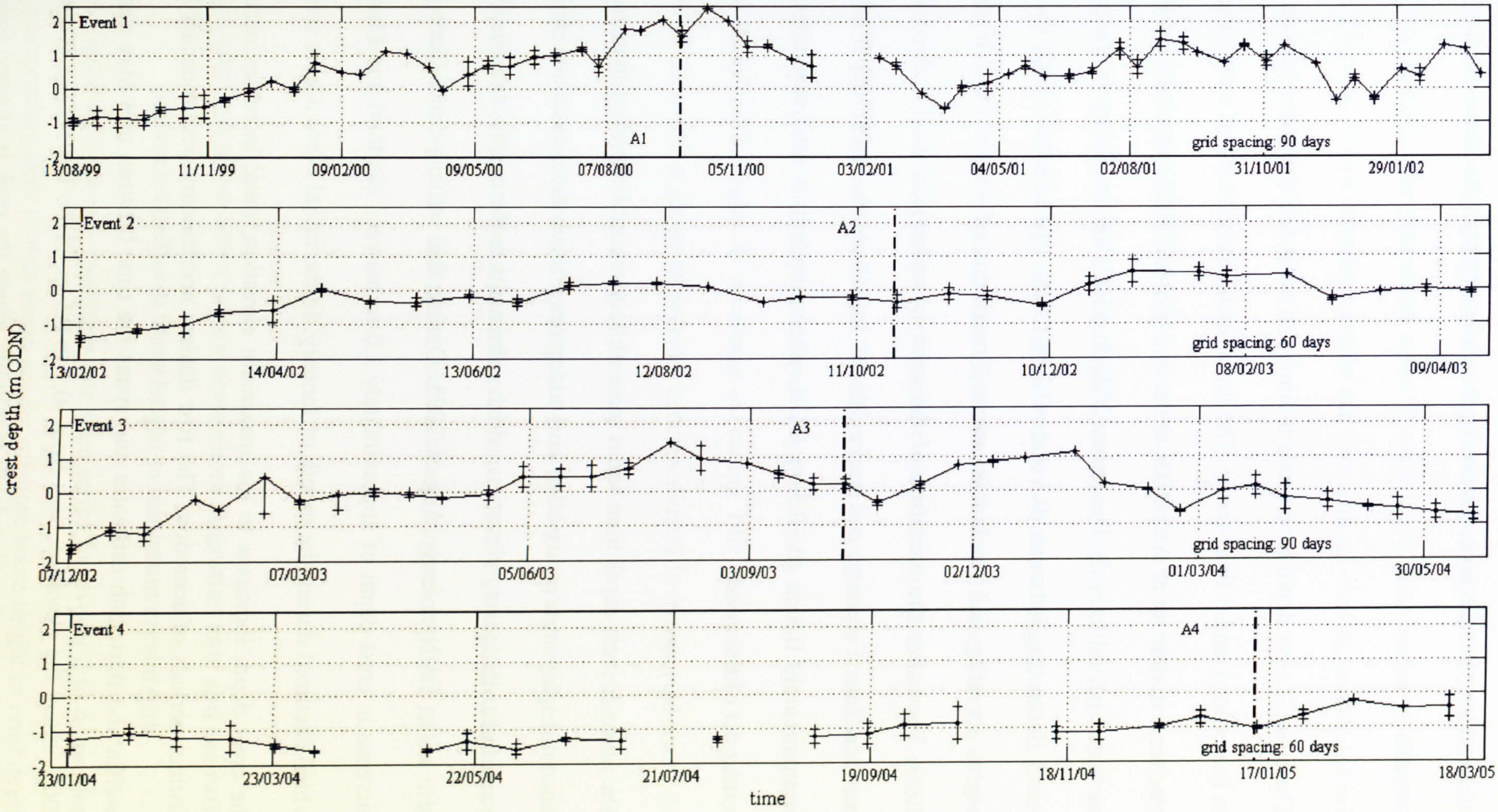

Figure 4.22: Sandbank crest depth time series for individual events. The vertical lines denoted by A1 to A4 indicate the approximate time of sandbank shore-attachment.

By mid-December 2001, the crest depth has been eroded to a depth of -0.35 m ODN after which the elevation gradually increases through the shore-attached dissipation process.

The event 2 crest depth time series is similar to event 4 in that it has less variability than in the event 1 and 3 time series. The initial quasi linear trend of increasing crest depth reaches a maximum at 0 m ODN at the end of April 2002, after which there follows a sustained period to early December 2002 in which the variability in the crest depth is small fluctuating between -0.3 and +0.2 m ODN. In December 2002, the crest depth begins accreting and reaches the event 2 maximum of +0.6 m ODN in early January 2003. Thereafter the elevation of the crest is maintained until a three week period between late February and early March in which the crest depth is eroded by approximately 0.8 m to -0.3 m ODN, after which it is relatively constant for the remainder of the event.

The event 3, crest depth time series more closely resembles event 1 than events 2 and 4 since it displays more variability and undergoes a much more sustained initial period of quasi linear increasing elevation, which culminates in the event's crest depth maximum of +1.5 m ODN in early August 2003. During this initial period, there is a notable increase in crest depth of approximately 1.0 m between the third and fourth estimates which occurred during the month of January. In the initial event 3 time series in which the crest depth increases to the maximum elevation, these increases occur during to distinct periods of accretion. The first distinct accretionary period occurs between the twelfth and thirteenth estimates and spans the time between mid May and early June 2003, where the elevation rises from -0.1 to 0.5 m ODN. The second distinct elevation increase relates to the crest depth maximum where the peak is attained following a rise

in elevation of 1.0 m during the month of July. After the August 2003 maximum in the event 3 crest depth, during the following 6 week period the crest was eroded by 1.9 m to -0.4 m ODN. The remaining event 3 crest depth time series is characterised by a succession of two accretion events and two erosion events, and ended with the crest depth at a depth of -0.7 m.

Interestingly periods of accretion and erosion of the crest both occur during the lower energy summer months and the higher energy winter months. This may reflect the fact that higher wave energy does not necessarily equate to higher sediment availability at the Teign inlet. Previous studies have shown that at the location the littoral drift from the primary input direction (i.e. from the north) is sensitive to wave direction (Siegle, 2003; Whitehouse et al., 2001). Therefore high wave energy conditions that are not also high sediment availability conditions may potentially occur. For example when waves approach with angles of incidence exceeding 140° the primary longshore drift input from the north is prone to reversal hence sediment is transported away from the inlet entrance and not towards it. Ultimately it is likely to be the case that, only when the sediment budget of the migrating shoal is undergoing a period of net gain that there would be sediment available for increases in elevation though the sediment may equally be deposited at the shoreward extremity causing elongation rather than elevation increase.

4.4.3.4 Correlation between raw cross-shore migration rate and the ratio of mean offshore significant wave height to minimum crest depth

In Figure 4.23 the raw migration rate time series for events 2 to 4 are plotted with the corresponding ratio of root-mean-square offshore wave height to crest depth. Event 1 is

not included due to the significant data gaps in the time series (Figure 4.10). This resulted in there being no wave height data available for the first 11 month period of the migration and thereafter, it was only available for intermittent periods in which data gaps of varying lengths up to a maximum of 7 month duration occur. The ratio of root-mean-square offshore wave height to the crest depth ratio was calculated using the mean of the 10 minute resolution offshore significant wave height time series for the period between estimates. The estimated minimum depth of the sandbank's crest was derived from the Argus image time series as plotted in Figure 4.22. Note that the data in Figure 4.23 have intentionally been plotted using unequal y-axes to highlight the clearly visible correlation in the short (weeks) term variability.

The correlation between the time series is evident and particularly for the event 2 time series (Figure 4.23a). A linear regression of the migration rate with the H_{rms}/h ratio produced R^2 values of 0.70, 0.36, and 0.17 for events 2, 3 and 4 respectively indicating a decreasing correlation between the parameters though this can be partly attributed to the increasing number of missing data points with event number. An R^2 value of 0.70 for event 2 indicates that the two parameters are well correlated and this is evident in the manner in which the trends in both the short (weeks) and medium (months) term variability are largely in phase with each other. This degree of correlation is also inferred from the event 3 time series in the period prior to shore-attachment (Figure 4.23b) as the variability appear to be equally well-correlated. The lower 0.36 R^2 value for event 3 is a function of the divergent correlation between the time series after shore-attachment in which there are a number of transitions in which the pair of parameters are in anti-phase with regard to the short (weeks) term variability.

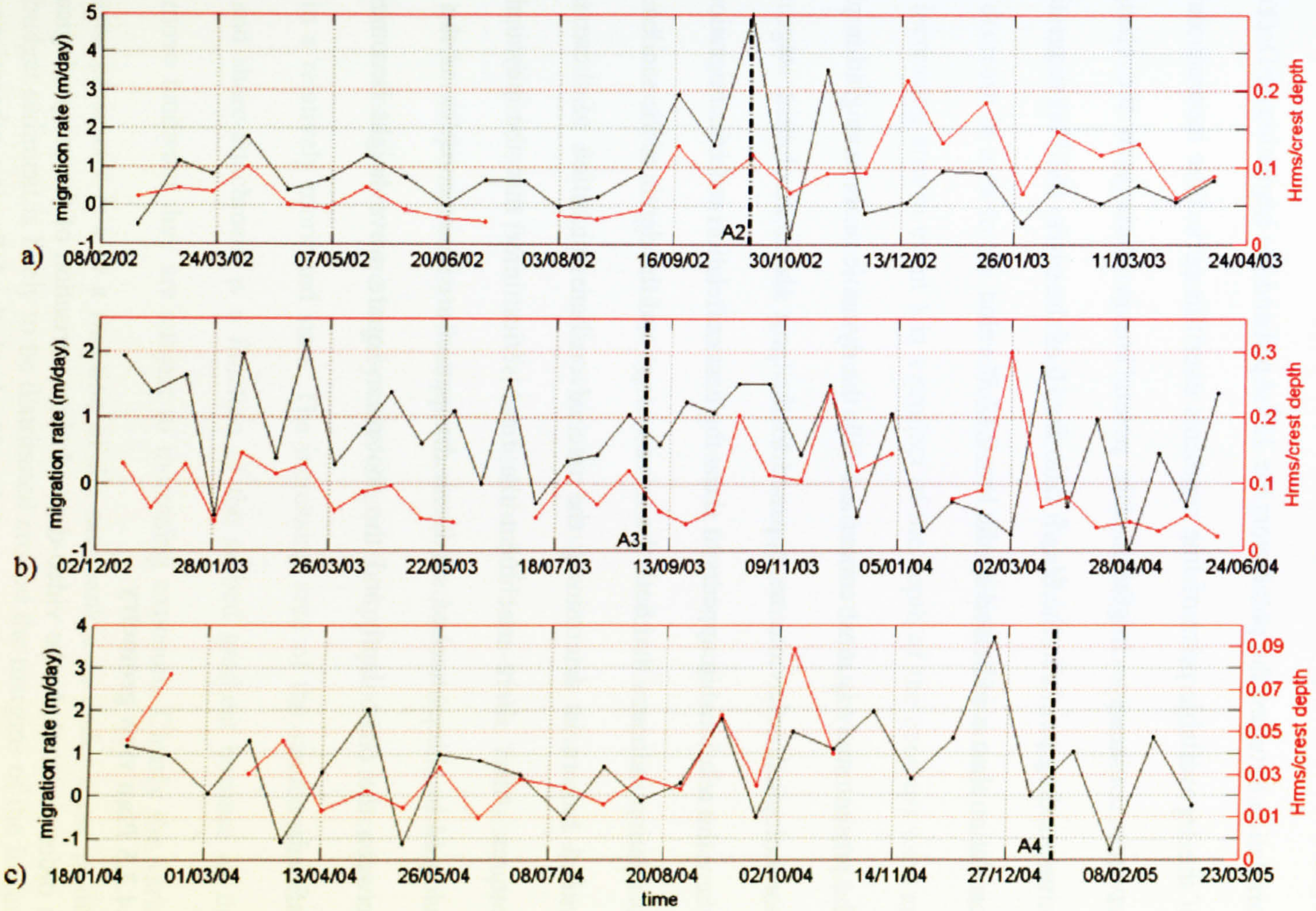

Figure 4.23: Time series of cross-shore migration rate (black) and the ratio of root-mean-square offshore wave height to crest depth (red) for the onshore migration events 2 to 4: a) event 1, b) event 2, and c) event 3. Vertical hatched lines indicate the approximate time of shore-attachment.

The event 4 time series is marked by a relatively large period of missing data which encompasses the time from 2 months prior to shore-attachment to the end of the dissipation stage. From the available time series which predominantly relates to the migration and elongation stage in the morphological evolution, there is reasonable correlation between the parameters the 13th April and the beginning of December 2004. Of the 16 available pairs of line segments over this period the increase and decreases between consecutive migration rate points are in phase with the changes in the corresponding points in the H_{rms}/h ratio for 10 of the cases (62.5%) suggesting a better correlation than is indicated by the low 0.17 R^2 value.

The present study is most concerned with the dynamic onshore migration phase of the morphological behaviour as opposed to the post shore-attachment stage and this is where the relationship appears to show the best correlation with the migration rate. This correlation indicates that both the wave energy and the depth of the sandbank crest are critical factors in determining the rate of onshore migration of these sedimentary features. After shore-attachment the time series infer that the physical processes involved in shore-attached sandbank dissipation are more complex as the correlation between the crest depth and the root-mean-square wave height becomes less well defined.

4.4.3.5 Plan view geometry

In order to conclude the video-derived characterisation of the morphological evolution in the onshore migration stage of the ebb shoal, the following subsections are used to describe the variability in the plan view geometric sandbank parameters which are the area, cross- and longshore axes lengths, and the aspect ratio which is computed from the

orthogonal axes using the longshore axis as the denominator. The data are plotted against time in Figure 4.24 and then the same data are presented in scatter plots in Figure 4.25 for the purpose of comparison.

The trends in the area time series (Figure 4.24a) for the four events show clear similarities with a quasi linear increase in area through the genesis and onshore migration/elongation stages. The area of the sandbanks typically reaches a maximum at around the time of shore-attachment and then this is followed by a similar near linear decrease in area to the time of sandbank dissipation. The scatter in the initial trend of increasing area in event 1 is a product of the depth of the contours used as the 9^{th}, 11^{th} and 13^{th} contours were in excess of 0.4 m below the target level of -1.80 m ODN. Due to the shallow sandbank gradients the area parameter is sensitive to the depth of the contour used hence the fluctuating values for this section of the times series. Event 3 deviates from the genesis to shore-attachment model of increasing area preceding shore-attachment due to a period in which the trend in the area time series decreases over a 2 month time scale from the 1^{st} May and the 30^{th} June 2003. This also appears to be an artefact of the sensitivity of the parameter to the contour depth as during these 2 months the sea conditions were largely calm (Figure 3, Appendix A3) hence the sandbank was in a relatively moribund state. The increasing area of the sandbanks between genesis and shore-attachment is a function of the seabed gradient because as the sandbanks move landward they are subject to increasing exposure. Clearly the variability in the area parameter is also a function of the sandbank's as under a net positive sediment budget sediment is likely to be distributed around the margins of the features as well as on the crest.

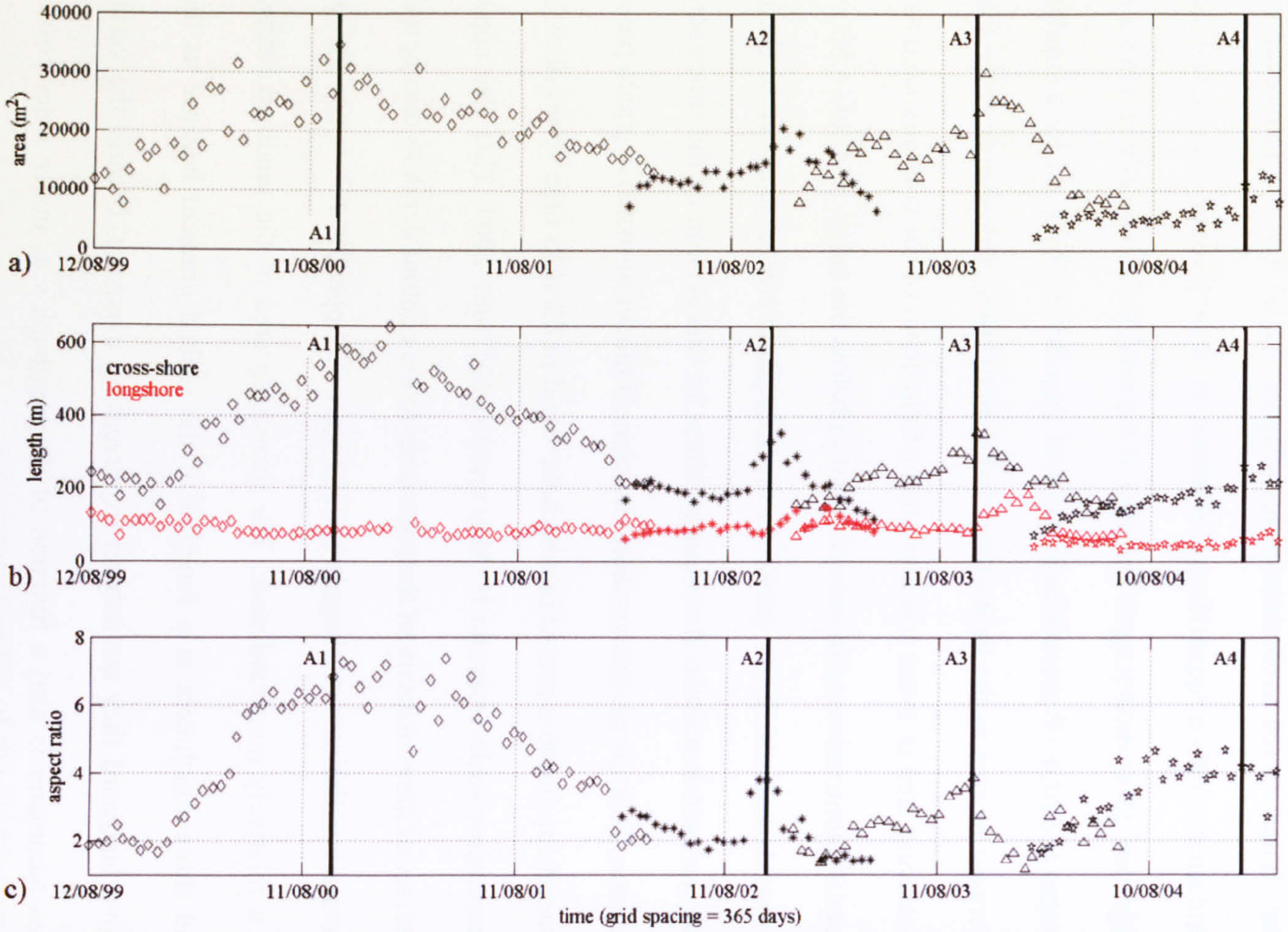

Figure 4.24: Time series of geometric sandbank parameters for all events: a) area, b) length of cross-shore (black) and longshore (red) axes, and c) aspect ratio (cross-shore length/longshore length). The approximate times of sandbank shore-attachment for events 1 to 4 are denoted by the vertical hatched lines A1 to A4 respectively. .Event key: event 1 diamonds, event 2: asterisks, event 3: triangles, event 4: stars.

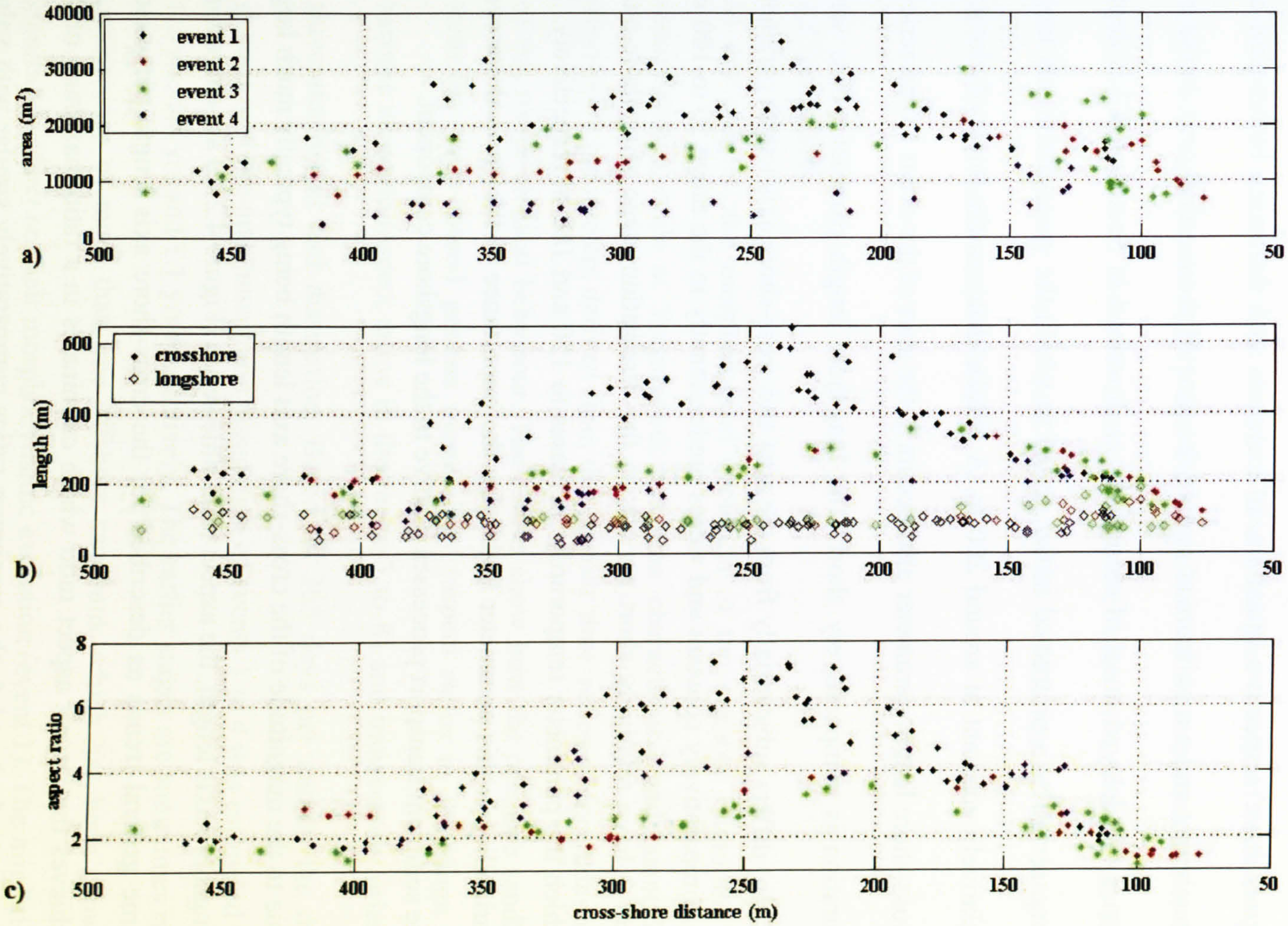

Figure 4.25: Scatter plots of geometric sandbank parameters with cross-shore distance for all events: a) area, b) length of cross-shore (dots) and longshore (diamonds) axes and c) aspect ratio. Colour denotes event number.

The event 1 maximum of 34,600 m^2 is the largest of all the events, events 2 and 3 have maximum areas of 20,600 and 30,000 m^2, whilst event 4 has the lowest maximum of 12,600 m^2. The described trends in the sandbank's area are reflected in the trends in the cross-shore axis length (Figure 4.24b) time series for events 1, 3 and 4. These time series have respective quasi linear increases and decreases before and after shore-attachment and a maximum at around the time of shore-attachment. In the event 2 time series the delayed onset of elongation as described in Section 4.4.2 is depicted in the time series by a protracted initial period in which the cross-shore axis length remains relatively constant at around 200 m. A similar delay in the onset of elongation in the cross-shore length parameter also occurs at the start of the event 1 time series though its duration is comparatively short. The longshore length parameter time series (Figure 4.24b) differs substantially from the area and cross-shore axis length parameters since it is comparatively constant and varies predominantly in the range 50 to 100 m. Events 2 and 3 have relatively short periods in the dissipation stage after shore-attachment in which the parameter temporarily increases to 150 and 180 m respectively. The lack of variability in this parameter highlights the importance of the cross-shore component of the sediment transport processes relative to the longshore component.

Due to the magnitude of the cross-shore axis length being typically much larger than the longshore axis length, the aspect ratio time series (Figure 4.24c) are characterised by the same general trends as described for the cross-shore axis length parameter. Event 1 achieves the largest aspect ratio which culminates in a ratio maximum of 7.4, and for the events 2, 3 and 4, the maximum ratios comparatively similar with values 3.8, 3.8 and 4.7 respectively. The trends in the aspect ratio time series reflect those in the major axis length time series with a peak at around the time of shore-attachment.

In the scatter plot of the area parameter versus cross-shore distance (top panel, Figure 4.25) the data show the absence of any distinct relationship as there are no clearly identifiable trends. The scatter plots of the orthogonal axis lengths and the aspect ratio derivative do show similar trends to those identified in the time series but there is considerable scatter between events. The scatter plot trends of increasing major axis length and aspect ratio signify that the magnitude of these parameters is a function of cross-shore position. However since the absolute value for a given cross-shore position is subject to scatter this is most likely to be a function of the long term (years) chronology of sediment availability.

4.5 Summary

In this chapter, the morphological evolution of the onshore migration stage of the sedimentation cycle at Teignmouth has been characterised and quantified from the descriptive parameters derived from the contour time series of four consecutive events of this morphological behaviour. The results show how the offshore sandbanks evolve from the more rotund genesis morphology (aspect ratios in the range 1.5 to 2) to become elongate (aspect ratios in the range 3 to 8) and transversely orientated before shore-attachment and dissipation. Based on 365 days per annum the duration from genesis to shore-attachment and dissipation of events 1 to 4 was estimated to be 2.6 yrs, 1.2 yrs, 1.5 yrs and 1.1 yrs respectively. The earlier stages are sometimes marked by the coalescence of more than one offshore sandbank which has been shown to have a significant effect on their morphodynamic evolution (event 1). The migration rate of the sandbanks in the shore-attached stage can also in influenced by other sandbanks on the ebb tidal delta depending on the degree of overlap between events. Offshore genesis typically occurs whilst the previous sandbank is still in shore-attached mode therefore

the dissipation of the shore-attached feature will be affected by the degree of sheltering from wave energy depending on the direction of incident waves.

The characteristics of the morphological evolution of the Teign inlet in its current morphologic mode have been defined using three generic chronological stages which are manifest in both the cross-shore COM position (Figure 4.17) and the smoothed and interpolated migration rate (Figure 4.19). The typical mode of onshore migration has been ascribed to events 2 to 4 since event 1 varied from the basic model on account of the sandbank coalescence event (Figure 4.18). Initially it was thought that the short term (weeks) migration rate of the COM of the sandbank would be a directly proportional to the intensity of the wave forcing but cross-correlation analyses in both the time and frequency domains of the two parameters yielded no statistically significant relationships. It was subsequently determined that the migration rate of the COM of the contour time series was significantly correlated with the ratio of offshore wave height to minimum crest depth particularly prior to shore-attachment (Section 4.4.3.4). This key result of the video remote sensing component of the study suggests that the onshore migration phenomenon is primarily wave driven but modulated by the tidal variation in water level relative to the crest depth. The relationship suggests that large waves combined with a shallow crest produce the largest migration rates. The observed behaviour was characterised by mean migration rates of approximately 1 $m.day^{-1}$ with maximum migration rates of up to ≈ 3 $m.day^{-1}$.

The importance of the depth of the crest is evident from the direct relationship between the migration rate and the ratio of offshore wave height to minimum crest depth as described in the previous paragraph. In the inlet's current mode the crest of the sandbanks at genesis is between 1 and 2 m below mean sea level. Typically the

sandbanks undergo an initial quasi linear increase in crest elevation as they begin to migrate onshore. This period of accretion appears to end shortly thereafter whereupon the sandbank's crests are subject to apparently random consecutive periods of erosion and accretion. The initial period of crest elevation increase occurs due to the sandbanks being in close proximity to the primary accretion zone at the distal end of the main channel during the energetic winter period. The subsequent random variability occurs when the sandbanks have migrated away from this zone. Under low energy conditions the sandbank's vertical and lateral morphological changes are considered to be primarily a function of the re-distribution of surficial sediment in the absence of high sediment availability conditions which are associated with higher energy waves. Under high energy conditions with high sediment availability, morphological change is also likely to be affected by transport pathways that lead both to and from the migrating sandbanks. Under these conditions the addition of new sediment is expected to add a degree of complexity to the morphological response (vertical versus lateral) which is difficult to determine.

In terms of the sandbank's plan form geometric parameters the area was shown to increase from genesis to shore-attachment (Figure 4.24a) which is assumed to be caused by their increasing sub-aerial exposure as they traverse the nearshore gradient (FitzGerald, 1988). The data indicate that increases in area occur contemporaneously with increases and decreases in sandbank crest depth which reflects the complexity of processes governing shoal sedimentation through their morphological evolution. The inter-event trend in sandbank area is one of decreasing area and this is reflected in the decreasing trend in the major axis length and aspect ratio parameters. The large area of the event 1 sandbank evolution was attributed to a shoal coalescence event and its occurrence infers that there was high sediment availability during winter, 1999. During

the next three events there is a downward trend in sandbank area and this coincides with an increase in the minimum depth of the features suggesting that the availability sediment to the ebb tidal delta decreased over the 5 year observation period. Bernardes (2005) estimated that the inlet was infilling at a rate of 20 $cm.yr^{-1}$. The observed trends in the area and length parameters could therefore be evidence of the infilling process whereby there is a net loss of sediment from the ebb tidal delta to the outer estuary.

The methodology used in this video remote sensing analysis is not without its shortcomings which include the inherent subjectivity involved in determining some of the criteria such as at what depth to extract the contours from, when should the first contour be taken, and in the delineation of the shoreward extremity of the feature when it has merged with the beach face. Furthermore, it was not possible to extract contours from the images at precisely the same depth which increases the inherent error particularly during the genesis and dissipation stages when the sandbank is in the periphery of the image. Despite these shortcomings the video analysis has achieved the objective of characterising the plan view meso to macro scale morphological evolution of the offshore sandbank during its onshore migration stage and quantifying the cross-shore migration rate in relation to its COM. In the following chapter the short term (micro to meso scale) physical processes responsible for the observed morphological behaviour are investigated in detail using a unique set of in-situ measurements that were obtained from the surface of the migrating sandbank during the May 2003 Coastview fieldwork program.

5 In-situ measurements

This chapter presents the results and analyses of the in-situ measurement component of the study focussing on the cross-shore dimension. The chapter begins first with a description of the data analysis methods used. The objective of the in-situ measurement analysis is to determine the physical processes responsible for the onshore sandbank migration cycle observed at the Teign inlet but which is also a common feature associated with tidal inlets on different coastlines around the world (Chapter 2.2).

5.1 Data analysis techniques

5.1.1 Sampling theory

The physical processes of interest in this study originate as continuous data which are converted to digital form during the sampling process. Sampling theory considers the question of how often a signal can be sampled so that all of the frequencies present are detected. The highest sampling frequency, also known as the Nyquist or folding frequency (N_y) is given by:

$$N_y = \frac{1}{2\Delta t} \tag{5.1}$$

Where Δt is the sampling interval. If frequencies higher than the Nyquist frequency are present in the signal being sampled then these will be 'folded back' into the time series of measurements and appear as erroneous signals of lower frequency than their true value. These erroneous signals termed aliasing errors are caused by the discretisation of continuous signals prior to digitisation. In order to avoid them, the frequency range of the signal being recorded is restricted prior to digitising using an analogue low pass

filter. The lowest resolvable frequency, which by definition is also the bandwidth, is given by:

$$B_e = \frac{1}{N.\Delta t} \tag{5.2}$$

Where Δt is the sampling interval and N is the number of points in the Fast Fourier Transform (Section 5.1.3). The choice of bandwidth determines the resolution of the estimated spectrum and is used for normalisation of spectra for the inter-comparison of multiple estimates.

5.1.2 Time series analysis

The purpose of time series analysis is to quantitatively describe the characteristics of a measured signal which are typically subsets of continuous processes that are sampled at discrete intervals. The standard techniques used in time series analysis make use of statistical procedures to parameterise the principle characteristics of the data set and so permit the analysis and inter-comparison of the variables of interest. The principle variables of interest in the present study are the water depth (h), the cross-shore (u) and alongshore (v) components of the current field, and the concentration of suspended sediment (c). The type of analysis technique to be used is determined by the nature of the data concerned of which there are two fundamental groups and these, along with their subgroups are summarised in Figure 5.1. In theory, a discrete (digital) time series of tidal variations in water depth could be categorised as deterministic data due to its periodicity and hence predictability. Conversely, a discrete time series of water depth under the influence of wind driven waves could be described as random or stochastic data by virtue of the fact that its variation in time or space cannot be described or

predicted by an explicit mathematical relationship. In practice the nature of oceanographic data is such that its classification usually falls somewhere in between the two categories. It should be noted that the ability to mathematically predict a phenomenon is limited by the accuracy of the prediction whereby if the prediction is associated with a significant error, then the variable could erroneously be classified as non-deterministic. Similarly, the inability to be able to predict a phenomenon may be the result of insufficient knowledge or understanding as opposed to it being unpredictable.

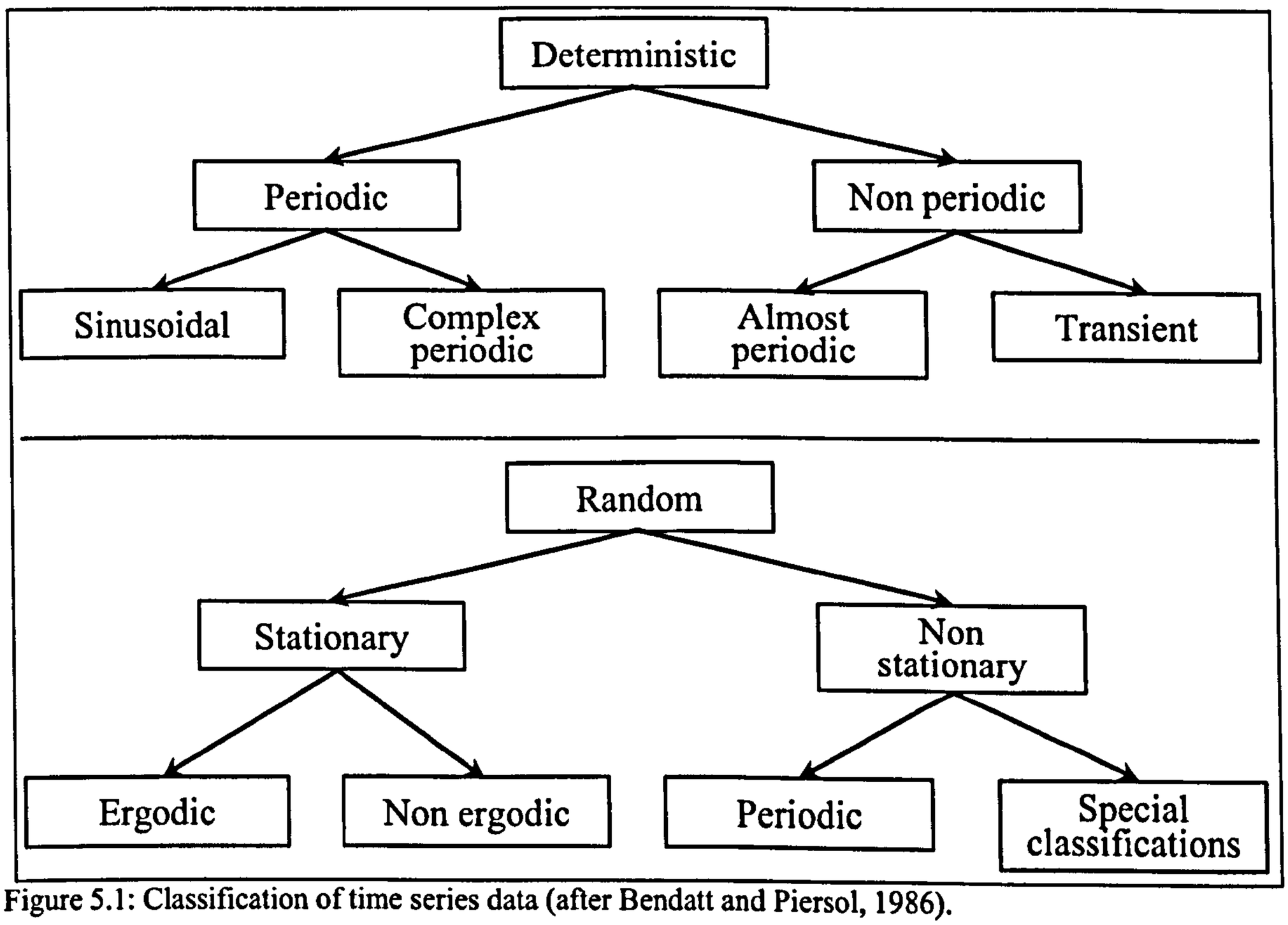

Figure 5.1: Classification of time series data (after Bendatt and Piersol, 1986).

In order for the results of statistical analysis to be meaningful the data need to be both stationary and ergodic. Physical data are time series of finite sample records and stationarity in this context is considered to mean that the process can be adequately described by the lower moments of its probability distributions, i.e. by its mean, variance and covariance, and that these will not vary significantly between sample records within the ensemble. Most actual stationary physical phenomena can also be

described as ergodic, which relates to the inter-changeability of the time average with the ensemble average. Therefore, if the ergodic assumption is justified, then verification of stationarity for a sample record is usually adequate verification that the record, and hence the process, is both ergodic and stationary. Thus assumptions regarding a physical stochastic process can be derived with some confidence from a single sample record (Laws, 1997).

5.1.2.1 Sediment transport calculations

In Section 5.6.3 the Eulerian (local) time averaged (net) sediment transport rate is estimated from the in-situ measurements after Jaffe *et al.* (1984) using the product of the instantaneous cross-shore current magnitude and sediment concentrations as defined in the following equation:

$$< uc > = \frac{1}{n}\sum uc \qquad (5.3)$$

Where n is the number of samples, u is the instantaneous cross-shore transport and c is the instantaneous sediment concentration. If it is assumed that u and c can be separated in to steady and oscillatory components which are denoted by the overbar and prime symbols respectively, then it follows that the local time averaged sediment transport rate ($< uc >$) can also be as expressed as follows:

$$< uc > = < (\overline{u} + u')(\overline{c} + c') > \qquad (5.4)$$

The expansion and simplification of equation 5.5 results in:

$$< uc > = \overline{uc} + < u'c' > \tag{5.5}$$

Where the first term denotes the mean net transport rate and the second term denotes the magnitude of coupling or correlation between the two flux components.

5.1.3 Frequency domain analysis and the Fast Fourier Transform

Analysis in the frequency domain is a useful extension of time series analysis as it facilitates an improved understanding of cyclical processes through the deconstruction of complex signals into constituent harmonics. The importance of this type of analysis relates to the product of the transformation which can be used to determine the relative contributions of each constituent to the total energy of a process. The technique uses the mathematics of Fourier and relies upon the principle that any function can theoretically be described by one or more sine and cosine functions of different frequencies and amplitudes. Classical Fourier series are applicable to periodic data and are integrated between the limits of $-\infty$ and $+\infty$ thus they require adaptation for application to the discretely sampled aperiodic data typical of measurements taken in the nearshore environment. The discrete Fourier transform was first developed for this purpose but has since been replaced by the computationally efficient Fast Fourier Transform (FFT) which uses complex exponent form derived from Euler's relation to generate an output with real and imaginary components (Equation 5.6):

$$x_t \xrightarrow{\text{FFT}} X_f \tag{5.6}$$

Where $X_f = a + jb$, $a = A.\cos\theta$ and $b = A.\sin\theta$, from the complex notation for a 2D vector (Figure 5.2).

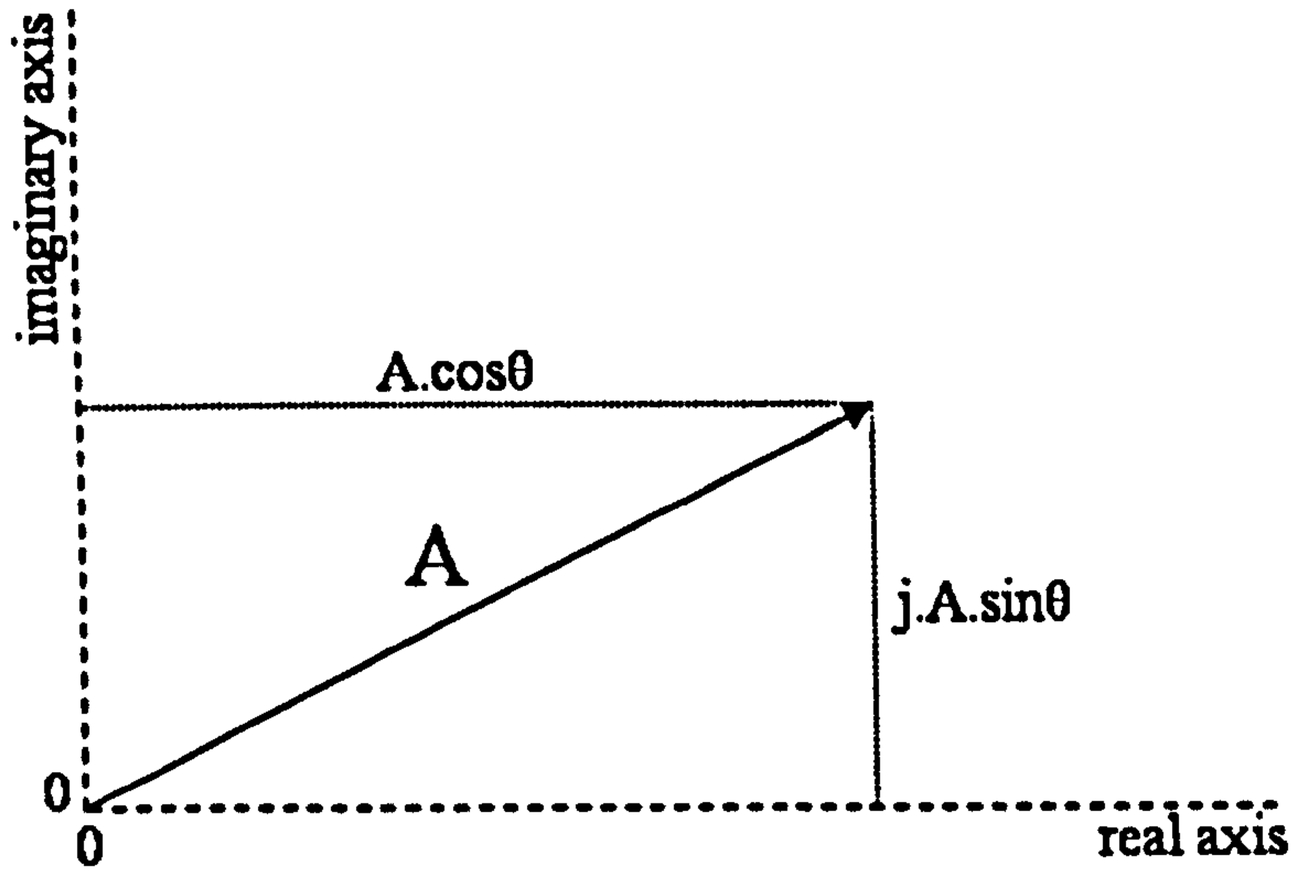

Figure 5.2: Argand diagram depicting the complex number representation of a vector.

A represents the amplitude of the signal being transformed thus the product of the FFT is an analysis of variance. From Pythagoras' theorem the squared amplitude of each harmonic is given by:

$$A_n^2 = a_n^2 + b_n^2 \tag{5.7}$$

Where *n* represents the *n*th harmonic of the spectrum and:

$$a_n = A_n.\sin\theta_n \tag{5.8}$$

$$b_n = A_n.\cos\theta_n \tag{5.9}$$

The product of the FFT also yields information about the phase relation between harmonics which is given by:

$$\theta_n = \tan^{-1}(b_n/a_n) \tag{5.10}$$

For further information on the FFT algorithm the reader is referred to Bendatt and Piersol (1986).

5.1.4 Spectral analysis

The sequence of operations required to transform a sample record in to the frequency domain can be summarised as follows:

1. Filter data to remove frequencies > N_y.

2. Digitise analogue data (automated process with equipment used).

3. Remove the mean and de-trend the time series.

4 Divide the time series in to overlapping sections and apply a suitable window function to each segment.

5. Apply the FFT algorithm to each segment.

6. Compute the power spectrum from the Fourier estimate and ensemble average each segment to obtain a stable estimate.

In the first operation, the filtering is usually executed during the instrument logging stage after signal amplification, and operations 3 to 5 are executed within Matlab's power spectral density (PSD) function. For a sample record of N data points, the FFT returns N-1 complex estimates of the variance which is symmetrical about (N/2+1), the raw estimate of the power spectrum is given by:

$$P_{xx} = (a + jb).(a - jb) \tag{5.11}$$

Therefore:

$$P_{xx} = a^2 + b^2 \tag{5.12}$$

The plot of variance versus frequency is termed the periodogram estimate. The use of the Fourier transform to convert a continuous signal from the time domain into the frequency domain introduces errors due to spectral leakage. Spectral leakage results from processing the infinite Fourier integral with finite limits, a problem that is further enhanced during segmentation of the time series prior to transformation. The leakage of energy caused by discontinuities at the end points of contiguous segments results in the distortion of the spectral density estimate as energy is redistributed to higher and lower frequency bins. The problem is minimised by forcing the data to approximate to an infinite series through causing it to smoothly decay to zero at both endpoints. This is achieved by multiplying each data segment by a suitable window function. An example of an appropriate 'data-tapering' window for surface elevation analysis is the cosine-squared or Hanning window. This window function has little leakage with minimal amplitude error which is further reduced by overlapping. The choice of function should be determined by the relative importance of leakage (frequency resolution) versus amplitude (accuracy) in respect of the time series being analysed.

The number of segments chosen determines the statistical confidence in the FFT estimate for segments which is derived using the following equation provided a Hanning window has been applied:

$$\text{Degrees of freedom (D.O.F.)} = 3.82N - 3.2 \tag{5.13}$$

Where m = length of the segment, N = number of points in the sample record. The number of degrees of freedom can then be used to calculate the error bar multiplication factor for each spectral peak using Figure 5.3 after Jenkins and Watts (1968).

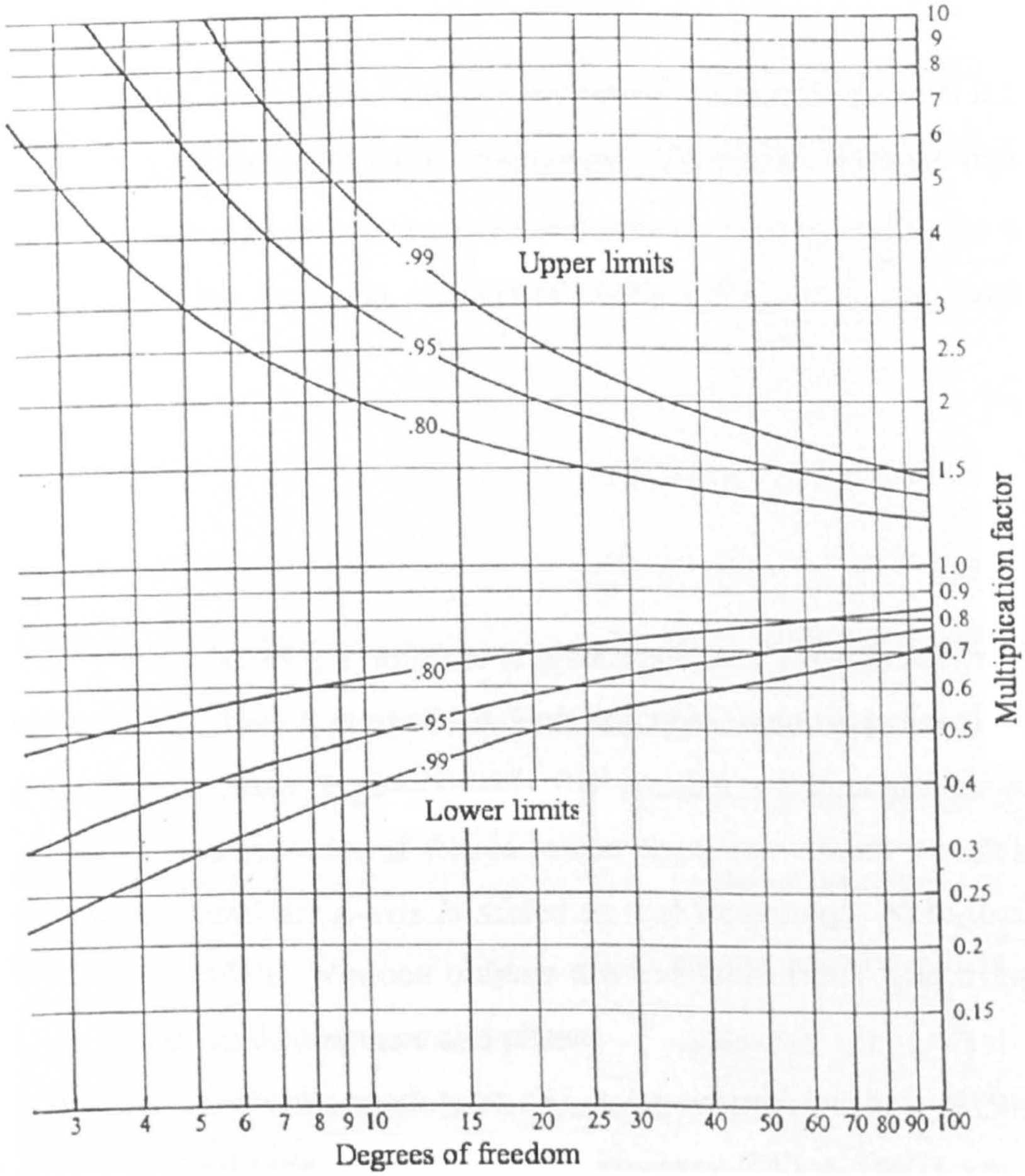

Figure 5.3: Spectral peak coefficient (y-axis) versus degrees of freedom (x-axis) with curves denoting the 80, 90 and 99% confidence levels for the upper and lower error bars.

5.1.5 Co-spectral analysis

Co-spectral analysis of a pair of signals enables the identification and quantification of coherent in-phase frequency based relationships between two variables that are measured simultaneously. The co-spectra and quadrature spectra are the principle components of cross-spectral analysis which yield information about the correlation and phase of two variables. Similar to spectral analysis, the variables are first FFT'd

generating complex outputs. The co- and quadrature periodograms are then estimated from the multiplication of the complex output of the first variable by the complex conjugate of the second. The raw estimate of the cross and quadrature spectra is given by:

$$P_{xy} = (a + jb).(c - jd) \tag{5.14}$$

Therefore:

$$P_{xy} = (ac + bd).+ j(bc - ad) \tag{5.15}$$

Where $(ac + bd)$ is the co-spectrum and $j(bc - ad)$ is the quadrature spectrum and the phase spectrum is defined as the cotangent of the former divided by the latter. The phase spectrum varies between $-\pi$ and π where a value of zero signifies that the variables are in phase, and values of $-\pi$ and π signify anti-phase. A tertiary component of co-spectral analysis is the coherence spectrum which is a measure of the frequency correlation between the variables. The coherence spectrum is given by:

$$C_{xy} = \frac{\hat{P}_{xy}^2}{\hat{P}_{xx}.\hat{P}_{yy}} \tag{5.16}$$

Such that $0 \leq C_{xy} \geq 1$ and the hats denote ensemble averaging. A value of zero indicates that the two variables are not correlated and a value of one indicates that there is correlation.

5.1.6 Energetics analysis

In order to assess the relative contributions of the mean and oscillatory cross-shore velocity components to the net sediment transport, an energetics analysis is undertaken after Bailard (1981). The analysis technique originates from the two dimensional stream flow theory developed by Bagnold (1963) which applies the principle of energy conservation and utilises an efficiency factor to give the following sediment transport equation:

$$i = K.\omega \tag{5.17}$$

Where i = total dynamic transport rate, k = efficiency factor, ω = available fluid power per unit boundary area, and the term 'total' means the combined transport due to bed load and suspended sediments. Bailard and Inman (1981) modified the analytical approach to incorporate the oscillatory flow component and key surf zone processes important to nearshore sediment transport such as wave skewness. They define the non-dimensional efficiency factor in the transport equation as follows:

$$K = \frac{rate\ of\ energy\ expended\ in\ transporting\ sediment}{rate\ of\ energy\ production\ of\ the\ stream} \tag{5.18}$$

The product of ω and K in Equation 5.17 includes a cubed cross-shore current term that can be decomposed into three components such that:

$$u_t^3 = (\overline{u} + \tilde{u}_s + \tilde{u}_l)^3 \tag{5.19}$$

Where u_t = the total cross-shore current, $\bar{u}$ = mean component, and $\tilde{u}_s$ = short wave oscillatory component, $\tilde{u}_l$= long wave oscillatory component. An expansion of Equation 5.19 generates a polynomial with ten third order velocity moment terms, each one representing a different nearshore hydrodynamic process (Table 5.1). According to the energetics theory, the transport rate (i) is proportional to the cross-shore current magnitude (u) therefore each term is a proxy for the sediment transport rate due to the hydrodynamic process that it represents.

No	Term	Description
1.	$\bar{u}^3$	mean velocity cubed
2.	u'^3_s	short wave velocity skewness
3.	u'^3_l	long wave velocity skewness
4.	$3\langle u'^2_s\rangle\bar{u}$	stirring by short waves & transport by mean flow
5.	$3\langle u'^2_l\rangle\bar{u}$	stirring by long waves & transport by mean flow
6.	$6\langle u'_s.u'_l\rangle\bar{u}$	non zero three way correlation
7.	$3\langle u'^2_l.u'_s\rangle$	long wave variance & short wave velocity correlation
8.	$3\langle u'^2_s.u'_l\rangle$	short wave variance & long wave velocity correlation
9.	$3\langle u'_s\rangle.\bar{u}^2$	time average of oscillatory component ≈ 0
10.	$3\langle u'_l\rangle.\bar{u}^2$	time average of oscillatory component ≈ 0

Table 5.1: Third order velocity moments generated by the expansion of the cubed cross-shore velocity component. A tilde denotes the oscillatory component and angle brackets denote a time average.

Terms 6, 7 and 8 each contain a product in the bracketed part of the expression which will only have finite values when the two components have a degree of correlation. If however, one of the components inside the brackets is a random signal or noise, then it is likely to be small in comparison to the other component and the whole term will tend towards zero. Similarly, the magnitude of terms 9 and 10 which have had the mean removed will also be close to zero since they are computed from the time average of a signal that oscillates about zero. Parameterisations of nearshore hydrodynamics and sedimentation involve assumptions and approximations that omit to incorporate all of the important physical processes and introduce uncertainty in to the estimates. Some of the assumptions and approximations included in the energetics analysis are the assumption that the drag coefficient is a constant, that there is no threshold condition for

the initiation of sediment movement, and that the approach does not properly consider the effects of breaking induced turbulence (Marino-Tapia, 2003). However, despite the limitations, Bailard-type models have a robust theoretical basis and have proved useful for the analysis of cross-shore sediment transport processes in a range of studies (Guza and Thornton, 1981; Marino-Tapia *et al.*, 2007; Ruessink, 2000; Russell and Huntley, 1999).

5.2 Instrumentation

Surf zone measurements of primary variables such as u (the cross-shore current component), v (the longshore current component), and c (the concentration of suspended sediment) are of fundamental importance in nearshore studies of sandy coastlines because they provide invaluable insight in to the physical mechanisms that constitute the hydrodynamics and sedimentation processes which drive the medium to long term morphological evolution. This chapter utilises unique measurements of u, v, and c obtained directly from the offshore sandbank during May 2003 when the feature was in the mid-term of its onshore migration (event 3), with the objective of elucidating the physical processes responsible for the persistent onshore migration of the feature as observed in the Argus image time series. Physical measurements of waves, orthogonal currents and the concentration of suspended sediment taken from an inlet sandbank in mid migration across the ebb tidal delta are thought to be unprecedented. These results therefore make an important contribution to the knowledge of ebb tidal delta shoal sediment dynamics in inlet research.

5.2.1 Synchronised logger for investigation into the transport of sediment (SLOT)

The field measurements were obtained using the Valeport SLOT system (see Figure 5.4) which enables the recording of synchronous, near bed measurements of hydrostatic pressure, biaxial currents and sediment suspension. The co-located pressure transducer (PT), electromagnetic current meter (EMCM) and optical back scatter (OBS) sensors are secured to a framework together with a power supply and data logger which is designed to be deployed in the inter-tidal zone. Power is supplied to the data logger and instrument array when a sea switch unit fixed at below sensor height to one of the piles becomes submerged

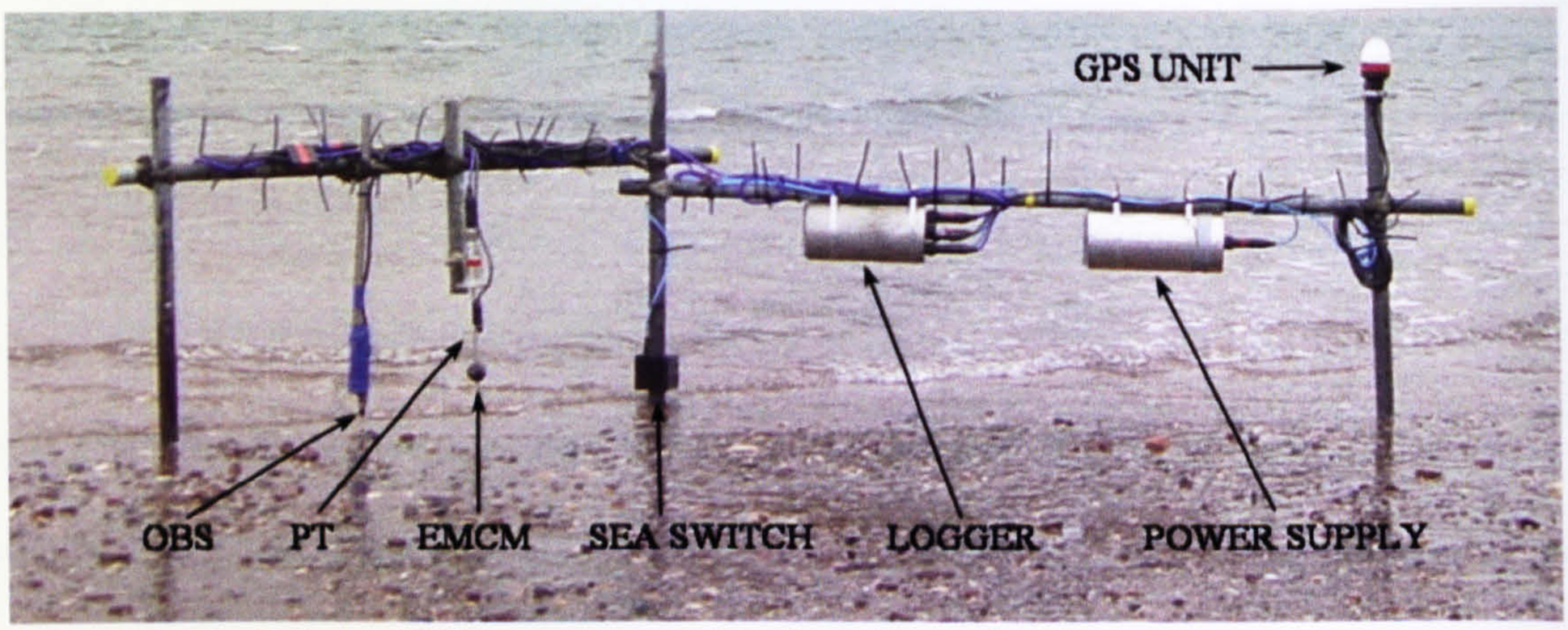

Figure 5.4: The Valeport SLOT system secured in-situ using steel tubing.

The data logger has a 12 bit resolution and logs data continuously during the submerged period obtaining time series of near bed measurements of h, u, v and c through the tidal cycle. The data are corrected for internal clock drift by a GPS receiver unit that applies corrections between submersion events. In respect of the vertical sign convention used in this study, the origin is the still-water surface level. Therefore increasing positive values of h denote increasing depth.

5.2.2 Pressure transducer

The pressure transducer (PT) used on the SLOT rigs is the Druck PDCR 1830 strain gauge model in which there is a micro-machined silicon element contained within a titanium pressure module assembly. The assembly is housed in a cylindrical titanium unit that is fully sealed from the surrounding media. The measurement of hydrostatic pressure depends on the near linear relationship between the pressure (p) exerted by a column of fluid above the sensor and the height of the column (z) ($z = -h$), such that the former expressed in decibars (dbar) is a good approximation of the numerical value of z expressed in meters. The hydrostatic pressure causes element displacement which is converted into a voltage output by means of a bridge configuration of piezo-resistance strain gauges. The voltage output is a function of the resistance change due to the strain exerted on the element (Morris, 1993). The very small voltages generated by the strain gauges are first amplified then low pass filtered before being output. The PT operates within a range of 0 to 200 kPa absolute with a resolution of 0.1 kPa and a corresponding voltage output range of 0 to 100 mV. The Druck PTs are calibrated in-house using precision pressure calibration equipment traceable to international standards. The process is undertaken in a controlled environment and involves simultaneous incremental pressure increases being applied to both the sensor undergoing calibration and a reference standard instrument, whereupon the output voltage of both can be directly compared. Calibration coefficients and offset values relating the pressure exerted on the transducer and the output voltage are obtained through linear regression. The calibration procedure is undertaken in a vacuum, hence a gauge pressure of 1 dbar is equivalent to $z = -1$ m which is derived from an equation of the following:

$$h = m(V_{output} - V_{offset}) + z_{inst} \tag{5.20}$$

Where h is depth (m), m is the calibration coefficient ($m.V^{-1}$), V_{output} is the output voltage (V), V_{offset} is the offset voltage at the start of the calibration (V) and z_{inst} is the height of the instrument above the seabed (m).

The measurement of surface elevation using a PT in the nearshore environment yields two parameters which are the depth due to the tidal excursion (mean component) and the wave height (oscillatory component). In terms of the mean component, the manufacturer specifies the error due to the combined non-linearity, hysteresis and repeatability of the PT as ±0.1% of the full scale which equates to a measurement error of ±1 cm in a depth of 1 m. The measurement error involved in the oscillatory component arises from the following equation (Miles, 1997):

$$Q = \cosh(k(z+h)).(\cosh(kh))^{-1} \quad (5.21)$$

Where Q is the attenuation, k is the wave number (m^{-1}), h is the water depth (m) and z is the height of the PT (m) above the seabed. The current study involved depth measurements in shallow water ($h_{max} \approx 3.5$ m) under low energy conditions (maximum $H_s \approx 0.6$ m), the primary objective of which is to determine the principle mechanisms responsible for onshore sediment transport. In order to estimate the maximum error in wave height measurement applicable to the PT data obtained, the following parameters have been used: h = 0.5 m, z = -0.25 m, wave amplitude (A) = 0.3 m and peak wave period (T_p) = 5 s thus wavelength (λ) = 11.07 m from shallow water wave theory hence k = 0.57 m^{-1}. Inserting these values into Equation 5.21 gives an under estimation of wave height by the PT of < 3%, therefore for a 0.6 m wave in a depth of 0.5 m, the wave height would be recorded as 0.582 m. The magnitude of this error is deemed sufficiently small to negate the application of a correction algorithm to the data for the

purposes of this study. The instruments are considered to have good measurement stability over the long term with the maximum drift error specified by the manufacturer at ±0.1 mV.annum^{-1}.

5.2.3 Electromagnetic current meter

The EMCM used on the SLOT rigs is the Valeport 2-axis flow sensor 802 model with a spherical 5.5 cm diameter moulded plastic head containing the flow sensor components which is mounted axially on a metal shaft. The measurement of flow is based on Faraday's laws of electromagnetic induction which state that:

- An electromagnetic force (EMF) is induced when a conductor is passed through a magnetic field.
- The strength of the EMF is proportional to the rate of change of the flux through the circuit.
- The direction of the induced EMF depends on the orientation of the field.

The EMCM head contains an electromagnetic coil and two pairs of orthogonal electrodes, seawater acts as the conductor thus the sensor is capable of measuring the strength and direction of flow of both components in accordance with Faraday's laws. Due to the very small voltages induced by the currents measured a preamplifier is incorporated into the head of the shaft to boost the voltage output range to ±5 V. The flow data is low pass filtered after amplification then logged in the range 0 to ±3.5 m.s^{-1} at a resolution of 1 mm.s^{-1}. The sensing volume of the EMCM's is three times that of the head diameter which translates to a requirement that no other solid object be placed within 5.5 cm of the face of the sensor head. The Valeport EMCMs are calibrated in-house using a series of tests in which the sensors are towed in a tank of water at

precisely known velocities. The experiment is repeated in both positive and negative flow directions. The output voltages are converted to flow measurements ($m.s^{-1}$) using an equation of the following form:

$$f = m(V_{gauge} - V_{offset}) \tag{5.22}$$

Where f is flow ($m.s^{-1}$), m is the calibration coefficient ($m.s^{-1}.V^{-1}$), V_{output} is the output voltage (V) and V_{offset} is the offset voltage at the start of the calibration (V). The magnitude of the EMCM offset of each instrument deployed in the field is verified before and after each experiment by immersing the sensor head in an in-situ water container. The manufacturer specifies the accuracy of the EMCM's as ±1% of the reading plus zero drift for average flow which has been estimated to translate to a maximum error of ±1.5 $cm.s^{-1}$ in a flow of 1 $m.s^{-1}$ (Miles, 1997).

5.2.4 Optical backscatter sensor

The optical back scatter sensor (OBS) used on the SLOT rigs is the Downing & Associates Instruments OBS-3 in which a high intensity infrared (IR) emitting diode and a detector consisting of four photodiodes are housed in a glass filled polycarbonate unit made of optical grade epoxy. The OBS sensor emitter radiates a high intensity conical beam and the subsequent measurement of material in suspension depends on a semiconductor detector changing its electrical characteristics in response to being illuminated by IR radiation scattered back from particulate matter in suspension. The strong attenuation of IR radiation in water, e.g. the intensity decreases by 63% per 5 cm travelled in clear water, makes this type of radiation particularly suitable for the measurement of suspended particulate matter in close proximity to the sensor head, and

also reduces the potential contamination due to the IR component of solar radiation. The beam width at a distance where the IR radiation has spread to half of its power density at source is 50° in the axial plane and 30° in the horizontal plane, the absolute distance being dependent on the optical properties of the surrounding fluid. The detector integrates back scattered IR radiation between 140° and 160° which is amplified and low pass filtered. The OBS-3 has a dynamic measurement capability of 2 to 100,000 $mg.l^{-1}$ with a frequency response of 10 Hz and a voltage output range 0 to 5 V.

The calibration of the OBS sensors used on the SLOT rigs needs to be undertaken prior to instrument deployment using sediment collected from the site under investigation. This is due to the fact that for a given volume of fluid, the amount of backscatter is a function of both grain size and sediment concentration. This is particularly important for suspended sediment measurements on the offshore sandbank at Teignmouth due to its coarse nature ($d_{50} \approx 3$ mm) which settle out of suspension rapidly. The rapid settling velocity of coarse sediment complicates the calibration process, for this reason it was decided to adopt the method developed by Butt *et al.* (2002) in which glycerol is used in place of water due to its higher viscosity, thereby reducing the settling velocity of the grains. The method involves the addition of measured quantities of sediment to a known volume of glycerol which is stirred to maintain the grains in suspension. Justification for the use of glycerol relates to the fact that stirring ceases at the moment the OBS reading is taken. The coarseness of the sediment on the offshore sandbank meant that it was difficult to maintain a spatially homogenous sediment suspension in water for the period between the cessation of stirring and taking the reading but this was greatly improved by using the higher viscosity medium. Measurement errors can occur should the gain be set incorrectly. As a consequence of there being a 5 V upper limit on the output voltage, if the gain is set too high, there is the potential to lose data due to

'saturation' of the detector at below-peak concentrations. Conversely, setting the gain too low could result in poor resolution of the data. The manufacturer specifies the OBS-3 error due to nonlinearity as 3.5% with a maximum additional contribution due to hydrodynamic noise of 5% RMS of the mean signal which is deemed insignificant.

5.3 Data collection strategy

Obtaining in-situ data for the present study site was facilitated by the Coastview project which required that six-monthly topographic and bathymetric surveys of the beach and nearshore regions were undertaken. The deployment of the instrumentation was synchronised with the project's survey program in order to optimise data collection. The Coastview survey program was scheduled to coincide with periods of maximum spring tide excursion for ease of instrument deployment, maintenance and data downloading. The measurements presented in this chapter were obtained during the Coastview survey in the summer of 2003 which occurred between the 12th and 19th May. At the time of the survey, the new offshore sandbank that had formed in the latter months of 2002 had already migrated a significant distance onshore ($\approx$ 200 m, see Figure 4.13) which meant that it became sufficiently exposed at spring low tide to afford the unique opportunity of deploying instruments on an migrating ebb tidal delta sandbank. The choice of where to position the instrumentation was primarily driven by observations of strongly oblique waves breaking along the flanks of the sandbank at times when it was not submerged. The oblique waves were considered to be important in the general onshore migration of the feature, but also it was thought that they may be a significant factor in the elongation of the sandbank that is typical of its observed morphological evolution. The principle aim therefore, was to concentrate the instrumentation on the flanks of the sandbank. The crest of the sandbank was selected as a secondary position for the location of

instrumentation since at times when the sandbank is completely submerged and the local water depth over the sandbank is shallow ($h \leq h_b$), strong wave refraction over the top of the feature creates a zone of wave convergence. It was thought that these periods in the tidal cycle were likely to be periods of increased sediment transport over the crest of sandbank and hence also important in the features sedimentation.

On the following page Figure 5.5 shows the bathymetry and topography of the Teignmouth nearshore region at the time of the fieldwork program along with the instrument deployment positions (SLOT rigs and ADCP). Two instrument rigs were deployed on the sandbank and these are denoted in Figure 5.5 by the numbers 1 and 2. Each rig was initially deployed at the positions denoted by the suffix A, and then moved to secondary positions denoted by the suffix B. The results presented in this chapter are supplemented by environmental data obtained from a pier-located meteorology station and pressure transducer, an offshore seabed located acoustic Doppler current profiler (ADCP), and surficial sediment samples taken from various locations around the sandbank morphology.

5.4 Data processing

The data for each instrument were sampled at 4 Hz and low-pass filtered to prevent aliasing errors (Section 5.1.1). After correcting the EMCM data for the temporal offset introduced by the integrated analogue filter, instrument calibration coefficients, gain and offsets were applied in order to convert the measurements into hydrostatic pressure, horizontal orthogonal current velocities and suspended sediment concentrations. Subsequently the data were subdivided into 17 minute data runs and scrutinised for the presence of dry runs and anomalies e.g. spikes and instrument drop out (Appendix A2). The length of the data subdivisions is determined by the need to satisfy the conditions

for stationarity and ergodicity (Section 5.1.2), and in order to have 2^n data points per data string (i.e. $2^{11} = 4096$ data points in this instance) so that the FFT algorithm could be applied (Section 5.1.3).

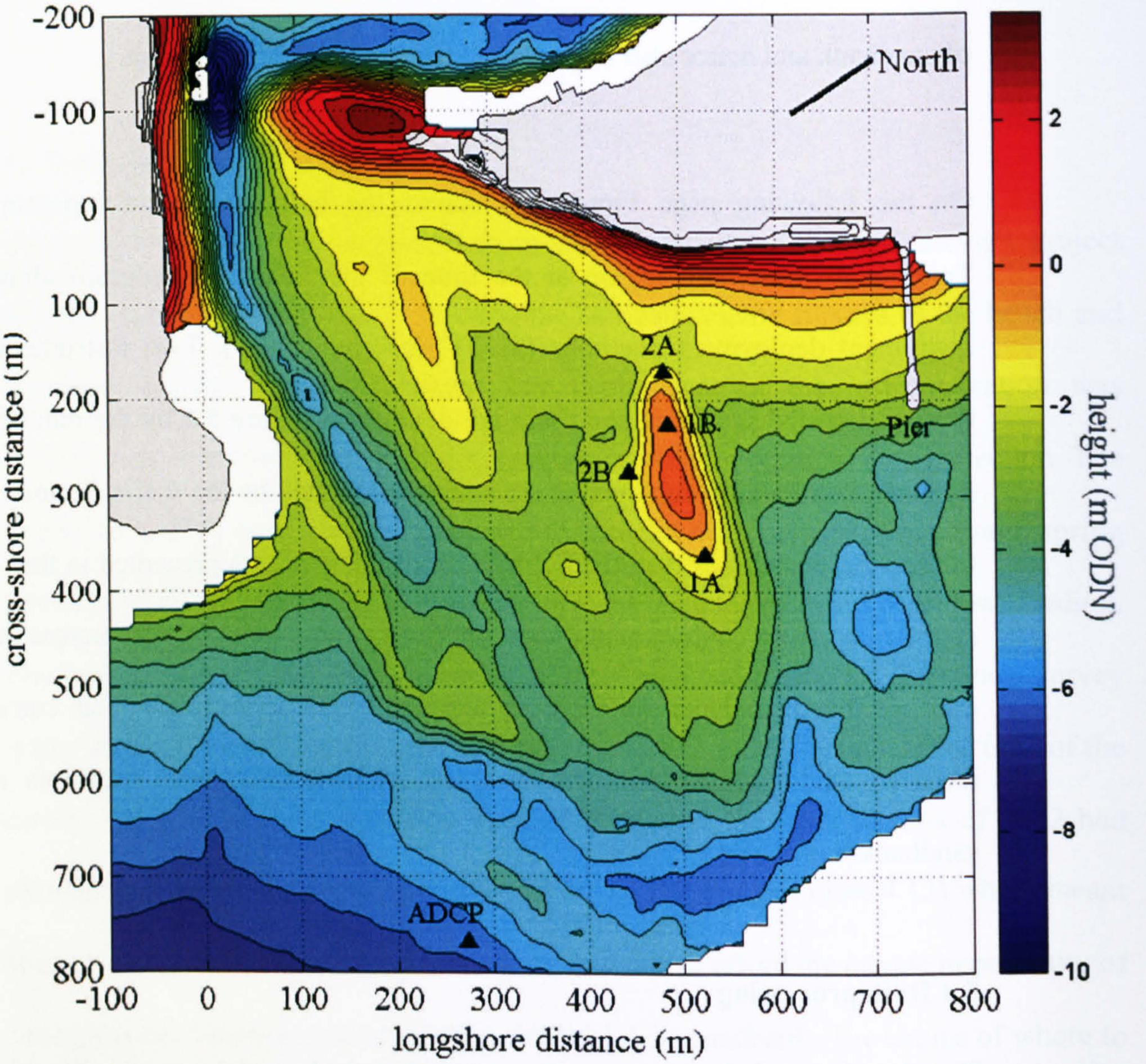

Figure 5.5: Contour plot of the bathymetry and topography of the study site during the May 2003 fieldwork program with SLOT and ADCP positions (▲) superimposed. The contours are in metres referenced to ODN.

5.5 Fieldwork environmental conditions

The field measurement period took place between the 14th and 19th May and the different conditions experienced can typically be expected to occur 75% of the time (Section 3.2). The wind and offshore wave conditions (h = -5.8 m ODN) for the field measurement period are presented in Figure 5.7 along with vertical lines denoting times

when noticeable changes occurred in the significant wave height conditions. In the following chapter the term 'calm conditions' is used to describe the 14th May conditions in which offshore winds produced a calm sea surface that was accompanied by small waves ($H_s \leq 30$ cm) which are typical conditions at Teignmouth when the wind has a westerly component (Figure 5.6a). The term 'low energy' is used to describe the choppy conditions of the 16th May that are generated by onshore winds producing significant wave heights of between 0.5 m to 1.0 m Figure 5.6b (Section 3.2). The three periods of differing incident wave conditions that are demarcated by the vertical lines in Figure 5.7 are summarised in terms of the significant wave height variability as follows:

1. 0000 hrs 14/05/08 to 1000 hrs 15/05/08: calm wave conditions, $H_s \approx 0.2$ m.

2. 1000 hrs 15/05/08 to 2200 hrs 16/05/08: H_s increases and peaks at a maximum of 0.79 m before decreasing to 0.3 m (low energy conditions).

3. 2200 hrs 16/05/08 to end of measurement period: H_s fluctuates in the range 0.3 to 0.6 m (low energy conditions).

The observed changes in the significant wave height during the measurement period were brought about by changes in the local wind strength and direction though it should be reiterated that at no time were high energy conditions recorded. In the first wave height subdivision, Teignmouth was under the influence of westerly winds in the range 2 to 5 $m.s^{-1}$ and as a consequence of these being offshore directed they produced calm sea conditions ($H_s \leq 0.2$ m). The ADCP struggled to resolve the period and direction of the incident waves during this initial period of low energy conditions which is manifest in the time series by the observed large and random variability in both parameters. On the morning of the 15th May at the start of the second wave height subdivision, a developing ridge of high pressure over the U.K. brought a period of onshore directed south-easterly winds (maximum strength $\approx$ 6 $m.s^{-1}$) which increased the significant wave height culminating in a peak of 0.8 m at approximately 1330 hrs on the 16th May.

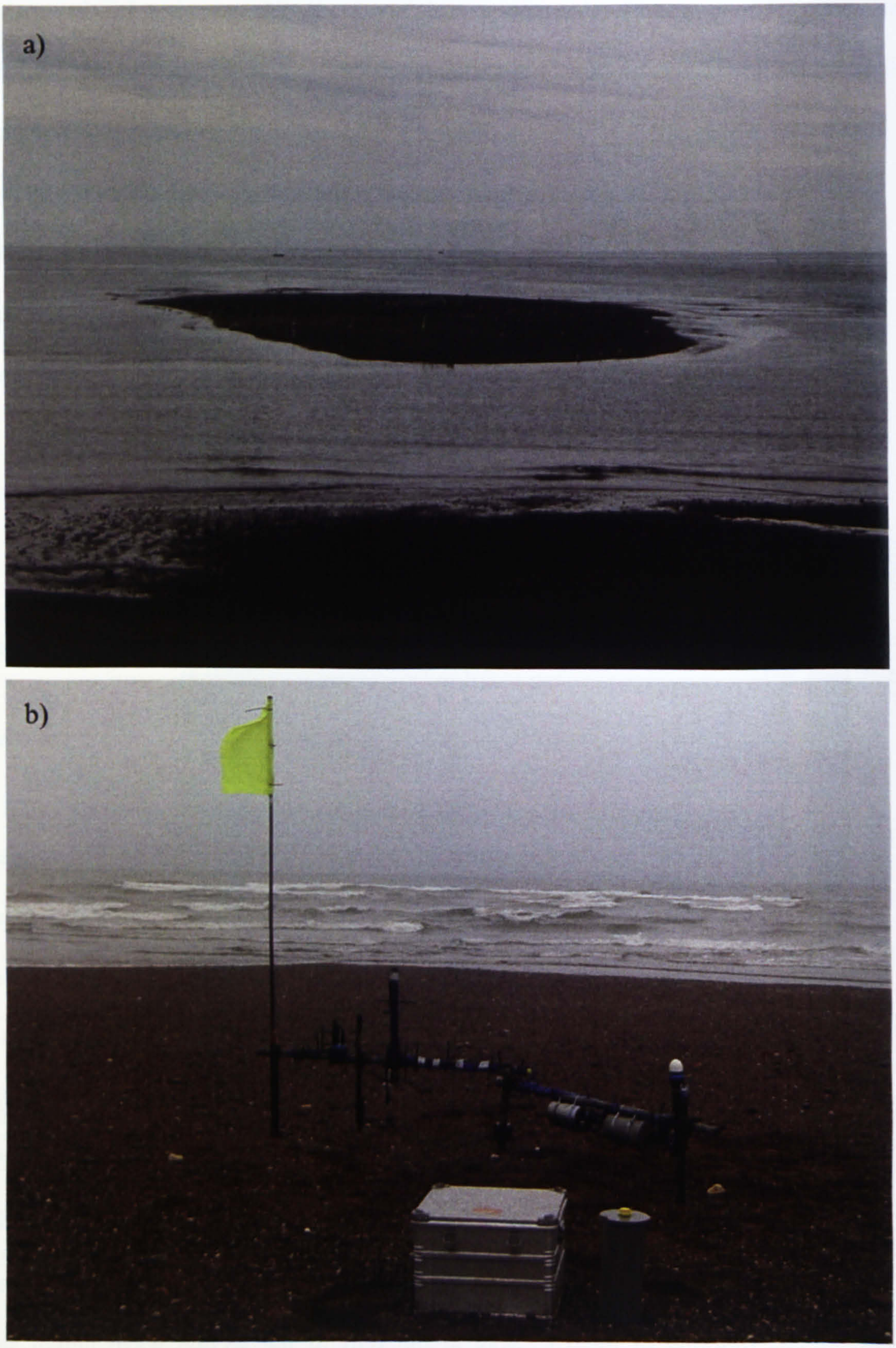

Figure 5.6: Images depicting the sea state at Teignmouth on a) the 14th May (calm conditions) and b) the 16th May (low energy conditions). (SLOT 1A deployment position is pictured in the foreground).

During this period of increased wave height, the wave period was observed to increase from 3 s to a maximum of 6 s with the predominant wave direction from the SSE.

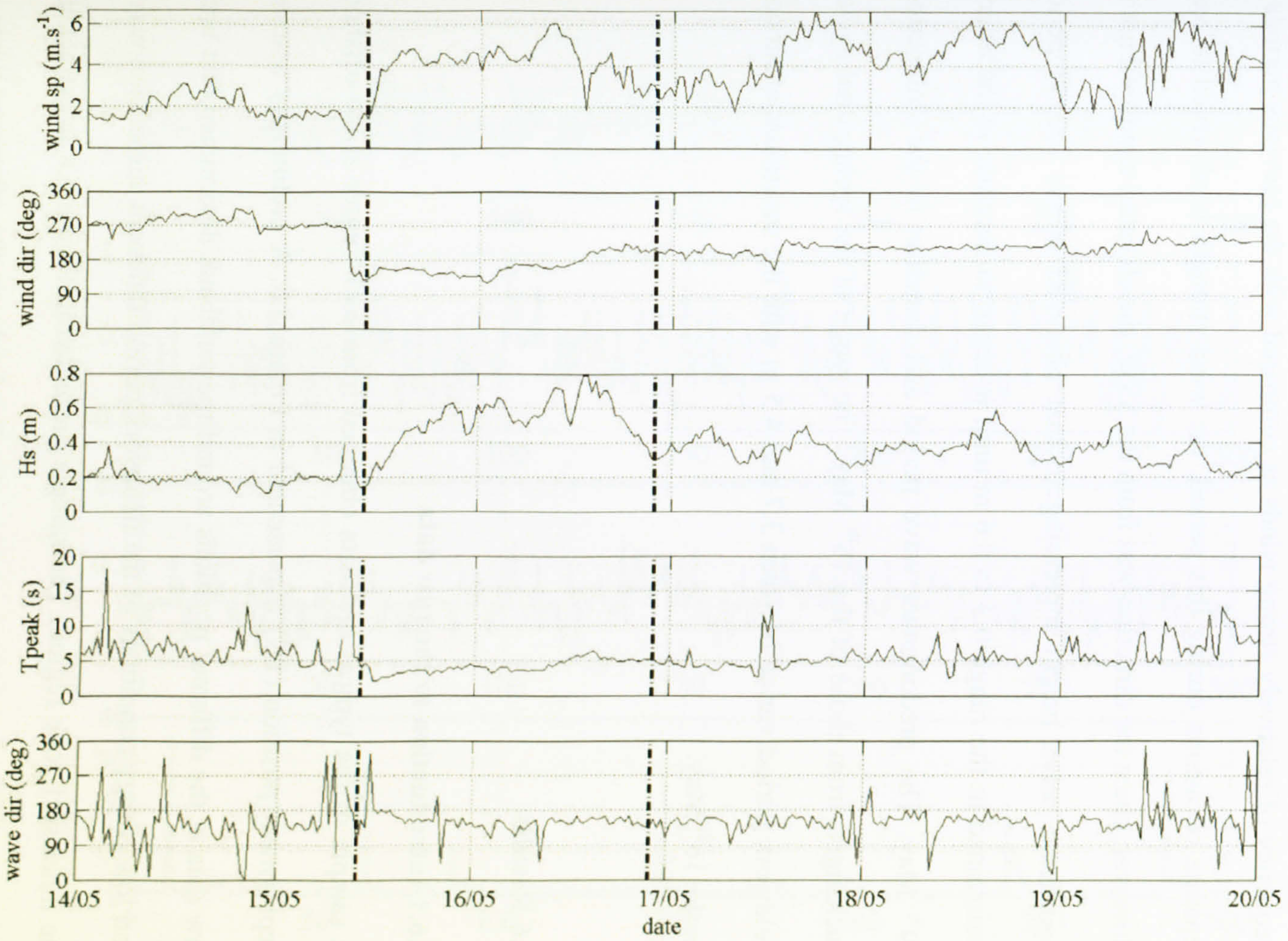

Figure 5.7: Wind and offshore ADCP (h = -5.8 m ODN) wave measurements during the fieldwork program. The vertical lines denote times when there was a noticeable change in the significant wave height conditions. Note: wind direction is measured relative to True North and indicates the direction from which the wind is coming from, wave direction is measured relative to the shore normal where a 180° wave direction indicates that the waves are propagating onshore in a perpendicular manner to beach face).

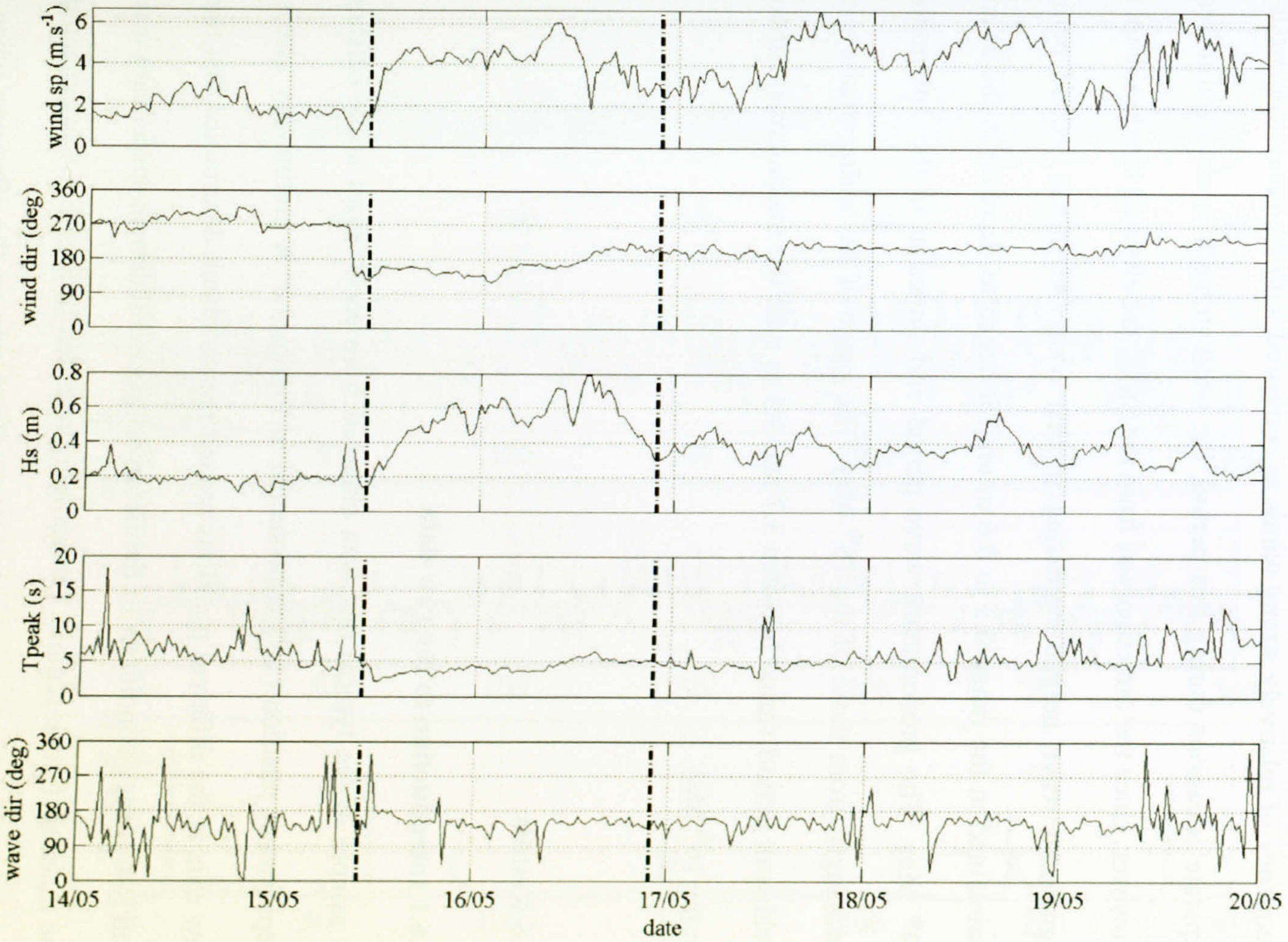

Figure 5.7: Wind and offshore ADCP (h = -5.8 m ODN) wave measurements during the fieldwork program. The vertical lines denote times when there was a noticeable change in the significant wave height conditions. Note: wind direction is measured relative to True North and indicates the direction from which the wind is coming from, wave direction is measured relative to the shore normal where a 180° wave direction indicates that the waves are propagating onshore in a perpendicular manner to beach face).

At approximately 0100 hrs on the 16th May the wind direction began to change and by 1300 hrs was observed to have a westerly component. Over the remainder of the fieldwork period the wind direction was from the SSW, whilst the wind speed fluctuated in the range between 1 and 6.5 $m.s^{-1}$. The 3rd period is noteworthy for the frequency of relatively strong winds as compared with the previous periods as on three separate occasions during this period, the wind strength is observed to reach 6 $m.s^{-1}$. However, since the direction was from the SSW, the elevated winds did not result in the significant wave height increasing to that observed in the second period but was maintained in the range 0.3 to 0.6 m until it began to decrease in the afternoon of the 19th May. The predominant wave period and direction in the 3rd period remained unchanged from those of the 16th May. The range of the spring tidal cycle during the fieldwork period varied between 3.7 and 4.5 m with the maximum excursion occurring on the 16th May.

5.6 Results

5.6.1 Introduction to the raw data

A sample of the typical raw data obtained from each sensor at the offshore extremity deployment position (1A) is presented in Figure 5.8. A preliminary assessment of the raw data at the different positions around the sandbank determined that under the calm and low energy conditions of the fieldwork period sediment suspension was confined to the inner surf zone region. The sample presented in Figure 5.8 is extracted from run 3 on the 16th May which was during the flood tide on the afternoon when the incident wave conditions were increasing to their maximum.

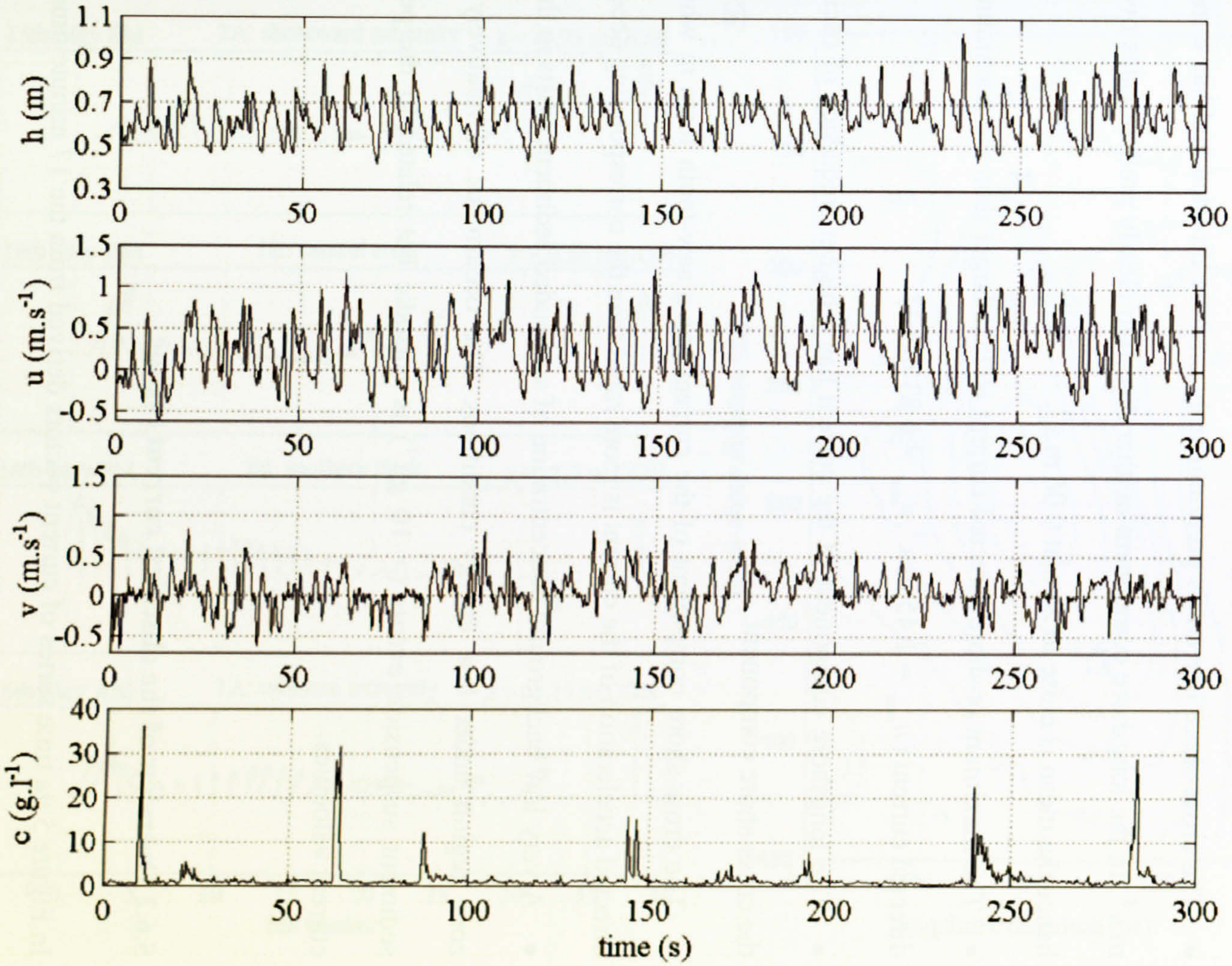

Figure 5.8: Raw data time series from run 3 (inner surf zone) on the 16th May for water depth (h), cross-shore current (u), longshore current (v), and suspended sediment concentration (c). Note for u and v, a positive value denotes an onshore directed current and a negative value denotes an offshore directed current.

The plotted data are particularly relevant to the current study because it is during the repeated incidences of low energy conditions that the onshore migration of the sandbank is maintained between storm events. The following observations are made on the time series:

- The cross-shore current is predominantly onshore directed and has a mean of 0.27 $m.s^{-1}$. In the longshore component neither direction clearly predominates over the other hence the mean is close to zero at 0.06 $m.s^{-1}$.
- The maximum onshore directed current is 75% larger than the maximum longshore directed current (u_{max} = 1.45 $m.s^{-1}$, v_{max} = 0.83 $m.s^{-1}$).
- The longshore component of the current has a higher frequency of oscillation than the cross-shore component.
- The cross-shore component of the current has a saw-tooth form in which onshore directed acceleration of the current is more rapid than the corresponding deceleration.
- A very low background concentration of suspended sediment exists in the inner surf zone region under low energy conditions. The occurrence of relatively significant sediment suspension events (> 10 $g.l^{-1}$) is episodic but related to the peak onshore current velocities.

5.6.2 Overview of the observed current regime

In Figure 5.9a time series of current vectors derived from the 17 minute time average of the *u* and *v* current data are presented from each of the SLOT rig deployment positions. A contour plot of the bathymetry of the offshore sandbank with the deployment positions overlaid is presented in Figure 5.9b.

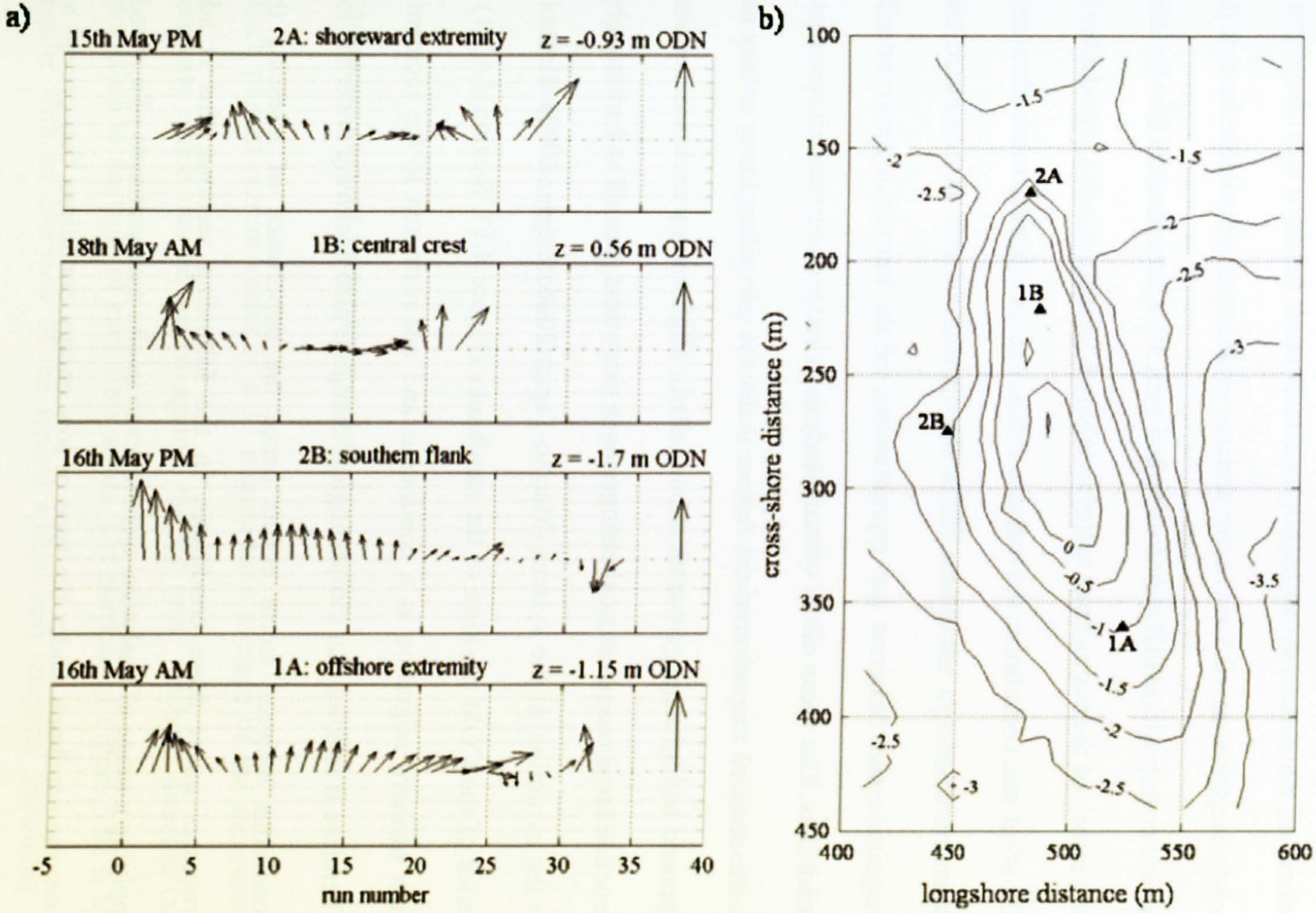

Figure 5.9: a) current vector time series from each SLOT rig deployment position using data averaged over 17 minute intervals for the duration of one tidal cycle. For scaling purposes a vertical vector denoting an onshore directed current of 0.5 $m.s^{-1}$ is positioned to the right of each vector time series plots, b) sandbank bathymetry with SLOT rig deployment positions overlaid. The abbreviations AM and PM relate to the 1st and 2nd tides of the day.

The deployment of two SLOT rigs in rotation between positions 1 and 2 means that contemporaneous vector time series for all four SLOT deployment positions cannot be presented. Wherever possible time series were selected from the higher energy 2nd period of wave activity as highlighted in Section 6.5 in which the significant wave height increases to +0.5 m. In the absence of data being available for this period at the central crest position (1B), time averaged current vectors for the 18th May are presented.

Since each of the vector time series in Figure 5.9a relates to the period after the onset of the wind sea conditions, the vectors define the sandbank's mean flow regime under typical low energy conditions. Therefore it follows that the observed trends in the magnitude and direction are representative of the current regime under low energy conditions. The focus of the current study is to better understand the processes that lead to the onshore migration of the feature under the prevailing lower energy conditions as opposed to high energy events (H_s > 1.0 m). High energy events have been shown to generate large morphological changes over short time periods and are thereby important to the evolution of the system (Marino-Tapia, 2006; Siegle, 2003). However the time series of the COM position of the sandbanks (Figure 4.17, Section 4.4.3.1) shows that their onshore migration is a continuous and not restricted to the incident of storms. Therefore it follows that morphological change is also occurring under the lower energy conditions between storm events hence the importance of assessing the physical processes under these conditions. In the following sections, this is addressed by applying a range of analytical techniques to in-situ measurements of *u*, *v* and *c* obtained from the sandbank under the type of low energy conditions that prevail at the Teign inlet.

Sandbank morphology

During the fieldwork program, the instrumented sandbank had an elongate transverse morphology that was 240 m in length and had a maximum width of 95 m that narrowed sharply on the southern flank, decreasing it to approximately 50 m for the shoreward 130 m section of its length. The sandbank had a maximum height of between 2.5 and 3.0 m and extended to a maximum depth of approximately -2.5 m ODN. Along the central axis of the sandbank, the relatively flat crest region of the feature extended for 100 m in the cross-shore direction at a constant level that was close to 0 m ODN (Figure 4.6, Section 4.2). The gradients of the slopes around the sandbank tend to be steeper on the northern flank and shoreward extremity (up to 1:10) when compared with the southern flank and offshore extremity (typically in the range 1:15 to 20). Due to the use of a 10 m grid spacing, the Matlab 'contour' function has not fully resolved the crest of the narrow shoreward section of the sandbank in the region of the central crest SLOT rig position (1B) and hence the apparent disparity between the SLOT *z* value at this location and the adjacent contour.

Resultant current vector time series

Each plotted current vector is a 17 minute time average of the measured orthogonal currents which can be scaled against the 0.5 $m.s^{-1}$ onshore directed current vector displayed to the right of each time series. The purpose of Figure 5.9a is to present the reader with an overview of the typical spatial and temporal variability in the mean current magnitude and direction under low energy conditions. A more detailed analysis of the hydrodynamics and sedimentation is provided in the following sub-sections. The vector time series reveal the spatial and temporal proliferation of onshore directed

The deployment of two SLOT rigs in rotation between positions 1 and 2 means that contemporaneous vector time series for all four SLOT deployment positions cannot be presented. Wherever possible time series were selected from the higher energy 2nd period of wave activity as highlighted in Section 6.5 in which the significant wave height increases to +0.5 m. In the absence of data being available for this period at the central crest position (1B), time averaged current vectors for the 18th May are presented. Since each of the vector time series in Figure 5.9a relates to the period after the onset of the wind sea conditions, the vectors define the sandbank's mean flow regime under typical low energy conditions. Therefore it follows that the observed trends in the magnitude and direction are representative of the current regime under low energy conditions. The focus of the current study is to better understand the processes that lead to the onshore migration of the feature under the prevailing lower energy conditions as opposed to high energy events (H_s > 1.0 m). High energy events have been shown to generate large morphological changes over short time periods and are thereby important to the evolution of the system (Marino-Tapia, 2006; Siegle, 2003). However the time series of the COM position of the sandbanks (Figure 4.17, Section 4.4.3.1) shows that their onshore migration is a continuous and not restricted to the incident of storms. Therefore it follows that morphological change is also occurring under the lower energy conditions between storm events hence the importance of assessing the physical processes under these conditions. In the following sections, this is addressed by applying a range of analytical techniques to in-situ measurements of *u*, *v* and *c* obtained from the sandbank under the type of low energy conditions that prevail at the Teign inlet.

Sandbank morphology

During the fieldwork program, the instrumented sandbank had an elongate transverse morphology that was 240 m in length and had a maximum width of 95 m that narrowed sharply on the southern flank, decreasing it to approximately 50 m for the shoreward 130 m section of its length. The sandbank had a maximum height of between 2.5 and 3.0 m and extended to a maximum depth of approximately -2.5 m ODN. Along the central axis of the sandbank, the relatively flat crest region of the feature extended for 100 m in the cross-shore direction at a constant level that was close to 0 m ODN (Figure 4.6, Section 4.2). The gradients of the slopes around the sandbank tend to be steeper on the northern flank and shoreward extremity (up to 1:10) when compared with the southern flank and offshore extremity (typically in the range 1:15 to 20). Due to the use of a 10 m grid spacing, the Matlab 'contour' function has not fully resolved the crest of the narrow shoreward section of the sandbank in the region of the central crest SLOT rig position (1B) and hence the apparent disparity between the SLOT *z* value at this location and the adjacent contour.

Resultant current vector time series

Each plotted current vector is a 17 minute time average of the measured orthogonal currents which can be scaled against the 0.5 $m.s^{-1}$ onshore directed current vector displayed to the right of each time series. The purpose of Figure 5.9a is to present the reader with an overview of the typical spatial and temporal variability in the mean current magnitude and direction under low energy conditions. A more detailed analysis of the hydrodynamics and sedimentation is provided in the following sub-sections. The vector time series reveal the spatial and temporal proliferation of onshore directed

currents across the majority of the sandbank, and throughout the tidal cycle. The strongest of these occur in the shallow surf zone region ($h < 0.5h_b$) with maximum mean values of 0.65 $m.s^{-1}$ for the initial flood tide runs at the central crest (1B) and southern flank (2B) SLOT positions. The general trend is one of relatively strong currents in the initial runs (inner surf zone) that abate with increasing water depth, though at the southern flank (2B) and offshore extremity (1A) positions there is a secondary resurgence in the current strength that peaks at around the time of high tide (up to 0.3 $m.s^{-1}$). During the first half of the ebb tide, the current vector time series display greater temporal variability in direction; at all SLOT deployment positions except the southern flank (2B), the currents increase in strength and rotate northwards until becoming approximately longshore orientated with respect to the shoreline of Teignmouth main beach. Subsequently, at the southern flank the mean current diminishes to near zero before becoming offshore directed and increasing in strength temporarily (up to 0.3 $m.s^{-1}$). Significantly offshore directed currents are only observed during the ebb tide and only occur at the offshore extremity (1A) and southern flank (2B) SLOT positions. They occur in the surf zone ($h < h_b$) during runs 24 to 28, and 31 to 34 respectively but the currents are relatively weak with maximum values of approximately 0.3 $m.s^{-1}$ and do not persist for more than four runs. Before the period of increased significant wave height (period 1 from Section 5.5) offshore directed currents were also observed in the surf zone at the offshore extremity SLOT position (1A) during the two flood tides (data not presented). However, upon the onset of increasing significant wave height, these offshore directed flood tide currents were replaced by onshore directed currents as seen in the time series for the 16th May presented in Figure 5.9. As the tide continues to ebb and the water depth decreases towards the breaker depth (h_b), the mean current at the offshore extremity (1A) which is at this time flowing in an approximately longshore manner (NNE), rotates offshore in a similar manner to the current at the southern flank

(2B) but these are then replaced by increasing onshore directed currents in the last three runs. The mean currents at the two shoreward SLOT positions (central crest and shoreward extremity) which are also very oblique initially decrease during this stage of the tide before increasing and becoming onshore directed in the shallowest run.

The mean flow over different parts of the sandbank is variable and complex but the key features of the current regime can best be summarised as follows:

- Onshore directed currents dominate over all areas of the sandbank on the flood tide.
- The strongest currents occur in the surf zone region ($h < h_b$) and are predominantly onshore directed.
- The current strength decreases with increasing water depth but the manner in which this occurred displayed some variability between locations.
- The ebb tide currents show greater directional variability. After high tide the mean current direction rotates northward and increases in strength until becoming approximately longshore directed with respect to the main beach. Subsequently the current becomes offshore directed at the two outermost SLOT positions and onshore directed at the two innermost.
- The incidence of offshore directed currents is comparatively rare and confined to the mid to outer surf zone region.

It is clear from the current vector time series in Figure 5.9 that there is a spatial and temporal dominance of onshore directed currents over much of the sandbank throughout the tidal cycle. However it is the concurrence of the onshore directed currents in the surf zone with sediment suspension events that provides the physical mechanism for the onshore migration of the morphological feature under low energy conditions. Mean

offshore and longshore directed currents (w.r.t. Teignmouth main beach) are also present on the sandbank under certain conditions, and they do reach similar magnitudes to the onshore component, but the incidences of these are relatively infrequent and they usually occur during deeper water runs. However, at the shoreward extremity, there is a strong component of the mean longshore current in run 1 but due to the cross-shore component being of similar magnitude, the net flow is still onshore directed.

It should be clarified at this point that the onshore directed currents that act over the sandbank particularly down the flanks when the feature is exposed by the tide are generated by waves that have been strongly refracted by the morphology of the feature. The strong refraction leads to the shoaling and breaking waves having very oblique angles of incidence therefore the currents are in effect longshore currents. With respect to the Teignmouth main beach these currents are actually of an approximate shore-normal orientation. In order to avoid potential confusion of terminology in the text these currents are referred to as onshore directed currents through the course of the work. In the following sections, the relative importance of the cross-shore current strength in relation to the incidence of sediment suspension is investigated through the use of time and frequency domain techniques. The offshore extremity SLOT position (1A) has been selected for this purpose because the data spans the period from the 14th May to the 17th May thereby enabling the comparison of sediment transport under the calm conditions versus the low energy conditions.

5.6.3 Comparison of cross-shore hydrodynamics and sedimentation under calm and low energy conditions

In Figure 5.10 the time averaged water depth (< h >), significant wave height (< H_s >), mean component of the cross-shore current (< $\overline{u}$ >), the oscillatory component of the cross-shore current (< u' >), and the concentration of suspended sediment (< c >) are presented for the calm (14th May PM) and low energy conditions (16th May PM). The longshore component has been omitted from this analysis since in the shallow water runs when sediment suspension is occurring, its magnitude is negligible when compared with the cross-shore component (Section 5.6.2) and therefore its contribution to the onshore migration of the sandbank is not considered significant. The following description of the form of the data focuses on the changes brought about by the onset of wind sea conditions.

Water depth

In Figure 5.10a the time averaged water depth shows the passage of the tidal cycle over the SLOT rig with high tide occurring during run 17 and maximum mean tidal heights of 3.0 m and 3.5 m ODN for the 14th and 16th May respectively. The increasing divergence of the two series as they tend towards high tide can be attributed to the difference in tidal range between the two days, the 16th May being the day with the largest spring tidal range (4.7 m) for the fieldwork period. There exists an asymmetry in the tidal curve with steeper gradients during peak ebb tide as compared with peak flood tide, which is accentuated in the 16th May dataset due to its greater range.

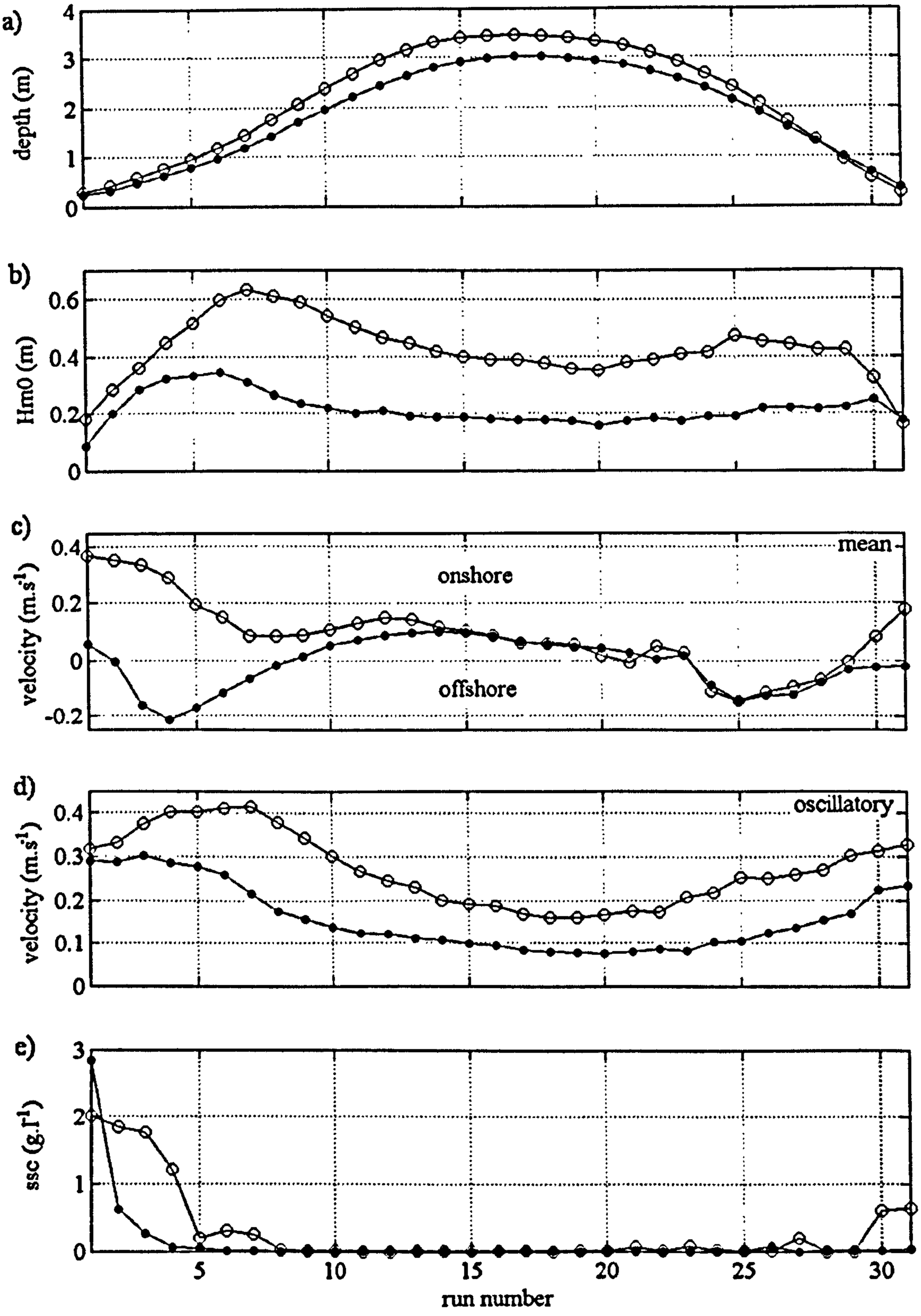

Figure 5.10: Comparison of hydrodynamics and sediment suspension under calm (dots) and low energy conditions (circles) for the offshore extremity SLOT position (1A): a) water depth (< h >), b) wave height (< H_s >), c) mean cross-shore current (< $\bar{u}$ >), d) the standard deviation of the cross-shore current (oscillatory component) (< u' >), e) the mean suspended sediment concentration (< c >), (Note: each plotted point is a 17 minute time average of the data).

Significant wave height

The time series of significant wave height on both days is asymmetric with larger waves occurring on the flood tide. On the 14th May, the maximum mean significant wave height was 0.35 m which occurred during run 6, whilst the maximum on the 16th May was 0.63 m which occurred during run 7. The occurrence of the maximum mean shoaling wave height in these two runs suggests that these represent the outer limit of the flood tide surf zone on the respective days but on the ebb tide, the outer limit of wave breaking is less clearly defined. On the 14th May, the conditions were effectively calm, though the data indicate that very small waves were breaking on the offshore extremity of the sandbank but only during the initial one or two runs, whilst on the 16th May, the larger ebb tide waves were still breaking in run 3. There is an apparent secondary peak in the mean significant wave height in run 5 on the 16th May, but with a mean water depth of 2.4 m, the water is too deep for the small waves ($< H_s > = 0.47$ m) to be breaking. In the deeper water outside of the surf zone the significant wave height decreases to minimum values in run 20 with mean significant wave heights of 0.16 m and 0.35 m for the 14th and 16th May respectively.

Mean and oscillatory cross-shore current components

In Figure 5.10c and d, the cross-shore current time series have been decomposed in to the steady (mean) and oscillatory (standard deviation) components in order to assess their relative contributions to the sediment transport on the offshore sandbank. The following description of the cross-shore current component concentrates on the inner surf zone runs where sediment is being brought in to suspension. The general form of the mean cross-shore current time series for the 14th May has a w-shaped profile which is the typical form usually found on open coast beaches. The profile takes this form due to the variability in the mean cross-shore current which can be onshore or offshore

directed depending on the conditions. Onshore directed mean currents occur in the initial runs which subsequently become offshore directed for most of the surf zone region. These are subsequently replaced by onshore currents in the deeper water depths beyond h_b. Typically, the same current profile is repeated on the ebb tide and hence the w-shape. The 14th May mean current profile emulates that typically found on open coast beaches exposed to wave action but with an asymmetry in which the ebb tide mean currents are generally weaker. The profile for the 16th May has a similar form to the 14th May profile but, importantly the weak inner surf zone mean currents (< 0.1 m.s^{-1}) have been replaced by significantly stronger onshore directed mean currents (≈ 0.4 m.s^{-1}). The general form of the mean oscillatory cross-shore current in both profiles is one of higher mean values in the surf zone region due to wave shoaling effects which then become abated in water depths > h_b. The effect is pronounced on the flood tide due to the tidal asymmetry in wave height. The magnitude of the mean oscillatory cross-shore current in the inner surf zone for both days is similar on the flood tide (≈ 0.3 m.s^{-1}) but over the majority of the profile, they are a minimum 0.1 m.s^{-1} stronger on the 16th May than on the 14th May owing to the higher energy conditions. The profiles of the mean cross-shore current on the two days converge outside of the surf zone (between runs 14 and 29) but inside the surf zone the currents diverge due to the contribution of the incident waves. There are significantly stronger mean currents in the inner surf zone on the 16th May when compared with the 14th May. the inner surf zone mean cross-shore currents reaches nearly 0.4 m.s^{-1} on the flood tide, and 0.3 m.s^{-1} on the ebb tide whilst on the 14th May the magnitude is close to zero in both cases and the maximum mean cross-shore current (≈ 0.2 m.s^{-1}) occurs in run 4.

Under low energy conditions, the key effects of the onset of the wind sea conditions that are important to the sediment transport at the offshore extremity of the sandbank occur in the shallow water runs and are as follows:

- Under calm conditions, the inner surf zone mean cross-shore current is close to zero but under low energy conditions, it increases to between 0.3 and 0.4 $m.s^{-1}$ depending on the state of tide and is onshore directed.
- Under low energy conditions the mean oscillatory currents throughout the tidal cycle are a typically 0.1 $m.s^{-1}$ larger than under calm conditions. In the shallow flood tide runs the mean values converge at approximately 0.3 $m.s^{-1}$.
- The mean cross-shore current profiles are asymmetric with stronger and more sustained inner surf zone currents on the flood tide than on the ebb tide.

Suspended sediment concentration

The maximum suspended sediment concentration on the 14th May occurred in run 1 (2.9 $g.l^{-1}$) and is significantly higher in terms of their relative magnitudes than the corresponding 16th May maximum concentration of 2.0 $g.l^{-1}$ (run 1). This apparent anomaly is considered to be a factor of the inherent errors introduced when undertaking the particularly difficult task of measuring key parameters in the nearshore. It is not intuitive for there to be higher suspended sediment concentrations occurring under calm conditions versus low energy conditions, but the results do suggest that even under calm conditions sediment is being brought in to suspension in the shallowest flood tide run, and that the concentrations may be of comparable magnitudes to those found under low energy conditions. On the 14th May, with increasing water depth there is a rapid decrease in the flood tide concentration of suspended sediment as compared with that on the 16th May. Under the higher energy wave conditions the rate of decrease over the

first three flood tide runs is negligible but subsequently decreases rapidly in run 4 culminating in a near zero concentration by run 5. As a consequence of the tidal asymmetry in the wave and current fields, the ebb tide mean concentration is near zero throughout the surf zone on the 14th May whilst on the 16th May, suspended sediment is confined to the two inner zone runs in which the maximum mean concentration in run 1 (≈ 0.7 g.l^{-1}) is less than 50 % of that on the flood tide (≈ 2.0 g.l^{-1}).

Key point summary:

- Under calm conditions, sediment is still being suspended in similar magnitudes to those under low energy conditions but only in the shallowest flood tide run.
- Under low energy conditions, the incidence of relatively significant sediment suspension events (> 10 g.l^{-1}) is confined to the inner surf zone.
- The asymmetry in the mean suspended sediment concentration profile reflects the asymmetry in the current profile with higher concentrations enduring for longer on the flood tide than on the ebb tide.

In the following sub-sections, the associated sediment transport resulting from the observed hydrodynamics and sedimentation are investigated in more detail.

Cross-shore sediment transport rates

The time averaged sediment transport rates for the offshore extremity position (1A) have been computed after Jaffe *et al.* (1984) (Section 5.1.2.1) and the results for the calm and low energy conditions are presented in Figure 5.11.

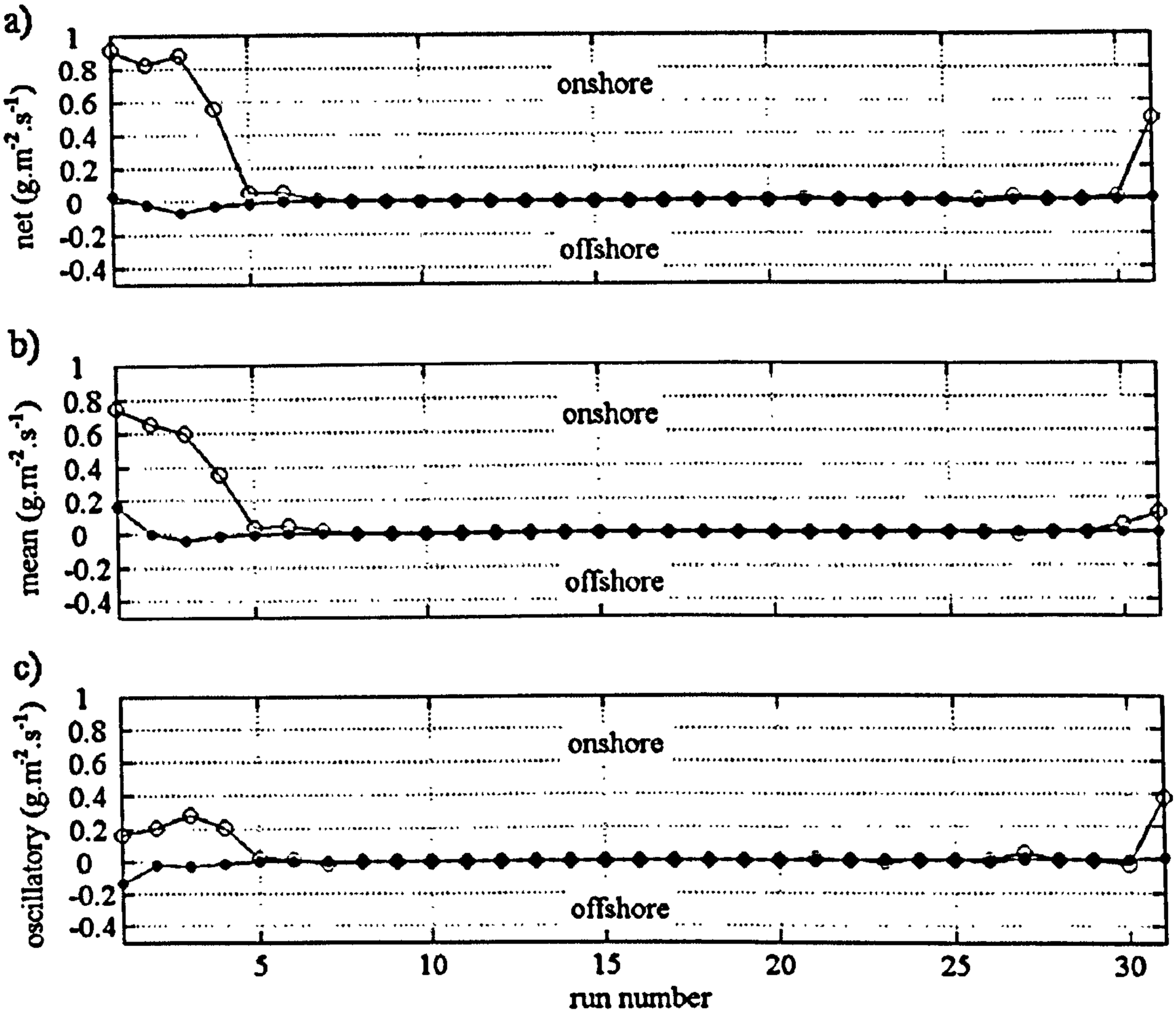

Figure 5.11: Comparison of the cross-shore sediment transport under calm (black dots) and low energy conditions (white circles) at the offshore extremity SLOT position (1A): a) net cross-shore sediment transport (< uc >), the mean component of the cross-shore sediment transport (< $\overline{u}\overline{c}$ >), and the oscillatory component of sediment transport (< $u'c'$ >). Each plotted point is a 17 minute time average of the data.

Since the strongest currents and highest sediment suspension events occur in the inner surf zone, this is where the mean net transport rates are highest. On the 14th May the calm conditions are generally not capable of suspending and transporting significant quantities of sediment and this is reflected in the negligible time averaged values over the tidal cycle. The peak 14th May sediment transport rate occurs in run 4 which is close to zero (-0.07 $g.m^{-3}.s^{-1}$) and is offshore directed on account of the mean flow that has the characteristics of an undertow current (Figure 5.10c). Correspondingly, the mean and oscillatory transport component rates on the 14th May are negligible over the whole tidal cycle. In run 1 when most suspension of sediment occurred the mean and oscillatory current components ($\overline{u}$ = +0.16 $g.m^{-3}.s^{-1}$, u' = -0.13 $g.m^{-3}.s^{-1}$) act in opposite directions

resulting in a negligible but onshore directed transport rate. In contrast to the 14th May, the higher energy conditions on the 16th May resulted in onshore directed sediment transport occurring in the inner surf zone on both flood and ebb tides as the asymmetry observed in the wave and current time series (Figure 5.10b and c) is translated in to the sediment transport time series. Consequently under the low energy conditions, there are higher maximum inner surf zone transport rates that endure for longer on the flood tide compared with the ebb tide. The run 1 maximum flood tide net transport rate is 0.9 $g.m^{-3}.s^{-1}$ (run 1), with comparable rates being sustained in runs 2 and 3 until a subsequent rapid decrease reduces the value to near zero by run 5. During the weaker ebb tide conditions, the maximum net sediment transport rate which occurs in the shallowest run (run 31) decreases to 0.5 $g.m^{-3}.s^{-1}$ which rapidly reduces to close to zero in the adjacent deeper run (run 30). Of the two cross-shore components, the mean cross-shore current is dominant on the flood tide through the inner to mid surf zone (runs 1 to 4) where the maximum mean transport rate of 0.7 $g.m^{-3}.s^{-1}$ (run 1) is 350 % larger than the maximum oscillatory rate of 0.2 $g.m^{-3}.s^{-1}$. The mean transport rate decreases in a near linear manner from the run 1 maximum value to close to zero by run 5 whilst the oscillatory rate increases to its maximum of 0.3 $g.m^{-3}.s^{-1}$ in run 3 before decreasing in a similar manner. Conversely on the ebb tide during the shallowest run, the situation is reversed with the oscillatory component being the greater constituent of the net onshore transport rate ($\overline{u} = 0.1$ $g.m^{-3}.s^{-1}$, $\tilde{u} = 0.4$ $g.m^{-3}.s^{-1}$).

The key points regarding the cross-shore sediment transport rates in relation to suspended sediment transport over the sandbank reflect the key points from the previous waves and current sub-sections:

- There is a strong tidal asymmetry in the transport rate magnitudes and, due to this it is primarily during the inner surf zone flood tide period in which the highest transport rates occur.
- On the flood tide, the transport due to the mean component dominates over that due to the oscillatory component with rates that are between 50 and 300% higher through the surf zone.
- During the weaker ebb tide conditions, onshore sediment transport also occurs in the shallowest inner surf zone, but in contrast to the flood tide, it is the oscillatory component that dominates the near bed sediment transport regime at this stage of tide.

5.6.4 Comparison of third order cross-shore velocity moments under calm and low energy conditions

In Figure 5.12 the 3rd order cross-shore velocity moments computed for the calm (Figure 5.12a) and low energy conditions (Figure 5.12b) are each presented in a series of three histograms for the inner, mid- and outer surf zone positions. Each histogram is orientated such that the velocity moment terms are the ordinates and their magnitude are the abscissas. Negative histogram values denote offshore transport and *vice versa*. In the absence of a clear and consistent spectral valley the short and long wave components were separated at a frequency of 0.05 Hz after Miles and Russell (2004). The magnitude of individual velocity moments are not considered in this analysis since they are derived from the cube of a velocity and therefore have units that are not meaningful in terms of sediment transport ($m^3.s^{-3}$) but it is their relative magnitudes and directions that is interest to the current study. The results of the analysis indicate that terms 1, 2, 4 and 5 are the most significant transport terms which are re-summarised in Table 5.2.

No	Term	Description
1.	$\bar{u}^3$	mean velocity cubed
2.	u'^3_s	short wave velocity skewness
4.	$3\langle u'^2_s\rangle\bar{u}$	stirring by short waves & transport by mean flow
5.	$3\langle u'^2_l\rangle\bar{u}$	stirring by long waves & transport by mean flow

Table 5.2: Velocity moment terms that constitute the sediment transport at the offshore extremity.

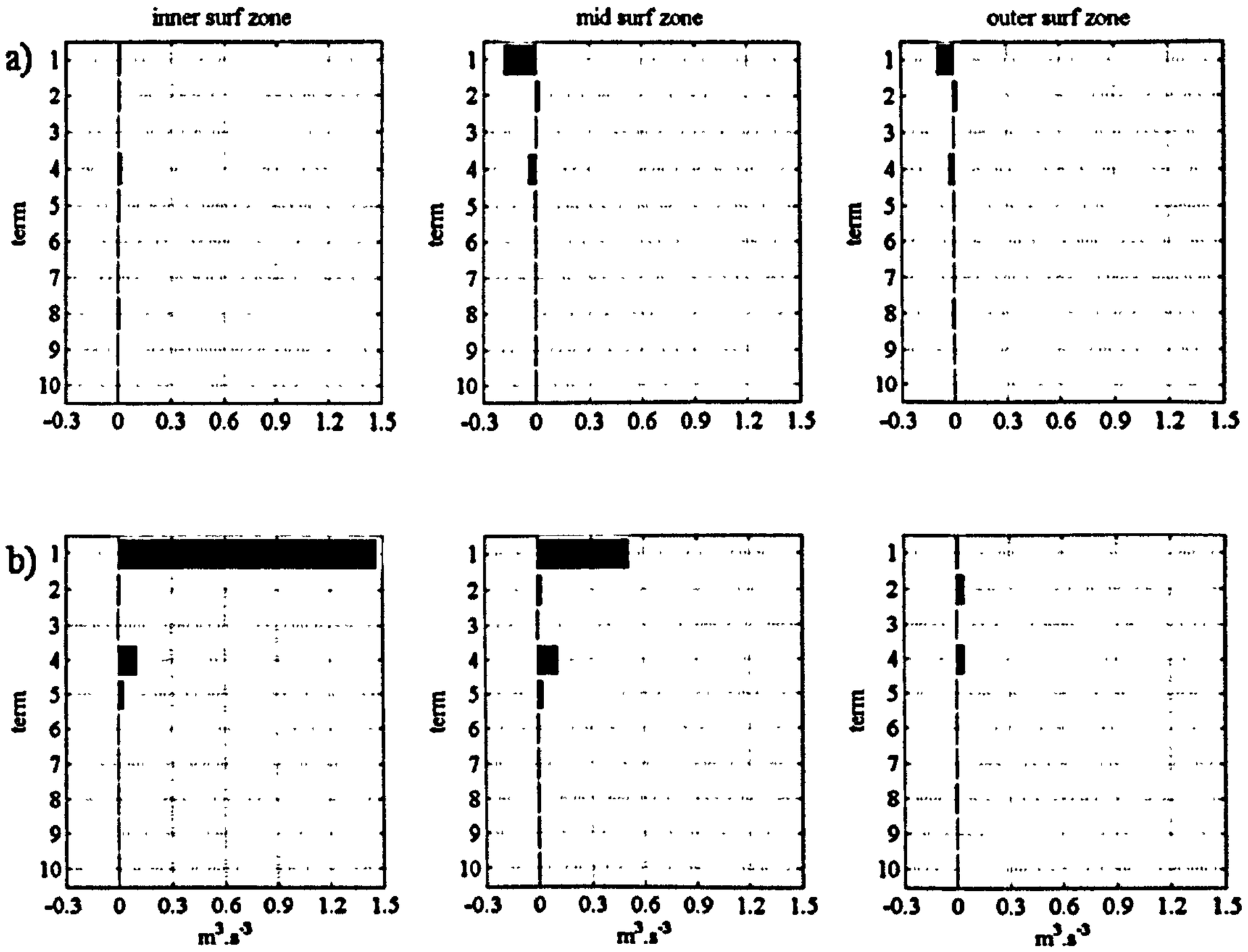

Figure 5.12: Third order cross-shore velocity moments computed for the offshore extremity position (1A) at the inner, mid- and outer surf zone positions for: a) calm conditions (14th May), and b) low energy conditions. The runs relate to the flood tide and positive values denote offshore transport, negative values denote onshore transport.

The energetics analysis produces a mean transport component (term 1) that dominates over the other terms and which has a variability in magnitude and direction that reflects that of the net transport computed after Jaffe *et al* (1984) in the previous section. The mean velocity moment term on the 14th May (Figure 5.12a) has a negligible magnitude and is onshore directed in the inner surf zone. It becomes offshore directed in the mid surf zone where it peaks in magnitude, before decreasing in the outer surf zone. On the 16th May (Figure 5.12b) the mean velocity moment term in the inner surf zone is much larger than on the 14th May and at its maximum in the inner surf zone, the positive sign indicating that the transport is onshore directed. The much larger magnitude of term 1

on the 16th May in the inner and mid surf zone as compared with the 14th May indicates the significant increase in sediment transport caused by the wind sea conditions. The energetics analysis also indicates that the wave stirring effects of short waves coupled with the onshore velocity phase (term 4) in the inner and mid surf zone is important to onshore sediment transport under low energy conditions which is intuitive given the fetch limited wave climate. A small contribution is made to the inner and mid surf zone onshore transport by the stirring effects of long waves (term 5). The contribution of short wave velocity skewness (term 2) to onshore sediment transport is comparatively small but largest in the outer surf zone where it is generally too deep for sediment suspension under low energy conditions. Conversely it is negligible in the inner surf zone where sediment suspension is highest and therefore only makes a small contribution to onshore sediment transport in the mid surf zone.

The results of the energetics analysis are in good agreement with the sediment transport analysis following Jaffe *et al.* (1984) (Section 5.6.3) as they predict both the significant increase in the sediment transport rates generated by the onset of the wind sea conditions. The results reiterate the importance of the mean component (term 1) to sediment transport on the offshore sandbank under low energy conditions. The wave driven mean flow in addition to secondary short wave stirring effects were also found to be important in the sediment transport regime and morphodynamics of the shore-attached mode of the sandbank (Marino-Tapia *et al.*, 2006).

5.6.5 Co-spectral analysis of the cross-shore current and sediment transport fluxes under low energy conditions

A co-spectral analysis of the components of the cross-shore current and suspended sediment data from run 3 on the 16th May has been undertaken and the results plotted in Figure 5.13. The periodograms were estimated using 16 segments containing 256 data points and a 50% overlap. A Hanning window function is applied to the data to reduce spectral leakage between adjacent bins and then the FFT applied. The averaged spectral density estimates have a bandwidth of 0.0016 Hz and 58 degrees of freedom at the 95 % confidence level with upper and lower error factors of 1.5 and 0.7 times the spectral estimate respectively. Since the process of converting a signal from the time domain in to the frequency domain involves removing the mean, the co-spectral analysis relates only to the oscillatory flow component. This has previously been shown to be the less important to the sediment transport over the sandbank under low energy conditions (Section 5.6.3) constituting between 20 and 50% of the transport depending on cross-shore position within the surf zone. However, though this contribution is smaller than that of the mean component it is not insignificant and the co-spectra are therefore worthy of investigation. Their analysis will provide further insight in to the contribution of the wave driven transport component under low energy conditions. Run 3 from the 16th May low energy was selected for the co-spectral analysis because there is a small peak in the computed sediment transport rate due to the oscillatory component in this run (Figure 5.11c).

The *c* and *u* auto-spectra (Figure 5.13a and b respectively) have two peaks, one at the incident wave frequency (0.17 Hz, $T = 5.9$ s) and one at infra-gravity frequency (0.016 Hz, $T = 63$ s). The two peaks in the *u* auto-spectrum are of similar magnitude though the peak at the incident wave frequency is the stronger and more dominant.

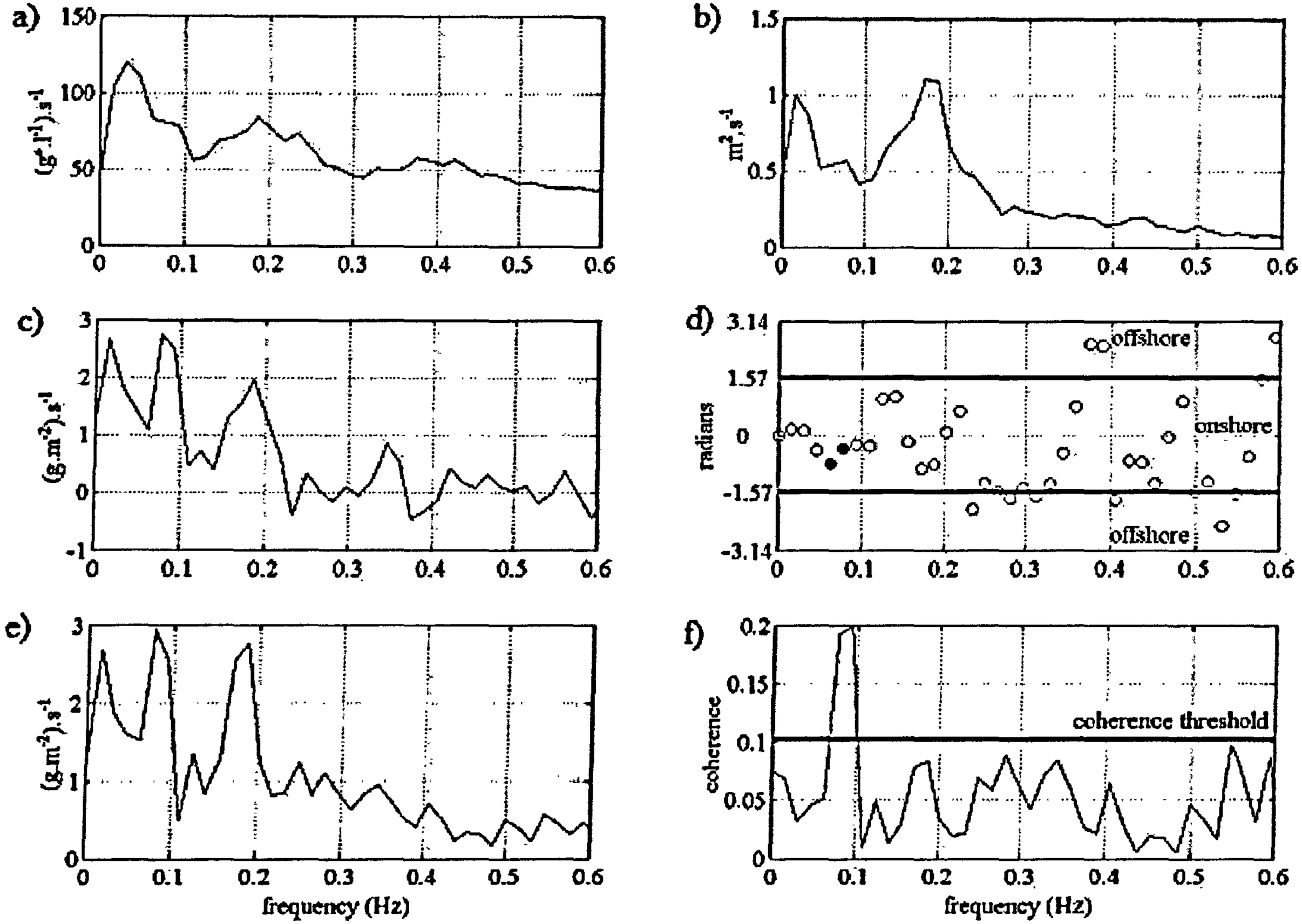

Figure 5.13: Cross-spectral analysis of suspended sediment concentration and cross-shore velocity for run 3, 16th May: a) SSC auto-spectrum, b) *u* velocity auto-spectrum, c) *c-u* auto-spectrum, d) *c-u* phase spectrum where white circles = non coherent phase relation , black circles = coherent phase relation, e) *c-u* cross-spectrum, and f) *c-u* coherence spectrum.

There are also two peaks in the *c* auto-spectrum at the incident wave and infra-gravity frequencies but in this spectrum, it is the lower frequency peak that dominates. The peaks at the incident wave energy and the infra-gravity frequencies are also present in the *c-u* co-spectrum (Figure 5.13c) but in addition to this there is a tertiary peak that occurs at a intermediate or harmonic frequency (≈ 0.05 Hz, $T = 20$ s). The positive sign of the co-spectral density at the peak frequencies indicates that the sediment transport is onshore directed. The black circles in the phase spectrum show the frequencies at which the phase relation between the cross-shore current and sediment suspension is coherent where the coherence threshold is given by:

$$\text{Coherence threshold} = 1-0.05^{(1/(0.5.\text{DOF})-1)} \tag{5.23}$$

Where DOF = number of degrees of freedom (Equation 5.13). A coherence threshold of 0.103 was computed for the data therefore the *c-u* phase relation is only coherent at the peak intermediate frequency (≈ 0.05 Hz) that was observed in the co-spectrum (Figure 5.13c). This is the frequency at which high cross-shore velocities occur simultaneously with sediment suspension events, and since the coherent phase relation occurs close to zero, *c* and *u* are in phase. Therefore the sediment is moved onshore under the onshore component of the cross-shore current, which concurs with the *c-u* co-spectrum.

A final point to note is that the lower frequency coherent peak in the *c-u* coherence spectrum is still in the short wave frequency energy band hence the dominance of term 4 over term 5 in the energetics analysis (Section 5.6.4).

5.7 Summary

The objective of the in-situ measurement analysis was to elucidate the physical processes responsible for the observed morphodynamic behaviour. The persistent onshore migration of the offshore sandbank at Teignmouth is the typical behaviour for sandbanks that form on the terminal lobe of ebb tidal deltas. When considered in the context of sedimentary features on exposed coasts (e.g. inter-tidal and sub-tidal alongshore uniform bars) which move both on- and offshore over comparable distances, the morphodynamic behaviour of these inlet sandbanks is aberrant. Typically, the effect of waves on open coast beaches is to generate an offshore directed bed return flow or undertow current and it is this physical process that provides the primary mechanism for the offshore migration of such features in these environments. Similarly, in nearshore environments adjacent inlet entrances strong offshore directed ebb tide currents flowing in shallow water over the shoals can entrain sediment and provide a potential mechanism for the movement of sediment offshore in addition to that occurring in the primary and secondary channels (Section 6.5.2.2). However at Teignmouth, the current vector time series from the four different SLOT rig positions indicate that offshore currents are relatively scarce and of low importance to the evolution of ebb shoals (Figure 5.9a). At the offshore extremity and southern flank positions where offshore currents are present, they occur outside of the surf zone which is where sediment is being suspended and transported under low energy conditions. It is this paucity of offshore directed currents in the surf zone that is the fundamental reason for the observed atypical morphodynamic behaviour of the offshore sandbank at Teignmouth.

The detailed analysis of the sedimentation at the offshore extremity SLOT rig position was undertaken since it permitted the comparison of calm versus low energy conditions. This comparative analysis revealed an important atypical response of the

hydrodynamics to increasing wave height that helps to explain the paucity of offshore directed currents at this position (Figure 5.10c). In contrast to the typical open coast scenario, an increase in significant wave height resulted in offshore directed flood tide surf zone currents being replaced by onshore directed currents. It should be mentioned here that this occurred when the sandbank was exposed by the tide as opposed to it being submerged. If the offshore directed surf zone currents were caused by the radiation stress of the incident waves then an increase in wave height is expected to strengthen the undertow (Masselink and Black, 1995) but this was not the case. A potential explanation for the disappearance of the flood tide undertow may be that larger waves are not able to cause setup against the offshore extremity of the sandbank due its narrow longshore dimension. Consequently, the onshore directed momentum generated by the incident waves is thought to be redirected around the flanks of the feature. This explanation for the lack of undertow under the larger waves infers that for isolated nearshore features exposed to wave action that have narrow longshore dimensions, there may be an upper radiation stress limit or threshold value that initiates the redirection of the onshore directed momentum upon being exceeded. Since the phenomenon only happens on the flood tide, this suggests that the specific combination of wind, wave and current conditions needed to initiate this hydrodynamic response exists in the continuum between the different conditions on flood and ebb tides of the 16th May.

The in-situ measurements results also showed that there is a considerable tidal asymmetry in the transport regime and that it is during the flood tide surf zone conditions that most sediment is being brought in to suspension and transported. The analyses revealed that it is the mean flow component that is most important to the net transport which can be as large as three times the magnitude of the oscillatory component under low energy conditions. However the oscillatory component is not

insignificant to the transport of sediment (Figure 5.11c) but it is the stirring action of the incident wave orbital motions that is of greatest importance (Figure 5.12b). The peaks in the *c-u* co-spectra indicate that the stirring action of the waves is suspending sediment at times of maximum onshore velocity at three different frequencies but only the longer period onshore oscillations of the cross-shore current at the infra-gravity and harmonic frequencies were of importance to mid surf zone (run 4) sediment transport at the offshore extremity. Previous studies have shown that towards the inner surf zone the infra-gravity contribution increasingly dominates the *c-u* co-spectra due to the dissipation of the incident wave frequencies (Davidson *et al.*, 1993; Miles and Russell, 2004), and under low energy conditions at the offshore extremity this is where the sediment transport is at its maximum. The coarse grained composition of the sandbank's sediment assists the process of onshore sediment transport because the coarse grains which are entrained in to the water column during the higher peak onshore velocities rapidly fall out of suspension before flow reversal can take place (Bowen, 1980; Richmond and Sallenger, 1984).

The analysis of the in-situ measurements has shown that in addition to the onshore directed mean flows, an additional primary factor in the persistent onshore migration of the offshore sandbank at Teignmouth under low energy conditions is the relative paucity of offshore directed currents over the sandbank. The physical process that results in this and is responsible for strong onshore directed inner surf zone currents is the strong refraction of the incident waves by the contours of the feature as evidenced by the linear form of its flanks (Figure 5.5b). During times when the sandbank is not fully submerged, sediment entrained at the offshore extremity is transported onshore along the flanks of the sandbank by significant onshore directed inner surf zone mean flows that are driven by the strong refraction of the incident waves. These currents are

in effect longshore currents with respect to the sandbank due to their very oblique angle of incidence. When the sandbank becomes submerged and $h \leq h_b$, the strong refraction leads to wave focussing over the sandbank's crest where the associated currents converge and transport sediment over the top of the feature to the shoreward extremity (Figure 5.9a). The intense wave refraction over the crest in the shallow submerged state on the flood tide produces flow constriction over the crest which has a jet-like form (Choi *et al.*, 2009) and this is when onshore transport is greatest.

It is the combination of these two transport regimes that erodes sediment from the offshore extremity and transports it along the flanks or over the crest to the shoreward extremity where it is deposited. This leads to the observed onshore migration of the morphological feature under the typical low energy conditions between storms. The effectiveness of these processes at transporting the sediment onshore between high energy events was highlighted when the SLOT rig sensors were found to have been completely buried during the tide on the morning of the 16th May indicating a local increase in seabed elevation of the order of 20 cm (Figure 5.14). The results clearly show that the transport over the sandbank under the typical low energy conditions is not negligible therefore the onshore migration of the features continues between storms albeit at a slower rate.

In Chapter 6 the depth-averaged 2D Mike 21 numerical model is used to investigate the patterns of erosion and deposition around the offshore sandbank to try to better explain the plan form morphological evolution of the feature, and to determine the relative contributions of the tide and wave driven components to the mean flow.

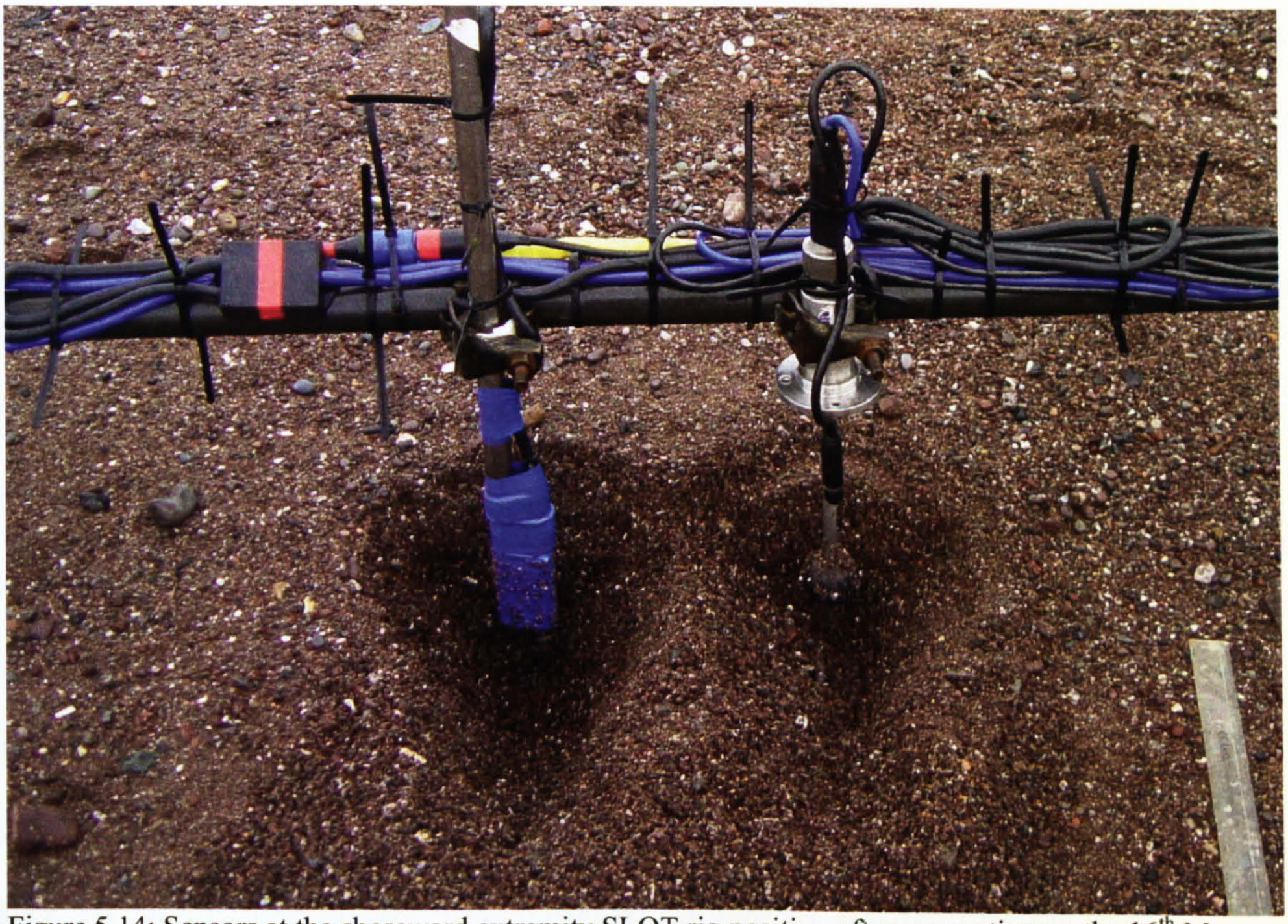

Figure 5.14: Sensors at the shoreward extremity SLOT rig position after excavation on the 16th May.

6 Numerical modelling

The increasing socio-economic importance of the coastal zone (Section 1.1) has led to the development of a wide range of numerical models for the study of nearshore processes. The different modelling approaches (e.g. conceptual, probabilistic, and deterministic) incorporate varying levels of complexity in order to simulate the marine environment over a wide range of temporal and spatial scales. The current state of the art numerical models are the two and three dimensional deterministic models that encapsulate theory through sets of complex governing equations that describe the underlying physical processes. These models are through necessity founded on simplifying assumptions which reduce the accuracy of model outputs but despite this they are still capable of making quantitatively reliable predictions (De Vriend, 1987). Consequently, their application has become standard practice in scientific and engineering disciplines. The numerical simulation of the marine environment enhances our analytical capability by helping to overcome the problems associated with an inherent paucity of measurements of key parameters and because it provides the scientist with a degree of experimental control that would not otherwise be attainable. Furthermore, the important advantage gained by undertaking numerical simulations in the present study is that they reveal how the physical Eulerian measurements fit (Chapter 5) within the 2D flow regime as it develops through the tidal cycle. In particular, the simulations show how the funnel flow conditions of higher states of tide evolve into the jet-like conditions during lower states when the flow becomes segregated in the channels between shoals. The combination of the modelling analyses with the physical measurement and video analyses provides detailed information about the system over a wide range of spatial and temporal scales thereby helping to overcome one of the primary limitations of research in to nearshore morphodynamics which is

poor data resolution. Studies taking a similar approach have already proved immensely useful in improving our understanding of the physical processes acting in the nearshore environment, and how they interact with, and control the morphological evolution of sandy coastal environments (Reniers *et al.*, 2001; Lafon *et al.*, 2005; Siegle *et al.*, 2004; Siegle *et al.*, 2007).

In this component of the study, the industry standard MIKE 21 model developed by the Danish Hydraulic Institute (DHI) is applied in two experiments which are as follows:

1. The effects of different hydrodynamic conditions on the geometry and distribution of the regions of erosion and accretion in the vicinity of a nearshore sandbank are investigated using a simplified modelling approach and idealised bathymetries.
2. Measured bathymetry, wave and tidal data are used as model boundary conditions to investigate the sediment transport regime of the offshore sandbank under the low energy conditions experienced during the May 2003 fieldwork program. The objective is to quantify the relative contributions of the cross-shore wave and tidal current components to the onshore transport of sediment over the migrating sandbank.

MIKE 21 is a two dimensional depth-integrated model with a suite of modules that can be used individually or in combination for the simulation of a wide range of nearshore processes. In this study the nearshore spectral wave (NSW), hydrodynamic (HD) and non cohesive sediment transport (ST) modules are applied using the modular framework presented in Figure 6.1 for the calculation of sediment transport fluxes and initial rates of bed level change in response to different hydrodynamics.

6.1 MIKE21: NSW, HD and ST modules

The first step in the application of the MIKE 21 modules is the initialisation of NSW model which is a parametric spectral model that describes the propagation, growth and decay of short period, short crested wind waves in nearshore areas. The numerical scheme solves the equations for the conservation of spectral wave action density (Holthuijsen *et al.*, 1989) for the computation of the stationary or quasi-stationary wind generated wave field.

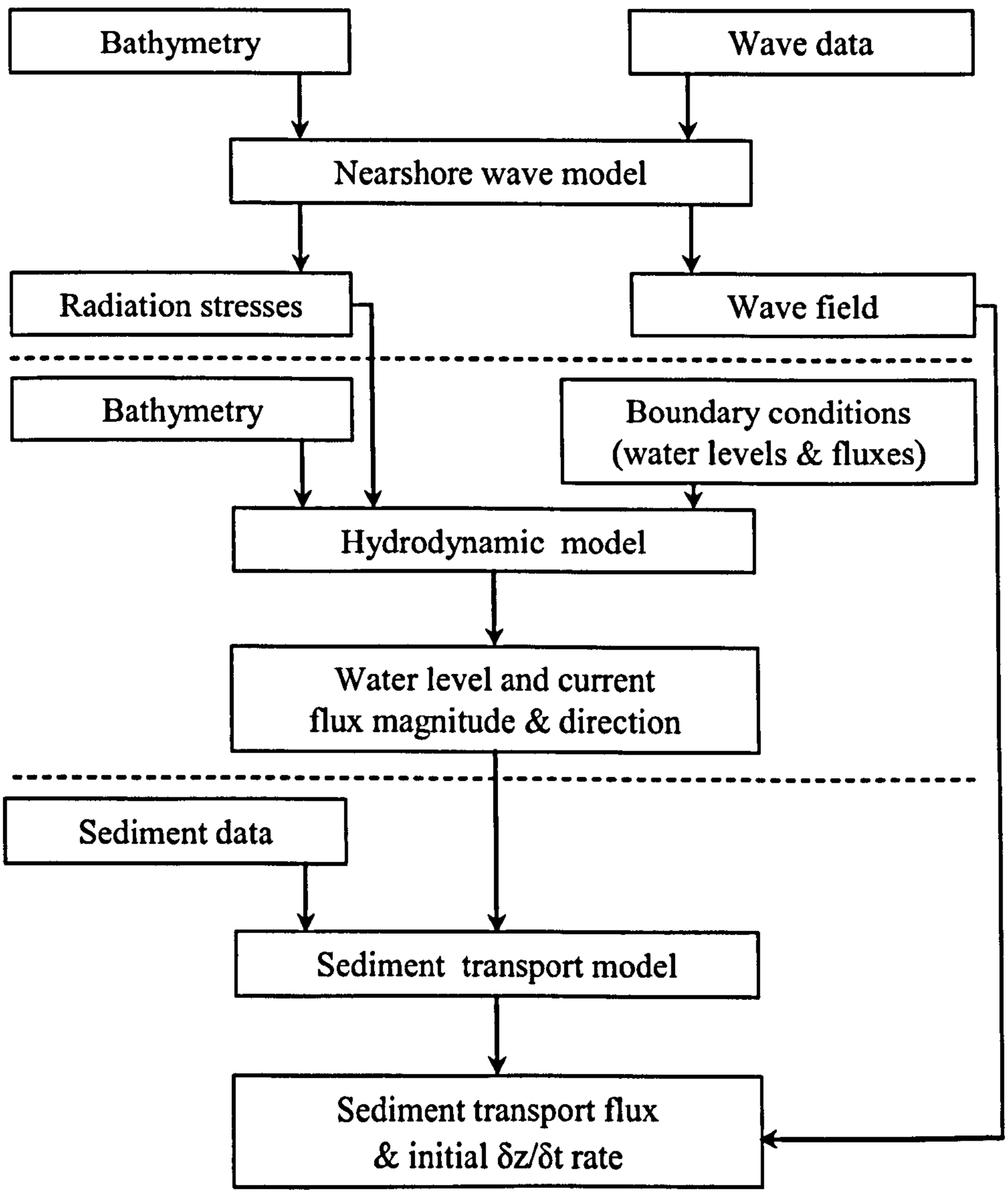

Figure 6.1: MIKE 21 modular framework.

The NSW model does not include wave reflection and diffraction, or non-linear wave-wave interaction and wave blocking but does incorporate the effects of:

1. Wave refraction and shoaling due to varying depth.

2. Energy dissipation due to bottom friction.

3. Energy dissipation due to wave breaking (Battjes and Janssen, 1978).

4. Wave-current interaction.

5. Directional and frequency spreading.

The output files are integral or spectral wave parameters such as significant wave height, mean wave period, mean wave direction, directional standard deviation and wave radiation stress. The spatial gradients in the surf zone radiation stresses determine the wave induced contribution to the flow field which is then used as input to the HD module. The second model to be initialised is the HD model which calculates water level and horizontal current field parameters due to a variety of forcing functions using the depth-integrated continuity and momentum equations. In addition to wave forcing, the model is able to incorporate tidal forcing and wind shear stress effects. The HD model outputs horizontal current velocity and fluxes which are then used as input to the ST model. The ST model is an advanced non-cohesive sediment transport model with a choice of two parameterisations (Bijker method and the DHI's deterministic STP formulation) for the computation of sediment transport fluxes and initial bed level change rates due solely to tidal currents or due to a combination of tidal and wave driven currents. The model incorporates the effects of breaking and non-breaking waves, complex bathymetry and sediment gradation.

6.2 Model calibration and validation

MIKE 21 has previously been used to investigate Teignmouth morphodynamics during which it was rigorously calibrated and validated using a comprehensive dataset from the COAST3D project (Siegle, 2003). The important implication of this for the present study is that the model is capable of simulating the complex horizontal circulation with a good degree of skill and without further model calibration. The process involved the iterative adjustment of tuning parameters (calibration) until the time series of modelled data most accurately replicated the time series of measured data (validation). Initially the hydrodynamic model was calibrated using the water level, wave height and horizontal current measurement data and after satisfactory comparative results were obtained, the validation process was then repeated for the sediment transport model. Using the comprehensive COAST3D dataset Siegle (2003) was able to calibrate the model at several locations across the model domain (Figure 6.2) and over a range of incident wave and tidal conditions. Siegle (2003) quantified the model's performance using a Relative Absolute Mean Error (RMAE) analysis for the hydrodynamic variables and a Brier Skill Score (BSS) analysis for the sedimentation. The validation was undertaken using a simulation period of one month which included the spring-neap tidal range and wave heights in the range 0.1 to 1.7 m. The results for the wave, water level and current fields are presented in Tables 6.1, 6.2 and 6.3 respectively. The low RMAE values for all variables indicate that the model is competent at simulating the hydrodynamic conditions at Teignmouth. The wave height and direction, and the tidal amplitude and phase were shown to be in very good agreement with the measured data. The HD model was less skilful in the prediction of the horizontal current velocity field as indicated by the higher RMAE values in Table 6.3.

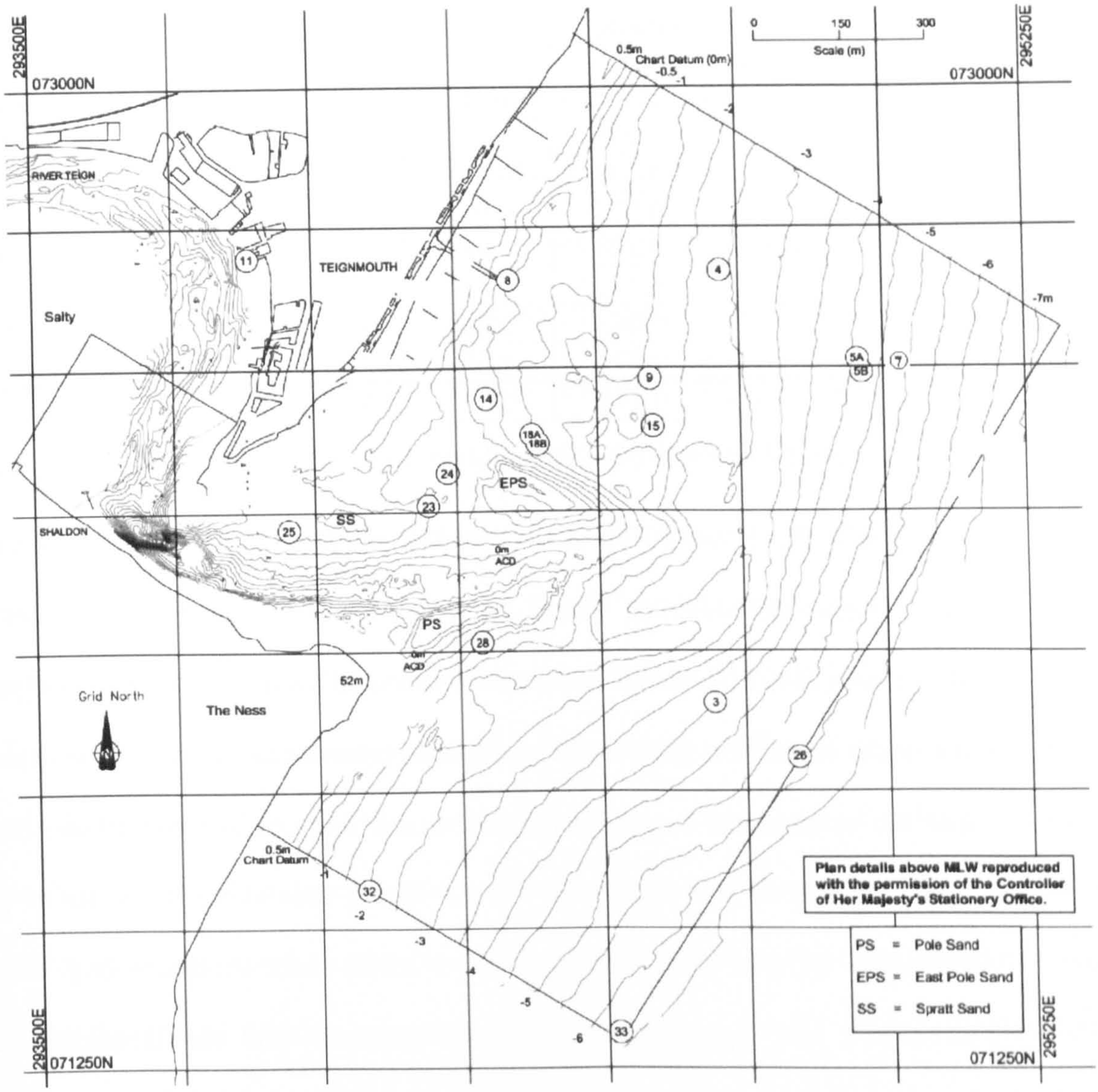

Figure 6.2: Teignmouth bathymetry with the stations used in the Siegle (2003) model calibration and validation.

Station number	Measured (m)	Predicted (m)	MAE	RMAE	Qualification
7	0.46	0.35	0.11	0.02	Excellent
4	0.46	0.36	0.10	0.01	Excellent
25	0.36	0.26	0.10	0.01	Excellent
Average	0.43	0.32	0.10	0.01	Excellent

Table 6.1: Significant wave height validation parameters (Siegle, 2003).

Station number	Measured (m) ODN	Predicted (m) ODN	MAE	RMAE
8	0.894	0.890	0.011	0.012
11	0.863	0.842	0.051	0.059
Average	0.878	0.866	0.031	0.035

Table 6.2: Water level validation parameters (Siegle, 2003).

Station number	Measured ($m.s^{-1}$)	Predicted ($m.s^{-1}$)	MAE	RMAE	Qualification
14	0.156	0.164	0.104	0.346	Reasonable
24	0.159	0.173	0.118	0.429	Reasonable
26	0.134	0.083	0.093	0.326	Reasonable
9	0.070	0.071	0.071	0.296	Good
28	0.126	0.184	0.107	0.450	Reasonable
25	0.377	0.432	0.139	0.237	Good
5	0.083	0.066	0.055	0.066	Excellent
33	0.070	0.054	0.055	0.071	Excellent
Average	0.146	0.153	0.092	0.277	Good

Table 6.3: Horizontal current velocity validation parameters (Siegle, 2003).

But despite this it was still able to reproduce the general circulation pattern and achieve an aggregate skill level of 'good' according to the stringent standards set out in Van Rijn *et al.* (2003). The modelled currents deviated from the measured data principally in the under estimation of both the alongshore current magnitude during calm conditions and the cross-shore current magnitude under larger wave conditions. Siegle (2003) attributed this to the coarseness of the model resolution (10 x 10 m grid) which prevented it from being able to resolve micro-scale processes (e.g. sub-grid scale turbulence and topographic steering of currents), and the inequality between the parameters being compared (i.e. depth-averaged values as compared with Eulerian point measurements). The latter point is supported by the notable improvement in current prediction capability for stations not in close proximity to the complex morphology associated with ebb shoal system (e.g. stations 5 and 33). For a complete description of the model calibration the reader is referred to Siegle (2003).

After obtaining satisfactory validation results for the hydrodynamic model, the sediment transport model is validated in a similar manner by comparing modelled erosion/accretion rates with Argus observations of the morphological evolution. Siegle (2003) used an iterative approach to bathymetry updating in which bed level changes were manually applied after one complete cycle of the modular framework. The BSS

used to quantify the performance of the ST model computes the accuracy of predictions relative to a baseline prediction after Sutherland *et al.* (2001). The validation of the ST model was undertaken for the region at the distal end of the estuary channel in which the offshore sandbank is observed to grow and begin migrating onshore. Siegle (2003) used surveyed bathymetries from the COAST3D project and 14 day simulation periods with which to make the comparisons. The results of the BSS analysis were measured against a predetermined threshold value (0.2) after Sutherland *et al.* (2001) whereby a BSS greater than the threshold indicated that the model was capable of simulating the morphological evolution and *vice versa*. The ST model permits the use of two distinct sediment transport formulations, the Bijker method and DHI's STP deterministic model. The former can be tuned using the bed load transport coefficient in the Bijker method which was defined as spatially varying in order to attain the best sediment transport predictions. The STP deterministic approach utilises user-generated sediment transport tables which are tuned to give the best prediction results at the table generation stage using the critical Shields parameter. After calibrating the ST model, Siegle (2003) demonstrated that it was satisfactorily able to predict the morphological evolution in the region of the offshore sandbank using both formulations with BSS values of 0.24 and 0.36 respectively, despite the limitations of the simplifying assumptions and the iterative approach to morphology updating. The rigorous model calibration and validation undertaken by Siegle (2003) showed that the NSW, HD and ST models within the MIKE 21 modular framework are capable of simulating the hydro- and morphodynamics at Teignmouth with sufficient accuracy and confirmed it's suitability for application to the study area. The modelling chapter begins with synthetic modelling experiment hence begins with a description of the methodology and the model setup used.

6.3 Idealised simulations

6.3.1 Methodology and model set up

The model domain in this experiment covers a 2 km square nearshore region at a 5 m resolution and is separated into two planar regions representing the beach face and the nearshore region from the foot of the beach face to the offshore boundary. The beach face occupies the shoreward 100 m of the domain and has a steeper gradient of 0.11 compared to the nearshore region which has a gradient of 0.01. The gradients used for each planar slope were estimated from the topographic and bathymetric surveys of the study site. The sandbank morphologies are derived from two orthogonal Gaussian curves superimposed on the slope of the nearshore region at a cross-shore distance of 380 m from the foot of the beach face. The generation of the morphologies using Gaussian formulae is useful since it allows the user to define the position of the feature relative to the model boundaries as well their cross-shore and longshore dimensions.

The addition of the simple linear equation describing an inclined plane with that for the Gaussian plane results in the equation of the form:

$$f(x,y) = mx + c + a_x e^{-\left(\frac{x-\bar{x}}{\sigma_x^2}\right)} . a_y e^{-\left(\frac{y-\bar{y}}{\sigma_y^2}\right)} \qquad (6.1)$$

Where m is the planar gradient, c is a constant, a is the amplitude, σ is the standard deviation, and $\bar{x}$ and $\bar{y}$ specify the location of the orthogonal peak in the Gaussian planar curve. Contour plots of the circular (aspect ratio $\approx$ 1) and elliptic (aspect ratio $\approx$ 2) sandbank geometries generated using Equation 6.1 are presented in Figure 6.3. A 2 km model domain was chosen so that the lateral boundaries would be sufficiently distant from the region of interest and therefore would not influence the modelled conditions in the vicinity of the sandbank.

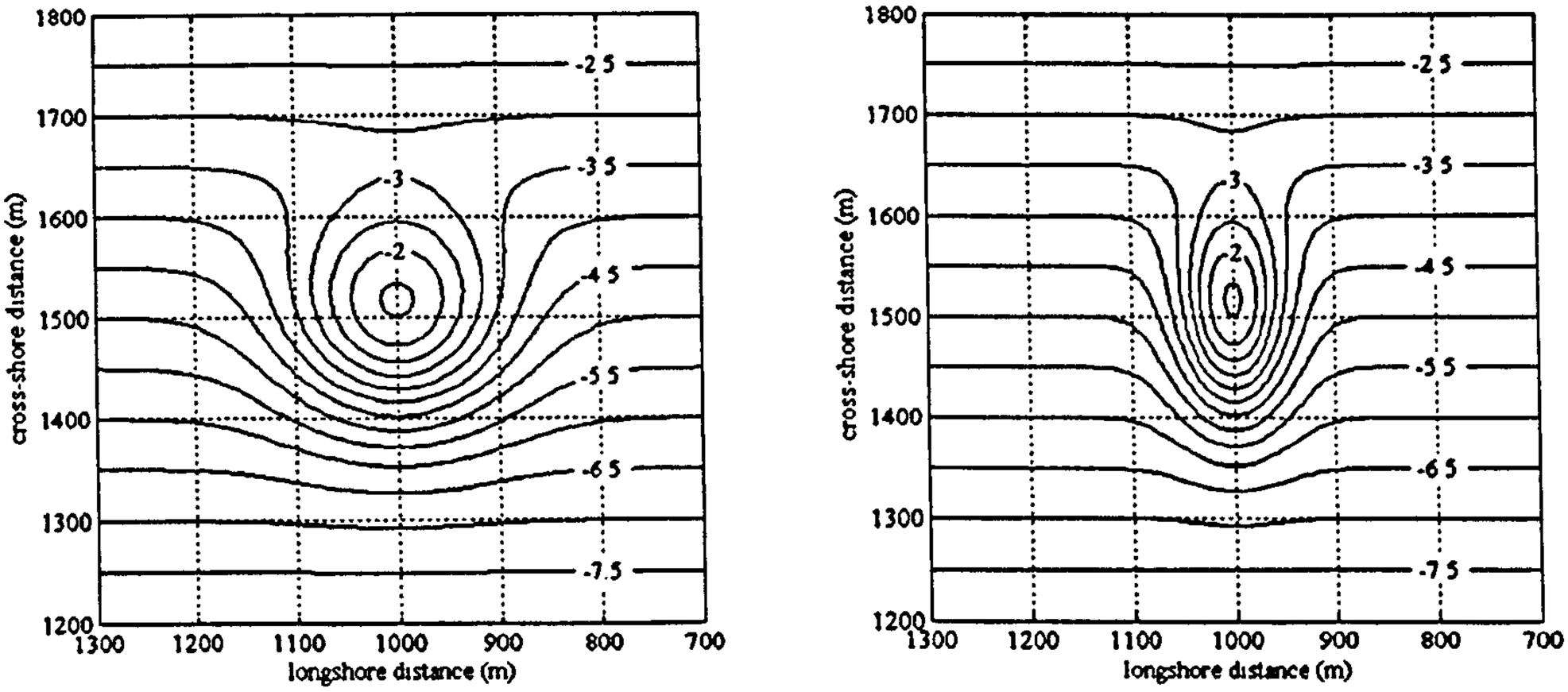

Figure 6.3: Contour plots showing the bathymetries for a subset of the model domain focussed on the sandbank morphologies: a) circular and b) elliptic. The contour units are depths (m) relative to an arbitrary datum and the cross-shore and longshore axes are relative to the model domain origin.

The choices of model grid resolution and the length of the time step to be used are a compromise between having a sufficiently fine grid to be able to resolve the physical processes of interest in addition to keeping the computation time down and maintaining model stability. The appropriate choice of model resolution and time step length is assessed using the dimensionless Courant number which is equated as follows:

$$C_r = c.\frac{\Delta t}{\Delta x} \tag{6.2}$$

Where Δt is the time step, Δx is the grid resolution and c is celerity which is given by:

$$c = \sqrt{g.h} \tag{6.3}$$

Where g is gravity and h is water depth. For the MIKE 21 HD module it is recommended that Courant numbers should not be allowed to reach values in the range 8 to 10 (Delft Hydraulics Institute, 2004). In this series of simplified numerical modelling experiments, a relatively fine grid resolution of 5 m was chosen which meant that a small time step of 2 seconds was needed to keep the Courant number below the

maximum recommended values. This combination generated a maximum Courant number of 5.6 during the HD module flow simulations which is comfortably inside the recommended limits. The modular procedure initially involves using the NSW module to model a single wave event (stationary time description) in order to generate the radiation stress, wave parameter fields which are used as input to the HD module. The HD module simulation period used was 1 hour which includes a half hour warm up period to enable the stationary conditions to be reached. The module computes the wave driven flow field from the radiation stress field at each time step which is subsequently applied in the ST module in order to estimate the sediment fluxes and initial rates of bed level change at each grid point.

Since the idealised numerical modelling experiments are used to investigate the effects of different hydrodynamic conditions on the plan form and distribution of the regions of accretion and erosion, this analysis is not concerned with the absolute magnitudes of the sediment transport fluxes and initial rates of bed level change output by the ST module but in the trends in their relative magnitudes, plan form and distribution. Initially a series of sensitivity tests were carried out to assess whether the inclusion or omission of the spatially varying bottom dissipation and eddy viscosity tuning parameters would significantly affect the trends. The tests revealed that their inclusion did not significantly affect the results of the experiments and so spatially constant values were used.

6.3.2 Results

6.3.2.1 Comparison of modelled hydrodynamics and sedimentation for circular and elliptic sandbanks under emerged and submerged states

From the Teignmouth Argus image archive it has been seen that during the genesis period of the offshore sandbank at Teignmouth, the feature typically has a rotund form which subsequently elongates in the shore-normal direction during the course of its onshore migration. In order to investigate how the hydrodynamics and sedimentation may result in elongation as the offshore sandbank migrates in to shallower water, idealised modelling experiments were undertaken using circular and elliptic sandbank morphologies where the former is representative of the rotund sandbank observed during the genesis stages and the latter is representative of the morphology observed during the elongation and migration stage of the inlet in its current mode. In the initial series of idealised modelling experiments, the sandbank crest height is at a depth of -1.42 m relative to the arbitrary water level datum (h = 0 m), and the hydrodynamics and sedimentation are modelled using water levels of -2.0, -1.0, +1.0 and +2.0 m, and offshore significant wave heights of 0.5, 1.5 and 2.5 m. In Figure 6.4 and Figure 6.5 the modelled results for the emerged (h = -2.0 m) and submerged (h = -1.0 m) tidal states are presented for the circular and elliptic sandbank bathymetries under an offshore significant wave height of 0.5 m. Each modelling experiment is encapsulated in a row of three plots per water level that define the wave, flow and sediment transport in the vicinity of the sandbank at the specified water level. The hydrodynamics and sedimentation are depicted using individual vectors plotted at each model grid point. In both the emerged and submerged states, the model results indicate that sediment is eroded from the offshore extremity and deposited shoreward of the region of erosion.

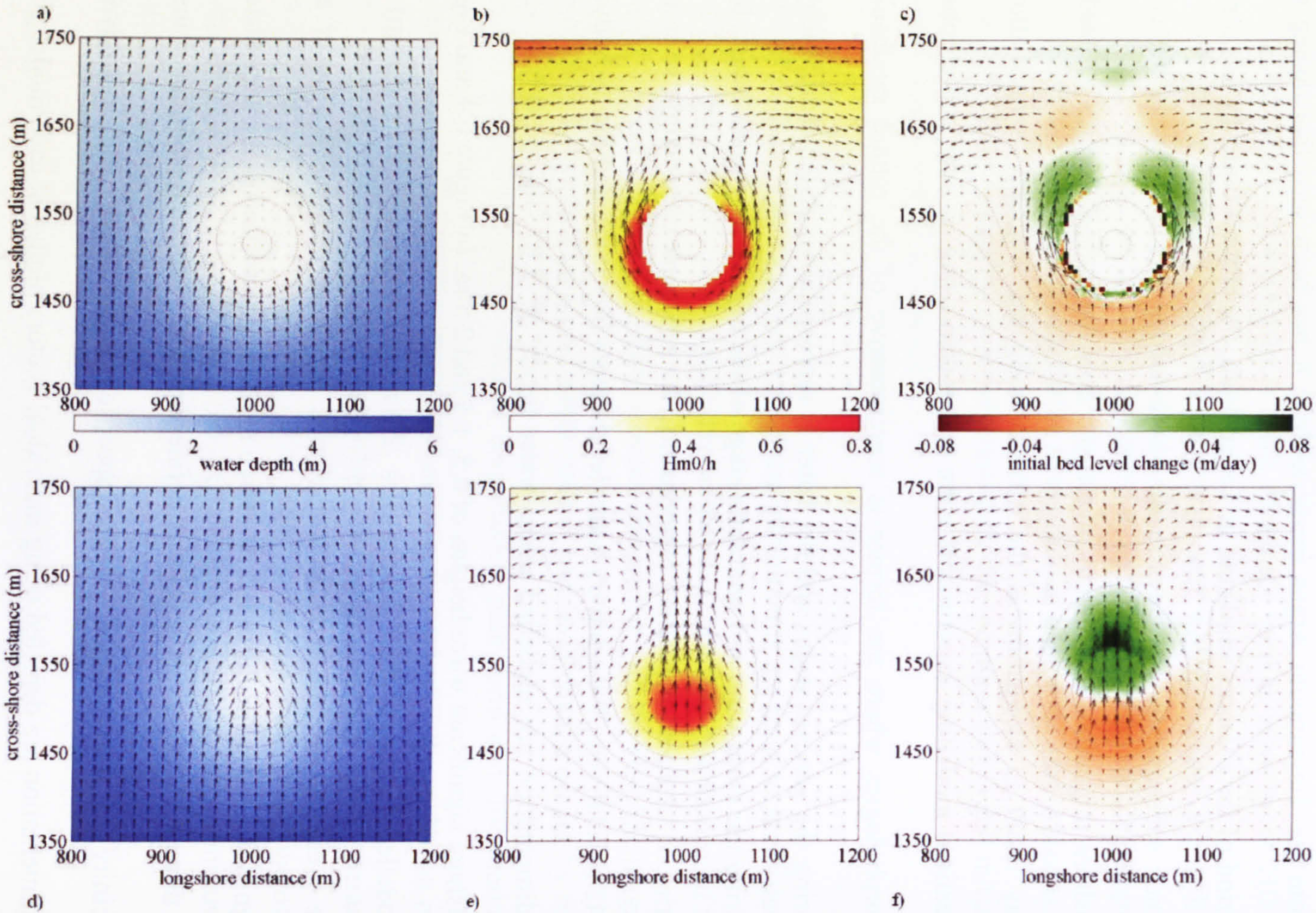

Figure 6.4: Modelled hydrodynamics and sedimentation for the emerged and submerged states of the circular morphology. Emerged state (h = -2.0 m): a) wave height and direction (vectors) with water depth (colour), b) current strength and direction (vectors) with H_s/h (colour), c) sediment flux strength and direction (vectors) with initial rate of bed level change (colour), Submerged state (h = -1.0 m): d) wave height and direction (vectors) with water depth (colour), e) current strength and direction (vectors) with H_s/h (colour), f) sediment flux strength and direction (vectors) with initial rate of bed level change (colour).

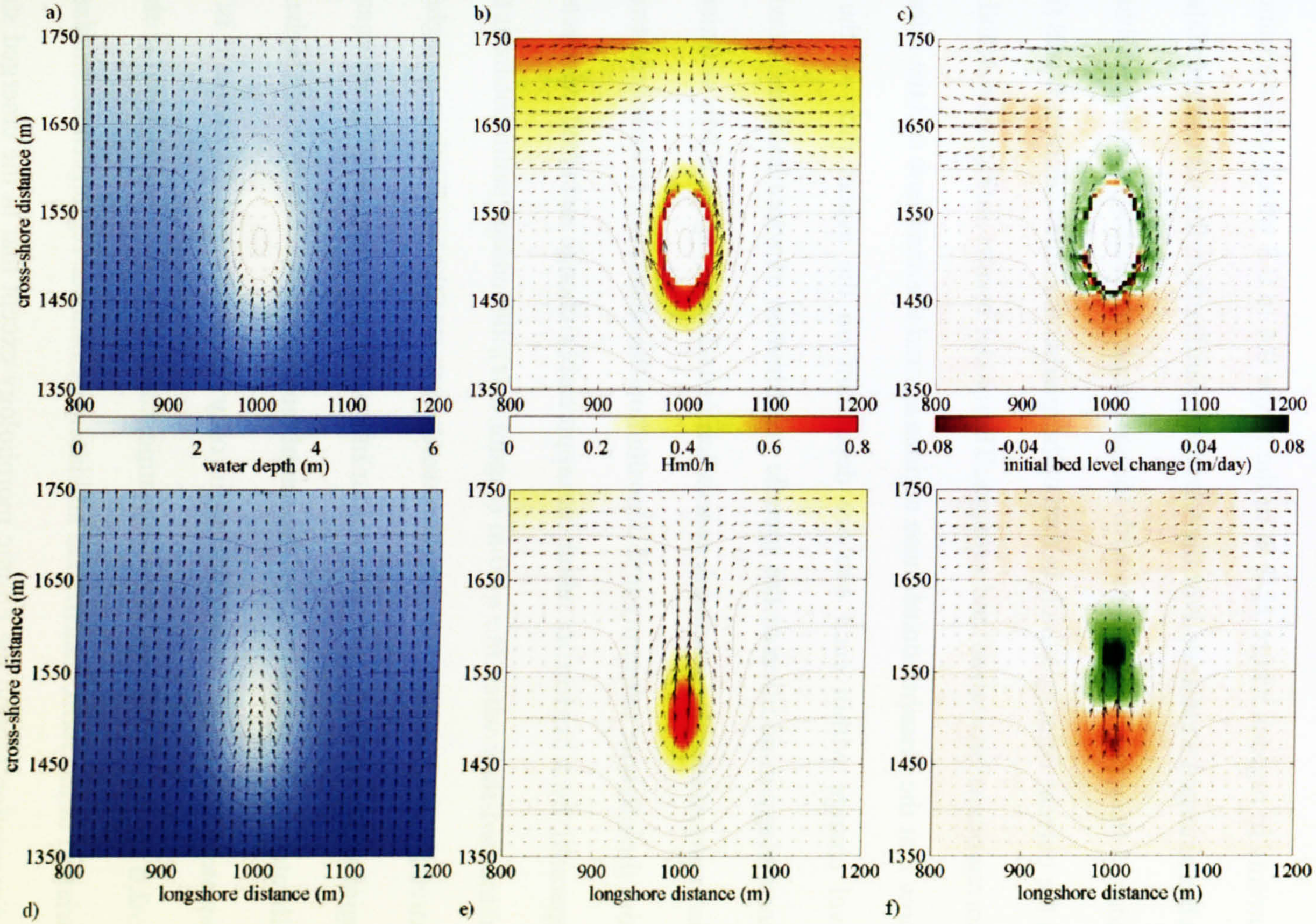

Figure 6.5: Modelled hydrodynamics and sedimentation for the emerged and submerged state of the elliptic morphology. Emerged state (h = -2.0 m): a) wave height and direction (vectors) with water depth (colour), b) current strength and direction (vectors) with H_s/h (colour), c) sediment flux strength and direction (vectors) with initial rate of bed level change (colour), Submerged state (h = -1.0 m): d) wave height and direction (vectors) with water depth (colour), e) current strength and direction (vectors) with H_s/h (colour), f) sediment flux strength and direction (vectors) with initial rate of bed level change (colour).

The different modes of erosion and deposition associated with the emerged and submerged states are both driven by the strong refraction of the shoaling incident waves by the morphology of the sandbanks as indicated by the wave direction arrows in Figure 6.4a and d, and Figure 6.5a and d. Wave breaking induces strong onshore directed currents in regions where H_s/h is in the range 0.4 to 0.8 which occur around the flanks in the emerged state and, over the top of the sandbank in the submerged state. The wave induced flow regime interacts with the sandbank morphology leading to sharp gradients in the current velocity which in turn cause gradients in the sediment fluxes that result in the regions of accretion and erosion. The model results in Figure 6.4 and Figure 6.5 show that the distribution of these regions around the sandbank and the intensity of bed level change within each one are dependant on the aspect ratio of the sandbanks morphology in addition to the specific combination of water level and wave height. In the emerged circular sandbank case when h = -2.0 m (Figure 6.4c), sediment is eroded from the offshore extremity and deposited on the shoreward extremity in two side lobes separated by a region in which no appreciable change occurred. Conversely, in the submerged state when h = -1.0 m (Figure 6.4f), the eroded sediment from the offshore extremity is deposited over the shoreward portion of the sandbank in a single centralised region of the crest. The varying colour intensities of the regions of erosion and accretion indicate that the magnitudes of the initial rates of bed level change are higher at the -1.0 m water level when the morphology is only just submerged than when it is emerged (h = -2.0 m). The different hydrodynamic states that are responsible for the observed variation in the form, distribution and intensity of these regions cause similar patterns of sedimentation around the elliptic morphology except that in the emerged state, the two side lobes are importantly replaced by a narrow, near continuous band of accretion around the flanks of the feature that extends to the shoreward extremity. In order to analyse the trends in the idealised modelling results, key hydrodynamic and

sedimentation parameters derived from the matrices output by the NSW, HD, and ST modules have been collated in Table 6.4 and plotted in Figure 6.6 to aid the identification of the underlying trends. The parameters are extracted from over and around the sandbank morphologies and are defined as follows:

a) The ratio of maximum shoaling wave height to the minimum water depth (H_s/h).

b) The maximum current strength ($m.s^{-1}$).

c) The maximum sediment flux ($m^3.day\text{-}1.m^{-1}$).

d) The mean initial rate of bed level change per unit area estimated over a 1 km^2 subset of the model domain that encompasses the sandbank bathymetry.

In the mean initial rate of bed level change estimate for the emerged sandbank state when h = -2.0 m, the calculation includes an inherent error due to the inclusion of the exposed area of the sandbank (≈ 8000 m^2 for the circular morphology), but since this area represents less than 1.0 % of that used in the estimate (1 km^2), the maximum error introduced is negligible. With the depth to the top of the sandbank at -1.42 m below the arbitrary reference level (h = 0 m) the crest is exposed in the -2.0 m water level experiments and submerged at the -1.0, +1.0 +2.0 m water levels. Based on the breaker index (γ_b) of 0.8 that was used in the model setup, the maximum water depth that the 0.5, 1.5 and 2.5 m waves can break in is estimated at 0.6, 1.9, 3.1 m respectively. The main trends under different wave heights and water levels in Figure 6.6 are summarised in the following sub sections along with the differences between the two morphologies.

Ratio of H_s/h

Figure 6.6a highlights the tidal water level control on the intensity of wave breaking over the surface of the sandbank.

Circular sandbank					Parameter	Elliptic sandbank				
		Offshore wave height (m)						**Offshore wave height (m)**		
		0.5	**1.5**	**2.5**				**0.5**	**1.5**	**2.5**
Water level (m)	**-2.0**	0.79	0.77	0.74	H_s/h	**Water level (m)**	**-2.0**	0.80	0.78	0.76
	-1.0	0.78	0.76	0.74			**-1.0**	0.79	0.78	0.77
	+1.0	0.25	0.57	0.62			**+1.0**	0.27	0.61	0.67
	+2.0	0.16	0.45	0.55			**+2.0**	0.17	0.48	0.58
		Offshore wave height (m)						**Offshore wave height (m)**		
		0.5	**1.5**	**2.5**				**0.5**	**1.5**	**2.5**
Water level (m)	**-2.0**	0.55	0.98	1.08	Current strength ($m.s^{-1}$)	**Water level (m)**	**-2.0**	0.59	1.15	1.28
	-1.0	0.59	0.99	1.12			**-1.0**	0.71	1.16	1.36
	+1.0	0.14	0.65	0.82			**+1.0**	0.11	0.74	1.21
	+2.0	0.11	0.32	0.82			**+2.0**	0.10	0.35	0.91
		Offshore wave height (m)						**Offshore wave height (m)**		
		0.5	**1.5**	**2.5**				**0.5**	**1.5**	**2.5**
Water level (m)	**-2.0**	2.39	7.59	9.17	Sediment flux ($m^3.day^{-1}.m^{-1}$)	**Water level (m)**	**-2.0**	2.64	9.18	11.43
	-1.0	2.37	7.29	9.89			**-1.0**	3.31	8.53	11.99
	+1.0	0.65	9.13	15.58			**+1.0**	0.71	9.89	17.61
	+2.0	0.52	4.49	15.16			**+2.0**	0.42	5.46	16.11
		Offshore wave height (m)						**Offshore wave height (m)**		
		0.5	**1.5**	**2.5**				**0.5**	**1.5**	**2.5**
Water level (m)	**-2.0**	0.10	0.28	0.28	Mean initial rate of bed level change ($cm.day^{-1}.m^{-2}$)	**Water level (m)**	**-2.0**	0.08	0.24	0.19
	-1.0	0.12	0.39	0.44			**-1.0**	0.09	0.34	0.28
	+1.0	0.03	0.32	0.39			**+1.0**	0.03	0.28	0.31
	+2.0	0.02	0.23	0.37			**+2.0**	0.02	0.17	0.28

Table 6.4: Summary of key hydrodynamic and sedimentation experimental parameters for circular and elliptic morphologies under a variety of stationary water level and wave height conditions. Values of H_s/h, current strength, and sediment fluxes are maximum values extracted from around the morphologies. The initial rate of bed level change is the mean value per unit area based on a 1 km^2 region of the model domain that encompasses the features.

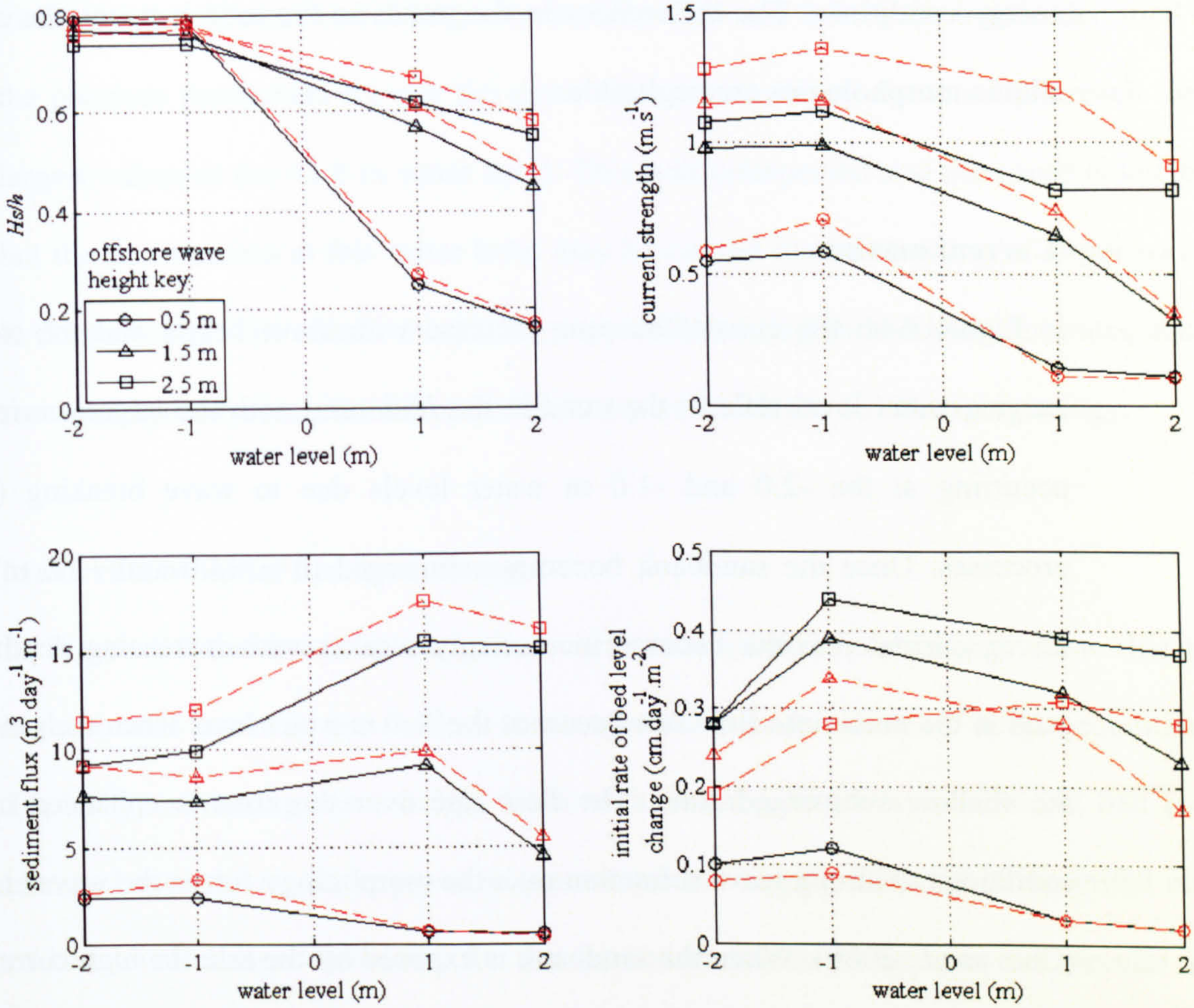

Figure 6.6: Hydrodynamic and sedimentation parameters for circular (black) and elliptic (red) morphologies from Table 7.4: a) ratio of maximum shoaling wave height to water depth, b) maximum current strength ($m.s^{-1}$), c) maximum sediment flux ($m^3.day^{-1}.m^{-1}$), and d) mean initial rate of bed level change per unit area ($cm.day^{-1}.m^{-2}$). Offshore wave heights of 0.5, 1.5, and 2.5 m are denoted by circles, triangles and squares respectively.

When the sandbank is in the exposed (h = -2.0 m) and shallow submerged (h = -1.0 m) states wave breaking occurs under all three wave height conditions. At these water levels the intensity of wave breaking around the flanks and over the crest is at a maximum and close or equal to the limit imposed in the model setup. Intuitively, as water levels deepen the magnitude of the ratio diminishes and fewer waves are break. The rate of decrease is highest for the smallest waves (H_s = 0.5 m) which highlights the ephemeral nature of the sandbank's low energy surf zone processes under meso to macro scale tidal water level variation. In this idealised experiment where the crest is positioned below mean tidal level, onshore directed wave driven sediment transport only occurs over the crest and around the flanks under lower states of tide under low

energy conditions. The differences in the trends in the ratio between the circular and elliptic morphologies are negligible.

Current maxima

In Figure 6.6b the current maxima increase with wave height and the trend due to varying water level reflects the trend in the H_s/h ratio with the largest current maxima occurring at the -2.0 and -1.0 m water levels due to wave breaking (surf zone) processes. Once the sandbank becomes submerged (h = +1.0 and +2.0 m) the wave driven current maxima become increasingly weaker with increasing depth. A minor peak in the maximum flow rate occurs at the -1.0 m water level when the sandbank is in the shallow submerged state. The flow rate over the crest is enhanced under these conditions as strong wave refraction over the morphology forces the waves to converge (Choi *et al.*, 2009). When the sandbank is exposed by the tide the high current maxima along the flanks (longshore currents) are due to the very oblique angle of the strongly refracted breaking waves. The current maxima for the elliptic morphology are typically higher than for the circular morphology under the same hydrodynamic conditions due to the stronger wave refraction over its steeper bathymetry. Under low energy conditions the difference between shoal current maxima is only appreciable in the shallow submerged state.

Sediment flux maxima

In Figure 6.6c the sediment flux maxima trend for the 0.5 m wave height case corresponds to the trends in the H_s/h ratio and current maxima with the highest magnitudes occurring in the exposed (h = -2.0 m) and shallow submerged (h = -1.0 m) states. With increasing submergence the flux maxima decrease to close to zero as the relatively weak surf zone radiation stresses cease to be effective in mobilising and

transporting sediment. Under larger waves (H_s = 1.5 and 2.5 m) the trends identified in the previous parameters are not the same since the sediment flux maxima reach their largest values at the +1.0 m water level. This was unexpected and the cause is unclear but the flux maxima at this water level may be caused by the breaking of larger waves in deeper water. The elliptic morphology typically has higher sediment flux rates under the same hydrodynamic conditions when compared with the circular morphology.

Mean rate of initial bed level change

In Figure 6.6 the trends in the mean initial rates of bed level change show that the highest rates occur in the shallow submerged state under all wave height conditions. Typically, increasing wave height leads to increasing mean rates of initial bed level change hence the trends in previous parameters are largely reflected in the initial rates of bed level change. However, for this parameter the trend between the circular and elliptic morphologies is opposite to that seen in previous parameters since the average rates of bed level change are consistently higher for the circular morphology than for the elliptic morphology. The reason for this unclear but it is likely to be a function of the larger area of circular sandbank which means that there is a greater area in which wave energy is eroding and depositing sediment at the higher rates hence the higher mean values.

Summary of key points:

1. Wave shoaling (outer surf zone) and wave breaking (inner surf zone) processes govern the distribution of the patterns of erosion and accretion depending on the water level.

2. Morphologies that are broad in the longshore dimension have significantly different patterns of erosion and deposition when compared with much narrower morphologies and this becomes significant when the sandbank is emerged at lower states of tide.

3. The elliptic shoal has relatively narrow patterns of erosion and accretion (i.e. constrained in the longshore dimension) under both submerged an emerged states. Importantly, due to the larger longshore length scale of the circular morphology these regions become separated under the emerged state leading to much broader patterns of deposition.

4. Strong wave refraction over the morphologies focuses the wave energy which intensifies wave breaking over the sandbank crest and around the flanks depending on the water level. These effects are often largest over the elliptic morphology which has steeper bathymetry along its flanks than the circular morphology.

5. The highest mean initial rates of bed level change occur when the two morphologies are only just submerged (h = -1.0 m) with the second highest changes occurring when the features are emerged (h = -2.0 m).

In this section, the idealised modelling experiment results for the emerged and submerged states of circular (aspect ratio ≈ 1) and elliptic (aspect ratio ≈ 2) morphologies have been presented with a description and analysis of the hydrodynamics and resulting sedimentation under a variety of different combinations of stationary water level and wave height conditions. The results underpin the findings of the video image and in-situ measurement analyses by reiterating the importance of wave shoaling and breaking processes on the sedimentation of discrete sandbanks. These processes are critically controlled by both the amount of wave energy and the vertical position of sandbank's crest relative to the water level since the manner with which they interact governs the nature of the patterns of erosion and deposition around the sandbank.

In the next section, the regions of erosion and accretion are used as a method of quantifying the propensity of different combinations of stationary hydrodynamic conditions to alter the aspect ratio of the morphologies. In particular this is investigated in relation to shoreward elongation in the cross-shore dimension through the comparison of the longshore length scales of the different regions with the original sandbank contour.

6.3.2.2 The propensity of different combinations of hydrodynamic conditions to alter the aspect ratio of an offshore sandbank

The principle objective of the idealised model experiments is to try to determine which physical processes cause the offshore sandbank at Teignmouth to elongate during its onshore migration. In the previous section the modelled results revealed how the spatial distribution and plan form of the regions of erosion and accretion vary under different water levels. In order to quantify the tendency of certain combinations of hydrodynamic conditions to cause shoreward elongation in the cross-shore dimension, the ratio of the longshore length scale of the contours of erosion and accretion at a prescribed level were used as an indicator. The basic premise for using the contours is that if the length of the longshore dimension of the primary region(s) of erosion in the vicinity of the sandbank is(are) less than that of the primary region(s) of accretion, then if the idealised conditions persisted then the sandbank's longshore dimension would tend to decrease causing an increase in the aspect ratio (longshore narrowing), and *vice versa* (longshore broadening). These mechanisms for morphological change have been defined conceptually in Figure 6.7. On the basis of this concept the ratio of the longshore lengths of these contours is considered to be a proxy for the tendency of the morphology to elongate or broaden. The erosion and accretion contours resulting from wave driven

sediment transport (tidal currents not modelled) for an arbitrary bed level change rate of ± 0.1 cm.day^{-1} per unit area were extracted from the modelled results at four individual tidal levels that spanned a vertical distance approximately equal to the spring tidal range at Teignmouth (4 m). The longshore lengths of the different regions were estimated from the contour data using the Matlab 'regionprops' function as described in Section 4.3

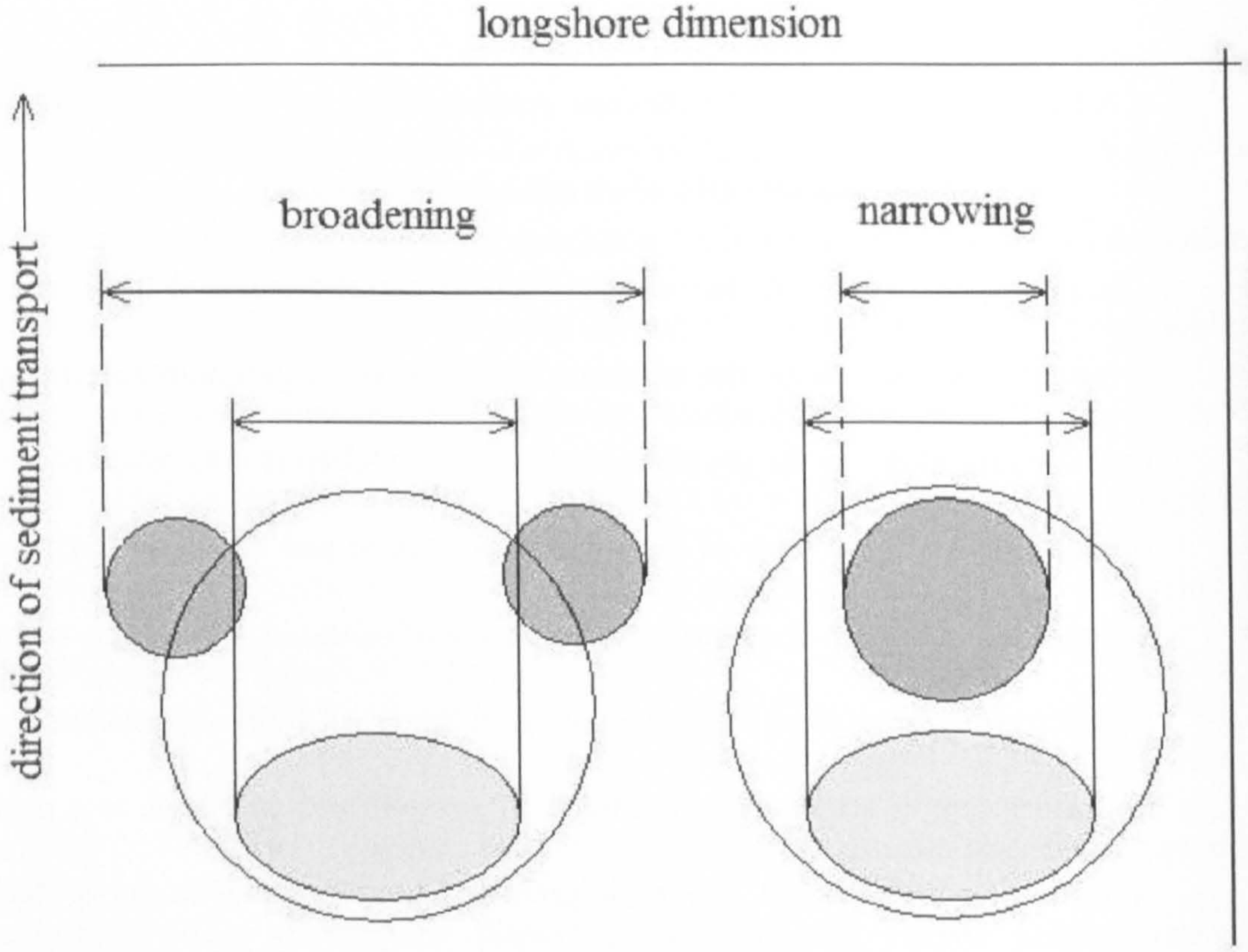

Figure 6.7: Conceptual diagram of the mechanisms of broadening and elongation due to the patterns of erosion (light grey shading) and accretion (dark grey) around the sandbank. The large circle denotes the plan form of the underlying sandbank.

The H_s/h ratios were calculated using the offshore significant wave height and the minimum depth over the crest which is situated at a level of -1.42 m relative to the arbitrary datum (h = 0 m). Negative values of the H_s/h ratio indicate that the sandbank is emerged and *vice versa*. The results for circular and elliptic morphologies are presented in Figure 6.8a and b respectively.

The effects of the different stationary hydrodynamic conditions on the ratio of the contours follow the results of the previous section and strongly suggest that the combination of wave energy with a submerged sandbank state (h = +1.0 and +2.0 m) generates the largest aspect ratios of the longshore dimensions of the selected erosion and accretion contours. These hydrodynamic conditions are therefore considered to promote elongation significantly whilst at lower states when the sandbank is just submerged or exposed by the tide there appears to be no such tendency.

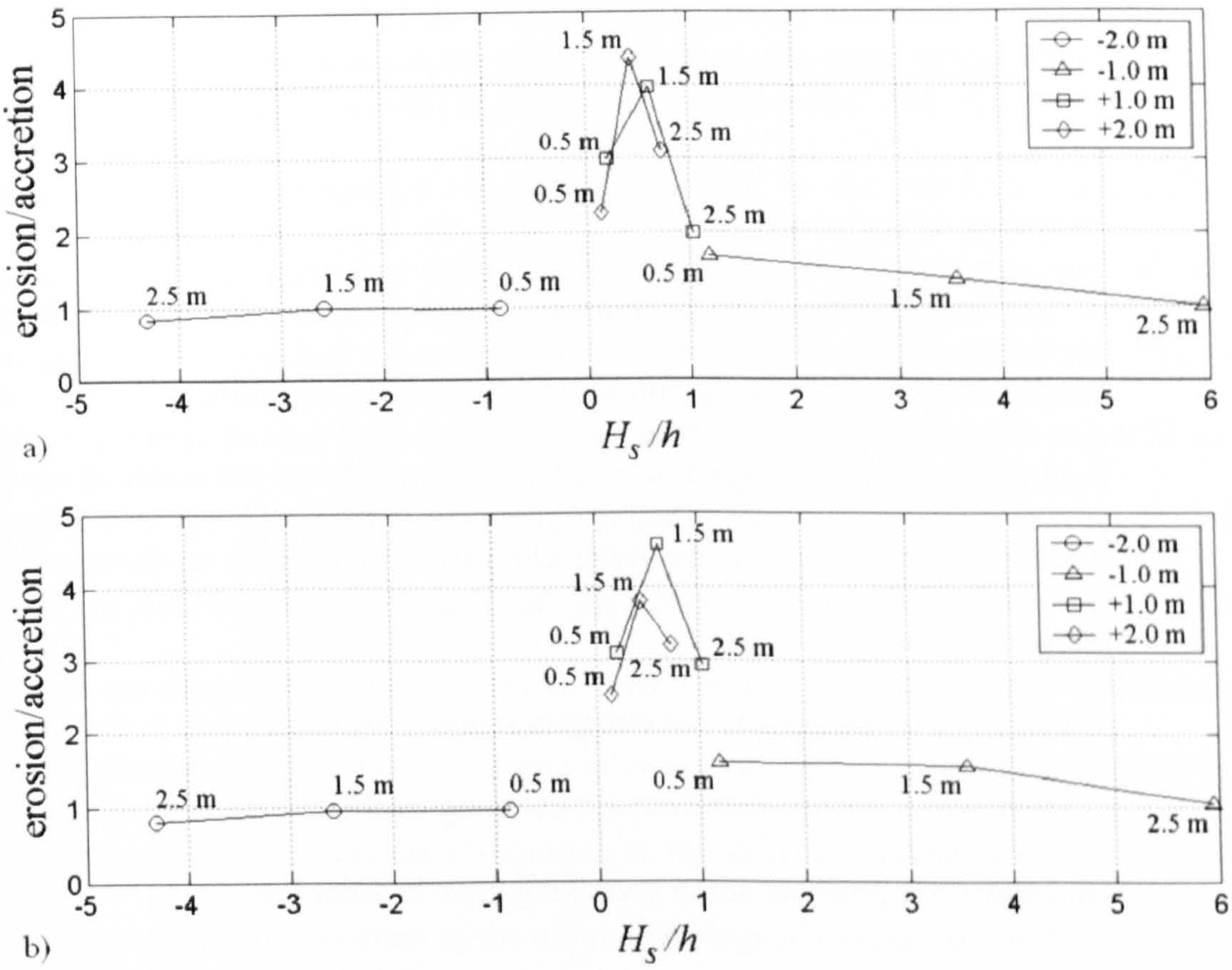

Figure 6.8: Comparison of the ratio of the longshore length scales of the erosion and accretion contours relating to initial bed level change rates of ±0.1 cm.day^{-1} per unit area under a range of water levels (h = -2.0, -1.0, +1.0, +2.0 m), and offshore significant wave heights (H_s = 0.5, 1.5, 2.5 m) for the: a) circular morphology, b) elliptic morphology. The H_s/h ratios are computed from the offshore significant wave height and the minimum depth over the crest of the sandbank which is located at a level of -1.42 m relative to the arbitrary datum (h = 0 m); negative H_s/h ratios indicate that the morphology is emerged.

For both the circular and elliptic morphologies the maximum aspect ratio generated in the experiments was approximately 4.5 (H_s = 1.5 m) for both morphologies. This indicates that the sediment is being eroded from regions that are significantly wider in

the longshore dimension than the regions of accretion. Sandbanks with relatively deep crests in relation to the tidal water level variation will therefore tend to narrow with shoreward migration causing a transverse and elongate geometry. Conversely, the more emerged the sandbank becomes the less elongation is promoted until under the largest waves (H_s = 2.5 m) and lowest water levels (h = -2.0 and -1.0 m) the shoal sediment transport regime may lead to a small longshore broadening effect. The results suggest that the propensity of the wave driven sediment transport regimes to promote elongation whilst submerged varies with wave height, though all wave height conditions do so to some degree especially in the case of the elliptic morphology.

Summary of key points:

1. The erosion-deposition patterns suggest that the combination of deeper submerged conditions with wave energy promotes shoreward elongation.

2. In the shallow submerged (h = -1.0 m) only the lower the levels of wave energy (H_s = 0.5 and 1.5 m) appear to promote elongation and this is accentuated for the elliptic morphology.

3. There is a no propensity for elongation under the exposed (h = -2.0 m) conditions.

2. High wave energy conditions coinciding with low water levels in relation to the sandbank crest promote small scale longshore broadening.

The idealised modelling experiments have been conducted using stationary water level conditions and therefore do not provide insight into the net effect of the different sediment transport regimes on the morphologies through the typical tidal cycle. The significance of tidal water level variation is that it imposes a temporal constraint on the on the residence times of the wave driven processes. This is exacerbated under low energy conditions since small waves are only able to break in shallower water depths. In

the next section an idealised modelling experiment is undertaken which estimates the aggregate morphological change due to one complete tidal cycle. The effect of the tidal cycle is introduced by the addition of the bed level change data at each grid point over a range of water levels which together represent the spring-neap variation in tidal range. These are subsequently used to update the original bathymetry to provide an estimate of the net morphological change.

6.3.2.3 Wave driven morphological change over spring and neap tidal ranges

In order to estimate the morphological change associated with the passage of one complete tidal cycle a similar conceptual approach to the previous experiments is adopted which uses stationary water levels. The water levels used span vertical ranges of 4 and 2 m to simulate the spring and neap tide excursions respectively. The tidal ranges were first divided in to equal intervals of 0.5 m for the spring tide and 0.25 m for the neap tide. The wave and flow conditions under each stationary water level and wave height combination are modelled and the output initial rates of bed level change matrices are then weighted according to their vertical position. This is undertaken in order to simulate the variation in the rate of change of tidal level through a typical cycle since this governs the duration of exposure to the different sediment transport regimes. This was considered important to the net morphological change following the results of the previous idealised modelling experiments which revealed how water level exerts a significant control on the variation in the plan form, distribution and intensity of the regions of erosion and accretion. The resultant matrices are summed to obtain an aggregate estimate for one tidal cycle and subsequently multiplied by a factor of 30. The data are multiplied by 30 in order to exaggerate the effects of the different permutations on the morphological evolution and so aid in the identification of trends between

experiments. The modelling experiment applies to the situation where the crest of the sandbank is relatively deep (h_{crest} = -1.42 m) with respect to the tidal range. This reflects the typical depth to the crest at the start of the onshore migration-elongation stage in events 2, 3 and 4 (Figure 4.22b, c and d). The idealised experimental setup does not include the tidal current component or updating of the bathymetry but despite such limitations, the approach is useful because it reveals the potential aggregate effects of the variable residence times of the different wave driven erosion-deposition patterns under the large water level changes associated with meso to macro scale tides.

The morphological change between the original (black contours) and resultant (red contours) morphologies for each of the modelling experiments is represented in a series of 3D contour plots in Figure 6.9. In the figure, the upper panel shows the estimated change due to offshore significant wave heights 0.5, 1.5 and 2.5 m and neap tides, whilst the lower panel shows the same but for spring tides.

The predicted contours of the resultant morphologies suggest that the aggregate effects of meso to macro scale water level variation when combined with wave energy on a discrete sandbank can lead to onshore elongation or longshore broadening. The experiments predict that elongation is promoted the most under low energy wave conditions. Under increasing wave energy conditions the aspect ratio of the sandbank undergoes a small degree of broadening which reflects the predicted morphological response for an exposed sandbank under high wave energy conditions in the previous experiment (Section 6.3.2.3). The plan form geometry of the upper contours in Figure 6.9c and f infer that the small broadening effect of higher energy waves is not appreciably different under spring and neap tidal ranges.

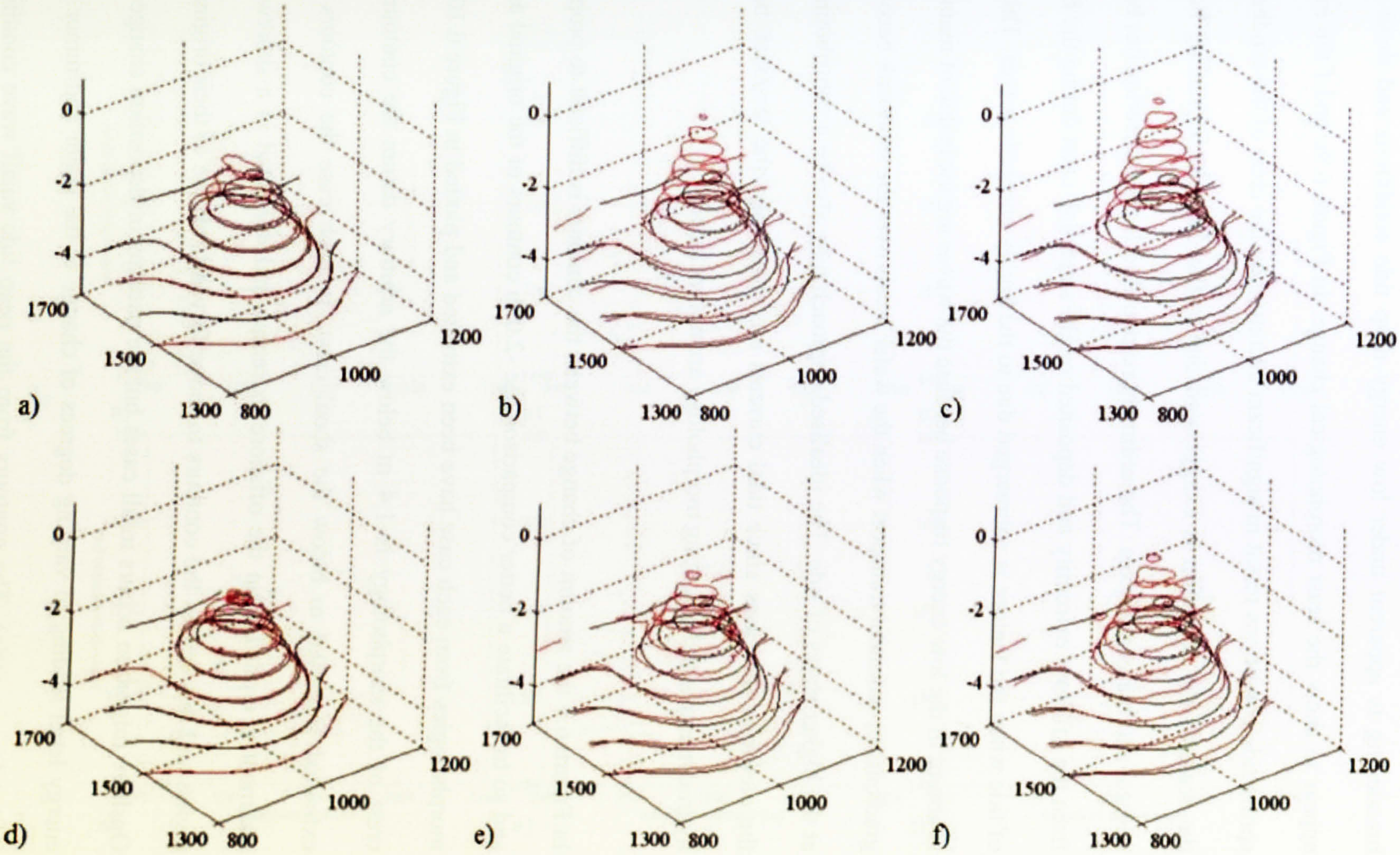

Figure 6.9: 3D contour plots showing the original circular sandbank morphology (black contours) and the estimated morphology after (red contours) 30 cycles of neap (tidal range = 2 m) and spring (tidal range = 2 m) tides under a range of offshore wave heights: a) H_s = 0.5 m, neap tide, b) H_s = 1.5 m, neap tide, c) H_s = 2.5 m, neap tide, d) H_s = 0.5 m, spring tide, e) H_s = 1.5 m, spring tide, and f) H_s = 2.5 m, spring tide. The contours are at 0.5 m intervals and all axes dimensions are specified in meters relative to an arbitrary datum (h = 0 m).

Under low energy conditions the difference in the upper contours in Figure 6.9a and d indicates that the neap tides significantly promote elongation but spring tides do not. No broadening is apparent under low energy neap tide conditions and these conditions appear to show the least morphological change. In Figure 6.9c and f the high energy spring tide conditions result in significant accretion on the crest of the sandbank though the scale of the accretion is exaggerated due to the disparity in scaling between the vertical and horizontal axes. The sediment responsible for the accretion has been eroded from the offshore extremity and deposited on the sandbank crest during the higher stets of tide when the feature is submerged due to the highly energetic waves. This accretion is absent in the low energy response because the waves are incapable of maintaining the gradients in sediment transport when the water levels over the sandbank become to deep at the higher states of tide. The idealised approach may also be a contributing factor to the elevation increases since tidal currents are absent and the feedback between the hydrodynamics and changing morphology are not included.

In Figure 6.9 the amount of change between the contours is difficult to properly assess and so to facilitate a better comparison the -2.0 m contours of the original and updated morphologies from each case have been extracted and plotted in Figure 6.10. Since the crest of the morphology is 1.4 m below the arbitrary datum the contours used are extracted from 0.6 m below the shoal crest. In each case the contours show that sediment is eroded from the offshore extremity and deposited in a shoreward central region and this causes the contours to move forward relative to their original position. Onshore migration occurs in all cases but the patterns of deposition change with wave energy level leading to varying degrees of change to the major and minor axis length scales (aspect ratio). The contours from the neap tide small wave condition (Figure 6.10a) indicate that the sediment deposition pattern is laterally constrained.

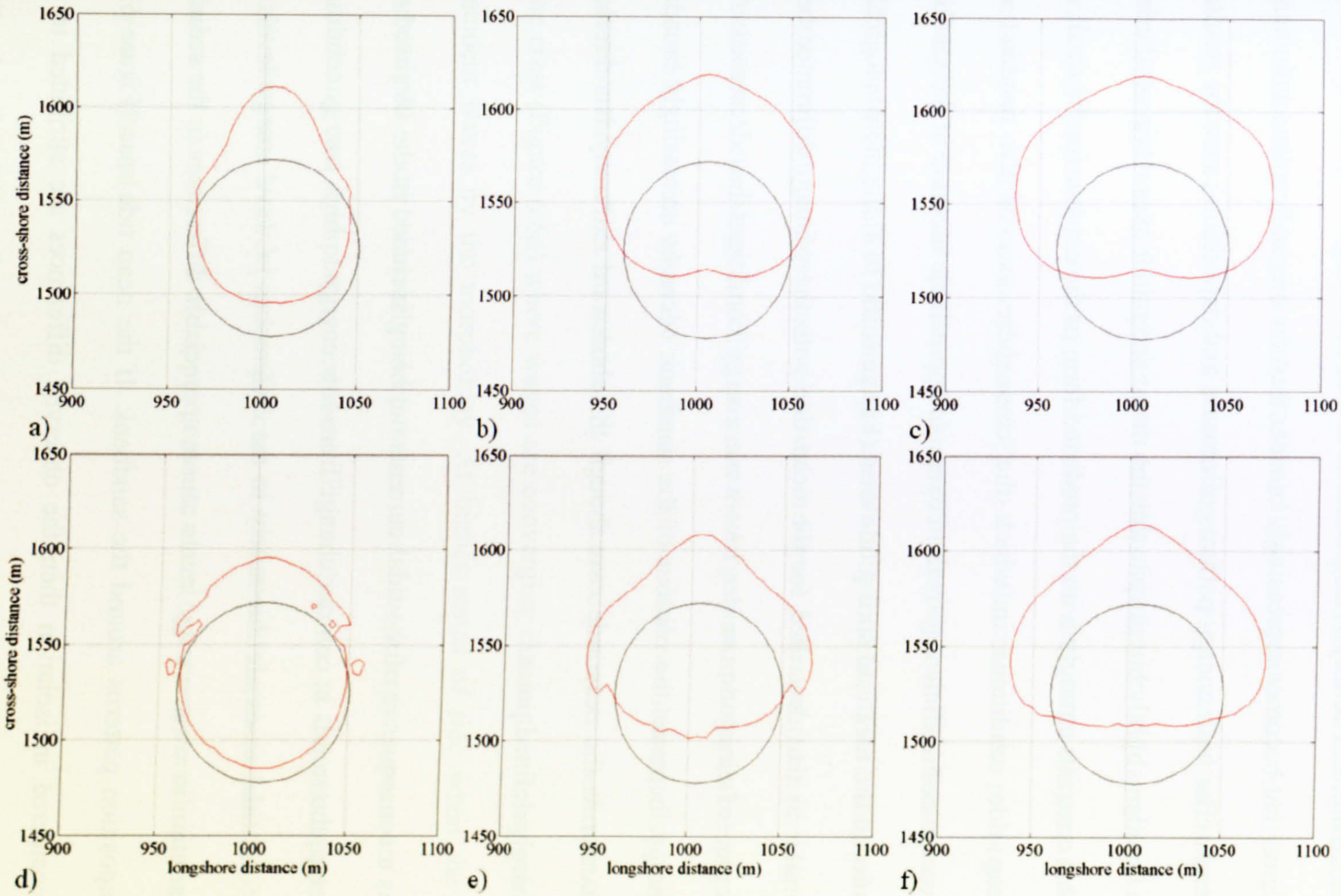

Figure 6.10: 2D plan view contour plots from the -2.0 m level from the original (black contours) and updated (red) sandbank morphologies in Figure 7.7: a) H_s = 0.5 m, neap tide, b) H_s = 1.5 m, neap tide, c) H_s = 2.5 m, neap tide, d) H_s = 0.5 m, spring tide, e) H_s = 1.5 m, spring tide, f) H_s = 2.5 m, spring tide. Contours are in specified meters at 0.5 m intervals and referenced to an arbitrary datum.

Consequently the new contour has a slightly smaller longshore length scale than the original and narrows toward the shoreward extremity. With increasing wave height (Figures 6.10b and c) greater quantities of sediment are eroded from greater depths on the offshore extremity. This sediment is transported onshore and deposited in a central region that becomes increasingly broader than the original contour with increasing wave height. The high energy patterns of erosion and deposition cause the resultant contours to broaden slightly but despite this the major and minor axes retain similar length scales. This contrasts strongly with the predicted form of the contour for the small wave energy neap tide conditions in which the cross-shore axis of the resultant contour has experienced sufficient growth to cause an appreciable increase in the sandbank's aspect ratio. In the idealised spring tide case (Figure 6.10d to f) the morphological response is similar to that described for the neap tide with the primary difference being that the degree of elongation under low wave energy conditions has decreased. As the wave energy increases the contour of the sandbank becomes increasingly broad in a similar manner to the neap tide case though the shoreward extremity has developed a more sharply defined point.

As a consequence of the tidal currents not being included in the idealised experimental setup, the trends in contour change from low energy to high energy conditions in either of the tidal cases are due solely to the differences in wave energy levels. Clearly the variation in wave energy levels causes appreciable differences in the sediment erosion-deposition patterns around the sandbank. If the neap tide case (Figure 6.10a to c) is considered in isolation then the observed differences are attributed to two factors. Firstly the depth to which sediment is mobilised and transported under different wave energy levels varies, and secondly the residence time of the different sediment transport processes over the range of water levels also varies. Under increasing wave energy

levels, the gradients in sediment transport are maintained at increasingly greater depths and this is evident in the contours of the offshore extremity in Figure 6.9 for both of the idealised tidal conditions. The variable residence times due to the tide mean that the sediment transport regimes at the lower and higher states of the tide endure for longer and are therefore dominant compared with those at intermediate water levels. These two factors account for the observed broadening and crest accretion trends under increasing wave energy levels. The prolonged duration of the low tide gradients in sediment transport (exposed state) deposit sediment in two side lobes (Figure 6.4c) hence the broadening of the contour (Figure 6.7). In a similar manner the prolonged duration of the high tide transport gradients (submerged state) deposit sediment in a central region of the crest (Figure 6.4f) causing the elevation to increase. The combined effect results in the morphological response observed in Figure 6.9c and f. Under low energy wave conditions the analogy is different since the largest morphological response appears to occur after low tide when the sandbank is in the shallow submerged state and residence times are shorter. This is explained by the enhanced gradients in sediment transport over the crest (Figure 6.6d) where waves are converging due to the strong refraction of the incident waves by the morphology. At higher states of tide when the sandbank is submerged under relatively deep water the low energy waves are incapable of mobilising and transporting sediment. This imbalance in the residence times of the different water level dependant patterns of erosion and deposition leads to the observed shoreward elongation of the upper contours under low energy conditions as depicted in Figure 6.10a and d.

The observed differences in the trends between the idealised spring and neap tide cases are less well defined. However, the less pronounced elongation under low wave energy spring tide conditions is largely a product of the shorter residence times leading to less

wave driven sediment transport over the sandbank and therefore less morphological change. This is also reflected in the high wave energy cases where the lower residence times associated with the spring tide results in less accretion on the crest (Figure 6.9f) compared with the neap tide (Figure 6.9c).

Key point summary:

The following points apply to the case where the sandbank has a relatively deep crest (i.e. below mean sea level):

1. Wave shoaling and breaking on the sandbank create cross-shore gradients in sediment transport which result in the landward displacement of the sandbank contours hence onshore migration.

2. The response of the morphology is determined by the dominance of sediment transport regimes at certain stages of the tide, and on the depth to which the gradients in sediment transport are maintained under the different wave energy levels.

3. High energy waves combined with both spring and neap tidal conditions are predicted to promote a degree of broadening in the longshore dimension and crest accretion due to the dominance of both the low and high tide sediment transport regimes. These dominate over the intermediate water levels due to their longer residence times.

4. Low energy waves combined with neap tides are predicted to promote shoreward elongation due to the dominance of the sediment transport regime in the shallow submerged state. Under these conditions the gradients in sediment transport over the crest are enhanced due to the convergence of refracted waves. This generates larger morphological change than at low tide state despite the shorter residence time of the physical processes.

6.3.3 Summary

In relation to the morphological evolution of the offshore sandbanks at Teignmouth, the results of the idealised modelling experiments have been useful in identifying potential mechanisms for shoal elongation following genesis. The findings of the idealised experiments support those of the Argus video analyses by reiterating the importance of the water level relative to the vertical position of the crest in controlling the wave driven sedimentation over and around the sandbanks. In addition to this, the initial experiments revealed the existence of a dichotomy of erosion-accretion patterns that depends on whether the sandbanks are submerged or exposed. When the sandbank is exposed, sediment eroded from the offshore extremity is transported onshore and deposited along either flank, whereas when the feature is submerged deposition occurs in a single centralised region of the crest. Typically, the pattern of deposition is constrained in the longshore dimension due to the strong refraction of the incident waves. This is exacerbated in the case of the elliptic morphology which has steeper gradients along its flanks than the circular morphology. The regions of accretion on the shoreward extremity of the exposed circular sandbank differed from the elliptic case since deposition occurred in two side lobes. Subsequently further idealised experiments were performed that investigated the effects of variable wave energy and meso to macro scale water level variation. When the aggregate effects of the water level variation were incorporated the results suggested that low energy wave conditions when combined with neap tides promote the most shoreward elongation. High energy conditions were predicted to promote a degree of broadening in the longshore dimension and an increase the elevation. These morphological responses are attributed to the dominance of sediment transport regimes at certain stages of the tide, and on the depth to which the gradients in sediment transport are maintained under the different wave energy levels. High energy waves are capable of maintaining gradients in sediment transport in deeper

water than low energy waves. Consequently, the morphological response under high energy conditions is primarily a function of the longer residence times of both the high and low tide sediment transport regimes. In contrast to this when low energy conditions exist, morphological change is restricted to the lower states of tide and is predicted to be dominated by gradients in transport under shallow submerged conditions which promote elongation.

The experiments concerning the aggregate effects of meso to macro scale water level variation on the sandbank's sedimentation relate to the circular sandbank morphology and to the case where the crest of the sandbank is positioned below mean sea level (MSL). At Teignmouth the elevation of the sandbank crest typically rises above MSL during the migration-elongation stage and in the inlet's current mode, the morphology has already become elongate and transversely orientated by this time. Therefore the resultant patterns of erosion and accretion will be constrained in the longshore dimension regardless of the relationship between the crest height, tidal excursion and the chronology of wave energy. Consequently, after the sandbank morphology has become elongate and transversely orientated it will retain the form through to the shore-attachment and dissipation stage.

This result appears to account for the observed morphological behaviour of the offshore sandbanks on the ebb tidal delta at the Teign inlet in its current mode. Genesis occurs when the sandbanks crests are deep with respect to MSL and this combined with the prevailing low energy wave conditions promotes the initial shoreward elongation. The hydrodynamics and sedimentation were investigated in respect of the specific case where the crest is deeper than the mid tidal level but the identified trends are more generally applicable and lead to a set of hypotheses. The hypotheses initially concern

sandbanks in genesis where it is proposed that those with deeper crests (h_{crest} >> MSL) will undergo preferential shoreward elongation under prevailing conditions of low energy waves and meso to macro scale tides. Sandbanks that occur under high sediment availability conditions are likely to accrete more and therefore have higher elevations at genesis (h_{crest} > MSL). For these sandbanks the duration of the exposed state increases with the elevation of the crest, therefore it is proposed that the aspect ratio of these sandbanks may remain relatively unchanged or have a tendency to broaden in the longshore dimension under the same conditions. If higher energy conditions prevail then it is proposed that the tendency for ebb tidal delta sandbanks to broaden will increase. These concepts are subsequently used in a conceptual model of the plan form evolution of the sandbanks on the Teign inlet ebb tidal delta in Section 7.5.

6.4 Teignmouth simulation

The idealised modelling experiments did not incorporate the tidal current component and in order to be able to assess their effect on the patterns of erosion and deposition around and over the migrating shoal it was necessary to conduct further simulations. In these experiments the measured bathymetric, wave and tidal data from the May 2003 Coastview Project fieldwork program are used as the simulation boundary conditions. The next section of the thesis begins with a brief description of the model setup.

6.4.1 Methodology and model set up

The analysis of the in-situ measurement data revealed that strong onshore directed mean flows were the primary mechanism for onshore directed sediment transport under typical hydrodynamic conditions (Sections 5.6.2 to 5.6.4). This was reflected in the idealised modelling experiments which showed how the wave driven mean flow (depth

averaged) creates gradients in sediment transport that lead variable patterns of erosion and deposition. These patterns appear to explain the mechanism that causes the sandbanks at Teignmouth to evolve into their elongate and transverse forms (Section 6.3.2). Therefore it is reasonable to assume that it is the mean flows that lead to the observed morphological behaviour. The primary objective of using the model to simulate the physical conditions at Teignmouth is to determine the relative importance of the wave and tidally driven components of the mean flow field. This is particularly important in the case of the tidal currents since their effect on the patterns of erosion and deposition has not yet been investigated. In order to achieve this, two identical modelling experiments were set up but in the second experiment the waves were omitted in order to isolate the flow due to the tide. Subsequently, the current due solely to the waves was estimated from the difference between the two time series.

The topographic and bathymetric survey data from the May 2003 Coastview fieldwork program were merged to provide the surface data for the model domain. This covers the coastline 2 km to the north, 1.5 km to the south of the Teign estuary and extends approximately 3.5 km offshore at a resolution of 10 m. A plot of the bathymetry focussed on the region of interest is presented in Figure 5.5 (Section 5.3). The wave and water level boundary conditions were obtained using a regional sized model that encapsulates the Teign estuary and utilised the wave and water level data from the seabed located offshore ADCP. The model runs covered two complete tidal cycles which spanned the afternoon of the 15th and morning of the 16th May. The bottom dissipation and eddy viscosity parameterisations were defined after Siegle *et al.* (2003) using spatially varying values of the Nikuradse roughness parameter and Chezy number. The simulation covered the period between 1600 hours on the 15th May and

1230 hours on the 16th May using a time step of 10 minutes and a warm up period of 30 minutes.

In order to simulate the south easterly incident wave direction on the 16th May, 2003, it was required to rotate the bathymetry in the NSW model setup but owing to an error in this procedure, the resultant mean wave direction (MWD) time series used was in the range 109 to 112° as opposed to the 143 to 160°. The impact of this error is however small due to the strong refraction of the incident waves which results in little directional variation over the sandbank morphology (Bird *et al*, 2001). The simulation did not incorporate the bed level changes therefore the morphology is not updated between time steps.

6.4.2 Results

6.4.2.1 Qualitative validation of the modelled and measured hydrodynamics using the data for the offshore extremity SLOT rig position

To provide a qualitative validation of the model setup, in this section the modelled hydrodynamics and sedimentation are compared with the data May 2003 fieldwork data for the same period. Initially, the current vector time series are compared (Figure 6.11) and in order to facilitate the comparison the 10 minute resolution of the model output current vector time series has been interpolated on to a 17 minute resolution. The parameters that are being compared in Figure 6.11 are time averages of the measured Eulerian currents at z = 14 cm, (Figure 6.11a, previously presented in Figure 5.6a), and the modelled depth averaged currents over one tidal cycle (Figure 6.11b).

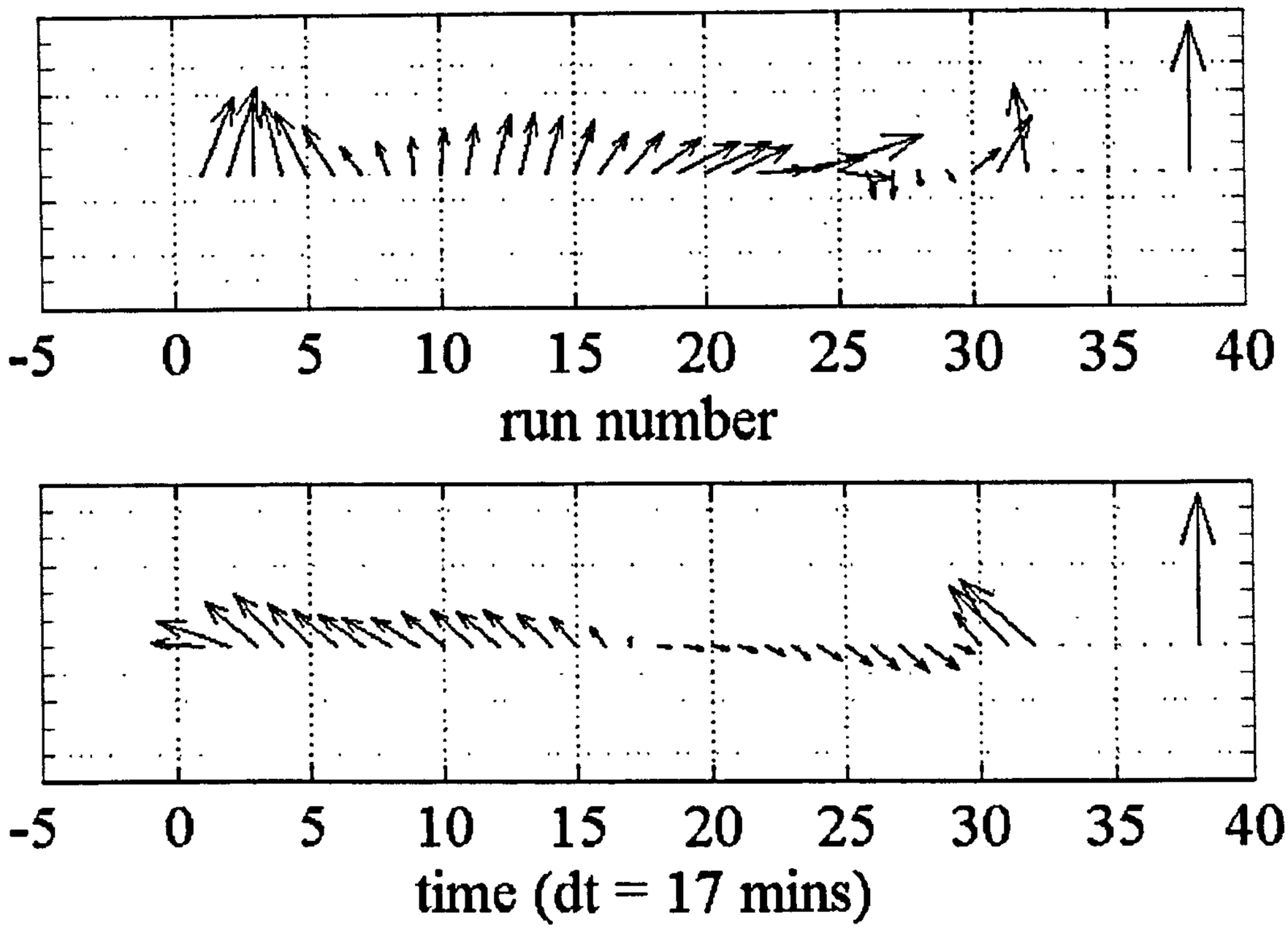

Figure 6.11: Modelled and measured current vector time series for the offshore extremity SLOT rig position (1A) under similar hydrodynamic conditions. a) in-situ measurement data from May 16th, 2003, and b) modelled data. A vector denoting a 0.5 $m.s^{-1}$ onshore directed current is plotted to the right of the time series for scaling purposes.

The general trends in the magnitude of the cross-shore component of the modelled vector time series show similar trends to those in the in-situ measurement vectors whilst in the longshore direction the differences become more appreciable. The longshore component of the sediment transport has previously been shown to be less important in the sedimentation of the sandbanks with the inlet in its current mode so the impact of the greater inaccuracy of the modelled longshore currents on this analysis is mitigated. Some of the differences in the time series can be attributed to the fact that the parameters being compared are not precisely equivalent with the model data being depth averaged estimates whilst the in-situ data are time averaged Eulerian measurements at one vertical position.

In terms of the trends in the cross-shore component of the modelled and measured current vectors there are identifiable similarities between the two time series. In the

shallow flood and ebb tide water the currents are strongest and onshore directed in both datasets. The manner in which the measured time averaged currents decrease during the flood tide is reflected in the modelled currents. The same also applies to the current variability that occurs on the ebb tide where it first becomes offshore directed before reversing in the shallow waters at the end of the ebb tide. The principle discrepancy between the trends in the measured versus modelled results for the cross-shore component is in the relative timing of when the onshore directed flood tide currents turns offshore. The model prediction occurs at around the time of high tide whilst in the measurement time series it occurs approximately 1 hour 40 minutes later. Additionally, the model does not predict the short but significant increase in the current strength that occurs at around the mid ebb tide (Figure 6.11a, run numbers 23 and 24). The error in the modelled incident wave direction may have affected the longshore component of the modelled current time series which is skewed about the cross-shore axis in the direction of the estuary mouth though the impact on the relative strength of the cross-shore current through the tide is considered to be negligible. The modelled current vectors show less randomness in their longshore variability when compared with the measured vector time series and the cause of this unclear but may be due to non-linear wave-current and wave-wave interactions that are not accounted for in the model parameterisation (Delft Hydraulics Institute, 2004). In terms of the variation in the magnitude of the modelled versus measured currents, the modelled currents tend to be smaller than the measured currents though this is considered to be a function of the depth averaging used in MIKE21 estimate.

An additional qualitative validation of the model set up for the Teignmouth experiment is now undertaken using the comparative measured and modelled parameters profile plots presented in Figure 6.12 which show the water level, cross-shore current and

cross-shore sediment transport from the offshore extremity SLOT rig position. The plotted parameters pertain to the morning on the 16th May, 2003 therefore the data are equivalent with the exception that the mean wave direction input to the model was in error (Section 6.4.1). In this comparison the in-situ measurement data have been interpolated from the 17 minute resolution of the original time series on to the higher 10 minute resolution of the model data. The model data are depth averaged compared with the in-situ measurement data which are Eulerian point measurements. The data are presented in a similar manner to the earlier time series plots in the in-situ measurement chapter (Section 5.6.3) with the depth and cross-shore current profiles depicted in a) and b) respectively. In Figure 6.12c the modelled cross-shore sediment flux profile is plotted with the net cross-shore sediment rate computed after Jaffe *et al.* (1984).

From the comparison of the measured and modelled data in Figure 6.12 it can be seen that the accuracy of the model prediction varies for the three parameters. The trends in the water depth and cross-shore sediment fluxes are well correlated. The modelled and predicted cross-shore current time series display the largest divergence which is most pronounced in water depths greater than 1.5 m. At the start of the flood tide, the shallow surf zone current strength is initially under estimated by approximately 33%, but over the subsequent three time steps the two datasets converge. On the ebb tide, the profiles begin to converge at time step 56 and the model subsequently predicts the changes in the cross-shore current strength reasonably well. The model is unable to simulate the atypical mid ebb tide surge in the resultant current strength. This response of the current regime to the hydrodynamic forcing appears to be a real hydrodynamic response as it also observed in the resultant current datasets at other SLOT rig positions. The cause of this phenomenon has not been determined but its occurrence highlights the complexity

of the hydrodynamics that govern the sedimentation of migrating sandbanks on ebb tidal deltas.

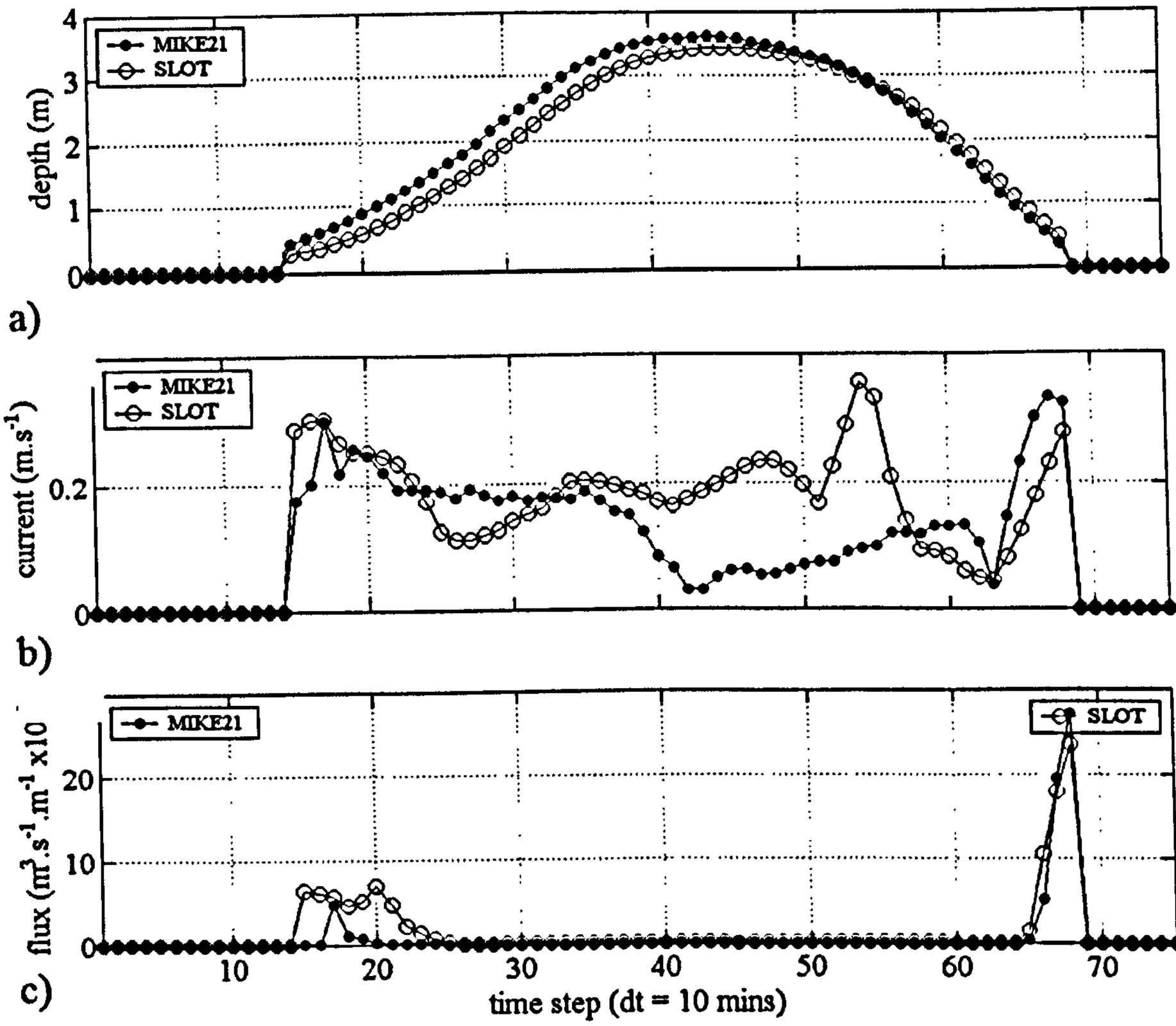

Figure 6.12: Modelled (black circles) and measured (white circles) hydrodynamics and sedimentation under comparative offshore wave and tide conditions for the offshore extremity SLOT rig position (1A): a) water depth, b) cross-shore current velocity, and c) cross-shore sediment flux (model) with the estimated suspended cross-shore sediment transport rate after Jaffe *et al.* (1984) (in-situ measurements).

The trends in the modelled cross-shore sediment fluxes are well correlated with the trends in the fluxes that were estimated from the in-situ measurements. The coarse-grained sediment combined with low energy conditions only generates appreciable sediment fluxes in the shallowest water depths around the low tide mark. The trend in the ebb tide sediment transport rate is predicted particularly well but the duration is underestimated on the flood tide when compared with the measurement profile.

Despite some divergence between the correlation in the trends in the time series in Figure 6.11 and Figure 6.12 shows that MIKE21 is reasonably well calibrated and

encapsulates the fundamental physical processes concerned. In the following two sections the experimental results are first presented for a range of discrete tidal levels then the relative contributions of the wave and tidally driven components to the mean flow at the different offshore extremity SLOT rig position are quantified and compared.

6.4.2.2 Spatial and temporal variation in the modelled hydrodynamics and sedimentation

The spatial and temporal variation in the current and sediment flux strength and direction in relation to the sandbank morphology at discrete tidal levels through the duration of one tidal cycle are presented in Figure 6.13 to 6.18. Each figure is comprised of upper and lower panels showing the modelled flow and sediment transport regimes at each respective tidal level. Each vector plot shows a subset of the model domain focussed on the sandbank morphology. To the left (south) of the plotted grid domain the bathymetry begins to shallow towards the channel margin bar termed Spratt Sand whilst at the top of the grid (north) the bathymetry shallows more sharply due to the contours of Teignmouth main beach. On the northernmost flank of the sandbank the contours define a gently gully which ceases abruptly next to the shoal and more gently in the direction of the adjacent beach. In the following paragraphs a brief description of the synoptic scale hydrodynamics is followed by a discussion of the important aspects of the predicted patterns of sedimentation in respect of the migrating shoal.

At the turn of the tide in Figure 6.13a the tidal circulation is weak and since the wave energy is low the submerged shoal is subject to weak onshore directed current over the crest.

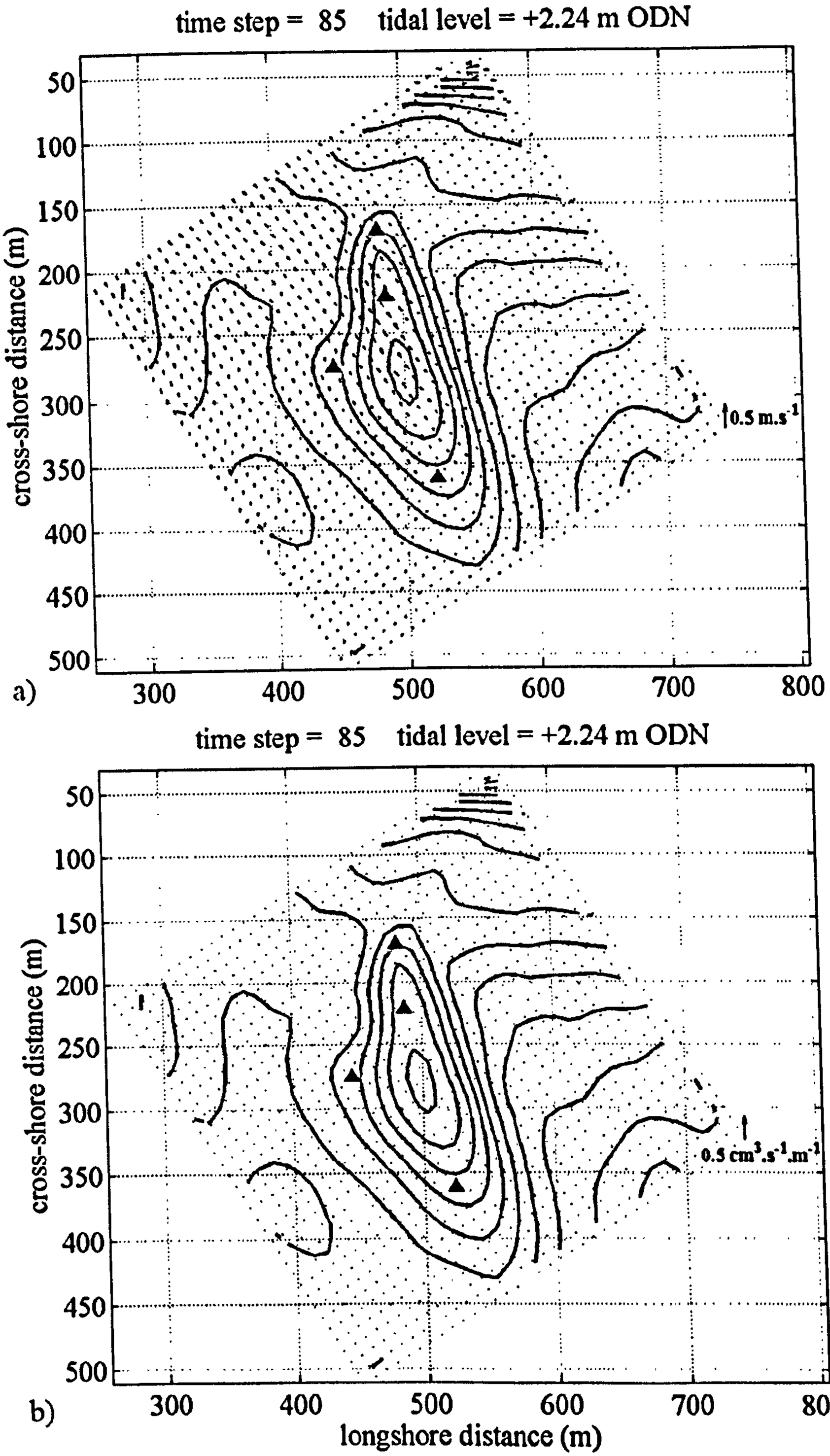

Figure 6.13: Simulated hydrodynamics and sedimentation in the vicinity of the offshore sandbank at Teignmouth for the 16th May, 2003. Time ≈ high tide: a) current strength and direction, b) sediment flux strength and direction. Black hatched lines indicate the shoreline position and black triangles indicate the nearest grid point to the SLOT rig positions used in the fieldwork program. Reference vectors are plotted at the furthest right hand grid point position for scaling purposes.

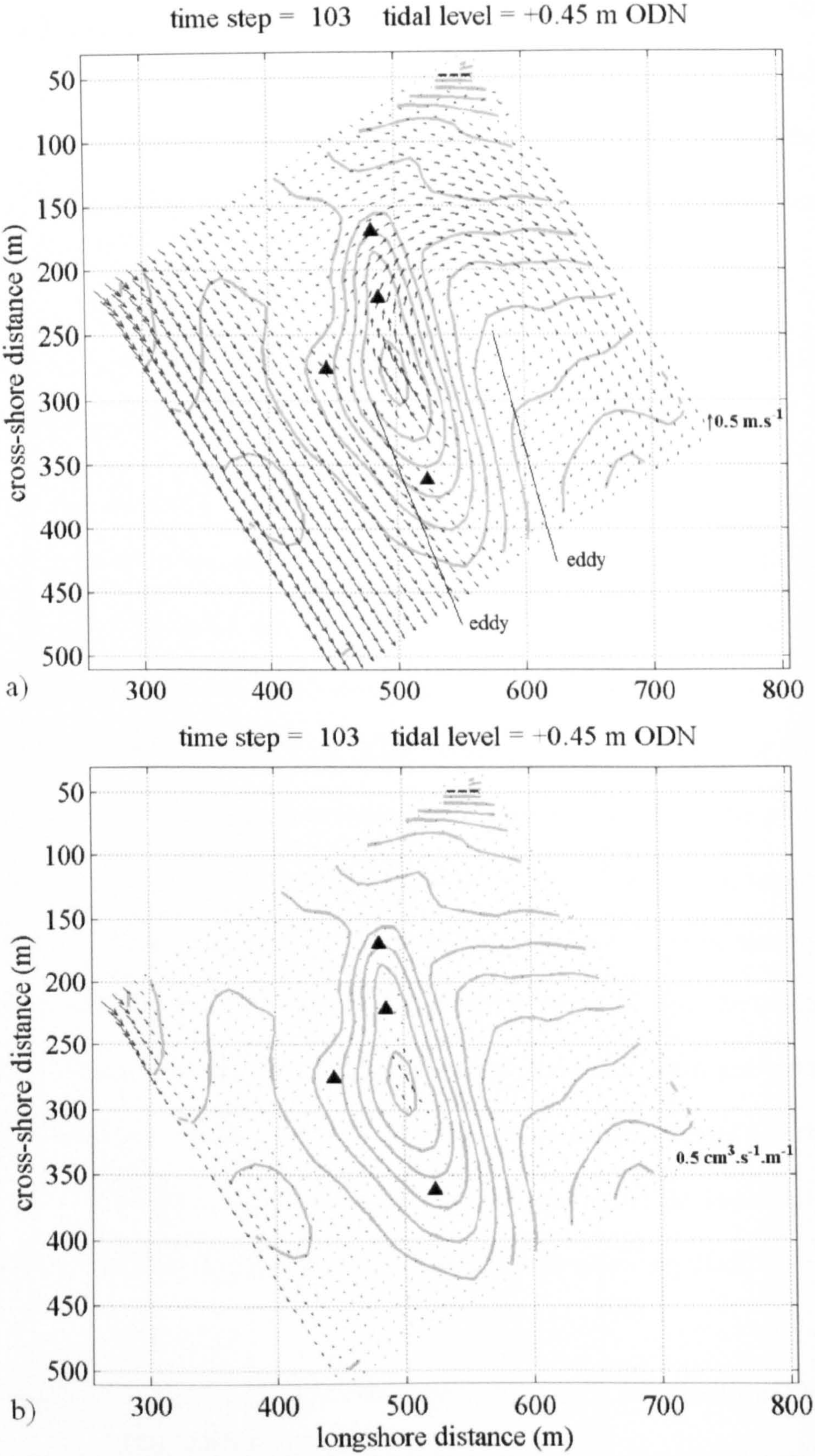

Figure 6.14: Simulated hydrodynamics and sedimentation in the vicinity of the offshore sandbank at Teignmouth for the 16th May, 2003. Time ≈ high tide +2 hours: a) current strength and direction, b) sediment flux strength and direction. Black hatched lines indicate the shoreline position and black triangles indicate the nearest grid point to the SLOT rig positions used in the fieldwork program. Reference vectors are plotted at the furthest right hand grid point position for scaling purposes.

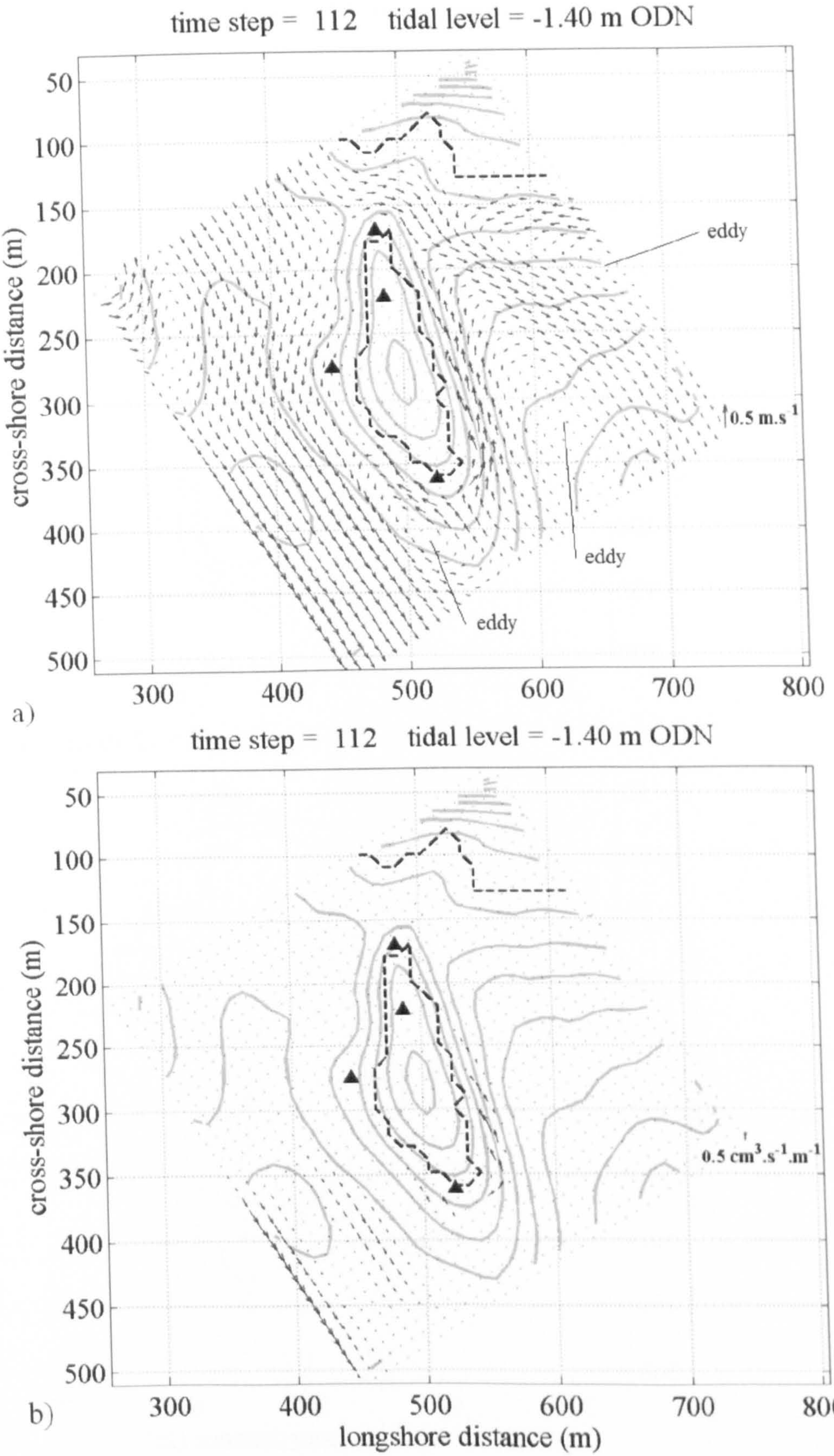

Figure 6.15: Simulated hydrodynamics and sedimentation in the vicinity of the offshore sandbank at Teignmouth for the 16th May, 2003. Time ≈ high tide +4 hours: a) current strength and direction, b) sediment flux strength and direction. Black hatched lines indicate the shoreline position and black triangles indicate the SLOT positions during the fieldwork program. Reference vectors are plotted at the furthest right hand grid point position for scaling purposes.

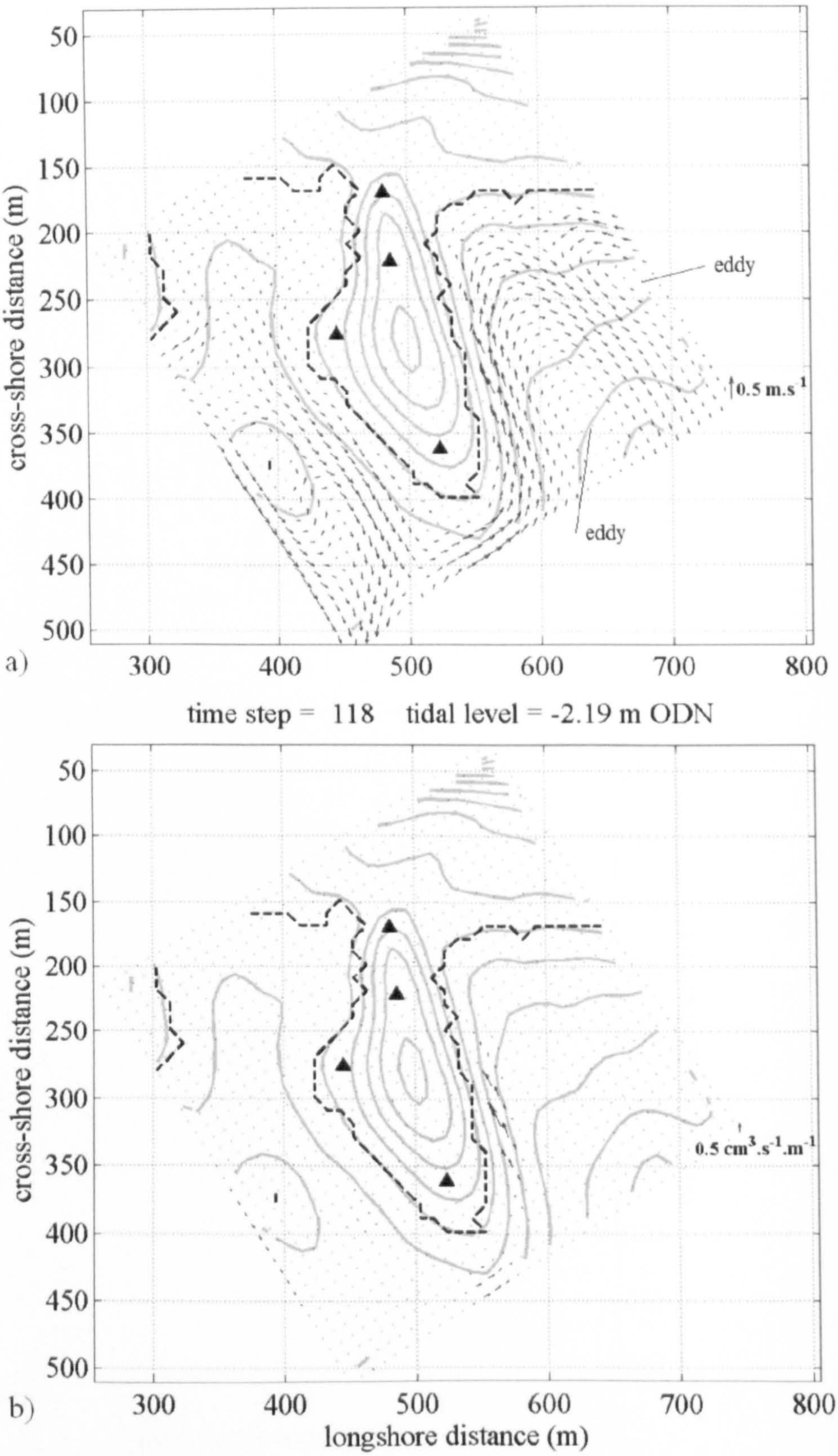

Figure 6.16: Simulated hydrodynamics and sedimentation in the vicinity of the offshore sandbank at Teignmouth for the 16th May, 2003. Time ≈ low tide: a) current strength and direction, b) sediment flux strength and direction. Black hatched lines indicate the shoreline position and black triangles indicate nearest grid point to the SLOT rig positions used in the fieldwork program. Reference vectors are plotted at the furthest right hand grid point position for scaling purposes.

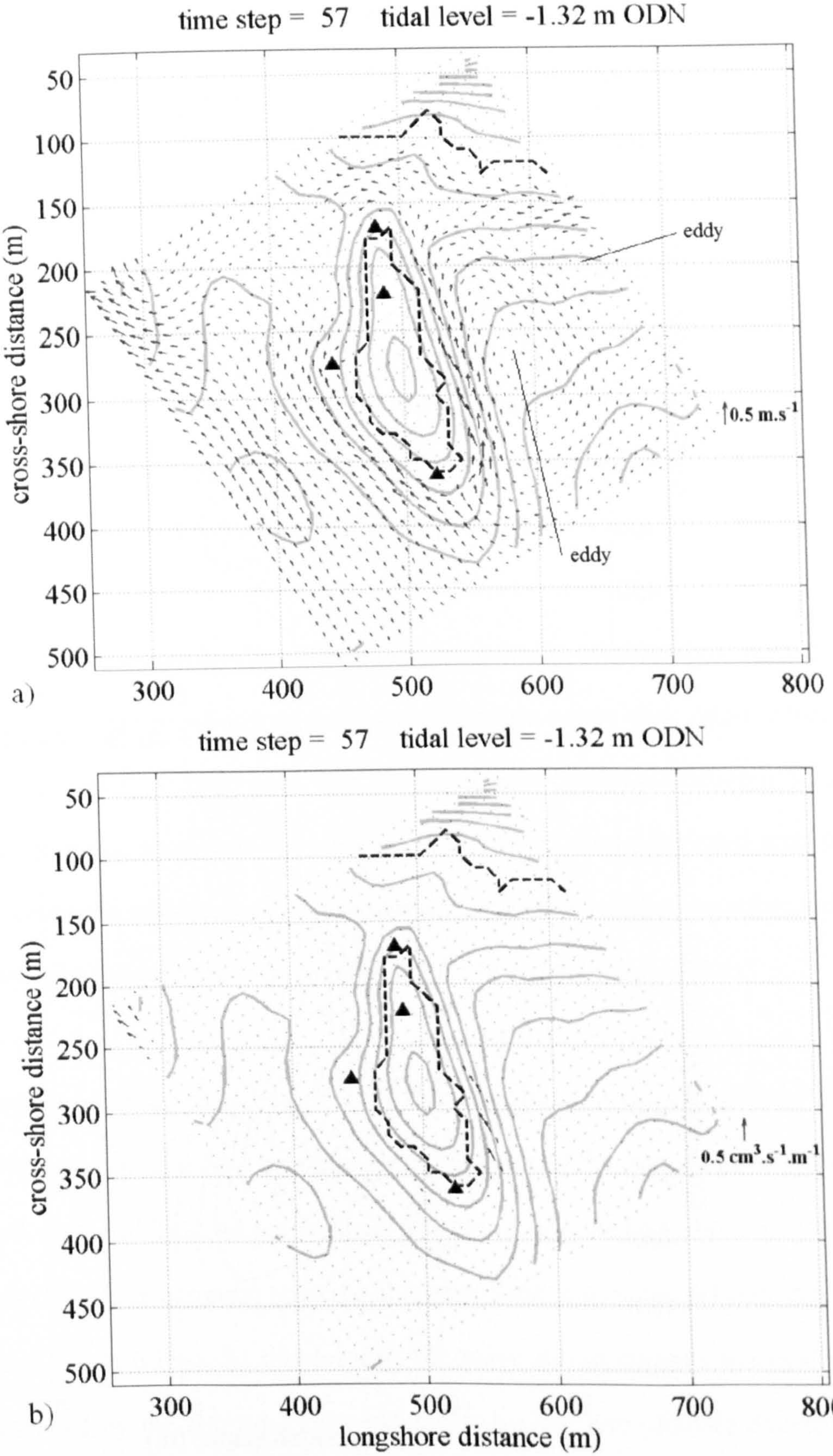

Figure 6.17: Simulated hydrodynamics and sedimentation in the vicinity of the offshore sandbank at Teignmouth for the 16th May, 2003. Time ≈ low tide +2 hours: a) current strength and direction, b) sediment flux strength and direction. Black hatched lines indicate the shoreline position and black triangles indicate nearest grid point to the SLOT rig positions used in the fieldwork program. Reference vectors are plotted at the furthest right hand grid point position for scaling purposes.

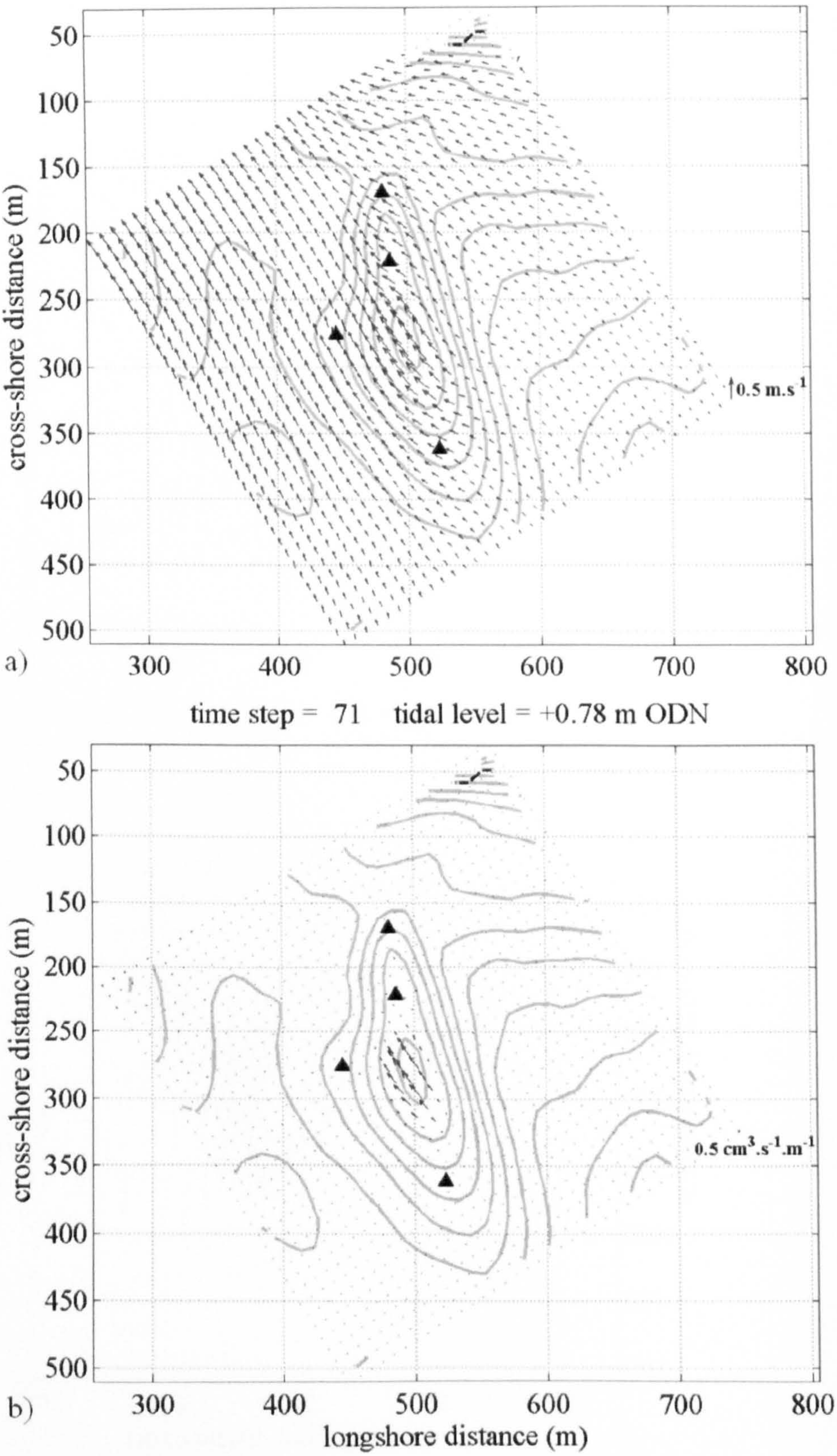

Figure 6.18: Simulated hydrodynamics and sedimentation in the vicinity of the offshore sandbank at Teignmouth for the 16th May, 2003. Time ≈ low tide +4 hours: a) current strength and direction, b) sediment flux strength and direction. Black hatched lines indicate the shoreline position and black triangles indicate the nearest grid point to the SLOT rig positions used in the fieldwork program. Reference vectors are plotted at the furthest right hand grid point position for scaling purposes.

Following mid ebb tide (Figure 6.14a) the sandbank is only just submerged and the depth to the crest has decreased ($h_{crest} < 0.5$ m) strong offshore directed currents $O(0.5$ m.s^{-1}) have developed to the south of the shoal and over Spratt Sand due to the fully developed ebb tidal currents issuing from the inlet entrance. This offshore directed tidal current regime weakens with distance from the inlet entrance until it becomes completely reversed by the strong onshore wave driven currents ($O(0.5$ m.s^{-1})) over the crest of the migrating shoal. Strong wave refraction particularly on the steeper northern flank focuses the wave energy over the shallow crest causing the onshore gradients in current strength to become locally enhanced.

At the shoreward extremity the onshore directed currents over the shoal are deflected to the east due to the proximity of the beach shoreline where they return offshore in a manner resembling a rip current. The reversing flow conditions between Spratt Sand and the migrating shoal, and the rip current-like circulation associated with the latter feature cause the formation of two temporary meso scale eddies on either side of the sandbank which have been marked in Figure 6.14a and subsequent plots.

The circulation observed in Figure 6.14a forms the basic circulation pattern throughout the ebb tide except that flow becomes segregated around the emerging sandbank. On the exposed southern flank of the offshore extremity, the onshore directed wave driven currents (longshore currents) breaking along the flank oppose the offshore directed tidal currents (Figure 6.15a). At this location the wave driven currents eventually become overwhelmed by the ebb tidal currents so that by low tide offshore directed currents dominate the southern flank (Figure 6.16a). This contrasts with the sandbank's northern flank which is subject to strong onshore directed wave driven currents throughout the ebb tide. At low tide the feature connects with the beach forming a transverse shore-

attached sandbank. The flow regime on the flood tide is similar except that onshore directed currents proliferate and the magnitude of those around (Figure 6.17a), and over (Figure 6.18a) the sandbank are stronger due to the additive flood tide component.

The small predicted sediment transport rates for the boundary conditions made scaling of the individual transport plots difficult. The data were plotted using Matlab's 'quiver' function which does not facilitate the scaling of vectors between different plots. Consequently, a single vector has been added to each of the vector plots to enable the relative scaling between different figures.

Under the low energy simulation the predicted synoptic scale sediment transport regime is relatively simple when compared with the hydrodynamics. There are two principle regions where sediment transport is predicted to occur through the tidal cycle and these were on the left of the plotted domain near the Spratt Sand bar and in the vicinity of the migrating shoal.

Initially under the high tide conditions there is no sediment transport evident in any part of the plotted domain (Figure 6.13b) since both the tidal and low energy wave driven currents are too weak to mobilise sediment. Shortly before mid tide (Figure 6.14b) the water depth has become sufficiently shallow for a zone of comparatively strong offshore sediment transport to develop close to the Spratt Sand bar on the left side of the plotted domain. At the same stage of tide a zone of onshore sediment transport has developed over the crest of the migrating sandbank ($h_{crest} < 0.5$ m). When the morphology becomes exposed with the ebbing tide (Figure 6.15b) this central zone of onshore directed sediment transport diverges creating gradients in sediment transport down the either flank. Relatively strong gradients occur on the northern flank where the slope of the

morphology is steeper. On the southern flank where the ebb tide currents oppose the wave driven currents the gradients in sediment transport are weaker and restricted to the outer portion of the flank. The zone of offshore directed transport close to Spratt Sand has moved further offshore which it brings it into close proximity to the southern flank of the offshore extremity. As the low tide is reached sediment transport becomes concentrated along the northern flank of the migrating sandbank (Figure 6.16b). On the flood tide the gradients in transport are maintained along the flanks of the sandbank (Figure 6.17b) until the feature becomes submerged which once more focuses the zone of transport over the crest (Figure 6.18b).

The marginal sediment transport conditions predicted by the model appear to reiterate the findings of the in-situ measurement chapter by demonstrating that low wave energy conditions can maintain morphological change between storms. The degree of transport is however marginal therefore when $H_s < 0.5$ m morphological change is expected to become negligible. The Teignmouth modelling experiments have also revealed that there is no appreciable littoral drift from the updrift beach therefore the addition of sediment to the system is unlikely unless there is particularly high fluvial discharge. In addition to this, the results suggest that there is a net export of sediment from the channel during the ebbing phase of the spring tide. This could be important to the migrating shoal since its close proximity means that it represents a potential source of new sediment to the sandbank when it is in mid term onshore migration and far removed from the terminal lobe accretion zone.

In the following section the relative importance of waves and tides to the cross-shore flow regime at the different SLOT rig deployment positions are investigated using the data from the present experiment. The longshore contribution has been omitted on the

basis that the hydrodynamics and sedimentation being studied are dominated by cross-shore flows in shallow water depths when sediment transport occurs (Section 5.61.1) and this is also evidenced by the lack of longshore growth of the migrating shoals during their evolution in the current inlet sedimentation mode (Section 4.4.2).

Key point summary:

1. Onshore directed sediment transport under low energy conditions occurs over the crest and along the flanks on the sandbank. No offshore directed transport was apparent.

2. In the shallow submerged state the gradients in sediment transport over the crest move surficial sediment from the crest toward the shoreward extremity

3. In the exposed state the zone of sediment transport is redirected along the flanks and particularly the northern flank which has a steeper slope.

4. In the absence of onshore directed transport on the flood tide, Spratt Sand appears to be a net offshore transporter of sediment under low wave energy conditions. This may therefore be a potential source of sediment to the feature during the mid term of the sandbank's onshore migration. The export of sediment will be accentuated during spring tides and large river discharge.

5 Under the low energy conditions the model predicts that there is no appreciable longshore transport of sediment between the shoreward extremity of the migrating sandbank and the beach shoreline.

6.4.2.3 Temporal variation in the relative importance of the wave driven and tidal components of the mean flow regime

In Figure 6.19 the total cross-shore current strength under the combined effects of waves and tide (black) is plotted with the tide (red) and wave (blue) driven components

at the four SLOT rig deployment positions. The wave driven component was computed from the difference between the model runs with both waves and tide, and tide only. The plotted cross-shore current component profiles have been annotated with the principle periods of wave (WD) and tide driven current dominance (TD). Since the data have been plotted using equivalent axes the different elevations of the various positions around the sandbank are reflected in the relative start and end points of the four times series and their respective lengths. It should be noted at this stage that the May 2003 sandbank was in the mid term of its onshore migration therefore the crest had accreted to approximately 0 m ODN. The four plots reveal that the interaction of the two current components becomes increasingly complex in shallower water depths but despite this complexity similar trends are observed. In the following paragraphs the key aspects of the cross-shore current variability are briefly summarised.

Flood tide

During the initial flood tide onshore directed wave driven currents dominate to some degree in the shallow water depths at all positions on the sandbank. The duration of the wave driven current dominance varies at the four positions due to their different elevations. The duration is longer at the offshore extremity and southern flank positions since they have lower elevations. At the central crest position which is approximately 2 m above the offshore extremity and southern flank positions submergence occurs over 2.5 hours later. By this time the tidal flow has gained momentum and the rate of change of the rising water level has increased. Consequently the tidal current strength increases more sharply after submergence and the duration of the shallow submerged state has shortened. This is also observed at the shoreward extremity except that there is an initial period where the currents due to both waves and tide remain negligible. Once the water the level has increased sufficiently the wave driven current due to the low energy

conditions is negligible and onshore directed tidal currents dominate over all areas of the sandbank.

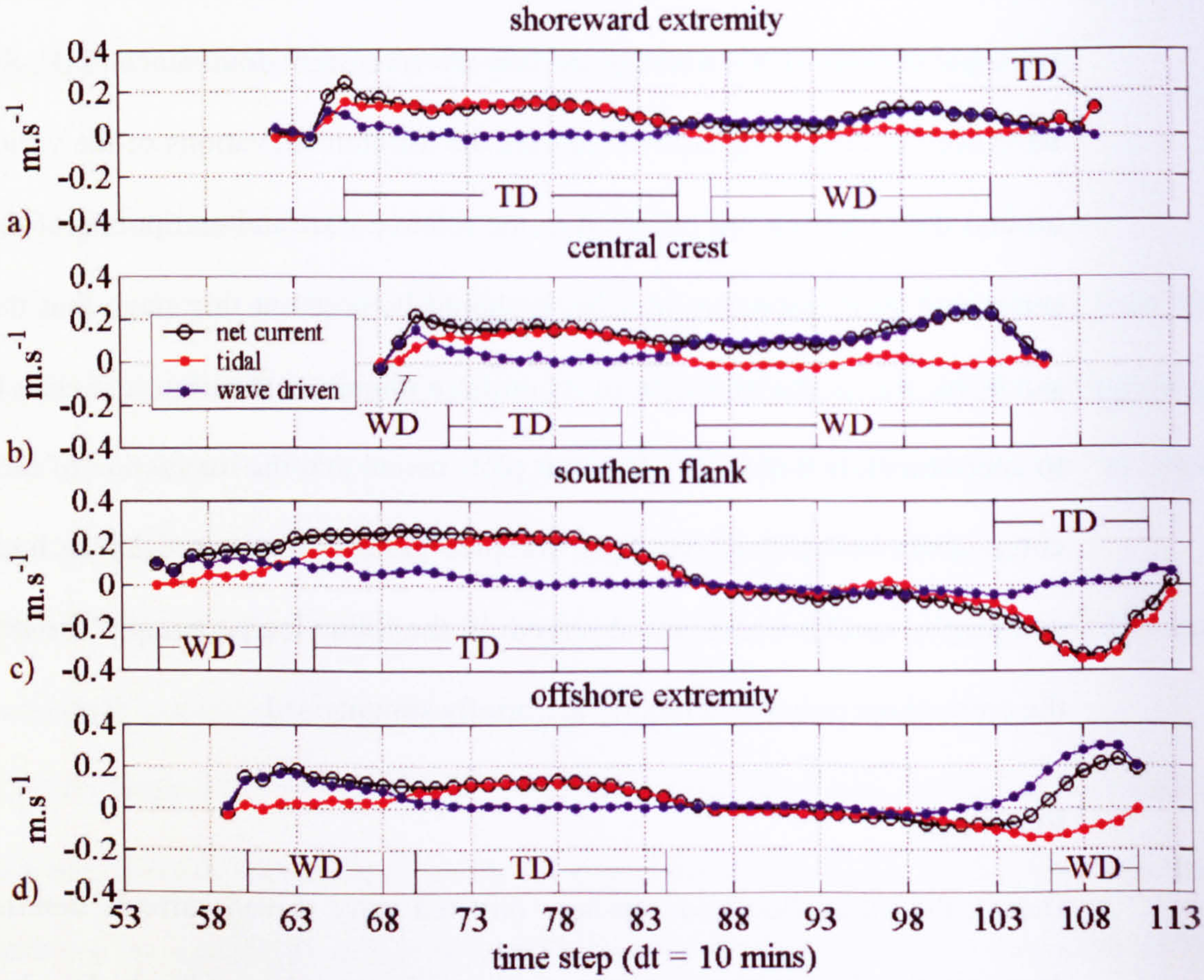

Figure 6.19: Comparison of modelled cross-shore current strength due to the combined effects of wave and tidally driven currents (black circles), the tide only (red circles), and waves only (blue circles) for the four SLOT rig deployment positions on the 16th May 2003: a) shoreward extremity (2A), b) central crest (1B), c) southern flank (2B), and d) offshore extremity (1A). Positive values denote onshore directed currents and *vice versa*. Abbreviation key: WD denotes wave dominance and TD denotes tidal dominance.

Ebb tide

At the offshore extremity and southern flank positions both the tidal and wave driven components of the cross-shore current are negligible during the initial stage of the ebb tide when the water depth is relatively deep (h = 3 to 4 m). In contrast to this the model predicts that there is a weak ($\approx$ 0.1 m.s^{-1}) onshore directed wave driven component to the depth averaged flow at the shallower central crest and shoreward extremity positions shortly after the tide begins to ebb and this persists through most of the ebb tide. As the tide ebbs further and conditions become relatively shallow over the sandbank the wave

driven current component at the central crest position increases and peaks first as the wave shoaling and breaking processes take effect. A similar wave driven cross-shore current dominance is later observed at the offshore extremity though the strength is diminished by the presence of an offshore directed tidal current. In the shallow emerged state the southern flank which is closest to the inlet channel is dominated by relatively strong offshore directed tidal currents.

Key point summary:

1. The meso to macro tidal regime imposes a temporal constraint on the residence times of the hydrodynamic processes and this also varies depending on vertical position within the sandbank's morphology. For the case where the sandbank crest is positioned at around MSL, the upper portions of the feature are exposed to shorter residence times than lower portions due to the differential rate of change in the tidal water level.

2. When the water depth is relatively shallow ($h \leq h_b$) on the flood tide, wave driven onshore directed currents dominate over all parts of the sandbank. Under similar ebb tide conditions, wave driven currents only dominate over the central crest and offshore extremity positions. The southern flank position is dominated by offshore directed tidal currents in shallow water due to its close proximity to the main channel.

6.5 General summary

The numerical modelling experiments were undertaken with the objective of trying to determine the mechanism for sandbank elongation and to verify that the tidally driven mean flow component was relatively unimportant to the physical processes that drive the onshore migration of ebb tidal delta sandbanks at Teignmouth.

In Section 6.4.2.3 it was determined that the cross-shore flow regime over the May 2003 sandbank was dominated by wave driven onshore directed mean flows. These occur in shallow water depths where they drive the gradients in sediment transport which result in the observed morphodynamic behaviour at Teignmouth. Offshore directed tidal currents were predicted to occur on the sandbank particularly on the southern flank but they are typically weak and ephemeral. Consequently they are not considered to be a significant factor in the evolution of the sandbanks though this may not be the case on the southern flank when extreme river discharge events coincide with spring tides. Tidal currents were however predicted to transport sediment offshore in the vicinity of Spratt Sand when it is in the shallow submerged state under spring tide conditions. This morphological feature was therefore identified as a potential net exporter of sediment to the terminal lobe region which may also have an important impact on sandbanks that are in the mid term of their onshore migration. The reason for this is that the transport pathway passes close to the sandbank therefore sediment may become advected into the shoal sedimentation system. Consequently this may represent a potential mechanism for the addition of sediment to the shoal budget long after the feature has become distant from the main accretion zone at the distal end of the inlet channel. A net offshore transport over a channel marginal bar is contrary to the findings of authors who have studied ebb tidal delta shoals in micro tidal settings (e.g. Hubbard, Oertel and Nummedal, 1979; Dean and Walton, 1973). This therefore suggests that the process may only be common to tidal inlet inlets with macro scale tidal regimes. A final point of note regarding the results of the Teignmouth modelling experiments was that negligible longshore sediment transport toward the inlet entrance was predicted to occur under low energy conditions. This infers that little sediment is returned to the main channel for transportation offshore to the terminal lobe, therefore in the absence of extreme river discharge events low energy conditions are associated with low sediment availability.

The results of the idealised modelling experiments were particularly useful with respect to the identification of the potential mechanism for sandbank elongation at Teignmouth. In Section 6.3.2.1 it was determined that there is a dichotomy in the patterns of erosion and deposition between the submerged and exposed states of the sandbank and particularly in the case of the broader circular morphology. When meso to macro scale water level change was introduced to the modelling experiments the divergent patterns of deposition were predicted to provide the potential mechanism for broadening in the longshore dimension under high energy conditions (Section 6.3.2.3). The effect was accompanied by an elevation increase and the combined morphological response was attributed to the longer residence times of the high and low states of the tide. In contrast to this low energy conditions were predicted to promote elongation under dominant spatial gradients in sediment transport when the sandbank is in the shallow submerged state. These promote elongation by mobilising and transporting surficial sediment from the top of the sandbank which when transported to the shoreward extremity promotes elongation. Under higher states of tide the low energy wave driven currents are too weak to maintain the gradients in transport over the feature therefore there exists a temporal constraint or bias on morphological change towards the lower states of tide.

The numerical modelling experiments have contributed significantly to the present study by revealing the spatial and temporal variation in the physical processes that govern the evolution of ebb tidal delta sandbanks. These results have led to the formulation of a set of hypotheses that are subsequently used to formulate a conceptual model in the following chapter. The hypotheses state that sandbanks with relatively deep crests (h_{crest} >> MSL) will undergo preferential shoreward elongation under prevailing conditions of low energy waves and meso to macro tidal water level variation. Additionally, sandbanks that occur under high sediment availability

conditions are likely to accrete more and therefore have higher elevations (h_{crest} > MSL) and as a consequence, they are more likely to broaden particularly under higher energy wave conditions.

7 Discussion and Synthesis

7.1 Primary physical controls on the short to medium term shoal morphodynamics

On time scales of weeks the average migration rate was found to have a linear dependency on the wave forcing through its correlation with H_s/h (Section 4.4.3.2) emphasising the dependency on the shoal crest depth (h). This parameter is important in that it influences when wave breaking occurs and its intensity during the submerged and exposed stages of the tidal cycle. Further evidence of the linear relationship between the sandbank's COM migration rate and the wave forcing over shorter time scales was determined from work undertaken by the author for the International Conference on Coastal Engineering at Lisbon, Portugal in 2004 (Aird *et al.*, 2005). In this study it was established that a net 42 m onshore migration of the event 3 sandbank during April 2003 was in direct response to the wave forcing. When a linear regression between the migration rate and wave energy between was performed the correlation was statistically significant ($R^2 = 0.9$). The wave forcing generated an average migration rate of 1.4 $m.day^{-1}$ for that month which was attributed to a sequence of elevated wave energy periods. This contrasted strongly with the following month in which there was only one appreciable wave energy wave event albeit of lower intensity than in the previous month. This had the effect of reducing the net onshore migration distance for a comparable period to just 8 m (Figure 3 and Table 2, Appendix A3).

The in-situ measurement (Section 5.6) and deterministic numerical modelling analyses (Section 6.5) showed that sediment transport under low wave energy conditions is confined to the shallow surf zone region where the residence time of the causative mean wave driven flows due to shoaling and breaking processes over the migrating sandbank are controlled by the water level variation due to the astronomic tide. When the shoal is

under the influence of wave energy the chronology of wave driven sediment transport processes has previously been found to be strongly modulated at semi-diurnal frequencies by the tidal water level variation (Bird *et al.*, 2001) and to a lesser extent at fortnightly frequencies by the variation due to the spring-neap cycle (Bernardes, 2005). These findings were also reflected in the results of the idealised experiments of the present study. The semi-diurnal modulation of the residence times of the sediment transport processes by the water level variation has been shown to be of primary importance to the sedimentation of the migrating shoal, whereas the spring-neap tidal variation affects the residence times (Section 6.3.2). However, the semi-diurnal water level variation is still of secondary importance to wave energy since without the waves the rate of morphological change would be negligible. The importance of the semi-diurnal tides stems from the meso to macro scale vertical change in water level over each tidal cycle which exerts a significant temporal constraint on the wave driven sediment transport processes. Under the prevailing low energy conditions this creates a bias towards the processes that occur at lower states of tide. In the inlet's current mode the crest of the sandbanks after genesis are typically deep in relation to mean sea level and this has been shown to promote shoreward elongation under low energy conditions (Section 6.3.2.3). The effect of tidal currents on the migrating sandbanks was predicted to be negligible (Section 6.4.2.3).

From the in-situ measurement analyses it was determined that the primary wave driven processes controlling sediment transport on and around the sandbank are the wave orbital motions which stir sediment into suspension, and the wave driven near bed mean flows that transport the suspended sediment and bed load around the shoal (Section 5.6). Under the wind sea conditions of the May 2003 fieldwork short wave stirring was the primary mechanism for sediment suspension in the surf zone whilst that due to long

waves played a secondary role. Short wave velocity skewness was found to make a tertiary contribution to the onshore directed sediment transport over the sandbank and this increased with distance offshore (Section 5.6.4). During the May 2003 Coastview fieldwork program the Teign inlet initially experienced near calm conditions followed by low energy wave conditions and no high energy conditions occurred (Section 5.5). Consequently, the estimated maximum net suspended transport rates for the main fieldwork wave event were relatively small (depth averaged transport flux maximum ≈ 0.9 $gm.s^{-1}.m^{-1}$) with the highest rates occurring on the flood tide as opposed to the ebb tide (Sections 5.6.3 and 6.4.2.2). This transport was predominantly onshore directed and despite the small magnitude of the estimated transport rates, the resultant transport due to the combined bed load and suspended sediment was significant since it was capable of initiating sufficient accretion at the shoreward extremity to bury sensor heads on the SLOT rig (Figure 5.14). By comparison, the estimated net transport rates for the near calm period preceding the low wave energy event (data not presented) showed that suspension still occurred to some extent on the flooding tide but the transport was not sustained, and suspension and transport was entirely absent on the ebb tide.

The described change in computed transport rates from negligible quantities to the more substantive quantities between the near calm and low wave energy states, infers that a threshold energy level for morphological change was exceeded. During times when the feature is subject to persistent near calm conditions for example in June and July, the negligible transport will cause the feature to be moribund. Conversely, under higher wave energy levels ($H_s \geq 0.5$ m) the flow regime is capable of mobilising and transporting sufficient concentrations of surficial sediments to initiate shoreward migration of the shoal with the distance traversed being directly proportional to the ratio of H_s/h. In-situ measurements on the mid term migrating shoal under large wave

conditions were not available but the same physical processes increase the intensity of onshore transport over the sandbank which has been shown to increase the rate of morphological change (Siegle, 2003). The high energy waves generate higher orbital velocities and depth of penetration (larger orbital radius of motion) which increase wave stirring hence there is greater sediment mobilisation and to greater depths. This sediment is subsequently transported onshore by the stronger mean flows.

The results of the idealised modelling experiment that simulated the effects of meso to macro scale water level variation showed that the morphological response was governed by two factors (Section 6.3.2.3). Firstly, the residence times of the wave driven sediment transport processes govern the duration of exposure to the hydrodynamic processes responsible for the sediment transport over and around the sandbank. Secondly, the level of wave energy determines the depth to which the gradients in transport can be maintained. Under high energy waves the longer residence times of the lower and higher states of the tide caused the sandbank morphology to undergo preferential broadening in the longshore dimension and increased crest elevation (Figure 6.9). The broadening response is caused by sediment deposition in two side lobes at the lower states when the sandbank is exposed. During higher states of tide when the sandbank is submerged the more energetic waves are capable of maintaining the gradients in sediment transport in deeper water. The eroded sediment is deposited over a central area causing the elevation to increase. Under low wave energy conditions the principle differences are that sediment transport is restricted to the lower states of tide and is dominated by the gradients created under the shallow submerged state. This promotes the observed shoreward elongation as surficial shoal sediment is eroded from the upper shoal surfaces and transported to the shoreward extremity.

Potential evidence of the erosion of deeper sediments from the offshore extremity under elevated wave energy levels and its subsequent deposition on a shoreward central portion may be in evidence when the cross-shore section through the approximate shoal centre line as presented in Figure 4.6 is considered in conjunction with the wave height time series for the weeks preceding the survey date (Figure 3, Aird *et al.*, 2004, Appendix A3). The cross-section which was derived from the May 2003 Coastview bathymetric survey shows an accretion of sediment (bulge) on the central region shoreward of the offshore extremity as described above. If the wave record for the 4 week period immediately prior to this is scrutinised, it can be seen that it was punctuated by a succession of elevated wave energy events in which H_{max} frequently exceeded 1.0 m. However, in the absence of high resolution survey data it is not possible to verify whether this deposition resulted from the episodic occurrence of higher energy waves. Additionally, if the crest depth time series in Figure 4.22 are studied in conjunction with the wave height time series for the each event (Section 4.4.2) then one might expect to observe periods of crest elevation increases more frequently during the winter months but this is not apparent. A potential explanation for this is that this morphological response (elevation increase) was elicited whilst using a circular morphology. In the inlet's current mode the sandbank morphologies after genesis are typically more rotund with the smallest aspect ratios compared with the other stages in their evolution (Figure 4.24c). Subsequently, the sandbanks rapidly become elongate and transversely orientated which results in their sediment transport patterns becoming constrained in the longshore dimension. Consequently, the steeper gradients on the flanks generate greater refraction and focussing of the wave energy over the submerged crest. This increases the onshore gradients in transport over the crest thereby reducing the potential for accretion on top of the features.

7.2 Refraction, diffraction and sheltering effects

Wave refraction around shoals and the focussing effect of their geometry has been shown to enhance transport over and around the shoal during the submerged and emerged states. The wave refraction induced by the sandbank morphologies is sufficiently strong to minimise the effect of variable wave direction. Consequently, the gradients in sediment transport are always strongest in the cross-shore dimension therefore shoreward migration is currently the prevailing mode of morphological change. West (2002) showed that for optimum refraction and wave focussing a reef needs to be longer (cross-shore dimension) than it is wide (longshore dimension) and should have a small elevation in relation to the horizontal dimensions. In the inlets current mode the geometry of the migrating sandbanks often meets these criteria during their evolution. For example they have typical elevations 2 to 4 orders of magnitude smaller than their typical horizontal dimensions, and elongate aspect ratios that are often 2 to 4 times longer in the cross-shore dimension than they in the longshore dimension (Figure 4.24c).

Once the sandbanks have migrated away from the terminal lobe accretion zone the wave driven sediment transport processes then become influenced by the wave diffraction and sheltering effects caused by the genesis of new offshore sandbanks that form on the terminal lobe. This usually coincides with the third stage of the morphodynamic evolution which is when the sandbanks have become shore-attached. This stage in their evolution is characterised by low migration rates that fluctuate close to zero. This is a function of two factors. Firstly, due to the fact that the shore-attached sandbanks are in effect anchored at the shoreward extremity, the migration rate of their COM is less dynamic due to them being largely determined by the on or offshore movements of the offshore extremity. Secondly, shore-attached sandbanks are also sheltered by the

presence of new offshore sandbanks that undergo genesis on the terminal lobe contemporaneously with the dissipation of the shore-attached features.

Wave refraction on the sandbanks and the sheltering effects of the ebb tidal delta and Ness headland are also important since they create alongshore gradients in the wave energy incident upon the adjacent shoreline. This is caused by the less proximal parts of the shoreline being more exposed to wave energy whilst those in the lee of the shoals are subject to varying degrees sheltering (Section 2.2). The degree of sheltering typically varies depending on wave direction which can initiate temporary reversals in the longshore transport that controls the nearshore supply of sediment to the ebb tidal delta. Furthermore, if these changes become more frequent over inter-annual time scales then this can lead to long term trends in the patterns of erosion and deposition. These are manifest by changes in the volume of the ebb tidal delta and morphology of individual shoals in response to changing channel hydraulics. Previous studies of the Teign inlet suggest that it is undergoing morphological change on inter-annual time scales (Bernardes, 2005, Kingston *et al.*, 2005) and this may be in evidence from the combined 35 year image archive of the Teign inlet used in the present study. In the period between 1976 and *c.*1990 one of the primary modes of the cyclic morphodynamics involved the genesis of large shore-parallel swathes of sand that extended northwards from the distal portion of the channel adjacent to the Ness headland (Ness Pole) (Section 4.4.2). Consequently, the major axes of the sandbanks that were released from the terminal lobe were often larger in the longshore dimension than in the cross-shore dimension. This behaviour does not typify the morphodynamic behaviour of the ebb tidal sandbanks in the inlet's present mode which may be indicative of long term changes to the ebb tidal delta volume. Similarly, the trends of decreasing sandbank area (Figure 4.24) and crest elevation (Figure 4.21) for the period

between 1999 and 2005 (Argus archive), could also be symptomatic of these long term changes. The mechanisms for ebb tidal delta volume change relate to changes in the littoral and fluvial supply of sediment to the inlet and a proposed explanation for this is presented in the following section.

7.3 Long term trends in the morphological evolution of the ebb tidal delta and landward migrating sandbanks

7.3.1 Seasonal trends (lower macro time scale)

The morphodynamic cycle of the Teign inlet ebb tidal delta was characterised by a three stage evolution which begins with the genesis of the sandbanks on the terminal lobe (stage 1). This is followed by landward migration and elongation in the cross-shore dimension (stage 2) which leads to shore-attachment and dissipation (stage 3) (Section 4.4.3.1). A three stage evolution was also manifest in the smoothed and interpolated migration rate time series (Figure 4.15), hereafter termed the average migration rate (S1 to S3) (Section 4.4.3.2). Following genesis there is a decelerating trend (S1) in the migration rate time series for events 2 to 4 (Figure 4.15b to d). The average migration rate of the COM then undergoes a period of acceleration and deceleration (S2) which creates a 'bulge' in the time series. This stage results in the sandbanks becoming shore-attached, after which the migration rate fluctuates close to zero as the offshore extremity is eroded (S3).This three stage evolution of the average migration rate time series is largely attributed to the seasonality in wave energy levels but it may also be a function of increasing sub-aerial exposure with proximity to the shoreline (Section 2.2.1). The seasonality in wave energy is evident in the ensemble histogram of average H_s that was compiled from the raw wave data from the pier mounted pressure transducer (Figure 7.1). This seasonality involves negligible wave energy levels in June and July (monthly

average $H_s \approx 0.1$ m), which increases to maximum levels in December and January (monthly average $H_s \approx 0.3$ m) before decreasing through spring.

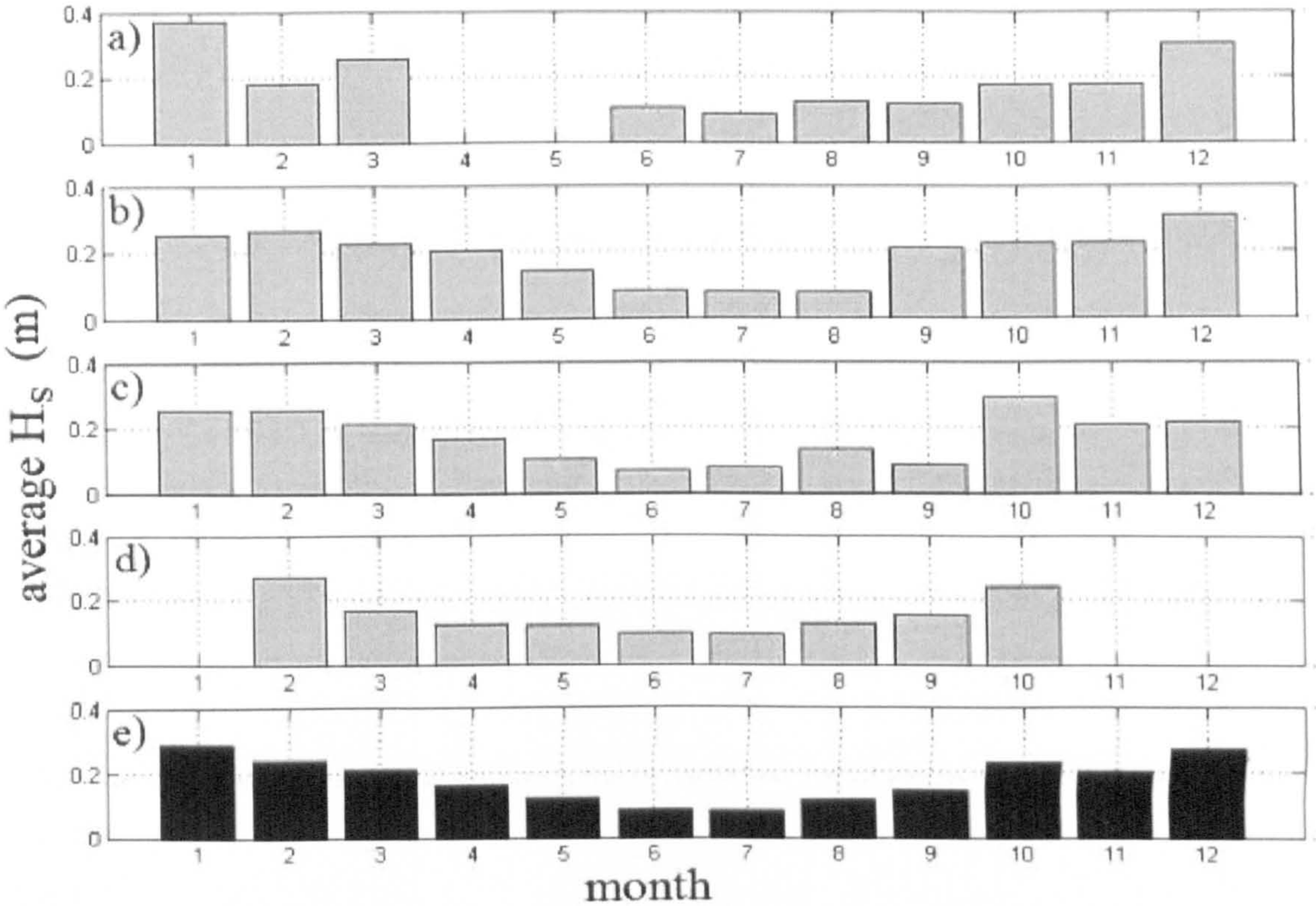

Figure 7.1: Histogram of monthly average significant wave height compiled from hourly pier-mounted pressure transducer data for a) event 1, b) event 2, c) event 3, d) event 4, and e) ensemble average.

The genesis of the offshore sandbanks in events 2 to 4 (S1) occurred in the energetic winter months when sediment is episodically input into the system via littoral drift and high river discharge events. The greater frequency of higher energy wave events ($H_s >$ 1.0 m) in winter causes the new offshore sandbanks to be relatively dynamic from the outset. As the season progresses towards the less energetic summer months and the shoreward migrating sandbanks become increasingly exposed during the tidal cycle the smoothed and interpolated migration rate gradually decreases (Figure 4.19). The migration rates reach minimum values June and July which is the least energetic period of the year. Subsequently, the sandbanks appear to undergo a relatively short period of acceleration then deceleration which causes a bulge in the time series (S2). The period of acceleration coincides with the onset of higher wave energy levels in autumn and

winter therefore the acceleration stage is attributed to increased wave energy levels. The subsequent deceleration period is considered to be a function the sandbanks becoming shore-attached which inhibits the dynamic of the COM as the migration rate largely becomes a function of the erosion or accretion of the offshore extremity. The last stage (S3) begins when the deceleration ceases and is characterised by a fluctuating migration rate that is close to zero. The decreased dynamic of the shore-attached dissipation stage is primarily attributed to the sheltering effects of the new offshore sandbank and the decreased residence times of the wave driven processes. At this stage in their evolution the offshore extremities of the sandbanks are high on the inter-tidal terrace and they are therefore exposed to wave driven transport processes for less time. Additionally, when wave energy is present, longshore transport processes become increasingly important with proximity to the shoreline and this may also account for the decreased cross-shore dynamic of the sandbanks whilst are being dissipated.

Event 1 was the only event in which coalescence occurred and this is considered to be due to the timing of the sandbank's genesis on the terminal lobe. Genesis for this event occurred comparatively early in August. This suggests the sandbank was either a relict feature from the previous winter season or that the wave energy levels in the summer-autumn months of 1999 generated high sediment availability conditions. Wave data are not available for the summer months of 1999 but the wave energy levels in this season are typically low (Figure 7.1). The wave energy levels through autumn were also low and only increased significantly in November (Figure 4.10). This fact favours the relict feature theory whereby the sandbank had begun accreting early in 1999 but the accretion was insufficient to cause it to be properly exposed it prior to the onset of summer. This is substantiated by the Argus video image archive in which the flanks of the horseshoe-shaped sandbank can be seen during the summer (Figure 7.2). The

sandbank lay in a moribund state through the summer and then quickly accreted when wave energy levels increased in autumn and this exposed it to the wave driven sediment transport processes causing it to begin its landward migration. Consequently, elevated wave energy levels and high sediment availability conditions through the winter of 1999-2000 caused the genesis of the next sandbank on the terminal lobe. This new sandbank was able to catch up and coalesce with the former sandbank due to sheltering effects of the outer sandbank on the inner feature.

Figure 7.2: Camera 4 image showing the relict sandbank on the terminal lobe on the 14th May, 1999.

7.3.2 Supra-annual trends (upper macro time scale)

The study by Robinson, (1975) indicated that the periodicity of the primary morphodynamic cycle was 3 to 5 years for the observation period from 1964 to 1974. The historic image archive taken by S Hook from the Ness headland over the period 1976 to 1990 were also used to determine the morphodynamic periodicity which was

estimated at 1 to 2 years (Section 3.4). This is similar to the estimated 1.5 to 2.5 year periodicities of the events analysed in the present study but it should be reiterated that the Argus video image-derived estimates were based on a subjective approach to genesis identification which means that the duration of each migration event might be longer depending on how genesis is defined. If the variability in the Teign inlet morphodynamic cycle from 1964 to 2004 are considered together then there appears to be evidence of long term changes (supra-annual) to the cycle periodicity and these appear to correlate with trends in the North Atlantic Oscillation (NAO) index which has been studied by Hurrell *et al.* (2003) (Figure 7.3). This is a measure of the winter sea level pressure differential between Portugal and Iceland and it is used to characterise the variability in the strength of the westerly winds.

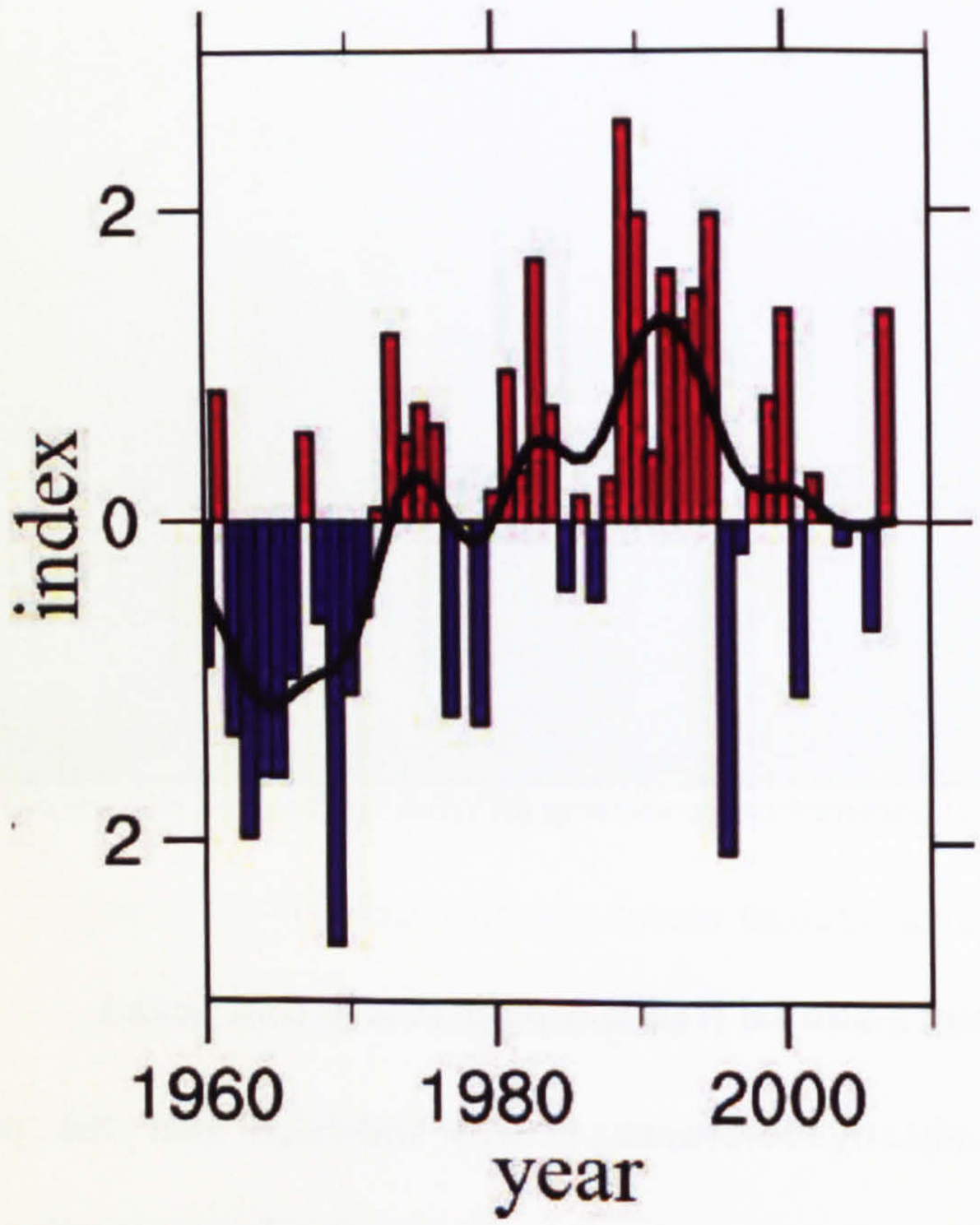

Figure 7.3: Index of the boreal winter (December-March) mean NAO constructed as the difference in sea level pressure between Lisbon, Portugal and Stykkisholmur/Reykjavik, Iceland from 1960 to 2007. The black line represents the index smoothed to remove fluctuations with periods less than 4 years (modified from Hurrell *et al.*, 2003).

The index used in the study by Hurrell *et al.* (2003) is based on the winter pressure differential when annual wave energy levels are at their maximum at Teignmouth. Westerly winds largely control the level of wave energy on west facing sections of the U.K. coastline that are exposed to the Atlantic Ocean. High positive NAO indexes are predicted to increase the incidence of storms but since the Teign inlet is sheltered from Atlantic Ocean swells it is not expected to be influenced by NAO index. The sensitivity of Lyme Bay to the NAO index was briefly cited in a report by the Department for Environment, Food and Rural Affairs (2005) which stated that 13% of the variance in the location's significant wave height can be explained by the variability in the NAO index. This is reflected graphically in Figure 7.4 in which the sensitivity of the winter monthly mean significant wave height in Lyme Bay is in the range 0.1 to 0.2 m per unit of index.

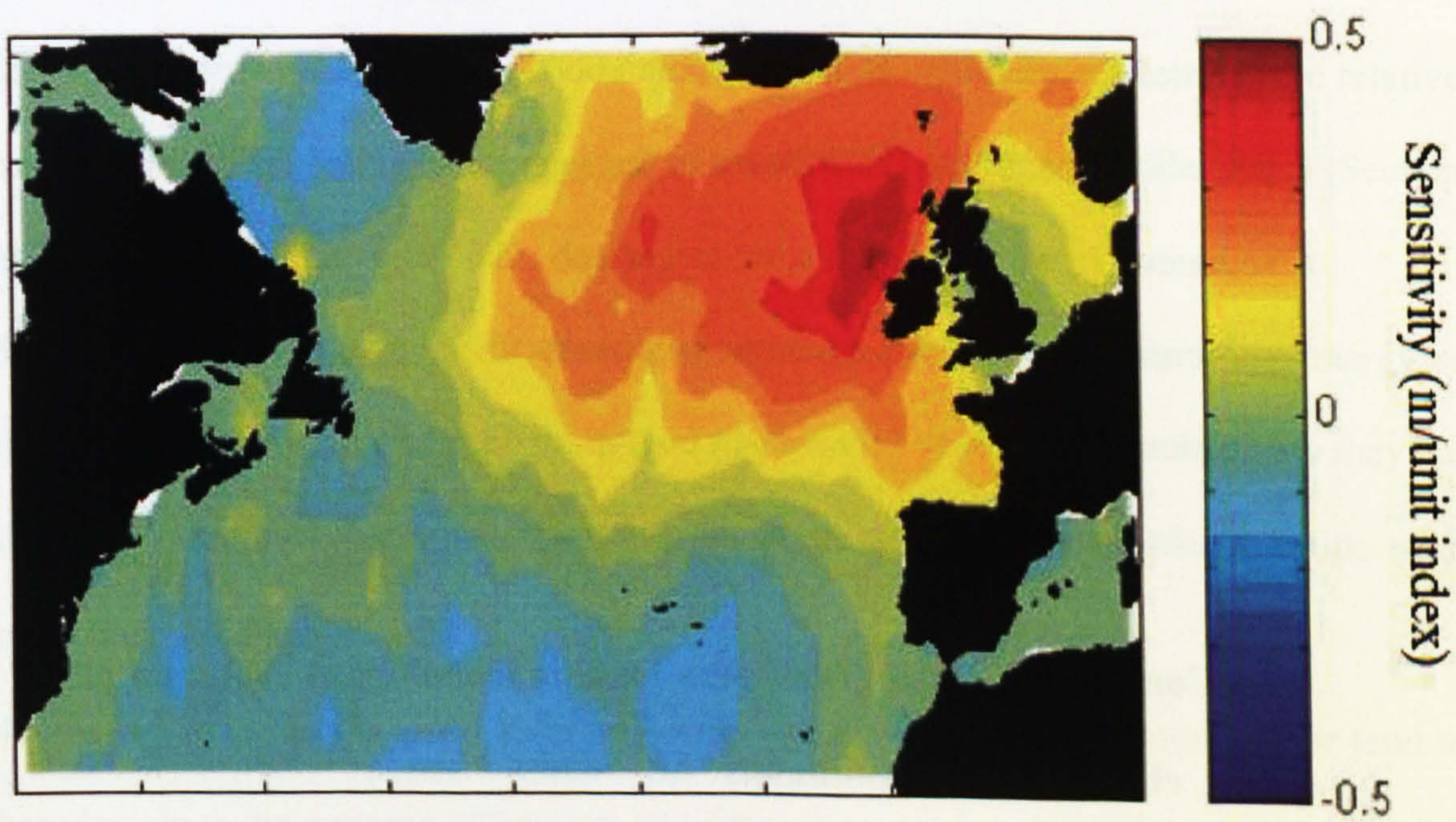

Figure 7.4: Sensitivity of winter monthly mean significant wave height to NAO around northern Europe (Image supplied to the Department for the Environment, Food and Rural Affairs courtesy of David Woolf, National Oceanographic Centre, Southampton).

In terms of the present study the evidence in support of this is summarised as follows:

1964-1974: high negative index with a decreasing trend which coincides with a relatively long cycle periodicity (≥ 3 years).

1975-1990: increasingly positive index that peaks c.1990 which is coincident with the minimum cycle periodicity (0.9 to 2.3 years, mean periodicity = 1.8 years).

1999-2005: decreasing positive index which is coincident with an increasing periodicity (+1.1 to +2.6 years, mean periodicity = +1.6 years).

For the last time period between 1999 and 2005 the positive sign in front of each figure denotes the fact that they are minimum estimates based on the subjective interpretation of when genesis occurred. The identified trends infer that there is an inverse linear relationship with the NAO index whereby a high positive index is coincident with short cycle periodicity and *vice versa*. It is proposed that the system is responding to fluctuations in the ebb tidal delta volume that are a function of wave energy levels and sediment availability. Higher volume ebb tidal deltas are associated with slower cycle periodicities and this is attributed to the migrating sandbanks having greater volumes of sediment. In addition to this, on larger ebb tidal deltas there are typically greater cross-shore distances for the dynamic sandbanks to traverse in order to reach the shoreline (Section 2.3).

7.4 Conceptual model of the plan form morphological evolution of the Teign inlet ebb tidal delta sandbanks

Based on the synthesis of the combined video, in-situ measurement and modelling analyses a conceptual model is proposed. The conceptual model accounts for the observed medium term (months) plan form evolution of the sandbanks from genesis to shore-attachment for the current morphologic mode of the Teign inlet. The results of the

analyses undertaken in the present study have shown that the shoal evolution is primarily controlled by the following key parameters:

1. The chronology of the wave energy level.

2. The relationship between the shoal crest depth and tidal water level variation.

3. The shoal geometry which governs the degree wave of refraction and focussing.

4. The variable level of sediment supply to the ebb tidal delta (sediment availability).

The key concepts relating to these parameters that are applied in the model are as follows:

1. Wave energy transports shoal sediment onshore and deposits it in a laterally constrained region of the shoreward extremity (Sections 5.6 and 6.3.2).

2. The response of the shoal plan form geometry is governed by the ratio of the relative longshore length scales of the regions of erosion (EL) and deposition (DL) (Section 6.3.2).

3. Deeper crests (h_{crest} >> MSL) undergo preferential elongation under wave energy as the patterns of erosion and deposition tend toward the submerged case in which they are the most laterally constrained, This process is most pronounced under low tide neap conditions (Section 6.3.2.3).

4. Shallower crests (h_{crest} > MSL) will tend to maintain similar proportions or tend to broaden since the patterns of erosion and deposition are less laterally constrained. This process is most effective under high energy conditions (Section 6.4.2.2).

5. The volume of sediment in the migrating shoals is primarily a function of the long term (supra-annual) evolution of the ebb tidal delta which is dependant on sediment availability (Sections 2.3, 3.4 and 7.3.2).

Together these factors govern the vertical (crest accretion and erosion) and lateral (onshore migration and elongation) redistribution of shoal sediment and therefore they control the morphodynamic evolution of the sandbanks. These five key concepts have been developed throughout the thesis and provide the framework for the conceptual model which is encapsulated in a schematic diagram in Figure 7.5. In the Teign inlet's current morphologic mode the onshore migration of sandbanks on the ebb tidal delta is characterised by two typical plan form geometries which are either horseshoe-shaped (crescentic), e.g. event 1 sandbank at genesis, or elongate and transversely orientated. The proposed conceptual model accounts for this morphologic behaviour based on the relationship between shoal elevation (crest depth) and mean sea level.

Time is represented on the vertical scale and the uppermost section denotes the sandbank just prior to the time when it has accreted sufficiently to be affected by the wave energy (shoal under genesis). Once the sandbank has accreted sufficiently and wave energy has begun to act on the shoal surfaces the patterns of erosion and deposition will control the features morphological evolution. The left hand transition from genesis (PG1) to the first post genesis phase represent low sediment availability which is primarily due to low littoral drift conditions ($Q_{IN} > Q_{OUT}$). This causes the shoal elevation to remain relatively deep after genesis ($h_{crest} >>$ MSL) hence the patterns of erosion and deposition will tend to the submerged state case. This is where the patterns of deposition are constrained in the longshore dimension and the length scale of the region of deposition (D_L) is less than that of the region of erosion (E_L) which promotes shoreward elongation. The right had transition (PG2) represents high sediment availability conditions which causes the sandbank to have a higher crest elevation at genesis ($h_{crest} >$ MSL) and the patterns of erosion and deposition tend to the exposed state case.

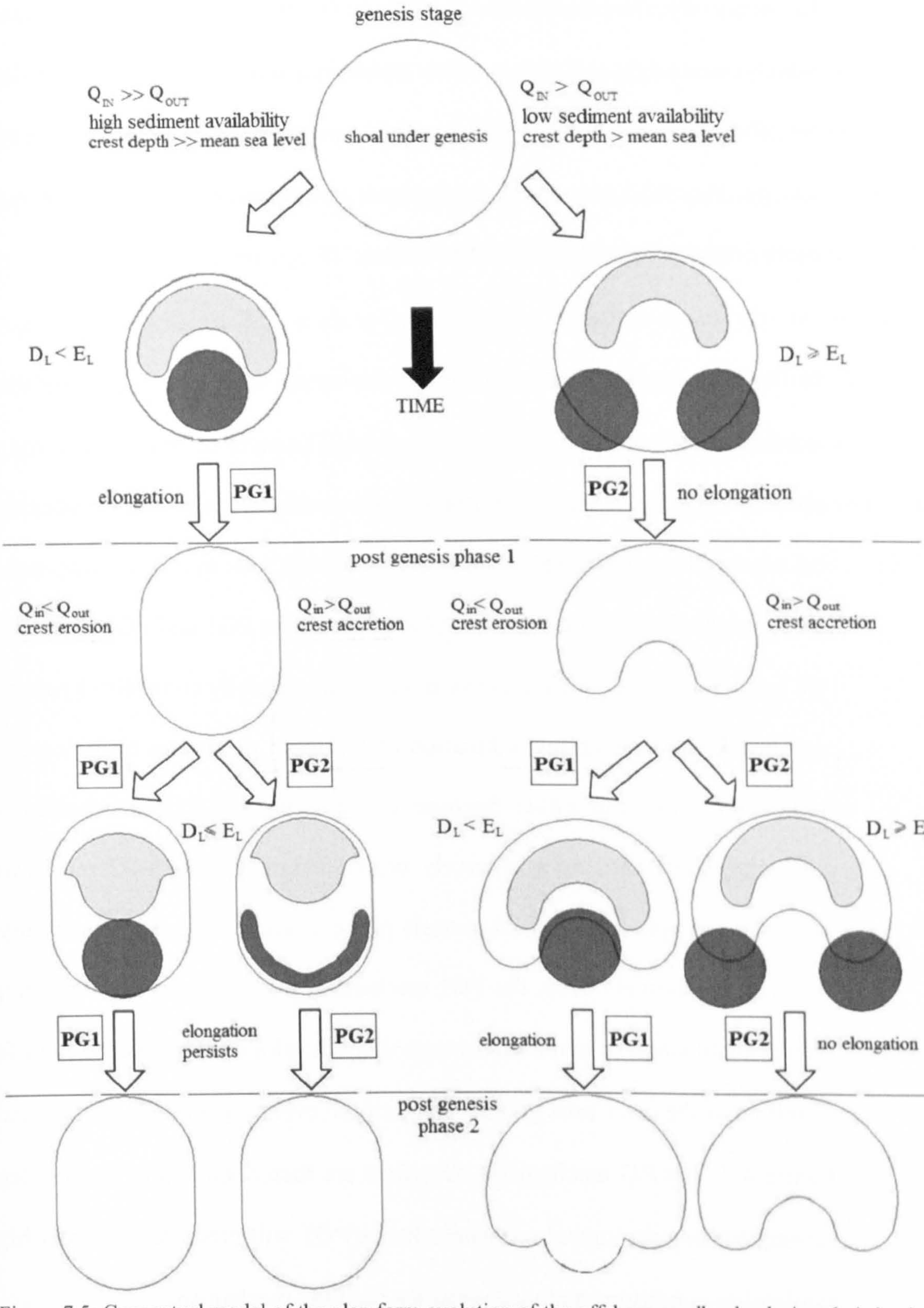

Figure 7.5: Conceptual model of the plan form evolution of the offshore sandbanks during their landward migration. Light and dark grey shaded areas represent regions of erosion and deposition respectively. The balance between Q_{IN} and Q_{OUT} represents sediment availability on the ebb tidal delta. D_L and E_L are the respective longshore length scales of the regions of deposition and erosion. Box codes denote the post genesis modes of morphological change due to the tendency towards the submerged (PG1) or exposed (PG2) patterns of erosion and deposition.

Consequently, the patterns of deposition are relatively broad in the longshore dimension which causes the sandbank to either maintain a similar aspect ratio or to broaden in the longshore dimension ($D_L \geq E_L$) depending on the chronology and intensity of the wave energy. This PG2 pathway naturally leads to the crescentic shaped morphology through more divergent patterns of deposition.

In the post genesis phases of the morphological evolution of the landward migrating sandbanks the same principles are applied. The main difference with the post genesis phases is that the supply of sediment to the sandbanks is more circuitous as the features become more distant from the primary accretion zone that is the terminal lobe. For an elongate sandbank in post genesis phase 1, both the PG1 and PG2 mechanisms result in the perpetuation of the elongate form due to the laterally constrained patterns of erosion and distribution which are a function of the shoal geometry. In the case of crescentic sandbanks these can either become elongate via the PG1 mechanism or continue migrating shoreward as a relatively broad feature via the PG2 mechanism. For the crescentic morphology in post genesis phase 1 where sediment availability is low and the crest is relatively deep, the PG1 mechanism will first lead to the development of an intermediate stage in which the morphology develops an arrowhead plan form. This is observed in the early post genesis stage of the event 1 evolution and depicted clearly in Figure 4.7. The PG mechanisms described are then reapplied in further steps to denote subsequent morphological sequences hence PG1 will predominate under high sediment availability conditions and *vice versa* for the PG2 mechanism.

This conceptual model is generally applicable to landward migrating sandbanks on the ebb tidal deltas of meso to macro tidal inlets since the physical mechanism that are responsible are not exclusive to the Teign inlet ebb tidal delta. The landward migrating

sandbanks at the Teign inlet have been observed to have markedly different morphologies between 1964 and *c.*1990. The cause of this appears to be that there was a much larger volume of sediment in the ebb tidal delta. One of the key morphologic responses of the sandbank system during such times is the formation of sandbanks on the terminal lobe that are significantly broader in the longshore dimension than in the cross-shore dimension. This leads to broad patterns of deposition in both the submerged and exposed states and these are typically maintained throughout the landward migration process. The broad patterns of deposition lead to the sandbanks developing landward facing protuberances or horns on either flank which can be observed in the lower panel of Figure A1 (28/03/1979) and the middle panel of Figure A3 (29/10/1987).

8 Conclusions

The present study has made a significant contribution to the knowledge of the morphodynamic behaviour of landward migrating sandbanks on the ebb tidal deltas of meso to macro tidal inlets. Previous studies of the landward migrating sandbanks on ebb tidal deltas have focussed on meso tidal environments and are typically based on qualitative analyses over mega time scales. In contrast to this the present study utilised a multi-faceted approach in order to quantify the morphodynamic behaviour of the dynamic Teign inlet ebb tidal delta sandbanks. Initially, four distinct episodes of the landward migration of the ebb tidal delta sandbanks were characterised and quantified on meso to macro time scales using an Argus video system developed by Oregon State University. The physical processes that are responsible for the observed behaviour which act over micro time scales were subsequently determined using a unique set of near bed Eulerian point measurements that were obtained directly from the surface of a sandbank in the mid term of its landward migration. The final data analysis strand utilised numerical modelling in order to analyse the spatial and temporal variability in the patterns of erosion and depositions on the sandbanks in order to understand how the physical processes lead to the plan form morphologies observed in the Argus image archive. The modelling was also used to assess the relative contributions of the wave and tidally driven current components to the observed behaviour as this was difficult to determine from the in-situ measurement data. In terms of the specific objectives of the present study that were set out in Section 1.2, the principle conclusions are as follows:

- To characterise and quantify the nature of the ebb shoal morphodynamics over short to long term time scales (weeks to years), in which the principle component is the episodic landward migration of large discrete shoals.

This was achieved using a times series of contours that were extracted from rectified Argus images at an approximate fortnightly resolution over the 5 year period between 1999 and 2004. During the observation period the landward migration of the ebb tidal delta sandbanks was characterised by three principle morphological stages which were are defined as follows:

1. Offshore genesis or growth of the bar in the distal portion of the main channel.
2. Onshore migration and elongation.
3. Shore-attachment and dissipation.

A set of six descriptive parameters were derived from the contours and this enabled the episodes of onshore migration to be quantified in terms of the dynamic of their centre of mass, crest depth, area and aspect ratio which is a function of the ratio of the orthogonal axes length scales. Genesis typically occurs at a cross-shore distance of between 400 and 500 m offshore relative to the origin of the Argus coordinate system. In the inlet's current mode the plan form geometry of the landward migrating sandbanks is predominantly elongate and transversely oriented after genesis. The aspect ratio which was computed with the longshore length scale as the denominator was closet to unity at genesis *O*(1.5 to 2). Subsequently, as the sandbanks migrate landward the aspect ratio increases until reaching maximum values at around the time of shore-attachment *O*(3 to 8). The minimum, mean and maximum contour areas at the target depth (-1.8 m ODN) across the four events were 2.2 x 10^4 m^2, 1.6 x 10^4 m^2 and 3.5 x 10^4 m^2 respectively. The area is observed to increase as the features traverse the nearshore slope which causes them to become increasingly exposed. The crest depth of the sandbanks is typically between 1 and 2 m below mean seal level at genesis. During the initial part of the onshore migration process the crest of the sandbank typically accretes before

undergoing apparently random periods of accretion and erosion for the remainder of the morphological evolution. Analysis of the centre of mass time series determined that the migration rate was linearly related to the ratio of the incident wave height to the tidally averaged crest depth. Typical migration rates between observations were in the range of 1 to 2 $m.day^{-1}$ with a maximum magnitude of 5 $m.day^{-1}$. When the raw migration rate time series were smoothed and interpolated to reveal the longer term trends the results strongly suggested that the migration rate was governed by the seasonal adjustment of wave energy levels.

- To determine which physical processes are responsible for the observed behaviour.

Analysis of the in-situ measurement data determined that the prevailing low energy conditions (H_s < 1.0 m) were capable of maintaining the onshore migration of the sandbanks between storm periods. Low wave energy levels typify the location and under these conditions it was found that onshore directed, wave-driven cross-shore currents dominate the shoal flow regime with maximum currents O(75%) larger than the longshore component. Analysis of the time averaged current strength revealed that the strongest flows ($< \bar{u} > = 0.5$ $m.s^{-1}$) occurred in the shallow surf zone ($h << h_b$). The maximum mean suspended sediment transport ($< c >$) occurred on the flood tide and was estimated to be O(1.0 $g.m^{-2}.s^{-1}$). This was five times the maximum magnitude of the corresponding oscillatory component (Figure 5.11). An energetics analysis of the data determined that under low energy short period wave energy short waves were the primary mechanism for sediment suspension over the migrating sandbank. The suspended sediment was then transported onshore by wave-driven mean flows. Undertow was not observed to develop on the offshore extremity of the sandbank under these conditions.

- To determine the role of the spring-neap variation in tidal water level on the landward migration of the ebb shoals.

The effects of meso to macro scale water level variation on the sandbank's sedimentation were investigated using idealised numerical modelling experiments under stationary water levels and variable wave energy. The model setup simulated the configuration of the sandbanks at the Teign inlet just after genesis when the aspect ratio is closest to unity and the crest of the sandbank is between 1 and 2 m below mean sea level. The experiments found that when low energy conditions coincide with neap tides the resultant patterns of erosion and deposition promote the shoreward elongation for sandbanks with an aspect ratio in approximate unity. With increasing wave energy levels the patterns of erosion and deposition caused the sandbank to undergo a degree of broadening in the longshore dimension and an increase in elevation. The differences in the between the two morphological responses was found to be a function of the variable residence times of the causative processes. Under low energy conditions these are biased towards the lower states of tides dominated by the patterns of erosion and accretion under the shallow submerged state. Tidal currents were found to have negligible sediment transport capability hence are not considered to significantly affect the evolution of the sandbanks.

- To explain the persistent elongate and transversely oriented geometry of the shoals through the course of their landward migration.

This morphodynamic behaviour is initially governed by the geometry of the sandbanks at genesis. In the inlet's current morphologic mode the aspect ratio of the sandbanks after they have undergone genesis is closest to unity. Consequently, they typically

evolve into elongate and transverse forms due to their crests being deep in relation to mean sea level. This causes their patterns of deposition to be constrained in the longshore dimension due to the effects of strong wave refraction and focussing over their crests. The resultant elongate and transversely orientated form the sandbanks is then maintained through to the shore-attachment and dissipation stage because the variability in wave direction is mitigated primarily due to the strong refraction of the incident waves by the sandbank morphologies. The process is assisted by the relatively infrequent occurrence of high energy waves which are predicted to promote longshore broadening.

Appendix A1: Teign inlet: *c.*1976-2009

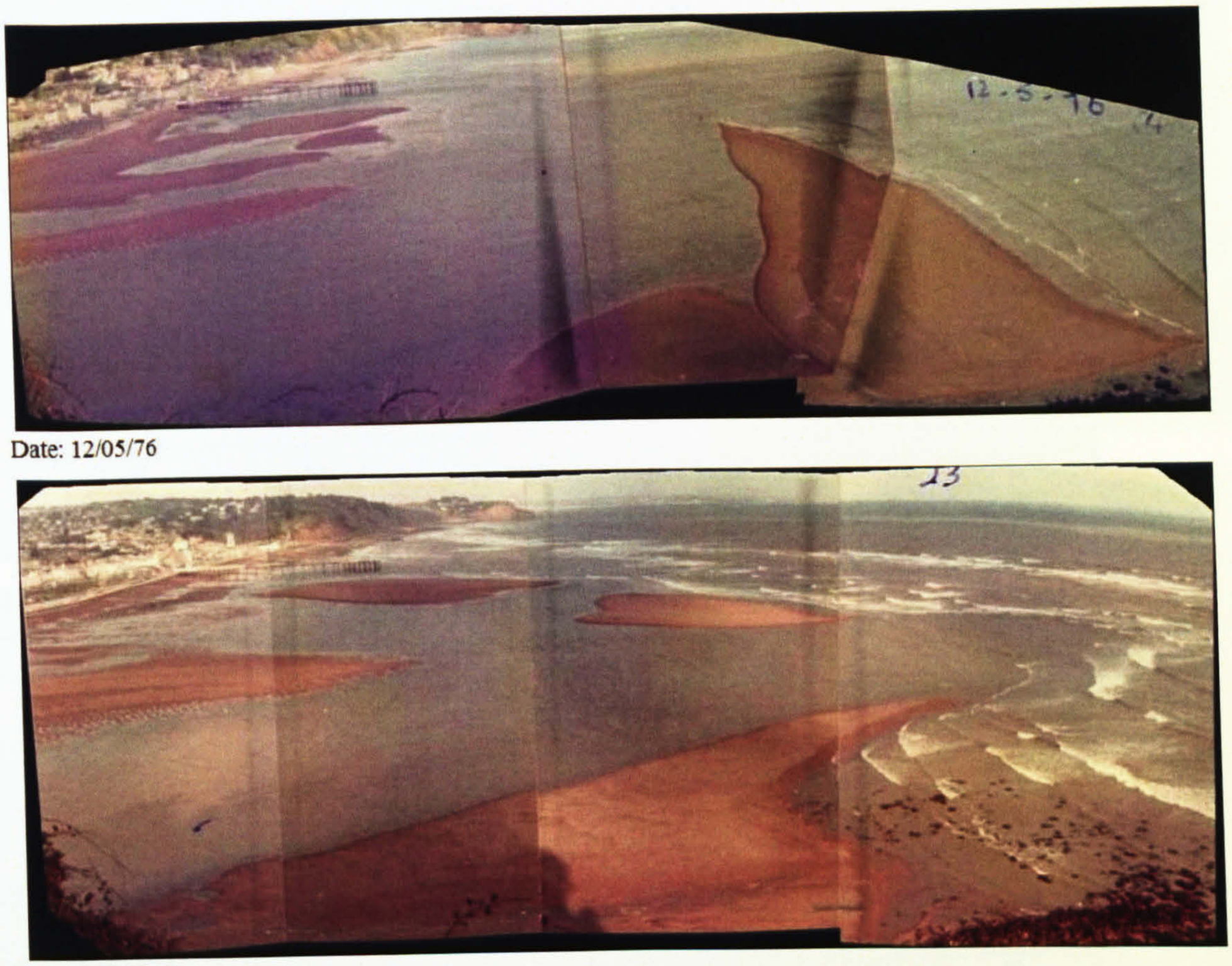

Figure A1: Chronology of the Teign inlet ebb shoal system photographed from the Ness headland, 1976-1979. (Courtesy of S.Hook). Upper panel: main ebb channel is orientated north due to the well developed Ness bar, an irregular-shaped, shore-attached sandbank is in the process of being dissipated. Middle panel: the main channel is orientated east, genesis and mid-term migration sandbanks are present. Lower panel: the main channel is orientated east, the migrating sandbank has a large area with crescentic horns developing at the landward margin of both flanks.

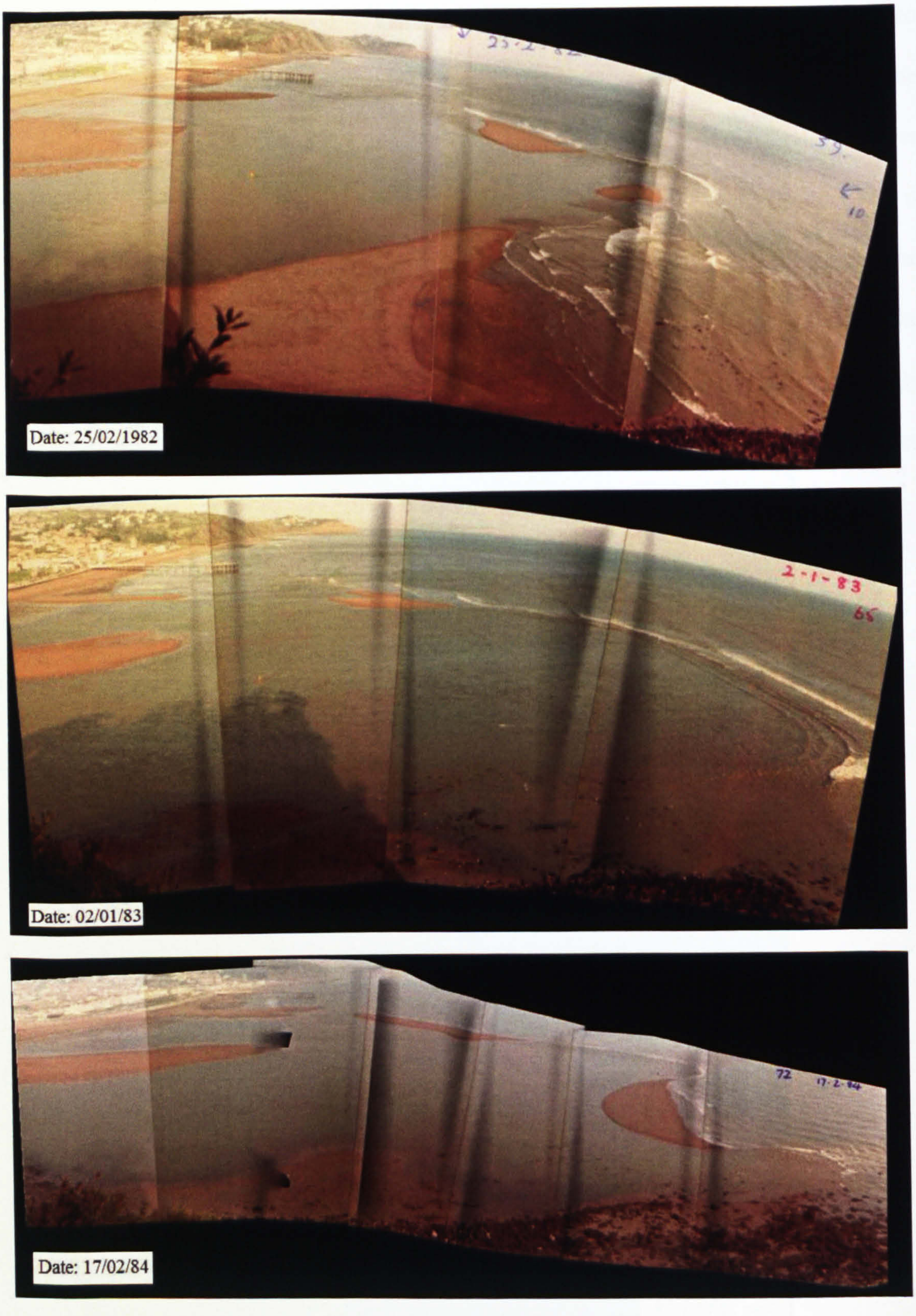

Figure A2: Chronology of the Teign inlet ebb shoal system photographed from the Ness headland, 1982-1984. (Courtesy of S.Hook). Upper panel: the main channel is orientated to the east, offshore sandbanks are developing on the terminal lobe and a relict shore-attached bar on Teignmouth main beach is in evidence. Middle panel: sandbank in mid-term onshore migration with crescentic horns on the landward side, the terminal lobe is completely submerged. Lower panel: the main ebb channel is orientated to the east and the Ness bar is well-developed, mid-term migration and shore-attached sadbanks are observed indicating high sediment availability.

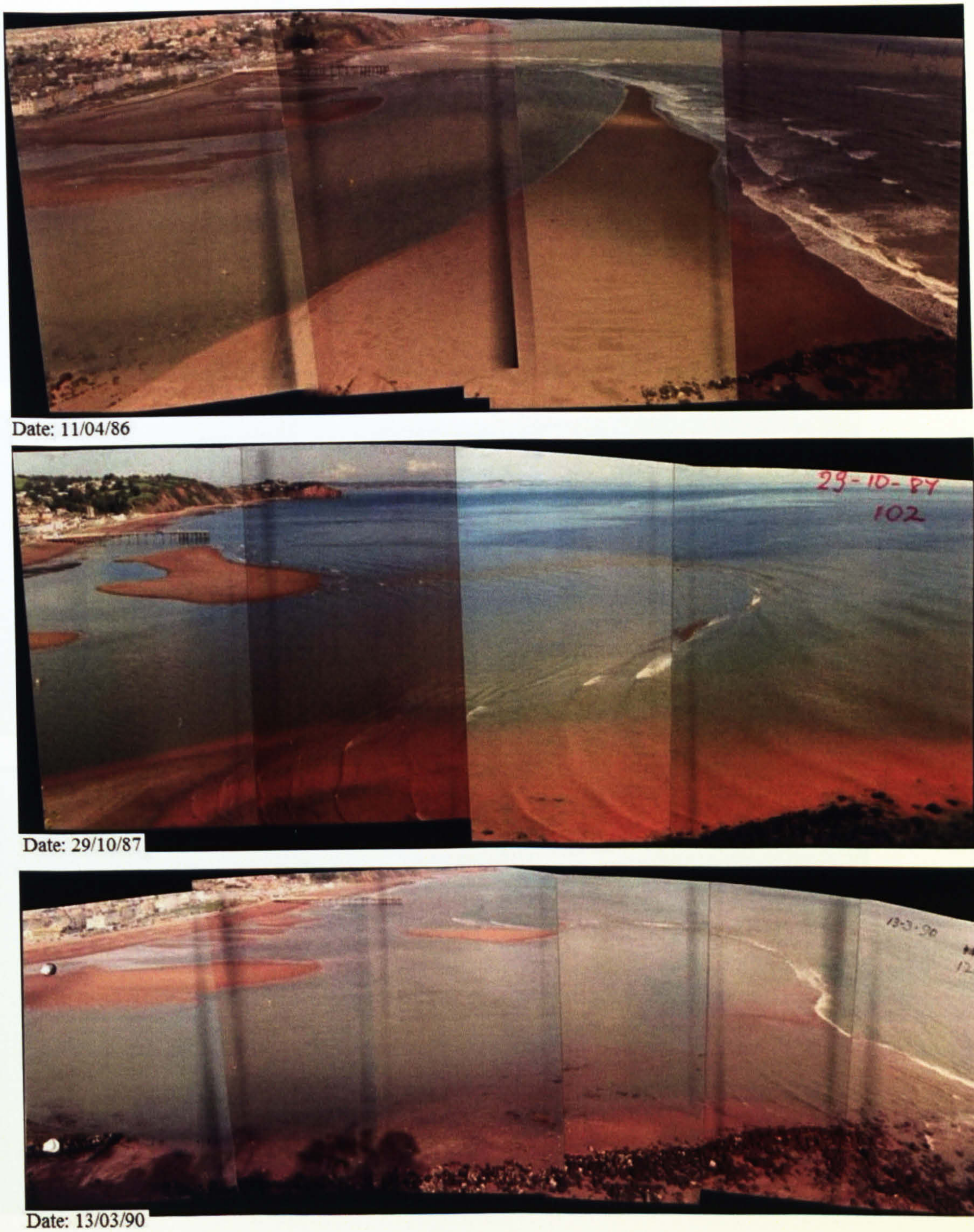

Figure A3: Chronology of the Teign inlet ebb shoal system photographed from the Ness headland, 1986-1990. (Courtesy of S.Hook). Upper panel: the main ebb channel is orientated to the north due to the well-developed Ness bar, the irregular-shaped, shore-attached bar is in the process of being dissipated. Middle panel: a large shore-parallel sandbank in mid-term migration has developed horns on the landward side. Lower panel: a single sandbank is in mid-term migration, there are no shore-attached bars in evidence on the main beach and the terminal lobe is completely submerged.

Figure A4: Chronology of the Teign inlet ebb shoal system photographed from the Ness headland, 1992-2009. Upper panel: A large oblique sandbank gas developed on the terminal lobe, the main channel has been deflected to the east, a shore-attached bar is in evidence (Courtesy of S.Hook). Middle panel; inner (shore-attached) and outer sandbanks occupy the nearshore region, both features are elongate and transversely oriented, (Argus image panorama). Lower panel: the sandbanks in the previous image have merged to form a single transverse bar approximately 600 m in length (Argus image panorama).

Appendix A2: In-situ measurement data quality tables for the different SLOT rig deployment positions during the May 2003 Coastview fieldwork program

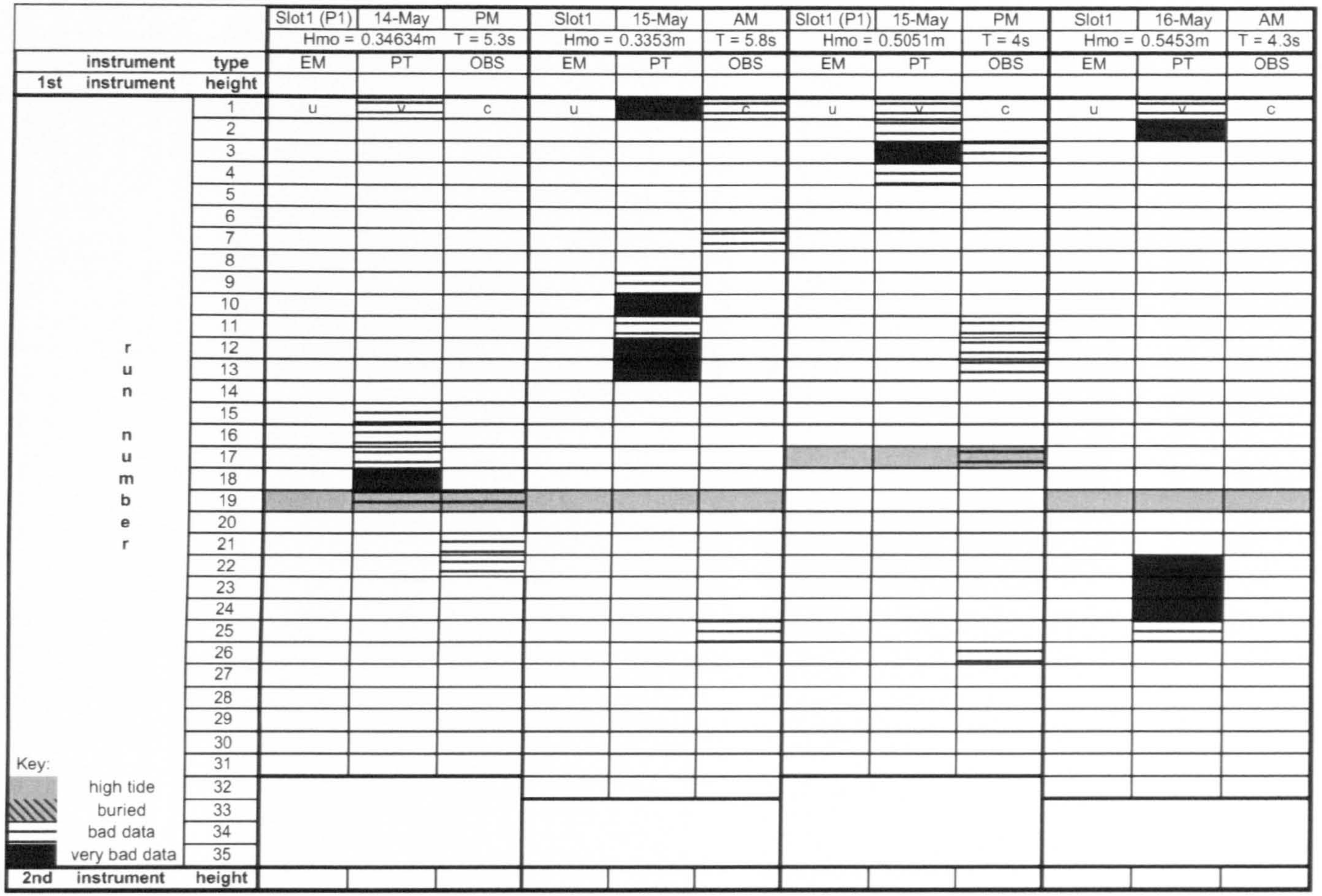

Table A3.1: Data quality tables for the in-situ measurements at SLOT rig deployment position 1A (SLOT1 P1) from the 14th May to the 16th May, 2003. P1 and P2 denote the first and second deployment positions respectively. AM and PM denote the first and second respective tides for a particular date; *u* and *v* denote the orthogonal current direction. Instrument abbreviations: EM: electromagnetic current meter, PT: pressure transducer, and OBS: optical back scatter sensor.

			Slot1 (P1)	16-May	PM	Slot1 (P1)	17-May	AM	Slot1 (P2)	17-May	PM	Slot1 (P2)	18-May	AM
			Hmo = 0.6297m		T = 5.3s	Hmo = 0.4841m		T = 4.9s	Hmo = 0.4654m		T = 4.9s	Hmo = 0.4322m		T = 4.9s
	instrument	type	EM	PT	OBS	EM	PT	OBS	EM	PT	OBS	EM	PT	OBS
1st	instrument	height												
		1	u		c	u	v	c	u	v	c	u	v	c
		2												
		3												
		4												
		5												
		6												
		7												
		8												
		9												
		10												
		11												
	r	12												
	u	13												
	n	14												
		15												
	n	16												
	u	17												
	m	18												
	b	19												
	e	20												
	r	21												
		22												
		23												
		24												
		25												
		26												
		27												
		28												
		29			?									
		30			?									
		31												
		32												
		33												
		34												
		35												

Key:
high tide
buried
bad data
very bad data

Table A3.2: Data quality tables for the in-situ measurements at SLOT rig deployment positions 1A (SLOT1 P1) and 1B (SLOT1 P2) from the 16th May to the 18th May, 2003. P1 and P2 denote the first and second deployment positions respectively. AM and PM denote the first and second respective tides for a particular date; *u* and *v* denote the orthogonal current direction. Instrument abbreviations: EM: electromagnetic current meter, PT: pressure transducer, and OBS: optical back scatter sensor.

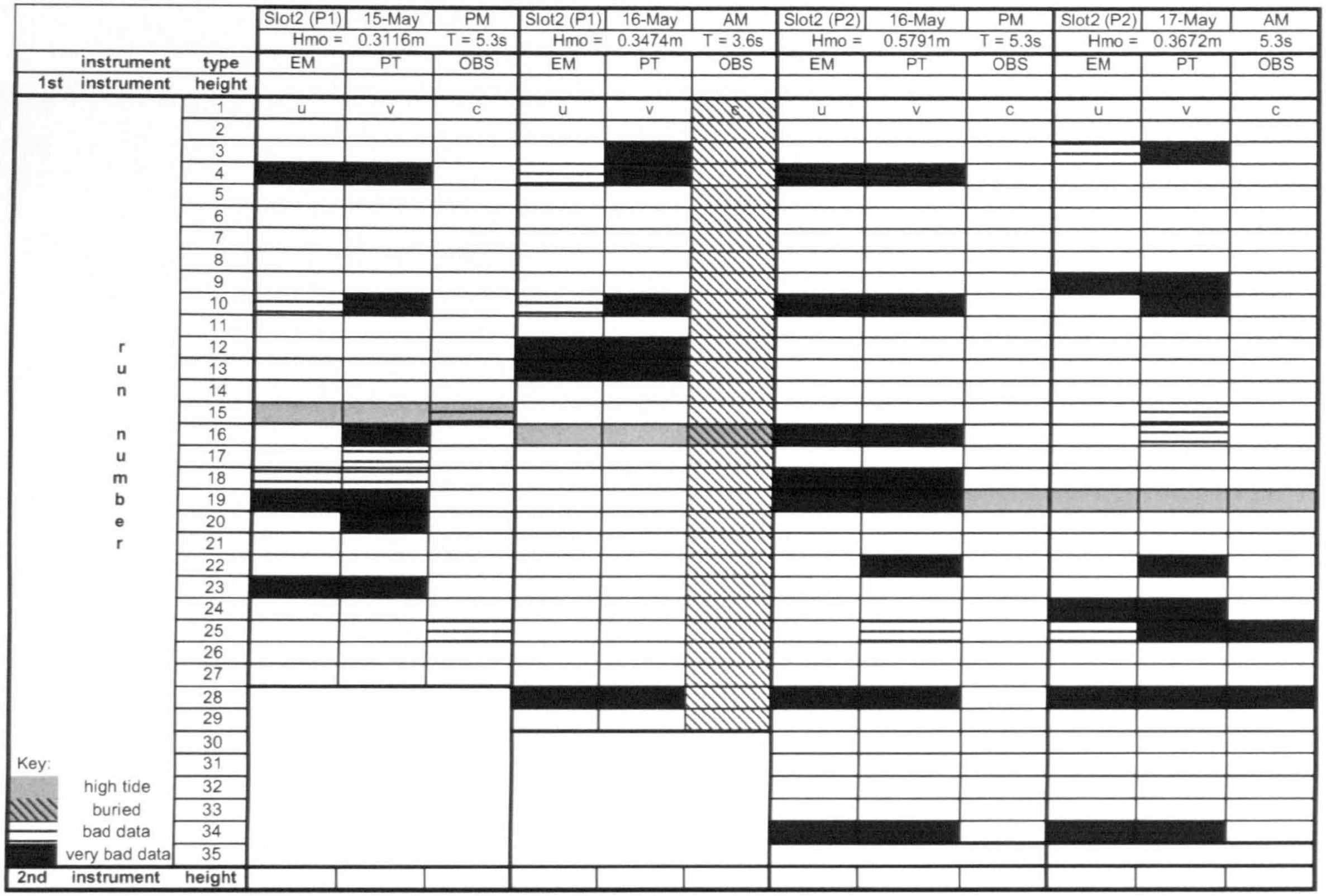

Table A3.3: Data quality tables for the in-situ measurements at SLOT rig deployment positions 2A (SLOT2 P1) and 2B (SLOT2 P2) from the 15th May to the 17th May, 2003. P1 and P2 denote the first and second deployment positions respectively. AM and PM denote the first and second respective tides for a particular date; *u* and *v* denote the orthogonal current direction. Instrument abbreviations: EM: electromagnetic current meter, PT: pressure transducer, and OBS: optical back scatter sensor.

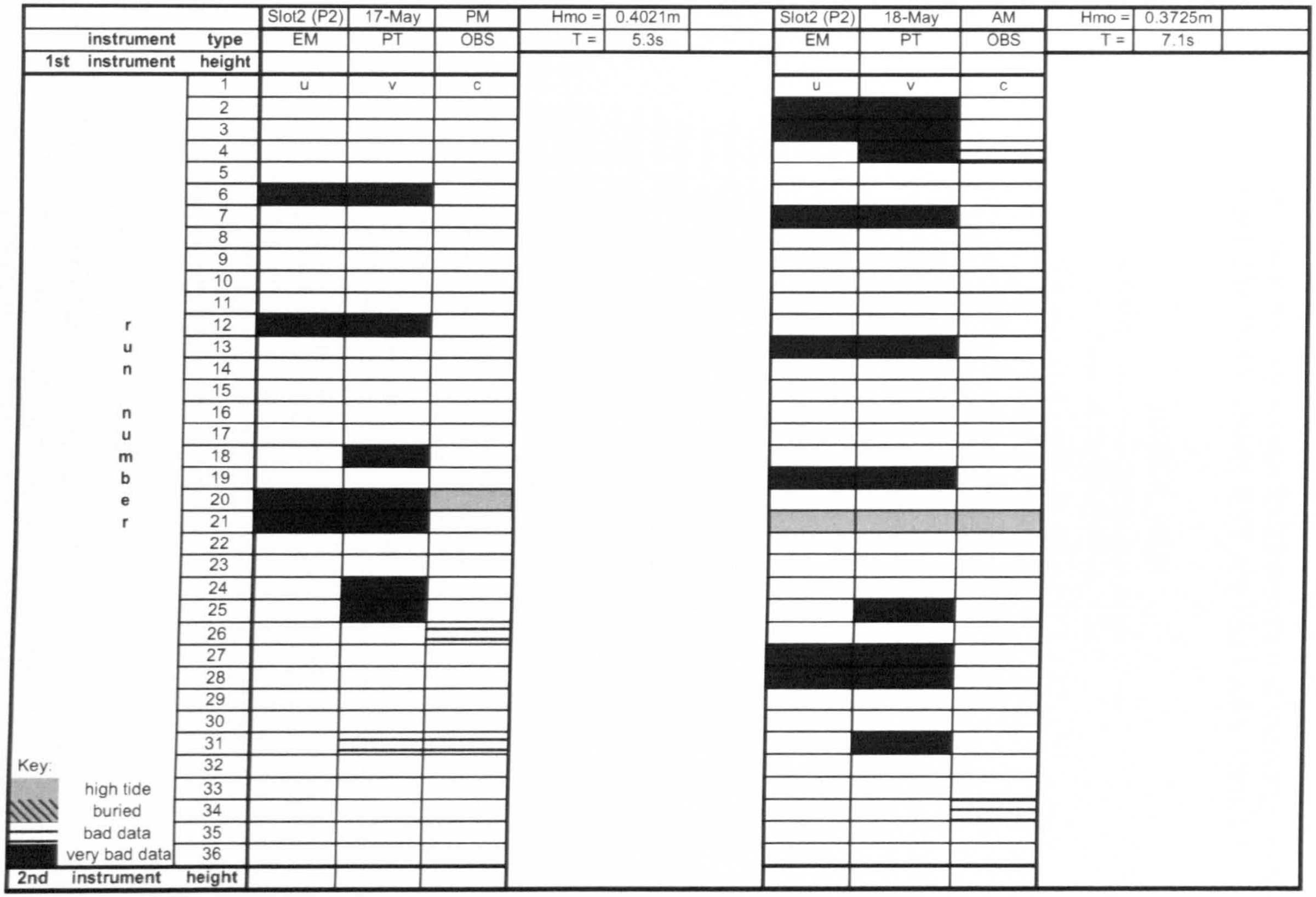

Table A3.4: Data quality tables for the in-situ measurements at SLOT rig deployment positions 2B (SLOT2 P2) from the 17th May to the 18th May, 2003. P1 and P2 denote the first and second deployment positions respectively. AM and PM denote the first and second respective tides for a particular date; *u* and *v* denote the orthogonal current direction. Instrument abbreviations: EM: electromagnetic current meter, PT: pressure transducer, and OBS: optical back scatter sensor.

Appendix A3: Proceedings paper from the 29th International Conference on Coastal Engineering, Lisbon, Portugal, 2004

PHYSICAL PROCESSES ASSOCIATED WITH ONSHORE SAND BANK MIGRATION ADJACENT AN ESTUARY MOUTH

NIGEL P. AIRD
S.E.O.E.S, University of Plymouth,Drake Circus
Plymouth, Devon PL4 8AA, U.K..

MARK A. DAVIDSON
S.E.O.E.S, University of Plymouth,Drake Circus
Plymouth, Devon PL4 8AA, U.K...

ISMAEL J. MARINO-TAPIA
S.E.O.E.S, University of Plymouth,Drake Circus
Plymouth, Devon PL4 8AA, U.K..

This paper utilises Argus video observations and in-situ measurements to elucidate the processes responsible for the onshore migration of a dynamic, coarse-grained sand bank situated adjacent an estuary on the south coast of the U.K during summer 2003. Using video observations combined with an image contouring technique, it was found that the sand bank had a net onshore migration during April and May, but that the rate during the former month (≈1.5 m.day^{-1}) was significantly higher than that of the latter (≈0.3 m.day^{-1}). The difference in migration rates is attributed to wave energy given that the tidal contribution for both months was approximately equal. April experienced a series of short term, higher energy wave events (offshore H_{max} ≈0.6 to 1.8 m) which occurred much less frequently, and on a reduced scale during May. Field measurements obtained during one such event showed that onshore directed sediment transport occurs in the inner to mid surf zone region at times when the sand bank is not submerged. Short wave stirring suspends sediment which is then transported by mean flows around the margins of the sand bank in a shoreward direction. The onshore directed sediment transport is further assisted by the absence of a well developed undertow on the offshore flank of the sand bank. Under the smallest wave conditions of the measurement period (H_{m0} ≈ 0.3 m), the onshore directed momentum flux is able to setup against the offshore flank of the sand bank producing a weak undertow current in the surf zone. However, under higher wave conditions (H_{m0} ≈ 0.6 m),, the undertow disappeared entirely on the flood tide and only manifest as a particularly weak offshore current on the ebb tide. This may be attributable to the geometry of the sand bank which is narrow in the longshore direction and approximately dome shaped, enabling the onshore directed momentum flux to be redirected around the sand bank margins, which in turn contributes to the onshore directed mean current along the sand bank margins.

1. Introduction

Accumulations of sand are important morphologic features in the coastal zone which occur in a wide range of geomorphological environments and exhibit diverse morphology. Their importance stems from two primary factors:

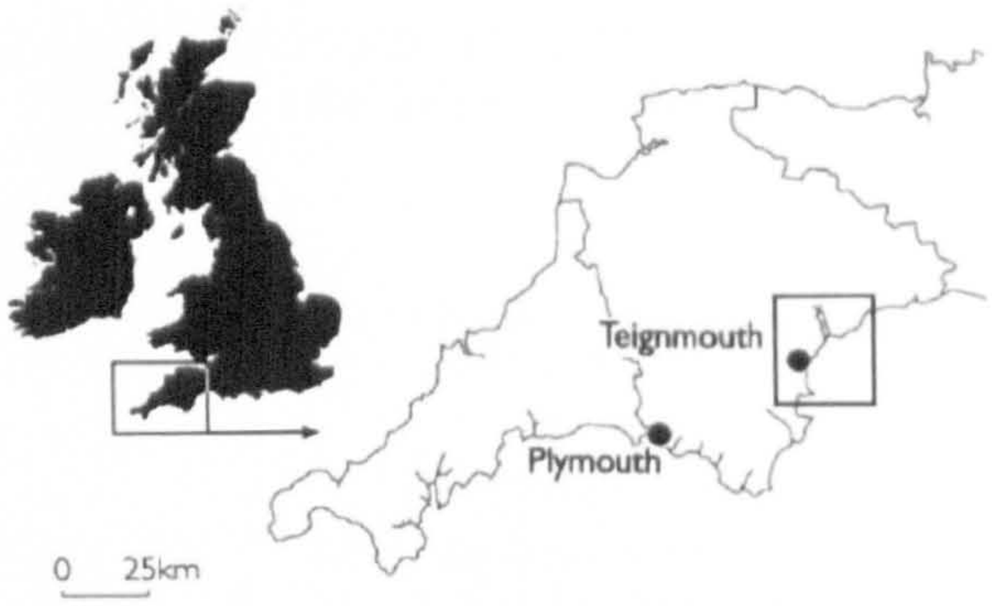

Figure 1: Site location map.

(i) their increasing use as a materials resource for the burgeoning construction industry, and (ii) their contribution to coastal stability through sedimentation processes and wave dissipation effects (Robinson 1980; Byrnes et al. 2004). They can exist in a variety of morphodynamic states; those occurring offshore can be moribund and in a state of static equilibrium with the local hydrodynamics, whilst those occurring in the nearshore on exposed open coast beaches are typically more dynamic and capable of attaining migration rates of 50 $m.day^{-1}$ (van Enckevort and Ruessink 2003). The processes controlling their morphodynamic evolution are fairly well understood as evidenced by their successful encapsulation in top-down models (Plant and Holman 2001; Marino-Tapia et al. 2003). However, the processes controlling the onshore migration component of their evolution are much less well understood (Hoefel and Elgar 2003). This contribution utilises Argus video images and in-situ measurements of waves, currents and sediment suspension in order to elucidate these processes in the context of an elongate nearshore sand bank at an estuarine location in the south west of the U.K (Figure 1).

2. Study Site and Data Collection

Data were obtained from the sand bank at Teignmouth on the south coast of the U.K. Figure 2(a) is a merged and rectified, Argus plan view image of the study site which has a uniform 2 km long beach that faces ESE into the English Channel. The beach is flanked to the north and south by red sandstone headlands and is backed by a sea wall. At the southern end of the beach, the entrance to the Teign estuary is situated which is considered to be in a state of near sedimentary balance (Dyer 2002). The estuary mouth has been deepened and narrowed due to the encroachment of 'The Denn' spit from the north which has resulted in significant tidal currents at peak tides creating a jet-like outflow which is ebb-dominated close to the mouth. The region experiences semi-diurnal macro-tides with a spring-neap cycle of 4.2 to 1.7 m that generate

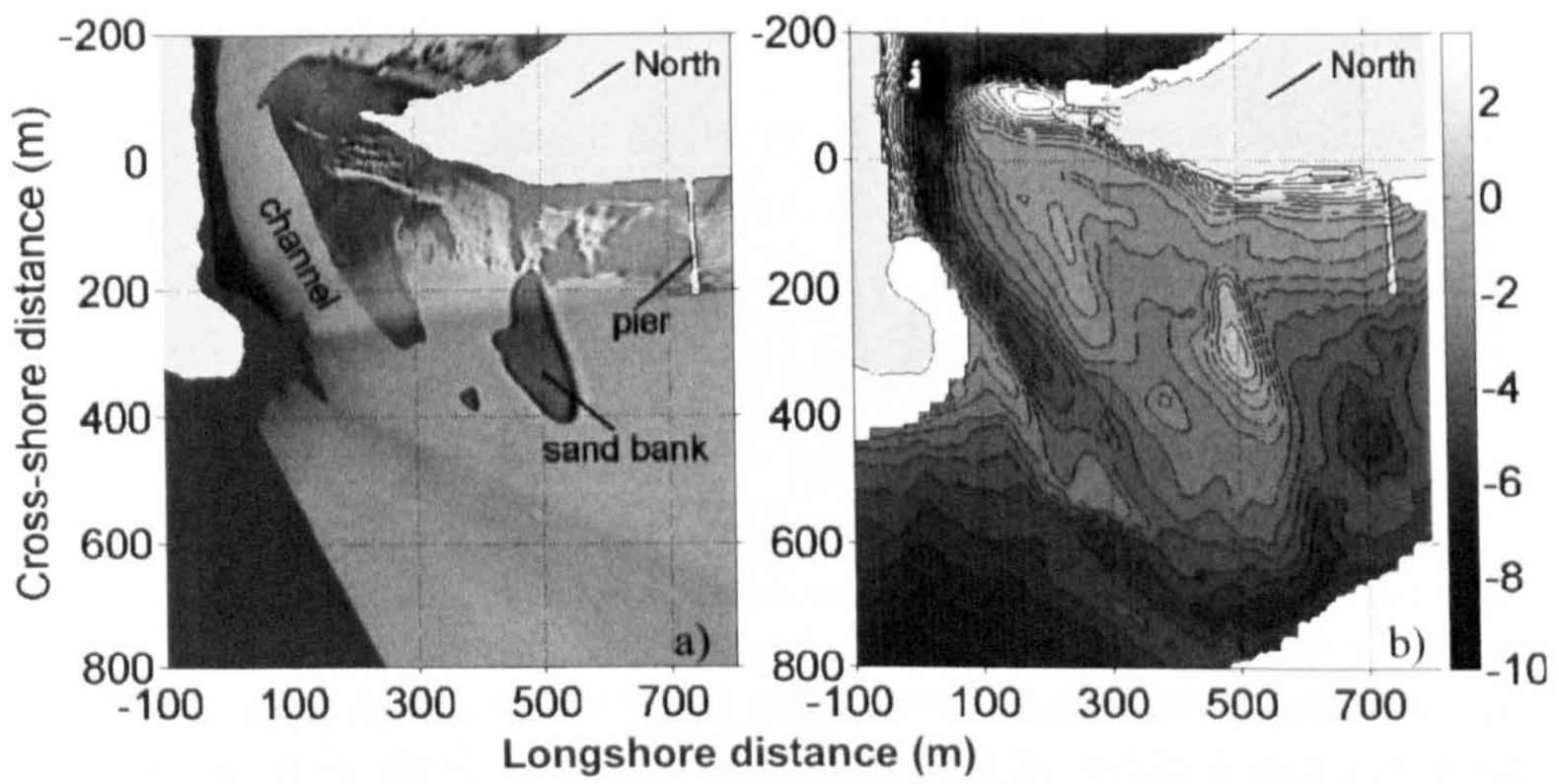

Figure 2. (a) Merged and rectified Argus image of Teignmouth, 15th May, 2003, and (b) Teignmouth morphology, May, 2003. Depths in meters relative to ordnance datum Newlyn,U.K.

dissipative conditions at low tide which become progressively reflective towards the high tide. Short period wind waves with typical heights of between 0 and 0.5 m dominate the surf zone 75% of the time although these can reach up to 3 m during gales with an easterly component. Coincident with the presence of the estuary mouth is the presence of an asymmetric, coarse-grained ebb shoal system. Complex 3D wave and current fields enhanced by refraction and dissipation processes have been observed to transport the sediment in a cyclical manner around the estuary mouth with a periodicity of between 3 and 5 years (Robinson 1975; Siegle 2003). The cycle begins with the growth of the offshore sand bank at the end of the estuary channel. As the volume of the sand bank increases, the shoreward margin of the sand bank begins to migrate onshore until becoming shore-attached. Subsequently, the offshore margin of the sand bank retreats shoreward until the feature has become entirely dissipated. Prevailing longshore currents transport the sediment south into the estuary channel which returns it offshore where the process begins again. The offshore sand bank is clearly visible in Figure 2(a) as the dark region situated between the estuary channel and pier. This sand bank is of particular scientific interest as it appears to migrate onshore under all conditions which is evidenced by 5 years of Argus video observations of the study site. The period of interest of this study are the months of April and May 2003, the latter being the month in which a field campaign was undertaken. During the field campaign, in-situ measurements were obtained between the 12th and 19th May from a number of locations on the offshore sand bank using two instrument rigs comprising pressure transducers (PTs), optical backscatter sensors (OBSs) and electronic

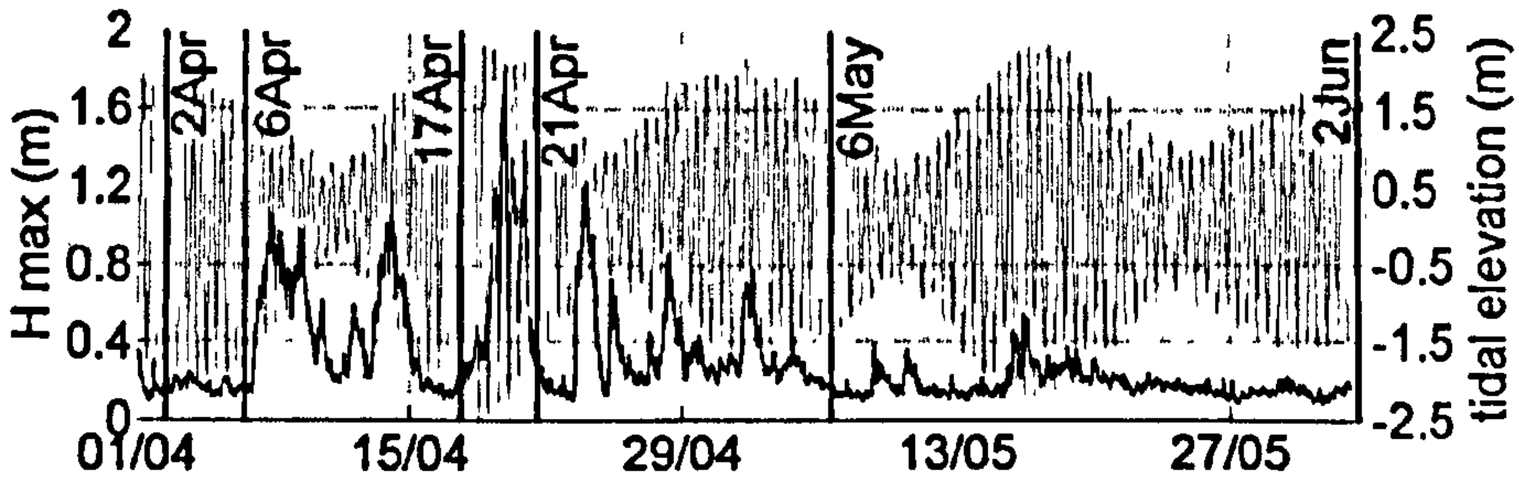

Figure 3. Offshore maximum wave height (H_{max}), and tidal elevation for the period between 1st April and 2nd June 2003. (Vertical lines indicate the times at which sand bank contours were extracted from the Argus archive).

current meters (EMCMs). Offshore wave height was recorded using an acoustic doppler current profiler (ADCP) located on the seabed at an approximate depth of 4 m, and a sensor situated at the end of the pier recorded meteorological conditions. This study focuses on the measurements taken from the instruments positioned on the seaward facing flank of the sand bank. The PT, OBS and EMCM instruments were secured to mountings which were buried deep into the sand to ensure stability during the measurement period, both the data logger and power unit were attached to the unit to avoid the problems associated with the use of cables. The PT, OBS and EMCM were fixed at elevations above the seabed of 25, 5 and 14 cm respectively and the data were sampled at a frequency 4 Hz. The beach topography and inter-tidal morphology (Figure 2(b)) were surveyed using Trimble real time kinematic GPS equipment and an ODOM portable echo sounder respectively.

3. Results

3.1. Argus Video Observations

The complex nearshore morphology in the vicinity of the estuary mouth is presented in Figure 2(b). The beach topography and nearshore bathymetry were surveyed during the May field campaign although, due to the absence of significant morphological change during this period, it is also representative of the morphology during April. Figure 3 shows the maximum offshore wave height (H_{max}) superimposed over tidal elevation at the study site for the period between the 2nd April and 2nd June 2003. Vertical lines indicate the times at which Argus video images focused on the sand bank were extracted for analysis from the Teignmouth archive. April and May experienced markedly different wave conditions. The former begins with daily offshore maximum wave heights

of approximately 0.2 m which are typical for the study site. After the 6th April, the remainder of the month is punctuated by short pulses of higher wave energy associated with incidents of easterly winds, which repeatedly cause H_{max} to increase to between 0.6 m and 1.0 m for short periods of time. In contrast to April, May experienced conditions of much lower wave energy with persistent H_{max} values of around 0.2 m.

Variable	Parameter
Location of centre of mass	Migration path, distance
Length of major and minor axes	Aspect ratio, orientation
Area/volume	Erosion, accretion

Table 1. Sand bank variables and their associated parameters.

In order to facilitate the analysis of the morphological evolution of the sand bank for the period between the 2nd April and the 2nd June, a manual contour extraction technique has been used to extract sand bank contours at a constant but arbitrary tidal level, in this case approximately -1.2 m below ordnance datum Newlyn, U.K. The technique enables the generation of a number of sand bank variables that can be used to facilitate the quantitative analysis of its morphodynamic evolution (see Table 1). The centre of mass of the sand bank can be used to document changes in position, the major and minor axes can be used to analyse changes in sand bank shape through calculation of the aspect ratio, and area can be used to analyse the extent of sand bank erosion or accretion through the analysis of changes in horizontal slices taken through the sand bank at different tidal elevations. Using the contours in Figure 4 panels (a) to (f), the set of variables have been calculated for the sand bank and the results are presented in Table 2. For the study period, the changes in the aspect ratio and orientation of the offshore sand bank were not significant when compared with the migration distance and rate of the sand bank's centre of mass. The maximum variation about the mean in area and orientation was of the order of 10% and the aspect ratio remained virtually unchanged. The latter factor has important implications when considering the sand bank's migration in terms of

Descriptor	Up to 2nd Apr	2nd - 6th Apr	6th - 17th Apr	17th - 21st Apr	21st Apr - 6th May	6th May - 2nd Jun
Migration rate ($m.day^{-1}$)	N/A	-0.4 (±0.1)	1.6 (±0.04)	1.4 (±0.1)	1.4 (±0.03)	0.3 (±0.01)
Migration distance (m)	N/A	-1.7 (±0.4)	17.5 (±0.4)	5.6 (±0.4)	20.7 (±0.4)	8.2 (±0.4)
Area (m^2)	10822	11383	10865	11419	9523	9959
Aspect ratio	2.7	2.6	2.7	2.7	3.0	2.7
Orientation (deg from longshore axis)	71.6	75.3	71.7	74.3	72.5	64.8

Table 2. Calculated sand bank parameters.

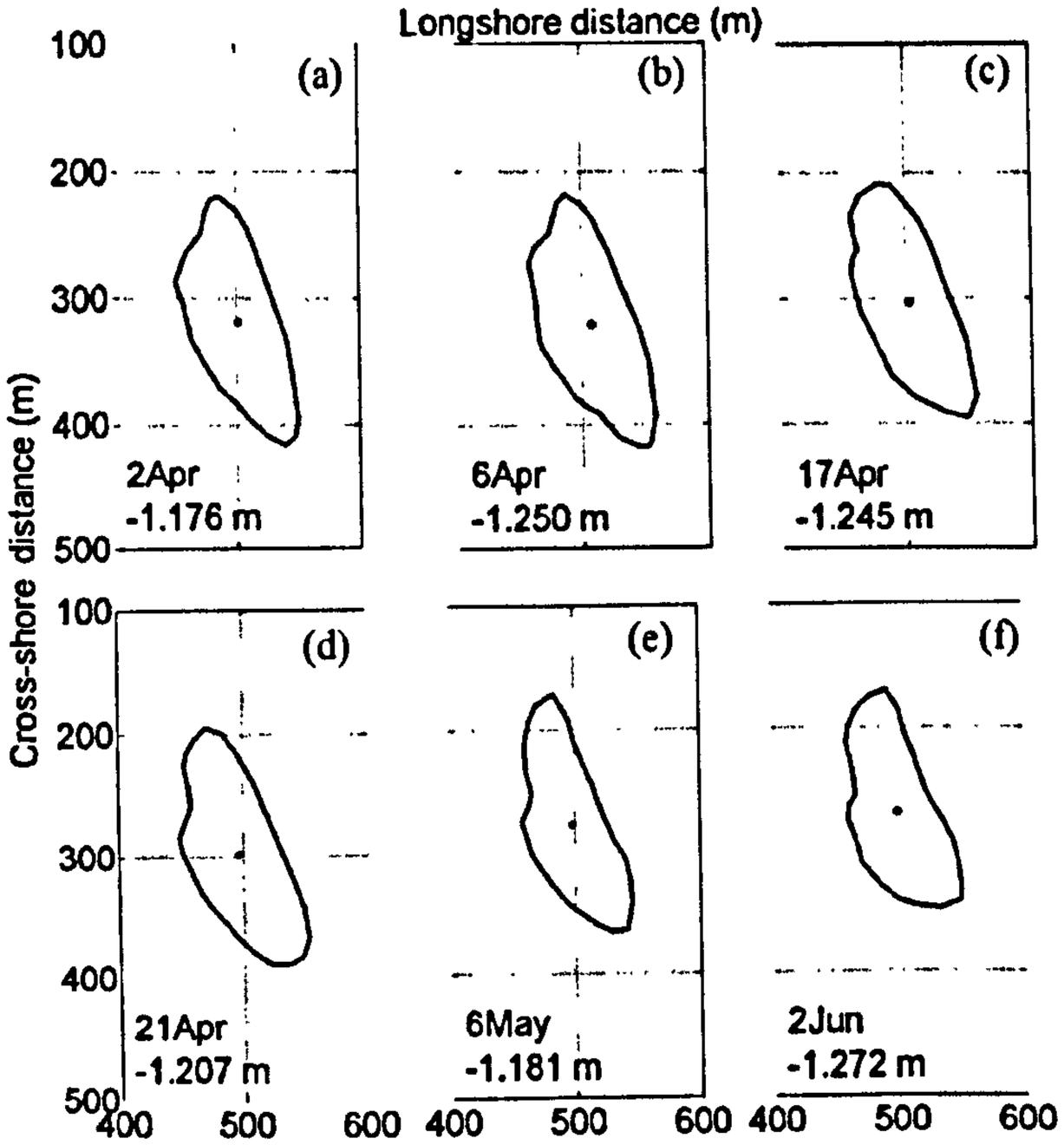

Figure 4. Offshore sand bank contours extracted from Argus images at an approximate depth of -1.2 m below ordnance datum, Newlyn, U.K. for: (a) 2nd April, (b) 6th April, (c) 17th April, (d) 21st April, (e) 6th May, and (f) 2nd June.

its centre of mass especially during periods when migration distances are small. The lack of significant changes in sand bank geometry during the period of study mitigates this potential source of error. Similarly, consideration of the inherent error associated with the contouring technique is also important hence the inclusion of the standard error values in the table which relate to the repeatability of the technique, other error sources were considered negligible. Figure 4 panels (a) to (f) show the time series of the morphological evolution of the sand bank at around the -1.2 m contour level. The date and tidal elevation for each image from which the contours were extracted are specified in the bottom left corner of each panel; each one covering the same spatial domain of the study site. The maximum variation in tidal elevation between contoured images is less than 10 cm and, plotted on each is the sand bank's centre of mass. Panels (a) to (e) document the sand bank's position from the 2nd April to the 6th May. Analysis of the position of the sand bank's centre of mass reveals that

there is a net onshore migration of 42 m (±0.6m) over this period (Table 2.). Conversely, the observed difference between the position of the centre of mass on the 6th May as compared with that on the 2nd June is very small and represents a net onshore migration of just over 8 m. The difference in the nearshore current field between comparative periods can be attributed to wave energy which suggests that the principle mechanism responsible for the onshore migration of the sand bank at Teignmouth is wave driven. Direct comparison of migration distance between periods is not appropriate due to the temporal disparity between them. However, a Spearman's non-parametric correlation test between the calculated wave intensity for each observation period and the corresponding migration distance produces a value of 0.9 suggesting significant correlation. This is reflected in the increased migration rates for the observation periods in April (≈1.5 $m.s^{-1}$ (±0.05)) as compared with May (≈0.3 $m.s^{-1}$ (±0.01)).

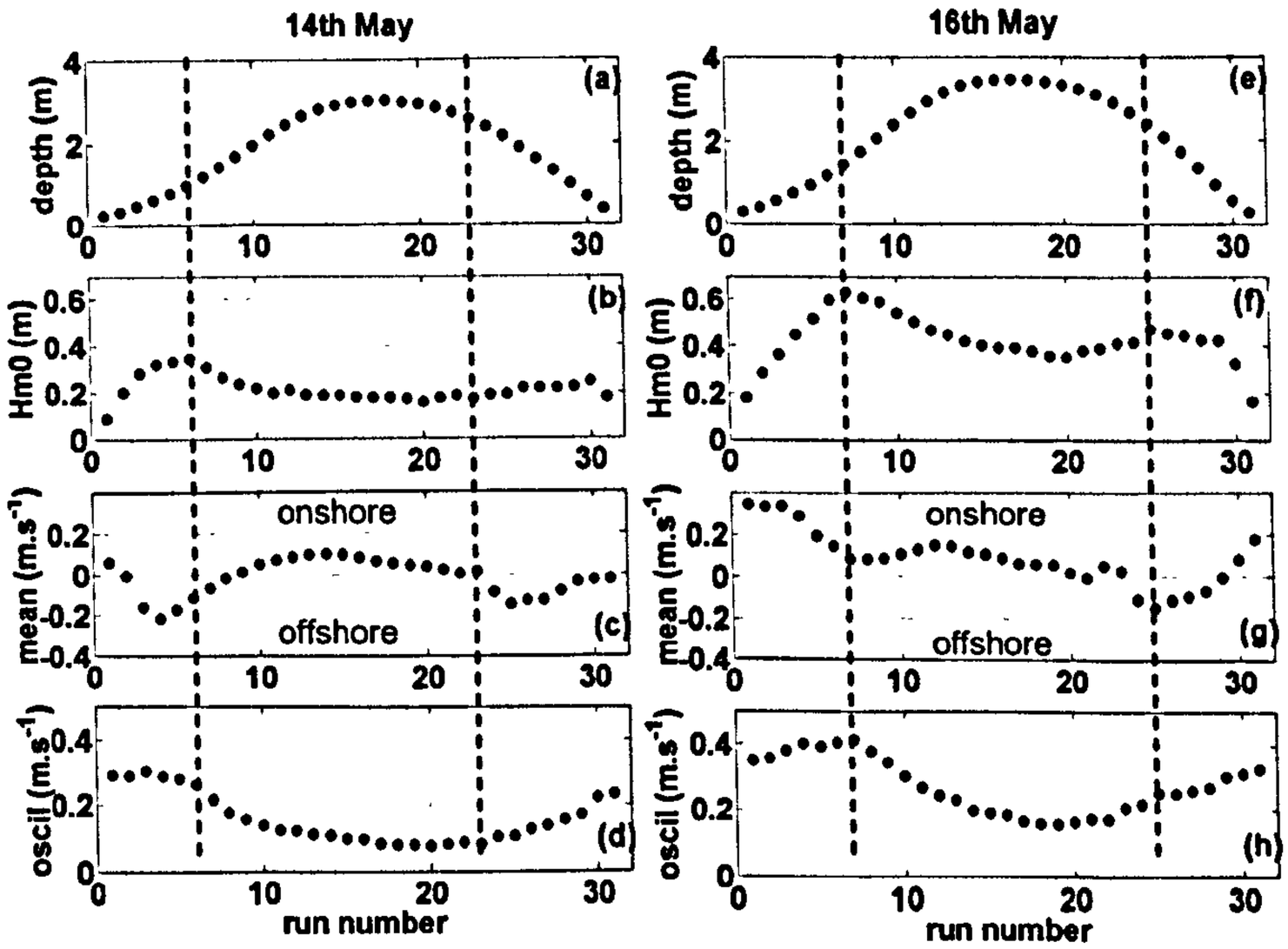

Figure 5. In-situ measurement time series for the 14th and 16th May: (a) & (e) surface elevation, (b) & (f), mean cross-shore current (c) & (g), and oscillatory cross-shore current (d) & (h). Vertical lines denote breaker depth position.

3.2. In-situ measurements

The field conditions during the May 2003 field campaign were typical of those experienced 75% of the time at the study site with small short period, wind sea waves with maximum offshore wave height of about 0.2 m (Figure 3) coming from the SSE, and with a period of approximately 7 s. On the morning

of the 15th May, the wind shifted onshore and increased from 2 to 7 $m.s^{-1}$, resulting in short-crested, sea conditions. The peak wave height during the following day had increased to 0.6 m with a period of 5 s. The peak direction of the incident waves was from the SSE which remained largely constant for the measurement period. The in-situ measurements recorded on the offshore sand bank before and during the period of increased wave height are presented in Figure 5 in which each plotted point represents a 17 minute time average. Panels (a) to (d) are the surface elevation, wave height (H_{m0}), mean cross-shore velocity and oscillatory cross-shore velocity respectively for the 14th May; panels (e) to (h) represent the same set of measurements for the 16th May. On the 14th May, the maximum tidal elevation was approximately 3.0 m above ordnance datum Newlyn and the maximum recorded wave height was 0.35 m which produced maximum mean and oscillatory cross-shore currents of -0.2 m and 0.3 $m.s^{-1}$ respectively. The structure of the mean cross-shore currents through the tidal cycle on the 14th May is typical of those experienced on open coast natural beaches with an offshore directed undertow in the surf zone and onshore directed currents outside the surf zone. Panels (e) to (h) represent the hydrodynamic conditions on the 16th May. The maximum tidal elevation increased to just under 3.5 m and wave height to approximately 0.6 m which generated mean and oscillatory cross-shore currents of approximately 0.3 $m.s^{-1}$ and 0.4 $m.\ s^{-1}$ respectively. On both days the maximum wave height occurred on the flood tide suggesting that the tide may be responsible for modulating incident wave height. This in turn has an effect on the current regime whereby on both days maximum cross-shore currents occurred on the flood tide. The combination of an increased tidal range combined with an increase in wave height on the 16th May resulted in an atypical mean cross-shore current time series (Figure 5(g)) which was persistently onshore directed during the flood tide. Figure 6 depicts the time

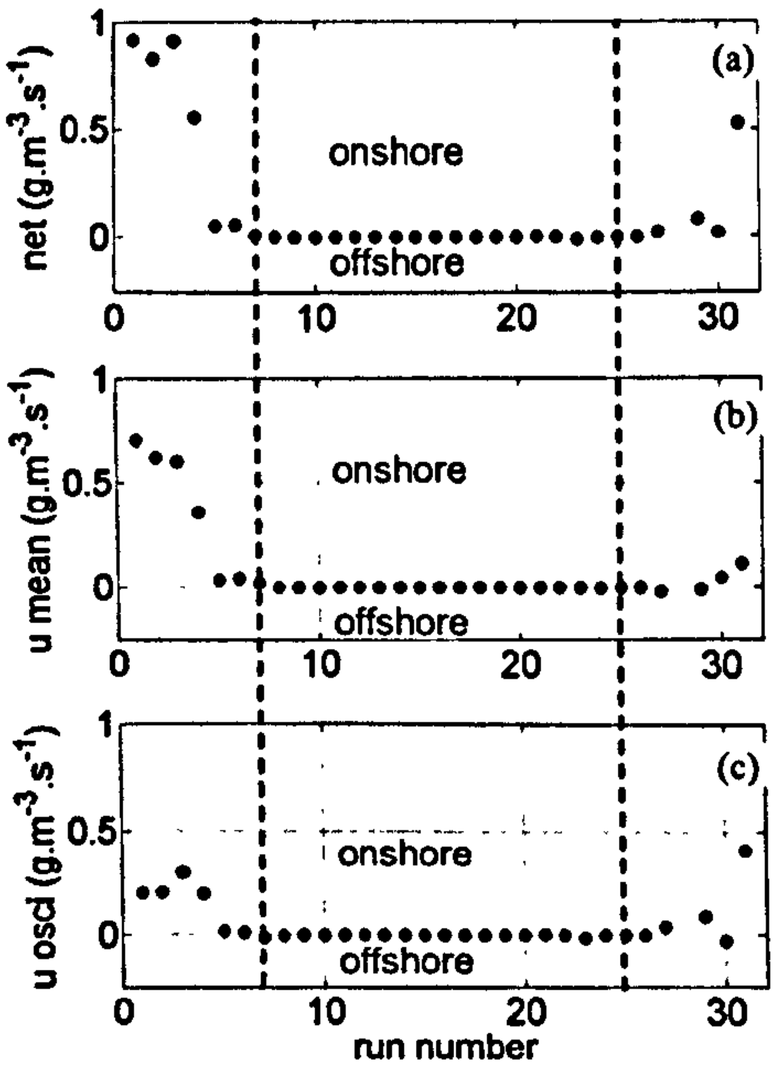

Figure 6. Computed sediment transport rates for 16th May 2003: (a) net transport, (b) mean transport component, oscillatory transport component.

averaged sediment transport rates for the 16th May computed after Jaffe *et al* (1984). Due to the small magnitude of the maximum currents on the 14th May and the coarse nature of the sediment on the sand bank, transport by sediment suspension was negligible on both the flood and ebb tides. Conversely, on the 16th May the increased mean and oscillatory currents on the flood tide in the inner to mid surf zone were sufficient to suspend particles and initiate onshore sediment transport. Significantly, at its maximum, the magnitude of the onshore sediment transport rate due to the mean current component was three times larger than that of the oscillatory component. On the ebb tide, the offshore directed undertow current in the mid to outer surf zone was again too weak to cause significant sediment suspension, whilst in the inner surf zone, onshore transport occurred but on a smaller magnitude compared to that on the flood tide.

No	Term	Description
1.	$\bar{u}^3$	mean velocity cubed
2.	$\tilde{u}_s^3$	short wave velocity skewness
3.	$\tilde{u}_l^3$	long wave velocity skewness
4.	$3\langle\tilde{u}_s^2\rangle\bar{u}$	stirring by short waves & transport by mean flow
5.	$3\langle\tilde{u}_l^2\rangle\bar{u}$	stirring by long waves & transport by mean flow
6.	$6\langle\tilde{u}_s\tilde{u}_l\rangle\bar{u}$	non zero three way correlation
7.	$3\langle\tilde{u}_l^2\tilde{u}_s\rangle$	long wave variance & short wave velocity correlation
8.	$3\langle\tilde{u}_s^2\tilde{u}_l\rangle$	short wave variance & long wave velocity correlation
9.	$3\langle\tilde{u}_s\rangle\bar{u}^2$	time average of oscillatory component ⇨ 0
10.	$3\langle\tilde{u}_l\rangle\bar{u}^2$	time average of oscillatory component ⇨ 0

Table 3. Computed third order velocity moments

4. Discussion

The results of the image analysis suggested that the increased onshore migration rate of the sand bank during April was driven by a sequence of short term (1 to 4 days) low energy wave events. Observations from the following month appear to support this as the migration rate decreased by 80% in the absence of such low energy wave events. The results of the in-situ measurements analysis reveal that mean flows are much more important in the transport of the coarse-grained sediment on the sand bank than the oscillatory flows which had larger but shorter duration maximum values. In order to further analyse the relative contribution of the mean and oscillatory components of the cross-shore velocity controlling the onshore migration of the sand bank, third order velocity moments were computed for the surf zone (Bagnold 1963; Bowen 1980; Bailard 1981) which are summarized in Table 3. The results of the analysis for the 14th and 16th May at shallow surf zone, mid surf zone and breaker depth locations are plotted in Figure 7. Negative values denote offshore

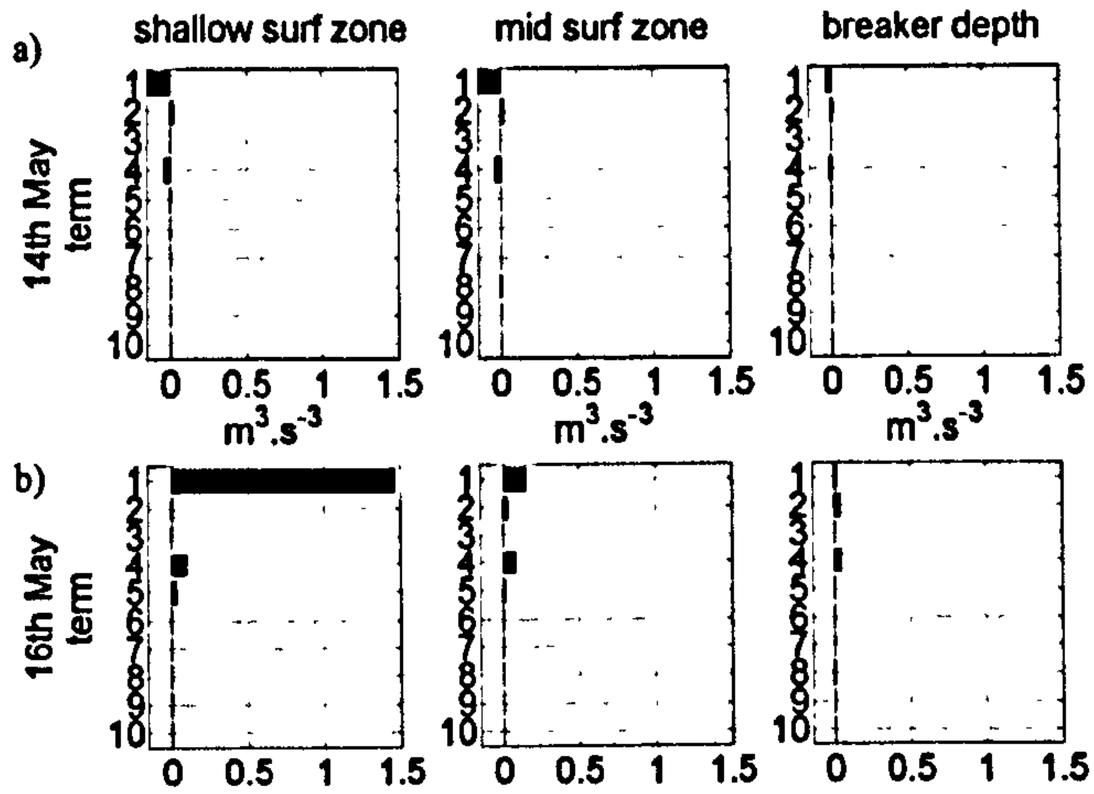

Figure 7. Computed third order velocity moments for the inner surf zone, mid surf zone and breaker depth on (a) 14th May and, (b) 16th May 2003 (not normalised).

transport potential and vice versa; short and long waves were separated about the location of a spectral valley which was situated at 0.05 Hz. Of the ten terms, the first five were found to be of most importance with the 'mean cubed' term dominating the velocity moments on both days. On the 14th May, a weak offshore undertow current that was strongest in the mid surf zone was measured which is reflected in the negative 'mean cubed' terms. Conversely, on the 16th May, the undertow was overcome by the significant onshore directed mean flow. This mean flow, which is strongest in the inner to mid surf zone during periods when the sand bank is not submerged are driven by strong refraction of the short period incident waves. The magnitude of terms 4 and 5 indicates the importance of both short and long wave stirring in suspending the sediment in the inner to mid surf zone. Wave skewness was not found to be important in the onshore transport of sediment under low energy conditions which is intuitive given that the majority of the transport occurs in the inner surf zone.

5.Conclusions

This study utilised Argus images and in-situ measurements to elucidate the processes that are responsible for the onshore migration of a sand bank adjacent an estuary under low energy conditions. The data showed that the process occurs in the inner to mid surf zone region through the suspension of sediment principally by short wave stirring but assisted by long waves. Strong refraction of the incident waves leads to a significant mean flow that drives the suspended sediment shoreward along the margins of the sand bank, at times when it is not submerged, and particularly on the flood tide. The onshore sediment transport is

further assisted by the absence of a well developed undertow on the offshore flank of the sand bank. Under the smallest wave conditions of the measurement period ($H_{m0} \approx 0.3$ m) the onshore directed momentum flux is able to setup against the offshore flank of the sand bank producing a weak undertow current in the surf zone. However, under higher wave conditions, the undertow disappeared entirely on the flood tide and only manifest as a particularly weak offshore current on the ebb tide. This may be attributable to the geometry of the sand bank which is narrow in the longshore direction and approximately dome shaped, enabling the onshore directed momentum flux to be redirected around the sand bank margins, which in turn contributes to the onshore directed mean current along the sand bank margins.

Acknowledgments

This contribution utilises Argus video technology developed by Rob Holman, John Stanley and the Coastal Imaging Lab of Oregon State University, U.S.A. The work was funded by the E.U. through the CoastView Project (contract no. EVK3-CT-2001-0054, website address: http://www.coastview.org.

References

Bagnold, R. A. 1963. Mechanics of marine sedimentation. *In M.N. Hill [Ed.]: The Sea*, **3**, Interscience, New York, 507-550.

Bailard, J. A. 1981. An energetics total load sediment transport model for a plane sloping beach. *Journal of Geophysical Research*, **86**, (C11) 10938-54.

Bowen, A. J. 1980. Simple models of nearshore sedimentation; beach profiles and longshore bars. *Canada. Geological Survey. Paper [Ottawa]*, **80**, (10) 1-11.

Byrnes, M. R., Hammer, R. M., Thibaut, T. D. and Snyder, D. B. 2004. Physical and biological effects of sand mining offshore alabama, USA. *Journal of Coastal Research*, **20**, 6-24.

Dyer, K. R. 2002. Futurecoast estuary assessment. On FutureCoast CD-Rom, Halcrow, Swindon, U.K.

Hoefel, F. and Elgar, S. 2003. Wave-induced sediment transport and sandbar migration. *Science*, **299**, (5614) 1885-1887.

Jaffe, B. E., Sternberg, R. W. and Sallenger, A. H. 1984. *The role of suspended sediment in shore-normal beach profile changes.* Edge, B.L. (Ed) 19th Coastal

Engineering Conference. Houston, Texas. New York: American Society of Civil Engineers. 3-7 September. pp 1983-1996.

Marino-Tapia, I. J., O'Hare, T. J., Russell, P. E., Davidson, M. A. and Huntley, D. A. 2003. *Onshore and offshore bar migration modelled with an energetics-type sediment transport model.* 28th International Conference on Coastal Engineering. Cardiff, U.K. ASCE. pp 2686-2698.

Plant, N. G. and Holman, R. A. 2001. *Nearshore morphology characterisation based on a predictive model for sand bar migration.* 4th Conference on Coastal Dynamics. Lundt, Sweden. ASCE. pp 530-537.

Robinson, A. H. W. 1980. Erosion and accretion along part of the suffolk coast of east anglia, england. *Marine Geology*, **37**, (1/2) 133-146.

Robinson, A. W. H. 1975. Cyclical changes in shoreline development at the entrance to teignmouth harbour, devon, england. *In: J. Hails and A. Carr [Eds]: Nearshore sediment dynamics and sedimentation*, pp181-200.

Siegle, E. 2003. *Sediment transport and morphodynamics at an estuary mouth: A study using coupled remote sensing and numerical modelling.* Ph.D. Thesis, University of Plymouth.

van Enckevort, I. M. J. and Ruessink, B. G. 2003. Video observations of nearshore bar behaviour. Part 1: Alongshore uniform variability. *Continental Shelf Research*, **23**, 501-512.

References

Aarninkhof S.G.I., Janssen P.C. and Plant, N.G., 1997. Quantitative estimations of bar dynamics from video images. In: Coastal dynamics '97, ed. E.B. Thornton, A.SC.E., pp 365-74.

Aarninkhof, S.G.J., 2003. Nearshore bathymetry derived from video imagery. PhD thesis, Delft University of Technology), 175p.

Aarninkhof, S.G J, Turner, I.L., Dronkers, T.D.T., Caljouw, M. and Nipius L., 2003. A video-based technique for mapping intertidal beach bathymetry. Coastal Engineering, 49, pp 275-89.

ABP Marine Environmental Research, 2002. Teignmouth quay development environmental statement. Report no. R.984a, pp 1-110.

Aird N.P., Davidson, M.A. and Marino-Tapia, I.J., 2005. Physical processes associated with onshore sand bank migration adjacent an estuary mouth. In: 29th International Conference on Coastal Engineering, ed. J.M. Smith, Lisbon, Portugal, pp 2519-30.

Bagnold, R.A., 1963. Mechanics of marine sedimentation. In: The Sea: Ideas and Observations, ed. M.N. Hill, Interscience, Vol. 3, pp 507-28.

Bailard, J.A., 1981. An energetics total load sediment transport model for a plane sloping beach. Journal of Geophysical Research-Oceans and Atmospheres, 86, pp 938-54.

Bailard, J.A. and Inman, D.L., 1981. An energetics bedload model for a plane sloping beach: local transport Journal of Geophysical Research, 86, pp 2035-43.

Battjes, J.A. and Janssen, J.P.F.M., 1978. Energy loss and set-up due to breaking of random waves. In: Proceedings of the 16th Conference on Coastal Engineering, Hamburg, Germany, ASCE, pp 569-87.

Bendatt, J.S. and Piersol, A.G., 1986. Random data: analysis and measurement procedures. New York, Wiley-Interscience.

Bernardes M E C 2005 Medium-term (months to years) morphodynamic modelling of a complex estuarine system. PhD thesis, School of Earth, Ocean and Environmental Studies, Univeristy of Plymouth, 194p.

Bird, P.A.D, Kingston, K.S., Mason, T.E. and Chadwick, A.J., 2001. Offshore and inshore wave measurements at Teignmouth. COAST3D Final Volume of Summary Papers, C4, pp 1-4.

Borrelli, M. and Wells, J.T., 2003. Swash bars and spit growth: evolution of a rapidly prograding spit along a sediment-starved coast. In: Coastal Sediments '03, ASCE, St. Petersburg, Florida.

Bowen, A.J., 1980. Simple models of nearshore sedimentation; beach profiles and longshore bars. In: The Coastline of Canada, Geological Survey of Canada, ed. S.B.McCann, 80- 10, pp 1-11.

Bray, M. Carter, D. and Hooke, J., 2004. South Coast Sediment Transport Study: Hope's Nose to Holcombe. In: SCOPAC Report, 5 Vols., 1200p. and CD-ROM, (http://www.scopac.org.uk/scopac%20sediment%20db/index.ht)

Bruun, P. and Gerritsen, F., 1959. Natural bypassing of sand at coastal inlets. Journal of Waterways and harbors Division, 85, pp 401-12

Buck, A.L., 1997. An inventory of UK estuaries; southern England. Joint Nature Conservation Committee, Vol. 6, Peterborough, U.K. 100p

Buonaiutoa, F.S. and Kraus, N.C., 2003, Limiting slopes and depths at ebb-tidal shoals. Coastal Engineering, 48, pp 51-65.

Burningham, H. and French, J., 2006. Morphodynamic behaviour of a mixed sand-gravel ebb-tidal delta: Deben estuary, Suffolk, U.K. Marine Geology, 225, pp 23-44.

Butt, T., Miles, J., Ganderton, P. and Russell, P., 2002, A simple method for calibrating optical backscatter sensors in high concentrations of non-cohesive sediments. Marine

Geology, 192, pp 419-24.

Byrnes, M.R., Hammer, R.M., Thibaut, T.D. and Snyder, D.B., 2004. Physical and biological effects of sand mining offshore Alabama, U.S.A. Journal of Coastal Research, 20, pp 6-24.

Cheung, K.F., Gerritsen, F. and Cleveringa, J., 2007. Morphodynamics and sand bypassing at Ameland Inlet, The Netherlands. Journal of Coastal Research, 23, pp 106-18.

Chickadel, C.C., Holman, R.A. and Freilich, M.H., 2003. An optical technique for the measurement of longshore currents. Journal of Geophysical Research-Oceans, 108, Art No: 3364.

Choi, J. Lim, C.H., Lee, J.I. and Yoon, S.B., 2009. Evolution of waves and currents over a submerged laboratory shoal, Coastal Engineering, 56, pp 297-312.

Cowell, P., Stive, M.J.F., Niederoda, A.W., de Vriend, H.J., Swift, D.J.P., Kaminsky, G.M. and Capobianco, M., 2003. The coastal tract (part 1): a conceptual approach to aggregated modelling of low-order coastal change. Journal of Coastal Research, 19, pp 812-27.

Cowell, P. and Thom, B., eds., 1997. Morphodynamics of coastal evolution.: Cambridge University Press, Cambridge.

Craig-Smith, S.J., 1970. A hydrographic analysis of the approaches to Teignmouth harbour. Unpublished M.Sc. thesis, University of Leicester, 174p.

Davidson, M.A., Huntley, D.A., Holman, R.A. and George, K., 1997, The evaluation of large-scale (km) intertidal beach morphology on a macrotidal beach using video images. In: Coastal Dynamics '97, Plymouth, U.K., ASCE, pp 385-94.

Davidson, M.A., Russell, P.E., Huntley, D.A. and Hardisty, J., 1993. Tidal asymmetry in suspended sand transport on a macrotidal intermediate beach, Marine Geology, 110, pp 333-53.

Davidson, M.A., Russell, P.E., Huntley, D.A., Hardisty, J. and Cramp, A., 1992. An overview of the British Beach and Nearshore (B-BAND) Programme. In: Proc. 23rd International Conference on Coastal Engineering, ed. B.L. Edge, ASCE, pp 1987-2000.

Davis, R.A. and Hayes, M.O., 1984. What is a wave-dominated coast? Marine Geology, 60, pp 313-29.

De Vriend, H.J., 1987. 2DH mathematical modelling of morphological evolutions in shallow water. Coastal Engineering, 11, pp 1-27.

Dean, R.G. and Walton, Jr. T.L., 1973. Estuarine Research II: Geology and engineering, ed. J.L. Cronin, New York, Academic Press, pp 129-49.

Defra, 2005. Marine Processes and Climate. Inter-Agency Committee on Marine Science and Technology, Report No. 2,. 138p.

Delft Hydraulics Institute, 2004. MIKE 21 Hydrodynamic module user guide and reference manual.

Douglass, S.L., 1991. Simple conceptual explanation of down-drift offset inlets. Journal of Waterway, Port, Coastal, and Ocean Engineering, 117, pp 136-42.

Draper, L., 1991. Wave climate atlas of the British Isles. OffshoreTechnology Report OTH 89 303, London, HMSO.

Dyer, K.R., 2002. FutureCoast Estuary Assessment. On: FutureCoast CD-ROM, Halcrow, Swindon, U.K.

Dyer, K.R. and Huntley, D.A., 1999. The origin, classification and modelling of sand banks and ridges Continental Shelf Research, 19, pp 1285-330.

Escoffier, F.F., 1940. The stability of tidal inlets Shore and Beach, 8, pp 114-5.

FitzGerald, D.M., 1982. Sediment bypassing at mixed energy inlets. In: Proc. Coastal Engineering Conference, ASCE, pp 1094-118.

FitzGerald, D.M., 1988. Shoreline erosional and depositional processes associated with inlets. In: Lecture Notes on Coastal and Estuarine Studies, eds.D.G Aubrey. and L. Weishar, 29, pp 186-225, Springer-Verlag.

FitzGerald, D.M., 1996. Geomorphic variability and, morphologic and sedimentologic controls on tidal inlets. Journal of Coastal Research, SI23, pp 47-71.

FitzGerald, D.M., Buynevich, I.V., Davis, R.A. and Fenster, M.S., 2002, New England tidal inlets with special reference to riverine-associated inlet systems. Geomorphology, 48, pp 179-208.

FitzGerald, D.M., Kraus, N.C. and Hands, E.B., 2000. Natural mechanisms of sediment bypassing at tidal inlets. USACE, report no: ERDC/CHL CHETN-IV-30. pp 1-10.

Galvin Jr., C.J., 1971. Inlets and wave direction; wave climate and coastal processes. In: Water environments and human needs. ed. A.T. Ippen, M.I.T. Parsons Laboratory for Water Resources and Hydrodynamics, pp 48-78.

Gaudiano, D.J. and Kana, T.W., 2001, Shoal bypassing in mixed energy inlets: Geomorphic variables and empirical predictions for nine South Carolina inlets. Journal of Coastal Research, 17, 2 , pp 280-91.

Guza, R.T. and Thornton, E., 1981. Velocity moments in the nearshore. Journal of Waterway, Port, Coastal and Ocean Engineering, 111, pp 235-56.

Hayes, M.O., 1975. Estuarine Research, 2, ed. L.E. Cronin, New York, Academic Press, pp 3-22.

Hayes, M.O., 1980. General morphology and sediment patterns in tidal inlets. Sedimentary Geology, 26, pp 139-56.

Hayes, M.O., Goldsmith, V. and Hobbs, C.H., 1970. Offset coastal inlets. In: Proc. 12th Conference on Coastal Engineering, ASCE, pp 1187-200.

Hicks, D.M. and Hume, T.M., 1996. Morphology and size of ebb tidal deltas at natural inlets

on open-sea and pocket-bay coasts, North Island, New Zealand. Journal of Coastal Research, 12, pp 47-63.

Hine, A.C., 1975. Bedform distribution and migration patterns on tidal deltas in the Chatham Harbor estuary, Cape Cod, Massachusetts. Journal of Coastal Research, 15, pp 303-13.

Hitchcock, D.R. and Bell, S., 2004. Physical impacts of marine aggregate dredging on seabed resources in coastal deposits. Journal of Coastal Research, 20, pp 101-14.

Holland, K.T., Holman, R.A., Lippmann, T.C., Stanley, J. and Plant, N., 1997. Practical use of video imagery in nearshore oceanographic field studies, IEEE, Journal of Oceanic Engineering, 22, pp 81-92.

Holland, K.T., Raubenheimer, B., Guza, R.T. and Holman, R.A., 1995. Runup kinematics on a natural beach. Journal of Geophysical Research-Oceans, Vol. 100, pp 4985-93.

Holman, R.A., Lippmann, T.C., O'Neill, P.V. and Hathaway, K., 1991. Video estimation of subaerial beach profiles. Marine Geology, 97, pp 225-31.

Holman, R.A. and Stanley, J., 2007. The history and technical capabilities of Argus Coastal Engineering, 54, pp 477-91.

Holthuijsen, L.H., Booij, N. and Herbers, T.H.C., 1989. A prediction model for stationary, short-crested waves in shallow-water with ambient currents. Coastal Engineering, 13, pp 23-54.

House of Commons Science and Technology Committee, 2007. Investigating the Oceans. Tenth Report of Session 2006-07, Volume 1, report no. HC 470-1, 151p.

Hubbard, D.K., Oertel, G.F. and Nummedal, D., 1979. The role of waves and tidal currents in the development of tidal-inlet sedimentary structures and sand body geometry: examples from North Carolina, South Carolina and Georgia. Journal of Sedimentary Petrology, 49, pp1073-92.

Hume, T.M. and Herdendorf, C.E., 1990. Morphologic and hydrologic characteristics of tidal inlets on a headland dominated, low littoral drift coast, northeastern New Zealand. In: Proc. Skagen Symposium, Journal of Coastal Research: SI 9, pp 527-63.

Hurrell, J.W., Kushnir, Y., Ottersen, G. and Visbeck, M., 2003. The North Atlantic Oscillation: Climate Significance and Environmental Impact. Geophysical Monograph Series, Vol 134.

Israel, C.G. and Dunsbergen, D.W., 1999. Cyclic morphological development of the Ameland Inlet, The Netherlands. In: Proc. of I.A.H.R Symposium on River, Coastal and Estuarine Morphodynamics: Dept. of Environment and Engineering, University of Genoa, Italy, pp 705-714.

Jackson, N.L., Nordstrom, K.F., Eliot, I. and Masselink, G., 2002. 'Low energy' sandy beaches in marine and estuarine environments: a review. Geomorphology, 48, p 147-62.

Jaffe, B.E., Sternberg, R.W. and Sallenger, A.H., 1984. The role of suspended sediment in shore-normal beach profile change. In: Proc. 19th Coastal Eng. Conf., ASCE, pp 1983-96.

Jarret, J.T., 1976. Tidal prism inlet area relationships. GITI Report No. 3, U.S.A.C.E., Vicksburg, MS, 76p.

Jenkins, G.M. and Watts, D.G., 1968. Spectral analysis and its applications. San Francisco, Holden-Day.

Kana, T.W., Hayter, E.J. and Work, P.A., 1999. Mesoscale sediment transport at southeastern U.S. tidal inlets: conceptual model applicable to mixed energy settings. Journal of Coastal Research, 15, pp 303-13.

Kingston, K., Davidson, M.A. and Holman, R.A., 2005. Video derived observations of estuarine sandbank migration, Teignmouth, U.K. In: Coastal Sediments '05

(CD-ROM), Paper 233, (Barcelona, Spain: A.S.C.E.), 10p.

Komar, P.D., 1996. Tidal inlet processes and morphology related to the transport of sediments. Journal of Coastal Research, SI23, pp 23-45.

Konicki, K.M. and Holman, R.A., 2000. The statistics and kinematics of transverse sand bars on an open coast. Marine Geology, 169, pp 69-101.

Kraus, N.C., 2000. Reservoir model of ebb-tidal shoal evolution and sand bypassing. Journal of Waterway Port Coastal and Ocean Engineering, ASCE, 126, pp 305-13.

Lafon, V., Dupuis, H., Butel, R., Castelle, B., Michel, D., Howa, H. and Apoluceno, D.D., 2005. Morphodynamics of nearshore rhythmic sandbars in a mixed-energy environment (SW France): 2. Physical forcing analysis. Estuarine Coastal and Shelf Science, 65, pp 449-62.

Laws, E., 1997. Mathematical methods for oceanographers: an introduction. New York, John Wiley & Sons.

Lippmann, T.C. and Holman, R.A., 1989. Quantification of sand bar morphology - a video technique based on wave dissipation. Journal of Geophysical Research-Oceans, 94, pp 995-1011.

Lippmann, T.C. and Holman, R.A., 1990. The Spatial and Temporal Variability of Sand-Bar Morphology. Journal of Geophysical Research-Oceans, 95, pp 11575-90.

Lippmann, T.C. and Holman, R.A., 1991. Phase speed and angle of breaking waves measured with video techniques. In: Coastal Sediments '91, ed. N Kraus *et al.*, Seattle, Washington, American Society of Civil Engineers, pp 542-56.

Maa, J.P.Y., Hobbs, C.H., Kim, S.C. and Wei, E., 2004. Potential impacts of sand mining offshore of Maryland and Delaware: Part I - Impacts on physical oceanographic processes. Journal of Coastal Research, 20, pp 44-60.

Madsen, A.J. and Plant, N.G., 2001. Intertidal beach slope predictions compared to field data.

Marine Geology,173, pp 121-39.

Marine Climate Change Impacts Partnership, 2008. Marine Cimate Change Impacts, Annual Report Card, 2007-2008. 8p.

Marino, J.N. and Mehta, A.J., 1987. Inlet ebb shoals related to coastal parameters. In: Coastal Sediments '87, Los Angeles, U.S.A., pp 1608-23.

Marino-Tapia, I.J., 2003. Cross-shore sediment transport processes on natural beaches and their relation to sand bar migration patterns. Ph.D. thesis, Institute of Marine Studies, University of Plymouth.

Marino-Tapia, I.J., Aird, N.P., Davidson, M.A., Kingston, K.S. and Ganderton, P., 2006. Tidally modulated sediment transport processes on a shore-attached bar. Journal of Coastal Research, SI39, pp395-400.

Marino-Tapia, I.J., Russell, P.E., O'Hare, T.J., Davidson, M.A. and Huntley, D.A., 2007. Cross-shore sediment transport on natural beaches and its relation to sandbar migration patterns: 1. Field observations and derivation of a transport parameterization. Journal of Geophysical Research-Oceans, 112.

Masselink, G. and Black, K.P., 1995. Magnitude and cross-shore distribution of bed return flow measured on natural beaches, Coastal Engineering, 25, pp 165-90.

Masselink, G. and Hughes, M.G., 2003. Introduction to coastal processes and geomorphology. London, Arnold.

Mehta, A.J., 1996. A perspective on process related research needs for sandy inlets. Journal of Coastal Research, SI23, pp 3-21.

Miles, J.R., 1997. Enhanced sediment transport near seawalls and reflective beaches. In: Institute of Marine Studies, Plymouth: University of Plymouth, 193p.

Miles, J.R. and Russell, P.E., 2004. Dynamics of a reflective beach with a low tide terrace, Continental Shelf Research, 24, pp 1219-47.

Miles, J.R., Russell, P.E. and Huntley, D.A., 1997. Introduction to the COAST3D field site at Teignmouth. In: COAST3D Kick-off workshop report, pp 1-10, (EC MAST Project No. MAS3-CT97-086).

Morris, A.S., 1993. Principles of measurement and instrumentation. London, Prentice Hall.

Nunny, R.S., 1980. A study of sediment dynamics in a shallow estuary. Unpublished PhD thesis, Faculty of Geography, University of Exeter, 364p.

Nunny, R.S., 1995. The physical environment: sediments. In: Lyme Bay environmental study, Vol. 2, pp 1-26.

O'Brien, M.P., 1931. Estuary tidal prisms related to entrance areas. Civil Engineer, 1, 8, pp 738-9.

O'Brien, M.P., 1969. Equilibrium flow areas of inlets on sandy coasts. Journal of the Warerways and Harbors Division 95 WW1, pp 43-52.

Oertel, G.F., 1972. Sediment transport of estuary entrance shoals and the formation of swash platforms. Journal of Sedimentary Petrology, 42, pp 857-63.

Oertel, G.F., 1975. Ebb tidal deltas of Georgia estuaries. In: Estuarine Research, ed. L E Cronin, New York, Academic Press.

Oertel, G.F., 1977. Geomorphoic cycles of ebb deltas and related patterns of shore erosion and accretion. Journal of Sedimentary Petrology, 47, pp 1121-31.

Reniers, A., Symonds, G. and Thornton, E., 2001. Coastal Dynamics '01, ed. H L M Hanson, pp 493-9.

Richmond, B.M. and Sallenger, A.H.J., 1984. Cross-shore transport of bimodal sands. In: Proc International Conference of Coastal Engineering, ed. B L Edge, Houston, Texas, ASCE, pp 1997-2008.

Robin, N., Levoy, F. and Monfort, O., 2007. Bar morphodynamic behaviour on the ebb delta of a macrotidal inlet (Normandy, France). Journal of Coastal Research, 23, pp

1370-8.

Robinson, A.W.H., 1975. Nearshore Sediment Dynamics and Sedimentation. Ed. J Hails and A Carr, John Wiley & Sons, pp 181-200.

Ruessink, B.G., 2000. An empirical energetics-based formulation for the cross-shore suspended sediment transport by bound infragravity waves. Journal of Coastal Research, 16, pp 482-93.

Russell, P.E. and Huntley, D.A., 1999. A cross-shore transport "shape function"' for high energy beaches. Journal of Coastal Research, 15, pp 198-205.

Seabergh, W.C., 1999. Physical model for coastal inlet entrance studies. Report no. CETN IV-19, USACE, 6p.

Sha, L.P., 1989. Cyclic morphological changes of the ebb tidal delta, Texel Inlet, The Netherlands. Geologie en Mijnbouw, 68, pp 35-48.

Sha, L.P. and Vandenberg, J.H., 1993. Variation in ebb-tidal delta geometry along the coast of the Netherlands and the German Bight. Journal of Coastal Research, 9, 3, pp 730-46.

Siegle, E., 2003. Sediment transport and morphodynamics at an estuary mouth: a study using coupled remote sensing and numerical modelling. PhD thesis, School of Earth Ocean & Environmental Sciences, University of Plymouth, 257p.

Siegle, E., Huntley, D.A. and Davidson, M.A., 2004. Physical controls on the dynamics of inlet sandbar systems. Ocean Dynamics, 54, pp 360-73.

Siegle, E., Huntley, D.A. and Davidson, M.A., 2007. Coupling video imaging and numerical modelling for the study of inlet morphodynamics. Marine Geology, 236, pp 143-63.

Small, C. and Nicholls, R.J., 2003. A global analysis of human settlement in coastal zones. Journal of Coastal Research, 19, pp 584-99.

Stive, M.J.F., 2004. How important is global warming for coastal erosion? An editorial

comment. Climatic Change, 64, pp 27-39.

Stockdon, H.F. and Holman, R.A., 2000. Estimation of wave phase speed and nearshore bathymetry from video imagery. Journal of Geophysical Research-Oceans, 105, pp 22015-33.

Stone, G.W., Pepper, D.A., Xu, J.P. and Zhang, X.P., 2004. Ship shoal as a prospective borrow site for barrier island restoration, coastal south-central Louisiana, USA: Numerical wave modeling and field measurements of hydrodynamics and sediment transport. Journal of Coastal Research, 20, pp 70-88.

Sutherland, J., Hall, L.J. and Chesher, T.J., 2001. Evaluation of the coastal area model PISCES at Teignmouth (UK). H.R. Wallingford.

Townend, I., 2005. An examination of empirical stability relationships for UK estuaries. Journal of Coastal Research, 21, pp 1042-53.

United States Army Corps of Engineers, 2002. Coastal classification and morphology. In: Coastal Engineering Manual , Part IV, Chapter 2, report no: EM 1110-2-1100, 83p.

Van Enckevort, I.M.J. and Ruessink, B.G., 2003. Video observations of nearshore bar behaviour. Part 1: alongshore uniform variability. Continental Shelf Research, 23, pp 501-12.

Van Enckevort, I.M.J and Ruessink, B.G., 2003. Video observations of nearshore bar behaviour. Part 2: alongshore non-uniform variability. Continental Shelf Research, 23, pp 513-32.

Van Lancker, V., Lanckneus, J., Hearn, S., Hoekstra, P., Levoy, F., Miles, J., Moerkerke, G., Monfort, O. and Whitehouse, R., 2004. Coastal and nearshore morphology, bedforms and sediment transport pathways at Teignmouth (UK). Continental Shelf Research, 24, pp 1171-202.

Van Rijn, L.C., 1998: Morphology of barrier islands and tidal inlets. In: Principles of coastal

morphology, Chapter 4, Part 6,Aqua Publications, 715p.

Van Rijn, L.C., Walstra, D.J.R., Grasmeijer, B., Sutherland, J., Pan, S. and Sierra, J.P., 2003. The predictability of cross-shore bed evolution of sandy beaches at the time scale of storms and seasons using process-based Profile models. Coastal Engineering, 47, pp 295-327.

Vinther, N., Aagaard, T. and Nielsen, J., 2005. Complex sediment transport pattern on a spit-platform in the Danish Wadden Sea. Journal of Coastal Research, 21, pp 710-9.

Walker, J.S., 1996, Fast Fourier transforms. CRC Press.

Walton, Jr. T.L. and Adams, W.D.,1976. Capacity of inlet outer bars to store sand. In: Proc. 15th International Conference on Coastal Engineering, ASCE, New York, pp 1919-37.

Walton, T., 2002. Tidal velocity asymmetry at inlets. United States Army Corps of Engineers, report no: ERDC/CHL CHETN-IV-47, pp 1-17.

West, A., 2002. Wave focussing surfing reefs: a new concept. MSc thesis, Delft University of Technology.

Whitehouse, R., 2001. Synthesis of Teignmouth process measurements and interpretation. COAST3D Final Volume of Summary Papers, C2, Report TR121, HR Wallingford, U.K., pp 1-10.

Whitehouse, R., Sutherland, J. and Waters, C., 2001. Water levels, wave and current climate at Teignmouth. COAST3D Final Volume of Summary Papers, C2, Report TR121, HR Wallingford, U.K., pp1-4.

Wright, L.D. and Short, A.D., 1984. Morphodynamic variability of surf zones and beaches - a synthesis. Marine Geology, 56, pp 93-118.